Characterisation of the cross-seeding of α-synuclein by Amyloid-β fibril polymorphs

Atenas Posada Borbon

University of Leeds

School of Molecular and Cellular Biology

Astbury Centre for Structural Molecular Biology

Submitted in accordance with the requirements for the degree of

Doctor of Philosophy

September 2020

The candidate confirms that the work submitted is his/her own and that appropriate credit has been given where reference has been made to the work of others.

Acknowledgments

First of all, I would like to thank my supervisors, Dr Eric Hewitt and Prof Sheena Radford, for their guidance and encouragement throughout the development of this research project. Eric, thank you for your everlasting patience and support. Sheena, thank you for setting the example to work hard and to always keep the big picture in mind.

It was a privilege to have been part of the Hewitt and Radford groups and to have coincided with past and current members of the labs. The work done in this investigation could not have been possible without the guidance of Dr Katie Stewart and Dr Matt Jackson, who helped me with the techniques and methods as I was settling into Leeds. Matt, thank you for the time and patience, but also your advice when I was in need of direction. I am grateful for the help of Mike Davies, Chalmers Chau and Sabine Ulamec, for having kindly spared their own protein (α-synuclein) so I could develop the assays in this thesis. I would also like to thank Dr Martin Walko and Maddie Brown, for their help with the purification of Aβ, a job not easy but a thousand times less problematic and more fun when accompanied by you. To Mr Nasir Kahn, thank you for always finding the time to take care of us. To Jess Ebo, Dr Anna Higgins and Maddie, thank you for providing a relief to the lab stress with your willingness to fight the cold, wind and rain and go for a run after work. Thank you to all the members of the Radford lab, for making me feel welcome in a place so far from my own home and made my time in Leeds an exceptional experience.

To my parents, Dora and Alvaro, I am forever grateful for your never-ending love and encouragement, you have been an inspiration to always try to be a better person. To my brothers, Oliver and Alvaro, thank you for showing me there are no limits to where one can go.

To Nik, thank you for your patience, your belief in my capabilities and giving me comfort in stressful times.

Lastly, I would like to convey my gratitude to the Mexican National Council of Science and Technology (CONACYT) for the financial support via the Programme “Becas al Extranjero 2016 Segundo Período” (beca No. 440768).

Abstract

Alzheimer's disease is the most common neurodegenerative disease whose main histopathological hallmark is the presence of extracellular plaques, primarily composed of Amyloid β (Aβ) fibrils. Recent finding suggest Aβ fibril polymorphism is associated with distinct clinical presentations of Alzheimer's disease. Moreover, intracellular inclusions of α-synuclein fibrillar aggregates known as Lewy bodies, classically associated with Parkinson's disease, are found in up to 60% of Alzheimer's disease individuals.

Using a set of *in vitro* biochemical and cellular approaches, the involvement of Aβ fibril polymorphism in α-synuclein aggregation and Lewy body-like formation is investigated here. Structurally defined $A\beta_{40}$ and $A\beta_{42}$ fibril polymorphs formed *in vitro* were used as models to study the effect of polymorphism on the ability to induce α-synuclein fibrillar aggregation. It was found that *in vitro*, there is a pH dependency on the cross-seeding of α-synuclein by Aβ fibril polymorphs. Fluorescence polarization and thioflavin T fluorescence kinetics showed that although binding between α-synuclein and Aβ fibrils can occur at pH 7.5, it is only at pH 4.5 that the fibrillar aggregation of α-synuclein can be accelerated by Aβ fibrils presence. Notably, the molecular mechanism of cross-seeding was found to be governed by surface-catalysed secondary nucleation. Further characterisation of the α-synuclein cross-seeded fibrils revealed differences in their curcumin fluorescence, denoting distinct structural arrangements.

Cellular analysis revealed that whilst not causing cell death, incubation with the Aβ fibril polymorphs differentially induced the formation of insoluble GFP-α-synuclein puncta. Furthermore, Aβ fibrils colocalized to acidic compartments, and increased resistance to lysosomal degradation was observed for α-synuclein monomeric samples in the presence of Aβ fibrils.

Taken together these results pose lysosomes as a site of α-synuclein cross-seeding by Aβ fibrils and suggest polymorphism may play a role in the extent of cellular cross-seeding, highlighting the importance of specific interactions between Aβ and α-synuclein in disease.

Table of contents

Acknowledgments ii

Abstract iii

Table of contents iv

List of abbreviations viii

List of Tables xi

List of figures xii

1. Introduction 1

1.1. Alzheimer's disease 1

1.1.1. Amyloid precursor protein and the amyloid pathway 3

1.1.2. Familial Alzheimer's disease 6

1.1.3. Sporadic Alzheimer's disease 8

1.1.4. Biomarkers of Alzheimer's disease 9

1.2. Amyloid β 10

1.2.1. Amyloid structure and assembly 12

1.2.2. Aβ fibril structure and polymorphism 16

1.2.3. Aβ toxicity 23

1.3. Parkinson's disease and other synucleinopathies 24

1.3.1. α-synuclein 24

1.3.2. α-synuclein fibril structure and polymorphism 26

1.3.3. α-synuclein toxicity 27

1.3.4. α-synuclein pathology in Alzheimer's disease 28

1.4. Project aims 30

2. Materials and Methods 31

2.1. $A\beta_{40}$ and $A\beta_{42}$ expression and purification 31

2.1.1. Expression of $A\beta_{40}$ and $A\beta_{42}$ in *Escherichia coli* 31

2.1.2. Inclusion body isolation 31

2.1.3. Anion exchange chromatography of $A\beta_{40}$ 32

2.1.4. Dialysis and lyophilisation....33
2.1.5. Size exclusion chromatography for $A\beta_{40}$ purification....33
2.1.6. High performance liquid chromatography (HPLC) for $A\beta_{42}$ purification....34
2.2. Aβ monomer fluorescent labelling and fibril formation....34
2.3. $A\beta_{40}$ and $A\beta_{42}$ fibril preparation....34
2.3.1. 2A and 3Q $A\beta_{40}$ fibril seeding....35
2.3.2. *de novo* $A\beta_{40}$ fibril generation....35
2.3.3. $A\beta_{42}$ fibril generation at pH 2 and pH 8....35
2.4. Fibril yields....35
2.5. Sodium dodecyl sulphate-polyacrylamide gel electrophoresis (SDS-PAGE)....36
2.6. Negative staining Transmission Electron Microscopy (TEM) of fibrils....36
2.7. Fluorescence polarization assays of Aβ fibrils and α-synuclein....36
2.8. Thioflavin T (ThT) fluorescence assays....37
2.8.1 Aβ fibril formation....37
2.8.2 Cross-seeding of α-synuclein monomer by Aβ fibrils....37
2.9. Curcumin binding assay....38
2.10. Cell culture....38
2.10.1 Recovery of cells from frozen stocks and maintaining....38
2.10.2 Cell stock maintenance (freezing)....38
2.11. $A\beta_{40}$ and $A\beta_{42}$ fibril polymorph cross-seeding α-synuclein in cells....39
2.11.1 Cell permeabilisation for insoluble GFP puncta formation analysis....39
2.12. Cellular viability assays after incubation with $A\beta_{40}$ and $A\beta_{42}$ fibrils....39
2.12.1 ATP assay....40
2.12.2 LDH assay....40
2.12.3 3-(4,5-dimethylthiazol-2-yl)-2,5-diphenyltetrazolium bromide (MTT) reduction assay....40
2.13. Live cell imaging of after $A\beta_{40}$ and $A\beta_{42}$ fibrils incubation....41
2.14. Cell fractionation....41
2.14.1 Sequential detergent fractionation of cells incubated with Aβ fibrils....41

2.14.2 Subcellular fractionation and lysosome isolation 42
2.15. Western blotting 43
2.16. Lysosomal degradation 43
2.17. Statistical analysis 44
3. $A\beta_{40}$ and $A\beta_{42}$ fibril polymorph formation 45
3.1. Introduction 45
3.2. Expression of $A\beta_{40}$ and $A\beta_{42}$ peptides 46
3.3. Purification of $A\beta_{40}$ 48
3.3.1 Inclusion body isolation and anion exchange chromatography of $A\beta_{40}$ 48
3.3.2 Size exclusion chromatography (SEC) of $A\beta_{40}$ 50
3.4. Purification of $A\beta_{42}$ 51
3.4.1 Inclusion body isolation of $A\beta_{42}$ 51
3.4.2 HPLC purification of $A\beta_{42}$ 52
3.5. Fibril production 54
3.5.1 2A and 3Q $A\beta_{40}$ fibril polymorph seeding 54
3.5.2 *de novo* $A\beta_{40}$ fibril generation 55
3.5.3 Characterisation of fibrillation of $A\beta_{40}$ 56
3.5.4 $A\beta_{42}$ fibril generation at pH 2 and pH 8 59
3.6. Discussion 61
4. Cross-seeding analysis of α-synuclein fibril formation by Aβ fibrils 64
4.1. Introduction 64
4.2. Binding of Aβ fibrils and α-synuclein monomer at pH 7.4 65
4.3. Analysis of cross-seeding of α-synuclein monomer by $A\beta_{40}$ fibrils at pH 7.5 67
4.4. Cross-seeding of α-synuclein monomer by $A\beta_{40}$ fibrils at pH 4.5 75
4.5. α-synuclein monomer cross-seeding by $A\beta_{42}$ fibrils 83
4.6. Molecular mechanism of aggregation of α-synuclein monomer by Aβ fibrils 90
4.7. Polymorphism characterisation of cross-seeded α-synuclein fibrils 96
4.8. Discussion 100
5. Cross-seeding of α-synuclein by $A\beta_{40}$ and $A\beta_{42}$ fibrils in a cellular model 105

5.1. Introduction 105

5.2. Development of a cellular model for α-synuclein seeding 106

5.3. Cellular toxicity of $A\beta_{40}$ and $A\beta_{42}$ fibril preparations 110

5.4. Cellular toxicity cross-seeding derived α-synuclein fibrils 115

5.5. Insoluble GFP-α-synuclein puncta formation in cells after incubation with $A\beta_{40}$ and $A\beta_{42}$ fibril preparations 117

5.6. Lysosomal co-localization with Aβ fluorescent fibrils 122

5.7. Cross-seeding of α-synuclein by Aβ in the presence of lysosomes 128

5.8. Discussion 131

6. Conclusions and future perspectives 136

References 142

List of abbreviations

Aβ	Amyloid β
$Aβ_{40}$	Amyloid β residues 1-40
$Aβ_{42}$	Amyloid β residues 1-42
AICD	APP intracellular domain
ApoE	Apolipoprotein E
APP	Amyloid precursor protein
ATP	Adenosine triphosphate
BACE1	β-secretase
CNS	Central nervous system
CSF	Cerebrospinal fluid
CTF	C-terminal fragment
CryoEM	Cryogenic electron microscopy
DTT	Dithiothreitol
E. coli	*Escherichia coli*
EDTA	Ethylenediaminetetraacetic acid
EEA1	Early endosome antigen 1
EM	Electron microscopy
ESI	Electrospray ionisation
ESI-MS	Electrospray ionisation mass spectrometry
fMRI	Functional magnetic resonance imaging

FT	Flowthrough
GAPDH	Glyceraldehyde-3-phosphate dehydrogenase
GFP	Green fluorescent protein
h	Hour
HPLC	High performance liquid chromatography
IAPP	Islet amyloid precursor protein
IC	Inclusion body isolate
IPTG	Isopropyl β-D-1-thiogalactopyranoside
LAMP-1	Lysosomal-associated membrane protein 1
LAMP-2	Lysosomal-associated membrane protein 2
LB	Lysogeny broth
LDH	Lactate dehydrogenase
MTT	3-(4,5-dimethylthiazol-2-yl)-2,5-diphenyltetrazolium bromide
MSA	Multiple system atrophy
MW	Molecular weight
NAC	Non-Amyloid β component
NaCl	Sodium chloride
NMR	Nuclear magnetic resonance
PAGE	Polyacrylamide gel electrophoresis
PBS	Phosphate buffered saline
PCA-AD	Posterior cortical atrophy Alzheimer’s disease
PDB	Protein data bank
PEG	Polyethylene glycol

PET	Positron emission tomography
PMSF	Phenylmethanesulfonylfluoride
PVDF	Polyvinylidene fluoride
PSEN1	Presenilin 1
r-AD	Rapidly progressive Alzheimer’s disease
rpm	Rotations per minute
sAPPα	soluble APP fragment α
sAPPβ	soluble APP fragment β
S.D.	Standard deviation
S.E.M.	Standard error of the mean
SDS	Sodium dodecyl sulphate
sec	Second
SEC	Size exclusion chromatography
ssNMR	Solid state nuclear magnetic resonance
t-AD	Typical progression Alzheimer's disease
TEM	Transmission electron microscopy
TFA	Trifluoroacetic acid
ThS	Thioflavin S
ThT	Thioflavin T
Tris-HCl	Tris(hydroxymethyl)aminomethane hydrochloride
WT	wildtype

List of Tables

Table 1.1. Molecular structure characteristics of in vitro generated $A\beta_{40}$ fibril polymorphs 19
Table 1.2. Molecular structures characteristics of in vitro generated mutant $A\beta_{40}$ fibril polymorphs 20
Table 1.3. Molecular structures characteristics of $A\beta_{40}$ fibril polymorphs generated from ex vivo material 21
Table 1.4. Molecular structures characteristics of $A\beta_{40}$ fibril polymorphs generated from ex vivo material 22
Table 3.1. Half times of the kinetic reaction of 2A and 3Q $A\beta_{40}$ fibril seeding. 55
Table 3.2. Significant differences of curcumin and ThT fluorescence observed between the $A\beta_{40}$ fibril preparations. 59
Table 3.3. Half times of $A\beta_{42}$ fibrils formed at pH 2 and pH 8. 60
Table 4.1 .Half-times of the α-synuclein aggregation reaction after adding 1%, 5% or 20% (v/v) α-synuclein seed. 70
Table 4.2. Half-times and lag-times of the α-synuclein aggregation reaction after 20% (v/v) α-synuclein seeding and cross-seeding with $A\beta_{40}$ fibrils at pH 4.5. 78
Table 4.3. Half-times and lag-times of the α-synuclein aggregation reaction after 20% (v/v) α-synuclein seeding and cross-seeding with $A\beta_{42}$ fibrils at pH 4.5. 86
Table 4.4. Comparison of half-times of $A\beta_{40}$ self-seeding reactions using 5 % (v/v) unsonicated or sonicated fibrils. 92
Table 4.5. Comparison of lag times of α-synuclein cross-seeding by unsonicated or sonicated $A\beta_{40}$ and $A\beta_{42}$ fibrils at pH 4.5. 95

List of figures

Figure 1.1. Braak stages of Aβ deposition. 2
Figure 1.2. Amyloid precursor protein structure domains. 4
Figure 1.3. The non-amyloidogenic and amyloidogenic pathways. 5
Figure 1.4. γ-secretase complex molecular structure. 8
Figure 1.5. $A\beta_{40}$ monomer structure and sequence. 12
Figure 1.6. Cross β-sheet structure 13
Figure 1.7. Amyloid fibril formation and kinetics. 14
Figure 1.8. The energy landscape of protein folding and aggregation. 15
Figure 1.9. Molecular structures of Aβ fibril polymorphs. 18
Figure 1.10. Molecular structure of α-synuclein bound to a micelle and protein sequence 25
Figure 1.11. Protofilaments of α-synuclein fibril polymorphs 27
Figure 3.1. $A\beta_{40}$ and $A\beta_{42}$ fibril polymorphs. 46
Figure 3.2. $A\beta_{40}$ and $A\beta_{42}$ peptide expression 47
Figure 3.3. Expression and purification of $A\beta_{40}$ and $A\beta_{42}$ workflow 48
Figure 3.4. SDS-PAGE gel of induction, inclusion body isolation and anion-exchange batch purification of $A\beta_{40}$. 49
Figure 3.5. Protein purification SEC of $A\beta_{40}$ peptide. 50
Figure 3.6. Mass spectrometry spectra of purified $A\beta_{40}$ peptide. 51
Figure 3.7. Isolation of $A\beta_{42}$ peptide from inclusion bodies. 52
Figure 3.8. HPLC spectra of $A\beta_{42}$ peptide purification 53
Figure 3.9. SDS-PAGE of HPLC purified $A\beta_{42}$ and high-resolution mass-spectrometry. 53
Figure 3.10. 2A and 3Q fibril seeding. 54
Figure 3.11. ThT kinetic analysis of the unseeded de novo $A\beta_{40}$ fibril generation 55
Figure 3.12. Fibril yields of the $A\beta_{40}$ fibril polymorphs. 57
Figure 3.13. Electron micrographs of the $A\beta_{40}$ fibril polymorphs. 57
Figure 3.14. Curcumin dye binding to $A\beta_{40}$ polymorphs. 58
Figure 3.15. Endpoint ThT fluorescence of the $A\beta_{40}$ polymorphs. 59
Figure 3.16. Fibrils of $A\beta_{42}$ grown at pH 2 and pH 8. 60
Figure 3.17. Endpoint ThT fluorescence of $A\beta_{42}$ fibrils. 61
Figure 4.1. α-synuclein short fibrils (seeds). 66
Figure 4.2. Binding of Aβ fibril polymorphs with α-synuclein monomer. 67
Figure 4.3. Cross-seeding analysis of α-synuclein monomer by $A\beta_{40}$ fibril polymorphs at pH 7.5. 69

Figure 4.4. Fibril yields and densitometry of unseeded and self-seeded α-synuclein samples from the ThT kinetic assay of self-seeding of at pH 7.5. 70
Figure 4.5. Fibril yields and densitometry of samples from the ThT kinetic assay of cross-seeding of α-synuclein monomer by $A\beta_{40}$ fibril preparations at pH 7.5. 71
Figure 4.6. Electron microscopy imaging of unseeded α-synuclein monomer and self-seeded α-synuclein after ThT kinetics at pH 7.5. 72
Figure 4.7. Electron microscopy imaging of α-synuclein monomer incubated with $A\beta_{40}$ fibrils after ThT kinetics at pH 7.5. 73
Figure 4.8. Molecular structures of ThT and ThS. 74
Figure 4.9. Cross-seeding analysis of α-synuclein monomer by $A\beta_{40}$ fibrils at pH 7.4. 75
Figure 4.10. Cross-seeding analysis of α-synuclein monomer by $A\beta_{40}$ fibrils at pH 4.5. 77
Figure 4.11. Lag time comparison of cross-seeded α-synuclein monomer by $A\beta_{40}$ fibril preparations at pH 4.5. 78
Figure 4.12. Fibril yields of samples from the ThT kinetic of unseeded and self-seeding of α-synuclein at pH 4.5 80
Figure 4.13. Electron microscopy imaging of samples after self-seeding of α-synuclein monomer at pH 4.5. 80
Figure 4.14. Fibril yields of samples from the ThT kinetic assay of cross-seeding of α-synuclein monomer by $A\beta_{40}$ fibril preparations at pH 4.5. 81
Figure 4.15. Electron microscopy imaging of samples after cross-seeding of α-synuclein monomer by $A\beta_{40}$ fibrils at pH 4.5. 82
Figure 4.16. Cross-seeding analysis of α-synuclein monomer by $A\beta_{42}$ fibrils at pH 7.5 and 4.5. 85
Figure 4.17. Lag time comparison of cross-seeded α-synuclein monomer by $A\beta_{42}$ fibril preparations at pH 4.5. 86
Figure 4.18. Fibril yields of samples from the ThT kinetic assay of cross-seeding of α-synuclein monomer by $A\beta_{42}$ fibril preparations at pH 7.5. 87
Figure 4.19. Fibril yields of samples from ThT kinetic assay of cross-seeding of α-synuclein cross-seeding by $A\beta_{42}$ fibril preparations at pH 4.5. 88
Figure 4.20. Figure 4.20. Electron microscopy imaging of samples after cross-seeding of α-synuclein monomer by $A\beta_{42}$ fibrils at pH 4.5. 89
Figure 4.21. Mechanism of amyloid formation. 90
Figure 4.22. Assessment of aggregation of $A\beta_{40}$ by seeding with sonicated and unsonicated fibril preparations. 91
Figure 4.23. Half-time comparison of 5% (v/v) self-seeded $A\beta_{40}$ by sonicated and unsonicated $A\beta_{40}$ fibrils. 92

Figure 4.24. Cross-seeding analysis of α-synuclein monomer by un-sonicated and sonicated $A\beta_{40}$ and $A\beta_{42}$ fibrils at pH 4.5. 94
Figure 4.25. Lag time comparison of cross-seeded α-synuclein monomer by sonicated and unsonicated $A\beta_{40}$ and $A\beta_{42}$ fibrils. 95
Figure 4.26. Curcumin molecular structure. 96
Figure 4.27. Curcumin dye binding to fibrils of α-synuclein after cross-seeding with 20% (v/v) $A\beta_{40}$ and $A\beta_{42}$ preparations at pH 4.5. 97
Figure 4.28. Curcumin λ_{max} fluorescence intensity of α-synuclein fibrils after cross-seeding by 20% (v/v) $A\beta_{40}$ or $A\beta_{42}$ fibril preparations at pH 4.5 98
Figure 4.29. Mean curcumin fluorescence intensity of α-synuclein fibrils after cross-seeding by 20% (v/v) $A\beta_{40}$ or $A\beta_{42}$ fibril preparations at pH 4.5 99
Figure 5.1. GFP-α-synuclein vector and predicted protein sequence. 107
Figure 5.2. Analysis of GFP-α-synuclein insoluble aggregate formation in unpermeabilised SH-SY5Y-GFP-α-synuclein cells..... 107
Figure 5.3. Insoluble GFP puncta formation in SH-SY5Y-GFP-synuclein cells after incubation with α-synuclein seeds. 109
Figure 5.4. Quantification of insoluble GFP puncta, average area of puncta and cell number in SH-SY5Y-GFP-synuclein cells after incubation with buffer, α-synuclein monomer or α-synuclein seeds. 110
Figure 5.5. ATP cellular viability assay after 48 h incubation with $A\beta_{40}$ and $A\beta_{42}$ fibril preparation. The ATP assay reaction (A) is based on the reaction of the D-luciferin substrate with the luciferase enzyme via ATP hydrolysis. 112
Figure 5.6. LDH cellular viability assay after 48 h incubation with $A\beta_{40}$ and $A\beta_{42}$ fibril preparation. 113
Figure 5.7. MTT cellular viability assay after 48 h incubation with $A\beta_{40}$ and $A\beta_{42}$ fibril preparation. 114
Figure 5.8. Cellular viability assays after 48 h incubation with the α-synuclein cross-seeded fibrils. SHSY5Y-α-synuclein-GFP cells were incubated with α-synuclein fibrils generated after the cross-seeding of α-synuclein with 20% (v/v) $A\beta_{40}$ fibrils preparations for 48 h. 116
Figure 5.9. Insoluble GFP puncta formation in SH-SY5Y-GFP-synuclein cells after incubation with $A\beta_{40}$ fibril preparations. 118
Figure 5.10. Insoluble GFP puncta formation in SH-SY5Y-GFP-synuclein cells after incubation with $A\beta_{42}$ fibril preparations. 119
Figure 5.11. Quantification of insoluble GFP-puncta, average area of puncta and cell number in SH-SY5Y-GFP-synuclein cells after incubation with $A\beta_{40}$ and $A\beta_{42}$ fibril preparations. 120
Figure 5.12. Sequential detergent fractionation of SH-SY5Y-GFP-α-synuclein cells after a 6-day incubation with $A\beta_{40}$ fibril preparations or α-synuclein seeds. 122

Figure 5.13. Fluorescently labelled $A\beta_{40}$ and $A\beta_{42}$ fibrils. 123
Figure 5.14. SH-SY5Y-GFP-α-synuclein cell seeding with fluorescently labelled 2A, 3Q and de novo $A\beta_{40}$ fibrils. 124
Figure 5.15. Quantification of fluorescently labelled $A\beta_{40}$ fibril in SH-SY5Y-GFP-α-synuclein cells. 125
Figure 5.16. Fibril colocalization with lysosomes: Buffer control. 126
Figure 5.17. Fibril colocalization with lysosomes: 2A. 126
Figure 5.18. Fibril colocalization with lysosomes: 3Q. 127
Figure 5.19. Fibril colocalization with lysosomes: de novo. 127
Figure 5.20. Percoll gradient fractionation of SH-SY5Y-GFP-α-synuclein cells. 128
Figure 5.21. In vitro degradation of α-synuclein monomer by lysosomes. 130
Figure 5.22. Lysosomal degradation of α-synuclein monomer in the presence or absence of Aβ fibril preparations or α-synuclein seeds. 131
Figure 5.23. Cellular model of α-synuclein cross-seeding by Aβ fibrils. 134
Figure 6.1. Model of α-synuclein cross-seeding by Aβ fibrils. 140

1. Introduction

1.1. Alzheimer's disease

About 20 to 40 million people are estimated to be currently living with dementia, with the incidence doubling every 20 years worldwide (Ballard et al., 2011), with an estimated cost of one trillion US dollars as of 2018 (DeTure and Dickson, 2019). Therefore, there is a pressing need to find a cure as well as to develop effective therapies to treat the disease.

Alzheimer's disease is the most common cause of dementia. Definitive diagnosis was for a long time only possible post mortem, but new techniques like functional magnetic resonance imaging (fMRI), positron emission tomography (PET) and cerebrospinal fluid analysis, have enabled physicians to identify Alzheimer's in living subjects (Scheltens et al., 2016).

Alzheimer's disease is pathologically characterized by the presence of insoluble proteinaceous aggregates in the brain, namely extracellular amyloid plaques and intraneuronal neurofibrillary tangles. Neuropathologically, extracellular accumulation of abnormal amyloid-β, from here onwards called Aβ, occurs in the brain of subjects with Alzheimer's disease (Selkoe, 2000). This accumulation leads to the formation of amyloid plaques, commonly known as senile plaques or neuritic plaques. Aβ plaques also present activated microglia, apolipoprotein E (ApoE), α_2-macroglobulin, interleukin-1 and 6, among other proteins and components (Thal et al., 2006).

Classification of amyloid plaques has been performed respective to their appearance and capability to be stained by amyloid dyes, such as Congo red, Thioflavin S or T (ThS or ThT) (Wu et al., 2006; Xu et al., 2020). Fibrillar plaques and dense-cored plaques are large, spherical structures that are surrounded by dystrophic neurites, reactive astrocytes and microglia. Fibrillar plaques have a central mass of Aβ with extensions that lead to an outer rim. In contrast, dense-cored plaques have a compact core of Aβ surrounded by a less densely packed Aβ. However, both of these plaques are strongly stained by Congo red and ThS (Xu et al., 2020). A third type of plaque that does not possess an identifiable substructure, known as diffuse plaques, has been identified in both Alzheimer's disease and aged brains. Diffuse plaques, which are often observed in association with microglia, present mostly non-fibrillar Aβ, as they are homogenously labelled by anti-Aβ antibodies, and are not stained by Congo Red and present weak or absent reactivity for ThS (Selkoe, 2000; Xu et al., 2020). (Selkoe, 2000). Simultaneously, irregular intracellular build-up of hyperphosphorylated tau tangles occurs in individuals with Alzheimer's disease, which leads to the formation of neurofibrillary tangles (Selkoe, 1999).

The spread of these protein accumulations, neurofibrillary tau tangles and amyloid plaques, occurs in specific patterns through the brain, seemingly in and independent way to each other (Braak and Braak, 1991; Ballard et al., 2011). The stages of propagation for amyloid burden have been thoroughly described by Braak and Braak (1991) and classified as Stages A, B and C (Figure 1.1). Stage A is demarcated by amyloid plaques confined to portions in the isocortex, particularly in basal portions in temporal, frontal and occipital lobe. In Stage B, accumulation progressively increases in the isocortical regions as well as part of the hippocampus, until all isocortical areas and the hippocampus are affected (stage C) (Braak and Braak, 1991).

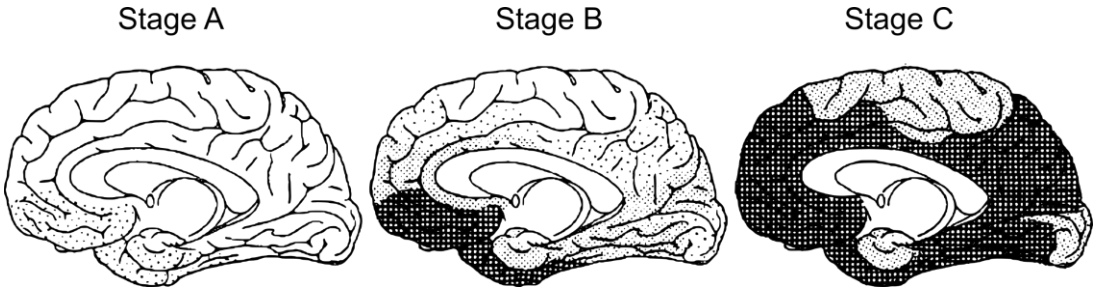

Figure 1.1. Braak stages of Aβ deposition.
Deposition of senile plaques, mainly composed of Aβ, appears to occur in a progressive manner, represented as increasing shades of grey/black. Initial confinement to basal portions of the isocortex gives way to spreading through the frontal and temporal lobes, affecting the hippocampus and ultimately appearing in all areas of the isocortex. Adapted from (Braak and Braak, 1991).

Classically, Alzheimer's disease patients, present a slow disease progression rate, with a survival of close to 8 years on average after diagnosis (Schmidt et al., 2011). However, some cases of Alzheimer's disease show a more acute presentation of the symptoms and cognitive decline (Drummond et al., 2017; Schmidt et al., 2011). This heterogeneity of symptom presentation makes it a difficult task to categorise it, but two main types, sporadic Alzheimer's disease and familial Alzheimer's disease, commonly encompass significant differences in the age of onset and genetic predisposition (Murphy and LeVine, 2010). Familial cases account for only less than 5% of the total cases of Alzheimer's disease and commonly present an earlier onset as well as a more severe symptoms (Ballard et al., 2011; Gessel et al., 2012; Murphy and LeVine, 2010).

The diversity of clinical presentations, including cognitive and biomarkers profiles, as well as disease progression rates are the probable outcome of an array of biologic causes that all converge on a common final disease pathway. Evidence of this has been shown by proteomic analysis of

amyloid plaques of the commonly used Alzheimer's disease mouse models, where a diversity in Aβ deposit morphology as well as distinct insolubility patterns was observed for Aβ plaques of the different mice models (Xu et al., 2020). The diversity of Aβ forms in these mice was accounted to the variations in each strain's background, such as the promoters used in the transgene vector constructs, the mutations to promote Aβ secretion, and co-expression of other protein mutants observed in familial cases of Alzheimer's disease. The following sections describe the main molecular commonalities that are observed in Alzheimer's disease and can determine the pathogenicity of the disease.

1.1.1. Amyloid precursor protein and the amyloid pathway

Amyloid senile plaques are mainly composed of Aβ fibrils, non-fibrillar forms of Aβ, cells and protein degradation products (Selkoe and Hardy, 2016; Selkoe, 1999). Aβ is the proteolytic product of the cleavage of the amyloid precursor protein (APP), a protein that has 8 isoforms that range in in length from 695-770 amino acids (Figure 1.2). Three regions have been identified independently *in vitro*. The E1 region is formed by the N-terminal domain and a copper binding domain (Wang and Ha, 2004). The N-terminal domain is a highly charged basic domain that binds to heparin and other glycosaminoglycans, that contains 9 short β-strands and 1 α-helix (Rossjohn et al., 1999). The copper binding domain is a cysteine-rich region that is implicated in binding and reduction of copper (Barnham et al., 2003). The second region, E2, is formed by the core domain of APP, which corresponds to residues 365-546 and lies adjacent to the Aβ sequence. The E2 region is known to have higher affinity to glycosaminoglycans than the N-terminal domain of APP. In solution, the isolated E2 region forms an antiparallel dimer, where the N-terminal of one monomer packs against the C-terminal of the second monomer of E2 (Wang and Ha, 2004). Lastly, the transmembrane domain is the anchor to the cell membrane and contains the C-terminal fraction of Aβ (Nadezhdin et al., 2011).

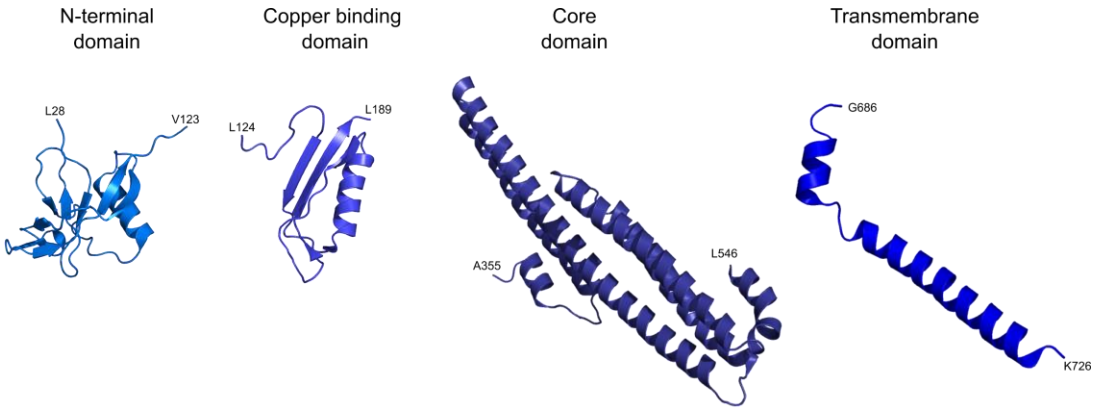

Figure 1.2. Amyloid precursor protein structure domains.
Four molecular domains have been identified independently in the amyloid precursor protein: The N-terminal domain (PDB: 1MWP) and the copper binding domain (PDB: 1OWT) form the E1 region, the core domain or E2 region (PDB: 1RW6) and the transmembrane domain (PDB: 2LLM).

APP is processed in the trans-Golgi network and transported to the cell surface or to the endosomal compartments via clathrin-coated vesicles. At the cell surface, APP is cleaved via several secretases, and two distinct processing pathways have been described (O'Brien and Wong, 2011).

The non-amyloidogenic α-secretase pathway (Figure 1.3 A), in which the α-secretase enzyme initially cleaves APP in the middle of the extracellular hydrophobic region that encompasses Aβ, releases a soluble fragment named sAPPα. As a consequence of this cleavage, there is no production of Aβ by this pathway (Nhan et al., 2015). The α-secretase cleavage of APP generates a carboxyterminal fragment (CTF) that is 83 residues long (Wilkins and Swerdlow, 2017). γ-Secretase cleaves CTF83 resulting in generation of the p3 peptide that is released into the extracellular space, as well as the APP intracellular domain (AICD) (Chow et al., 2010; O'Brien and Wong, 2011). The sAPPα peptide, observed as a component of the CSF, has been described as neurotrophic factor, and has been implicated in memory consolidation by increasing long term potentiation in mice models of Alzheimer's disease. In contrast, no specific physiological role has been described for the 3 kDa long p3 peptide. However, the p3 peptide has been implicated in neurotoxicity as it is often found as a component of senile plaques. The AICD fragment is thought to be translocated into the nucleus, where it promotes gene expression and activation of genes. It has recently been implicated in the activation of GSK-3β, a protein that phosphorylates tau, and therefore may contribute to Alzheimer's disease pathology (Nhan et al., 2015).

The amyloidogenic pathway of APP (Figure 1.3 B) begins with the action of β-secretase, or BACE1 enzyme. This cleaves APP into a 99 amino acid peptide, termed C-terminal fragment 99, that contains the hydrophobic Aβ region (Chow et al., 2010). After this cleavage the release of sAPPβ occurs, which as sAPPα is commonly found in the CSF and has neurotrophic effects in

the central nervous system (CNS) (Nhan et al., 2015). The APP cleavage by β-secretase is followed by that of γ-secretase, which has cleavage sites in the middle of the APP transmembrane. γ-Secretase initiates endoproteolysis at the region encompassing $A\beta_{48}$ or $A\beta_{49}$, which is then shortened by sequential cleavages every 3-4 amino acids (Chavez-Gutierrez et al., 2012). Ultimately, the 39-42 residue long Aβ peptide is released into the extracellular space, and the AICD fragment to the intracellular space (O'Brien and Wong, 2011). The main sites of cleavage of β-secretase γ-secretase (Figure 1.3 C) occur at residues flanking the Aβ region, before D1 and after V40 or A42 (O'Brien and Wong, 2011). However, it has been noted that the cleavage by both β and γ-secretase enzymes are not restricted to a specific site, but rather they have multiple cleavage sites that generate Aβ peptides of different lengths, denoted as N-terminal or C-terminal truncations of Aβ (Arber et al., 2019).

Mutations to the enzymes involved in the amyloidogenic pathway, as well as mutations in APP have been observed in individuals presenting familial Alzheimer's disease (Hatami et al., 2017).

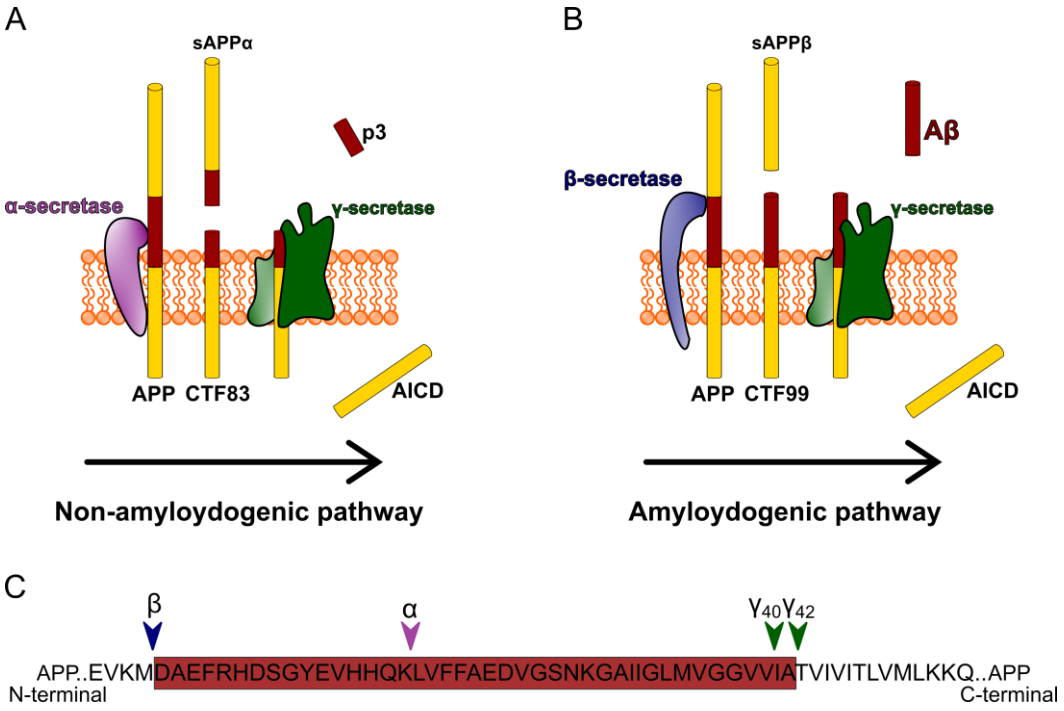

Figure 1.3. The non-amyloidogenic and amyloidogenic pathways.
In the non-amyloidogenic pathway (A), APP is initially cleaved by α-secretase, which releases a soluble APP fragment (sAPPα) into the extracellular space. The C-terminal fragment that remains bound to the membrane (CTF83) is then cleaved by γ-secretase enzyme, that releases a p3 fragment into the extracellular space and an intracellular APP fragment (AICD) into the cytoplasm. In the amyloidogenic pathway (B), APP goes through sequential cleavages by β-secretase and γ-secretase enzymes, at different sites than in the non-amyloidogenic pathway. First, β-secretase cleaves APP. In this case, the C-terminal fragment (CTF99) bound to the membrane contains the region encompassing Aβ. Aβ is then cleaved from CTF99 by γ-secretase and is released into the extracellular space. The APP sites of cleavage (C) by α-secretase (purple arrow), β-secretase (blue arrow) and γ-secretase (green arrows) fall within or flanking the Aβ region (red box). Adapted from (O'Brien and Wong, 2011).

1.1.2. Familial Alzheimer's disease

Familial Alzheimer's disease, or inherited Alzheimer's, disease represents 1- 5% of the total cases (Arber et al., 2019). Several genes and gene mutations are implicated in dominantly inherited Alzheimer's disease pathology (DeTure and Dickson, 2019). The *APP* gene, encoding APP, was the first to be discovered to be involved in the disease and mutations *APP* are thought to account for less than 0.1% of all cases (Tanzi, 1999). Other genes, whose mutations are thought to lead to degeneration, are *presenilin 1* (*PSEN1)* encoding for PSEN1 protein, the catalytic centre of γ-secretase and *PSEN2* encoding for the PSEN enhancer 2 protein, part of the γ-secretase protein complex formation (Selkoe, 1999). Mutations in these genes lead to the increased secretion of Aβ in the brain, and enhancement of the extracellular concentration and aggregation into plaques (Thal et al., 2006).
How these mutations and other genetic factors contribute to Alzheimer's disease pathology is described below.

1.1.2.1 APP mutations

In familial Alzheimer's disease, mutations to APP fall within residues 1-43 of the Aβ region or in sites adjacent to the N- or C-termini of the Aβ sequence, where cleavage by β-secretase or γ-secretase occur in the amyloidogenic pathway (Hatami et al., 2017). Close to 30 mutations have been described within the APP fragment that encompasses Aβ, and 14 mutations have been defined at sites neighbouring γ-secretase cleavage sites (Chiti and Dobson, 2017).

The mutations of APP that fall within the Aβ region are known to affect its fibrillar aggregation kinetics in vitro. ThT fluorescence analysis of 11 of the familial APP/Aβ mutants, showed that these Aβ variants apart from having distinct aggregation kinetics, displayed different ThT endpoint fluorescence, and in general acceleration of aggregation occurred compared to wildtype (WT) Aβ40 (Hatami et al., 2017). Examples of these are the APP D678N (D7N Aβ) Tottori mutation, known to promote the elongation phase of Aβ fibrillar aggregation; the APP E693 deletion (ΔE22 Aβ), which has been implicated in Aβ's acceleration of aggregation (Hatami et al., 2017); the APP E693G mutation (E22G Aβ) Arctic mutation, known to increase the rate of protofibril formation; the APP A692G mutation (A21G Aβ) Flemish mutation, at a site that is close to α-secretase cleavage and observed in some cases of early onset Alzheimer's disease (Gessel et al., 2012).

APP overexpression is observed in Down syndrome individuals. Trisomy of chromosome 21, where the APP gene is found, is observed in these individuals. This triplication results in APP overexpression, and leads to early brain Aβ deposition and plaque presence when individuals are

in their late 20s (O'Brien and Wong, 2011). In addition to an increase in amyloid burden, an emergence of dementia symptoms, aside from lifelong intellectual impairment, is observed from the age of 40 in ~55% of Down syndrome individuals. The development of dementia in this group seems to follow early onset Alzheimer's disease neuropathological changes, as an increase in Aβ plaques, changes in hippocampal volume and cerebral glucose metabolism are observed, compared to people with Down's syndrome who did not have dementia (Ballard et al., 2016).

1.1.2.2 PSEN mutations

More than 150 mutations have been described for *PSEN1* and *PSEN2* genes in Familial Alzheimer's disease (Chavez-Gutierrez et al., 2012).

The γ-secretase enzyme complex (Figure 1.4) is formed by 4 discrete protein regions: 1) PSEN1, the catalytic home of γ-secretase complex that works through a recognition motif (residues 433-435),a YD (residues 258 and 257) and GxD (residues 383-385) cleavage sites. 2) Nicastrin, a type 1 glycoprotein, composed by a large extracellular domain and a PSEN-interacting transmembrane site. 3) the PSEN enhancer 2 protein, a hairpin membrane protein directly adjacent to PSEN1, formed by 2 transmembrane with endoproteolysis activity related to PSEN1 activation. 4) The anterior pharynx defective-1, a 7 transmembrane protein complex that stably associates with PSEN1 through a GxG motif, important in the assembly of the complex (Bai et al., 2015; Tolia and De Strooper, 2009).

Mutations in PSEN1 observed in people diagnosed with Alzheimer's disease are thought to reduce the carboxypeptidase activity of γ-secretase, leading to longer Aβ fragments being released (Chavez-Gutierrez et al., 2012). Two mutational hotspots have been identified in PSEN1, located at the inner core of the structural subunits, and that modulate the cleaving activity of the complex *in vitro*. The first one affects residues in transmembrane domains 2 – 5 and altering and the second hotspot is located at the inner core of transmembrane domains 6 – 9, close to the catalytic site, where D257and D385 are (Bai et al., 2015).

Analysis of iPSC's derived from Alzheimer's disease individuals bearing mutations in *PSEN1* (Y115H, M139V and R278I) revealed an increase in the ratio of $A\beta_{43}$:$A\beta_{40}$ and $A\beta_{42}$:$A\beta_{40}$ by immune assay and mass-spectrometry. At the same time, they noted that the levels of PSEN1 expression were variable depending on the *PSEN1* mutation, suggesting that partial loss of function, lack of PSEN1 maturation or reduced catalytic activity are directly involved in the generation of longer Aβ peptides (Arber et al., 2019).

Figure 1.4. γ-secretase complex molecular structure.
The γ-secretase complex (PDB: 5A63) is formed by nicastrin in green, PSEN enhancer 2 in yellow, PSEN1 in blue, and pharynx-1 A in purple. The catalytic residues D257 and D385 in PSEN are coloured in cyan.

1.1.3. Sporadic Alzheimer's disease

The majority of cases of Alzheimer's disease are due to environmental and non-dominant genetic factors, as opposed to dominant inherited genes in Familial Alzheimer's (Lippa et al., 1996). It is also common to find people, not living with dementia, burdened with amyloid deposits in the neocortex, allocortex, grey nuclei and posterior fossa structure (Thal et al., 2002) which reveals the difficulty determining the disease and the necessity for additional biomarkers for this task.

Individuals with sporadic Alzheimer's disease tend to have a later age of onset of symptoms and less severity of pathology (Aβ deposits), compared to familial cases (Lippa et al., 1996). The histopathological markers, including neuronal loss, Aβ and tau deposition, remain the same in both types (Lippa et al., 1996). Sporadic cases have been suggested to be related to a decrease in degradation of Aβ by neprilysin, a plasma membrane bound metalloprotease that degrades peptides extracellularly (Murphy and LeVine, 2010), and insulin degrading enzyme (Thal et al., 2006). The strongest risk factor for late onset Alzheimer's disease is the presence of the ε4 allele of the *APOE* gene, and its frequency is increased to ~40% in sporadic Alzheimer's disease patients, compared to a 13.7% frequency in the general population worldwide (Liu, C.C. et al., 2013). In the same manner, ~80% of familial cases of Alzheimer's present at least one *APOE* ε4 allele (Corder et al., 1993).

1.1.3.1 Apolipoprotein E ε4 genotype

The Apolipoprotein E (ApoE), is a ~34 kDa lipoprotein involved in lipid metabolism, lipid transport and cholesterol mediation in a variety of cell types. In the CNS, ApoE synthesized in astrocytes delivers cholesterol to neurons via ApoE receptors (Liu, C.C. et al., 2013; Palta et al., 2020). The APOE gene is polymorphic, existing as ε2, ε3 and ε4 and resulting in six different genotypes. Three different isoforms of the ApoE that differ in the residues 112 and 158: ApoE2 has a C112 and C158, ApoE3 shows a C112 and a R158, and ApoE4 has an R112 and R158. These residue differences result in different binding affinities for Aβ (Liu, C.C. et al., 2013).

Loss of function in neuroprotection and gain of function in neurotoxicity seems to be the mechanism of pathogenesis in Alzheimer's disease. ApoE is deposited in senile plaques, and senile plaque load appears to occur in an ApoE-isoform dependent manner, where the presence of ε4 shows the highest plaque load (Nhan et al., 2015).

Although it is still not clear how the ApoE ε4 genotype renders such a drastic increase in pathogenicity, an involvement in Aβ clearance dysfunction, rather than increase in affinity in binding to Aβ is thought to be the main cause. Consistent with this, ApoE3 isoform, and not ApoE4, is the protein isoform with the highest binding affinity to Aβ (Yang, D.S. et al., 1997). One of the routes of clearance of Aβ occurs by receptor mediated uptake by neurons and glial cells and involves lipidated ApoE binding to Aβ and facilitating uptake through cell surface receptors. A decrease in efficiency in clearance of Aβ by ApoE4 could be therefore be at fault of increased pathogenicity (Liu, C.C. et al., 2013).

1.1.4. Biomarkers of Alzheimer's disease

The levels of Aβ in different fluids, as well as tau levels, β-secretase levels have been sought as indicators of early stages of Alzheimer's disease (Zetterberg and Blennow, 2013). Under physiological healthy conditions, the ratio of monomeric $A\beta_{42}$:$A\beta_{40}$ is thought to be ~1:9, and under pathological conditions a shift occurs, whereby the percentage of $A\beta_{42}$ is increased (Pauwels et al., 2012), with ratios 4:6 and 3:7 stimulating the aggregation of $A\beta_{40}$ into amyloid fibrils and modulating oligomer formation (Pauwels et al., 2012; Zoltowska et al., 2016). Biochemical changes in the brain are reflected in the CSF composition. Aβ concentration in the CSF is found in the low nanomolar range for both healthy controls and Alzheimer's disease patients (Mattsson et al., 2009). It has been found that $A\beta_{42}$ has a synthesis and clearance rate of 6.7% and 7.6% per hour, respectively, as is $A\beta_{40}$, with a 6.8% and 7% per hour clearance rate compared to the total amount of Aβ found in the CSF of healthy individuals (Bateman et al., 2006;

Mawuenyega et al., 2010). In Alzheimer's disease, the clearance rate, but not synthesis rate, is reduced to 5.3% per hour for $A\beta_{42}$ and 5.2% for $A\beta_{40}$ (Mawuenyega et al., 2010).

$A\beta_{42}$ concentration is reduced in the CSF of Alzheimer's disease patients compared to healthy individuals (Mattsson et al., 2009). A multicentre study showed that patients who developed Alzheimer's disease had a lower median $A\beta_{42}$ levels in the CSF (356 pg/mL, range from 96-1074 pg/mL), compared to patients with other mild cognitive impairments (579 pg/mL, ranging from 121-1420 pg/mL) and to healthy controls (675 pg/mL, ranging from 182-1897 pg/mL). Variation in the CSF biomarker levels was accounted to each centre's standard procedure of operation, but between tested groups the differences were consistent (Mattsson et al., 2009; Zetterberg and Blennow, 2013). A similar trend was observed in a small cohort study, where a reduction in the average concentration of $A\beta_{42}$ in the CSF was observed in Alzheimer's disease patients, compared to healthy age matched controls (Mawuenyega et al., 2010). Analysis by ELISA assay of CSF samples from healthy controls and Alzheimer's disease patients reported an average concentration of $A\beta_{42}$ of ~500 pg/mL for healthy controls and ~200 pg/mL for Alzheimer's disease patients. In contrast, the average $A\beta_{40}$ concentration for both groups was ~5000 pg/mL (Mawuenyega et al., 2010).

Plasma levels of Aβ are reported to be on the low nanomolar concentration in healthy controls and are thought to also reflect changes in the brain biochemistry and Aβ metabolism dysregulation (Ovod et al., 2017). $A\beta_{40}$ plasma levels were reported as ~244 pg/mL for Alzheimer disease individual, and ~276 pg/mL for healthy controls. Lower levels but a similar trend was observed for $A\beta_{42}$, where Alzheimer's patients showed ~13 pg/mL and ~19 pg/mL was seen in controls (Janelidze et al., 2016).

CSF biomarkers of Alzheimer's disease not only include monomeric $A\beta_{40}$ or $A\beta_{42}$, but also soluble oligomeric aggregates of both peptides (Holtta et al., 2013; Savage et al., 2014). Known to be metastable and polydisperse structures (Tycko, 2014), the generation of conformation-specific antibodies has enabled the characterisation of oligomers in the CSF. It has been found that Aβ oligomer levels are increased in Alzheimer's disease patients (1.52 pg/mL) compared to aged matched controls (0.52 pg/mL) when assayed by ELISA (Savage et al., 2014).

1.2. Amyloid β

Having discussed Alzheimer disease progression, characterisation and diagnosis with a focus on senile plaques, this section will provide an overview of the main molecular component of senile plaques, Aβ, its assembly into fibrils and pathogenicity.

Aβ is an intrinsically disordered peptide that is the proteolytic product of APP cleavage by γ-secretase. Aβ is released into the extracellular space in the brain, where is known to aggregate and form highly condensed plaques (O'Brien and Wong, 2011). The Aβ is found as a 39 – 43 residues peptide, with an average mass of ~4.5 kDa. The 40-residue peptide, $A\beta_{40}$ (Figure 1.5), is the most abundant form, accounting for 80% of Aβ molecules in humans (Murphy and LeVine, 2010). The other major form is the 42-peptide residue $A\beta_{42}$, which is thought to be more toxic, as it forms fibrils more readily than $A\beta_{40}$. $A\beta_{42}$ is more hydrophobic and therefore more prone to aggregate, due to the presence of the last two hydrophobic residues, alanine and isoleucine (Selkoe, 1999).

Residues 1-28 in Aβ contain the hydrophilic region, where 46% of residues are charged. In contrast, residues 29-40/42 comprise the C-terminal region, comprised of hydrophobic residues (Hou et al., 2004). Monomeric Aβ has been found to have an absence of well-defined secondary or tertiary structures (Hou et al., 2004), although recent NMR studies have found $A\beta_{40}$ to be partially folded in 50 mM sodium chloride (NaCl) at pH 7.3, where a central α-helix forms between residues 12-23 (Figure 1.3). The dynamic N and C-terminal regions were found to come in contact the helix and a resemblance between this Aβ structure to islet amyloid polypeptide (IAPP) has been suggested (Vivekanandan et al., 2011). Molecular dynamics studies have determined that both $A\beta_{40}$ and $A\beta_{42}$ are formed by 5 independent folding units connected by four turns, or peptide segments in which there is reversal in the chain's direction (Yang, M. and Teplow, 2008). The probability of presenting structured region, observed as a β-strand or α-helix, increases in regions adjacent to residues 17-21. It was also found that the C-terminal region in $A\beta_{42}$ is more stable and structured compared to $A\beta_{40}$. Specifically, residues 30-36 were found to have a higher likelihood to present a β-structure in $A\beta_{42}$ than in $A\beta_{40}$, and residues 39-40 have a 5% likelihood of β-structure in $A\beta_{42}$ compared to no β-structure in $A\beta_{40}$ (Yang, M. and Teplow, 2008).

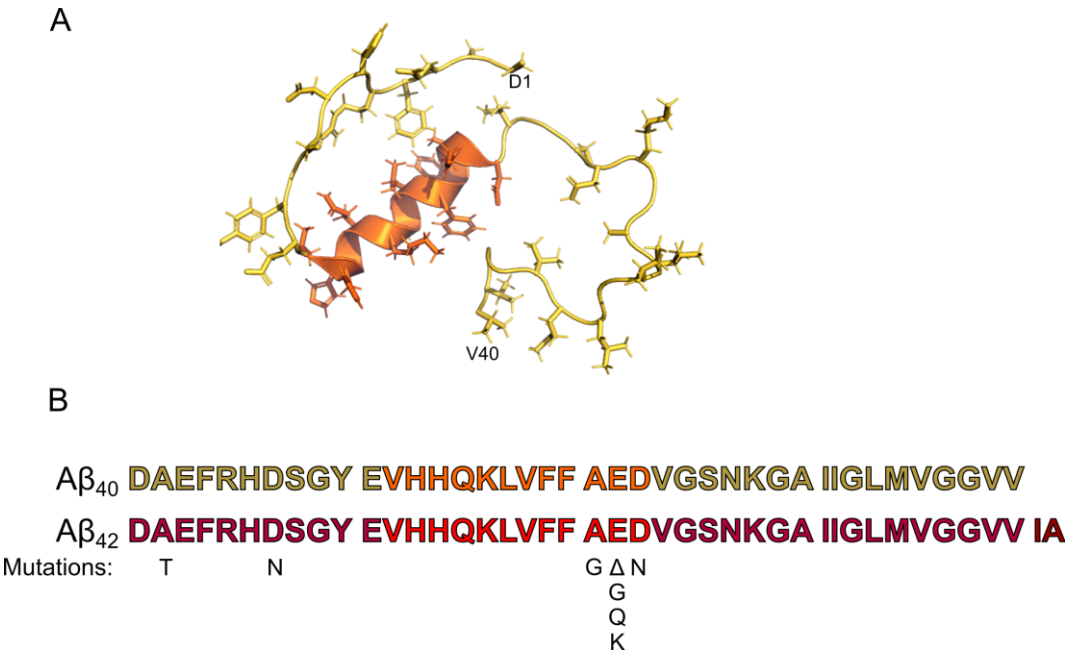

Figure 1.5. $A\beta_{40}$ monomer structure and sequence.
The NMR derived $A\beta_{40}$ monomer structure (A) shows the presence of an α-helix between residues 12-23 (bright orange), flanked by a dynamic N and C-terminal fragments (light yellow) that come in contact with it. The $A\beta_{40}$ and $A\beta_{42}$ peptide sequences (B) show that six of the most studied APP/Aβ mutants fall within the α-helix region. Denoted are the Icelandic A2T mutation, Tottori D7N mutation, Flemish A21G mutation, Osaka E22Δ mutation, Arctic E22G mutation, Dutch E22Q mutation, Italian E22K mutation and Iowa D23N mutation.

As for other proteins implicated in neurodegeneration, Aβ is subject to post-translational modifications, such as phosphorylation, truncation, ubiquination and pyroglutamation (Leissring, 2014). The majority of post-translational modifications appear to affect the N-terminal region of Aβ and are also thought that accelerate the rate of aggregation of Aβ. *In vitro* analysis of post-translationally modified $A\beta_{40}$ variants showed different fibril morphologies. In particular, phosphorylation to S8 of $A\beta_{40}$ shows a two-fold fibril structure that has accelerated seeded fibrillation kinetics as well as portrays higher toxicity compared to the wildtype $A\beta_{40}$ (Hu, Z.W. et al., 2019).

1.2.1. Amyloid structure and assembly

A major histopathological hallmark in Alzheimer's disease and of a number of other neurodegenerative diseases is the occurrence of insoluble proteinaceous aggregates, known as amyloid deposits (Chiti and Dobson, 2017).

The process of amyloid formation in human disease involves protein misfolding. This leads to the aggregation of proteins into amyloid fibrils, inherently non-crystalline insoluble material that is 5-15 nm in diameter (Tycko, 2014). Amyloid fibrils are highly ordered assemblies that characteristically contain cross-β structures. Arranged as β-sheets, the β-strands that form the fibrils run perpendicular to the fibril growth direction, and are linked together through hydrogen bonds with a 4.7–4.8 Å inter-strand distance between the β-sheets (Figure 1.6) (Adamcik and Mezzenga, 2018; Tycko, 2014).

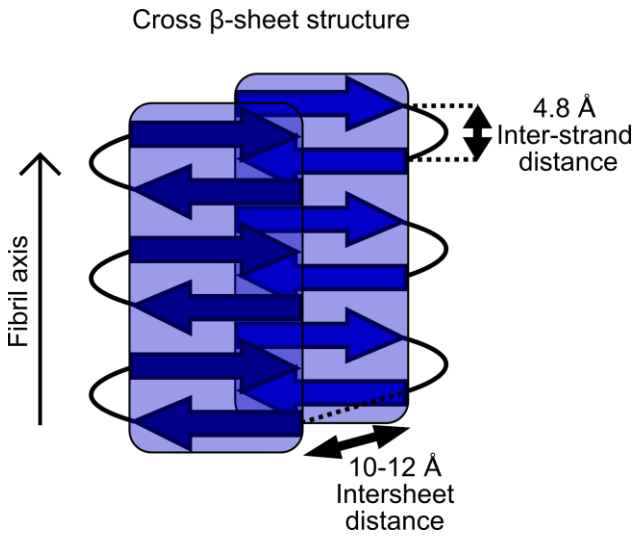

Figure 1.6. Cross β-sheet structure.
The cross β-sheet architecture is defined by β-strands that run perpendicularly to the fibril axis. The distance between the β-strands is 4.7–4.8 Å, while the separation between β-sheets is around 10–12 Å. Adapted from (Adamcik and Mezzenga, 2018).

Amyloid fibril formation is defined by a nucleation dependent polymerisation process. This polymerisation reaction begins by the formation of nuclei by monomers that are partially or completely disordered (Chiti and Dobson, 2017). Amyloid formation can then occur through elongation of monomers into fibrils, where the misfolded monomers are added to one another following the path of the fibril length, and ultimately creating larger insoluble amyloidal structures (Figure 1.7 A). Amyloid fibril formation can also occur through a secondary nucleation pathway, where a combination of both monomeric and aggregated species interact, and where the preformed aggregated structure acts as a catalyst for the formation of a secondary multimer (Linse, 2017).

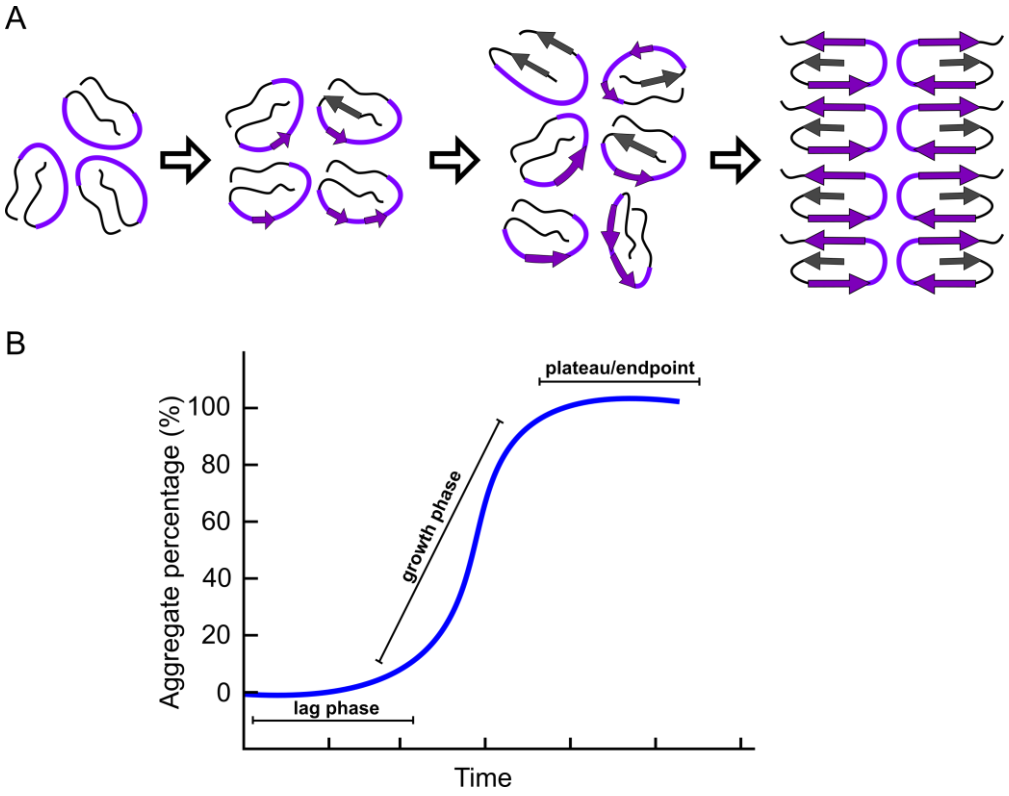

Figure 1.7. Amyloid fibril formation and kinetics.
Amyloid fibril formation and kinetics. A) Misfolded or partially folded peptides form nuclei in the early stages of amyloid fibril formation. Nuclei growth is characterised by molecular rearrangements occurring as small soluble aggregates and oligomers form. Stabilization as well as increased compactness of the molecular structure occurs as β-sheet formation and fibril formation progresses. B) Amyloid fibril formation is observed as a sigmoidal curve and is represented in terms aggregate concentration during the time elapsed since the reaction began. The kinetics are denoted by a lag phase, where nuclei and soluble aggregates form (Arosio et al., 2015), a growth or elongation phase, where fibrils are generated and a plateau at the endpoint of the reaction. Adapted from (Chiti and Dobson, 2017).

One of the first assemblies formed during the amyloid cascade are oligomers. These are aggregates formed by two or more monomers together, and generally include structures that contain up to 20 monomers, although not restricted to a specific number of monomers. Nonetheless, the structure they form is different from that observed in fibrils, as well as possessing a slower rate of growth to these (Arosio et al., 2015). Another species formed during the early stages of the amyloid cascade are protofibrils. These are soluble intermediate aggregates, that undergo structural rearrangements that can lead to the formation of a nucleus for fibril. They possess β-sheet structures that demonstrate the progressive order of segments in the peptide within the soluble aggregate (Kheterpal et al., 2006).

The kinetics of fibril formation generally shows a sigmoidal curve (Arosio et al., 2015) (Figure 1.7 B), in which misfolded monomers aggregate into nuclei, small and large oligomers and other

soluble aggregates during the lag phase, then fibril formation where turnover into amyloid forms occurs by primary or secondary nucleation during an exponential growth phase until fibril aggregate formation reaches a plateau, where a steady state of monomer at the endpoint of the reaction. Fibrillar amyloid structures can be identified by their filamentous morphology at this point. Fibril formation is usually monitored by Thioflavin T or S kinetics in *in vitro* assays, as these dyes, and others including Congo red, bind tightly to β-sheets (Chiti and Dobson, 2017).

The energy landscape of proteins (Figure 1.8), theoretically defined and visualized as a funnel, sees the unfolded monomer at the top of it, where entropy and free energy are high, whereas the rest of the proteins conformational states (the oligomers, soluble aggregates and fibrillar assemblies) get kinetically trapped in other individual peaks as they travel down-hill the energy landscape. It is generally agreed that amyloid fibrils are the most stable thermodynamic state in the energy landscape (Adamcik and Mezzenga, 2018; Tycko, 2014).

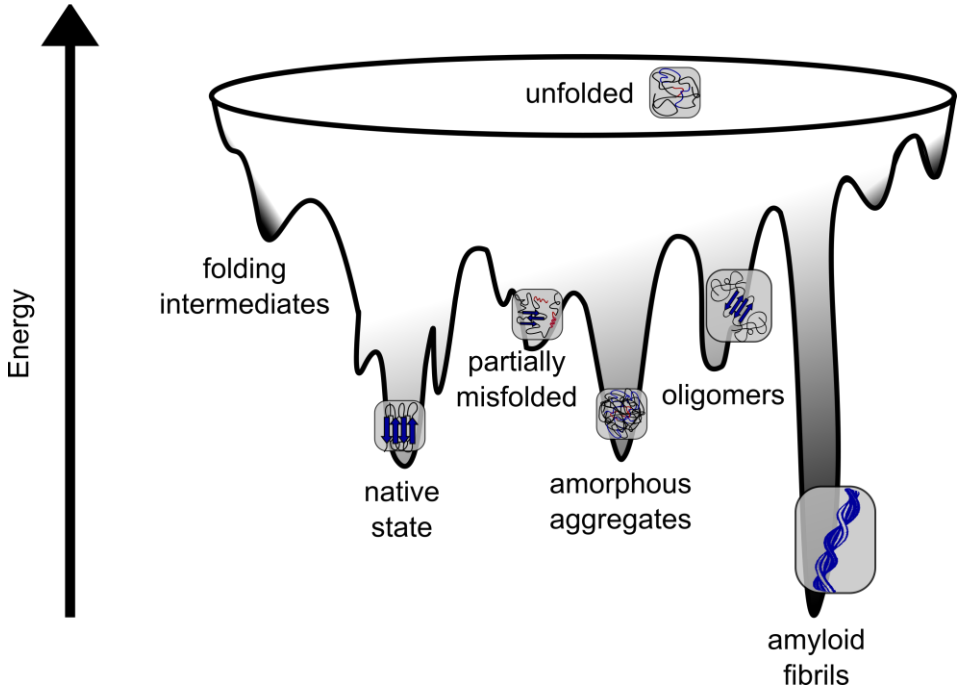

Figure 1.8. The energy landscape of protein folding and aggregation.
The different protein conformers fall into different wells of the energy landscape. Amyloid fibril. Adapted from (Adamcik and Mezzenga, 2018).

1.2.2. Aβ fibril structure and polymorphism

Fibrils are the endpoint of protein aggregation (Tycko, 2014). In disease, they represent the failure of native protein "on-pathway" folding and are the result of exposure of hydrophobic residues in the misfolded or partially folded protein and interactions between them. In particular, non-specific interactions between exposed residues on the misfolded protein lead to the previously described nuclei and initiate the amyloid cascade (Adamcik and Mezzenga, 2018). Inter-monomer and inter-fibril interactions vary between proteins or peptides, but can also differ within a protein, a consequence of the diversity of interactions taking place between misfolded proteins (Iadanza et al., 2018). All these interactions consequently produce amyloid fibril polymorphs, or structural varieties of fibrils of the same peptide sequence. Amyloid polymorphism is observed in neurodegenerative diseases. As mentioned previously, point mutations can generate peptides that aggregate faster, as well as have a biological effect, such as a more severe cognitive impairment and toxicity to cells (Iadanza et al., 2018).

A wide range of *in vitro* studies have shown Aβ fibril polymorphism. Aβ fibrils, generated from synthetic or recombinant peptide *in vitro*, have revealed that variation in growth conditions produce significant, reproducible alterations to the fibrillar molecular structures. In the case of $A\beta_{40}$ (Table 1.1), growing fibrils in quiescent conditions produces a 3-fold molecular structure (Paravastu et al., 2008), whereas agitative conditions are known to generate 2-fold fibrillar structures. Differences have also been observed in fibrils of phosphorylated S8 $A\beta_{40}$, that presents a unique mass-per-length, a measurement that reveals the amount of peptides within a cross-β-repeat, that established it as a two-fold structure with distinct toxicity than the latter two $A\beta_{40}$ fibril polymorphs (Figure 1.9 A) (Petkova et al., 2005).

It has also been noted that small changes in the peptide sequence (Table 1.3), such as a deletion or point mutation, as is the case for $A\beta_{40}$ E22Δ or $A\beta_{40}$ D23N, render different fibril structures from that of the WT Aβ (Figure 1.9 B). In the case of $A\beta_{40}$ D23N, in the same sample, the structure of two polymorphs could be determined in the same samples, one showing parallel in register β-sheets (D23N-p), and another with antiparallel β-sheets (D23N-a) that appeared to be a transient conformation (Figure 1.9 B) (Qiang et al., 2012; Tycko, 2014).

The difference in structures due to growth conditions is also applicable for $A\beta_{42}$ fibrils (Table 1.2), as it has been observed that acidic conditions (Gremer et al., 2017) produce significantly different fibrils that display the C-terminal of the monomer deeply buried within the core of the fibril, compared to basic or neutral grown fibrils where this is not observed (Figure 1.9 C).

Fibril structures have also been determined for $A\beta_{40}$ fibrils derived from *ex vivo* Alzheimer's disease and Lewy body disease brain (Table 1.4). In their study, Lu et al. (2013) were able to

determine a 3-fold molecular structure of $A\beta_{40}$ fibrils that had been generated after seeding with brain extracts from Lewy body disease individuals (Figure 1.9 D). In contrast, $A\beta_{40}$ fibrils extracted from meningeal tissue vascular amyloid deposits from Alzheimer's disease cases showed a distinctive two-fold structure, with a particular outward double C-shaped (Kollmer et al., 2019). These fibrils differ from *in vitro* generated fibrils in that both the C-terminal and N-terminal regions present and outward bend that leaves them solvent-exposed. In opposition, *in vitro* generated fibrils tend to have a protected C-terminal region located within the fibril core and an N-terminal region that is solvent-exposed.

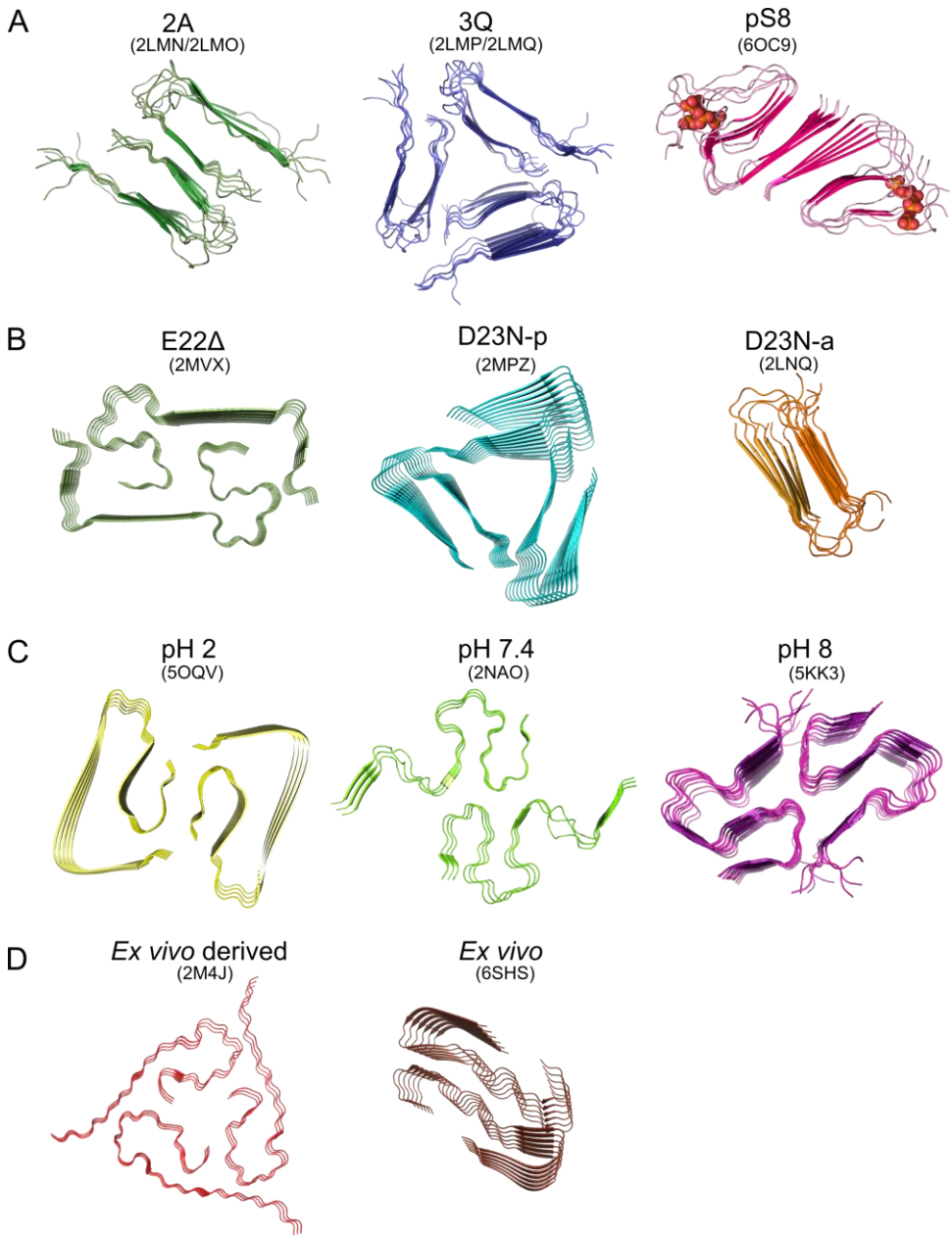

Figure 1.9. Molecular structures of Aβ fibril polymorphs.
Schematic of fibril structures in vitro generated $Aβ_{40}$ fibrils (A), mutant $Aβ_{40}$ fibrils (B), $Aβ_{42}$ fibrils (C) and ex vivo/ex vivo derived $Aβ_{40}$ (D). Two-fold or 3-fold arrangements were observed for the 2A, 3Q and phosphorylated S8 (pS8) fibrils WT $Aβ_{40}$ fibrils. Mutant $Aβ_{40}$ E22Δ, parallel (D23N-p) and antiparallel (D23N-a) D23N presented 1-fold to 3-fold molecular structures and were distinct from the structures observed in the WT fibrils. The structures of ex vivo derived fibrils of Aβ, generated by seeding monomeric $Aβ_{40}$ with Lewy body disease brain (ex vivo derived) showed a particular 3-fold structure. In contrast, fibrils extracted directly from vascular amyloid deposits from Alzheimer's disease brain (ex vivo) showed an outward double C-shaped morphology. PDBs are stated in brackets.

Table 1.1. Molecular structure characteristics of in vitro generated $A\beta_{40}$ fibril polymorphs

	$A\beta_{40}$		phospho-Ser 8 $A\beta_{40}$
	2A (Petkova et al., 2005)	**3Q (Paravastu et al., 2008)**	**pS8 (Hu, Z.W. et al., 2019)**
PDB	2LMN/2LMO	2LMP/2LMQ	6OC9
Morphology	2-fold, striated ribbons	3-fold, twisted fibrils	two-fold striated ribbon morphology
Conditions they were formed	210 μM peptide in 10 mM sodium phosphate, 0.01% (v/v) NaN3 pH 7.5	210 μM peptide in 10 mM sodium phosphate buffer, pH 7.4. Quiescently grown with intermittent sonication (once per hour for 9 days)	50 μM peptide in 20 mM sodium phosphate pH 7.4, 0.01% NaN3 at 37°C. Seeded quiescently to fresh monomer for 8 generations
Peptide type	synthetic	synthetic	synthetic
Type of structure	experiment based structural model	experiment based structural model	experiment based structural model
Method of structure determination	13C and 15N ssNMR, TEM, STEM	13C and 15N ssNMR, TEM, STEM	13C ssNMR, TEM, ThT kinetics
Residues assigned in structure	residues 10 - 40	residues 10 - 40	residues 1 - 40
N-terminal order	unstructured N-terminal (residues 1-10)	unstructured N-terminal (residues 1-10)	dynamic N-terminal (residues 1-7)
twist period (nm)	no resolvable twist	120 +/- 20 between minima and max period	-
width (nm)	5.5 +/- 0.5	At max period: 8.0 +/- 1.0	8.5
Mass-per length (kDa/nm)	Max at 21.4	Max at 26 ± 2	Max at 19.5
β-strand location	residues 10-22 and residues 30-36	residues 11-22 and 30-39	residues 9-12, 17-22 and 31-39
Type of beta sheet structure	in register parallel	in register parallel	in register parallel from residue 9-39
Fibril core	residues 28-40	residues 29-40	residues 31-39
Toxicity	Cortex neurons from rats incubated with 10-75μM sonicated fibrils for 48 h. Observed >50% neuronal death by cell count compared to vehicle control	Cortex neurons from rats incubated with 10-75μM sonicated fibrils for 48 h. Observed >80% neuronal death by cell count compared to vehicle control	BV2 cells incubated with 0.01-5μM fibrils and compared to 2A fibrils. Analysis after a 24 h incubation showed that MTT reduction was inhibited (~20%-60% decrease) in cells incubated with pS8 $A\beta_{40}$ from a 0.01 -5μM concentration.

Table 1.2. Molecular structures characteristics of in vitro generated mutant $A\beta_{40}$ fibril polymorphs

	$A\beta_{40}$ E22Δ	**$A\beta_{40}$ D23N**	**$A\beta_{40}$ D23N**
	Osaka mutation (Schutz et al., 2015)	**Iowa mutation – parallel (Sgourakis et al., 2015)**	**Iowa mutation – antiparallel (Qiang et al., 2012)**
PDB	2MVX	2MPZ	2LNQ
Morphology	2-fold, cinnamon roll-like interlaced protofilaments	3- fold, unbundled rough and irregular twisting	1- fold
Conditions they were formed	60 μM peptide in10 mM sodium phosphate pH 7.4, 100 mM NaCl. Grown at 37°C, magnetic stirring at 700 rpm for 80 min	100 μM peptide in 10 mM sodium phosphate pH 7.4, 0.01% NaN3. Grown quiescently at 4°C for 1 week, then 2 min sonication and seeded into fresh monomer (8 generations). 432 000 x g ultracentrifugation at endpoint	100 μM peptide in 10 mM sodium phosphate pH 7.4, 0.01% NaN3. Grown quiescently at 6°C for 1 week, then 10 min sonication at 10% cycle duty and seeding into fresh monomer by 48 h periods at 6°C for 8 generations
Peptide type	recombinant	synthetic	synthetic
Type of structure	experiment based structural model	experiment based structural model	experiment based structural model
Method of structure determination	13C and 15N ssNMR, TEM, STEM	13C and 15N ssNMR, TEM, Rosetta model building	13C ssNMR, TEM
Residues assigned in structure	resides 1 - 40	residues 15- 40	residues 15- 40
N-terminal order	-	unstructured N-terminal	unstructured N-terminal and residues 37-40
twist period (nm)	-	-	-
width (nm)	-	-	-
Mass-per length (kDa/nm)	Max at 21	Max at ~27	Max at 9
β-strand location	residues 5-7 and 11-19	residues 17-21 and 31-36	residues 16-21 and 31-36
Type of beta sheet structure	in register parallel	in register parallel	in register antiparallel
Fibril core		residues 29-40	residues 15-40
Toxicity	-	Primary hippocampal neurons from rat incubated with 1-30 μM sonicated fibrils. Observed >70% cell death (analysed by neuronal count) after 48 h incubation at 30μM compared to control	Primary hippocampal neurons from rat incubated with 1-30μM sonicated fibrils. Reported >60% cell death (by neuronal count) after 48 h incubation at 30μM compared to control

Table 1.3. Molecular structures characteristics of $A\beta_{40}$ fibril polymorphs generated from ex vivo material

	$A\beta_{42}$		
	pH 2 (Gremer, et al. 2017)	**pH 8 (Colvin, et al. 2016)**	**pH 7.4 (Wälti, et al. 2016)**
PDB	5OQV	5KK3	2NAO
Morphology	LS shaped, staggered protofilaments	Two S-shaped cross-β-sheet entitiy with hydrophobic residues hidden in fibril core	Double-horseshoe-like cross-β-sheet entity
Conditions they were formed	120.5 μM peptide in 30% (v/v) acetonitrile, 0.1% (v/v) TFA in water pH 2	50 μM peptide in 20 mM sodium phosphate, 0.2 mM EDTA, 0.02% NaN3, pH 8.0	30 μM peptide in 100 mM sodium phosphate pH 7.4, 100 mM NaCl, 100 μM ZnCl, grown at 37°C with 350 rpm shaking
Peptide type	recombinant	recombinant (Met at residue 1)	recombinant
Type of structure	structure	experiment based structural model	experiment based structural model
Method of structure determination	cryoEM, ssNMR, x-ray diffraction	13C and 15N ssNMR	13C and 15N ssNMR, TEM, STEM
Residues assigned in structure	residues 1 - 42	residues 11 - 42	residues 1-42
N-terminal order	-	unstructured N-terminal (1-10)	part structured and dynamic N-terminal (residues 1-14)
twist period (nm)	-	-	-
width (nm)	7	-	-
Mass-per lenght (kDa/nm)	-	Max at ~48, second at 24.7	Max at 19
β-strand location	residues 1-9 and 11-21	residues 16-20, 26-32, 35-36 and 39-41	residues 2-6, 15-18,26.28,30-32 and 39-42
Type of beta sheet structure	in register parallel	in register parallel	in register parallel
Fibril core	residues 36-42		residues 15-42, and and intramolecular (peptide) core at residues 19-34
Toxicity	PC12 cells. 24 h incubation. Sonicated fibrils. Tested 0 -3 μM. Decrease in >50% MTT reduction	SH-SY5Y cells, 24 h incubation. Tested 10 nM. Decrease of 20-40% MTS reduction.	-

Table 1.4. Molecular structures characteristics of $A\beta_{40}$ fibril polymorphs generated from ex vivo material

	$A\beta_{40}$		
	***Ex vivo* derived patient 1 (Lu et al., 2013)**	***Ex vivo* derived patient 2 (Lu et al., 2013)**	***Ex vivo* polymorph 1 (Kollmer et al., 2019)**
PDB	2M4J	-	6SHS
Morphology	3-fold molecular structure comprised of three cross-β units	3-fold molecular structure	C-shaped 2-fold molecular structure, with a right-hand fibril twist
Conditions they were formed	0.8 mg of synthetic 15N,13C-labeled $A\beta_{40}$ seeded with fibrils from temporal/parietal lobe tissue and occipital lobe tissue from LBD patient. Buffer: 10 mM phosphate buffer, pH 7.4	0.8 mg of synthetic 15N,13C-labeled $A\beta_{40}$ seeded with fibrils from temporal/parietal lobe tissue and occipital lobe tissue from AD patient. Buffer: 10 mM phosphate buffer, pH 7.4	Fibril extraction from vascular amyloid deposits (meningeal tissue) from AD cases. Centrifugation (12 000 xg) in Tris calcium buffer pH 8 followed by collagenase digestion (5mg/mL) overnight at 37°C. Sample was then subjected to a wash in ethylendiaminetetraacetic acid pH 8 buffer (4°C) and centrifuged to then be subjected to a water wash (4°C) and centrifugation. Water wash repeated 9 times
Peptide type	synthetic peptide seeded with ex vivo material	synthetic peptide seeded with ex vivo material	ex vivo material
Type of structure	experiment based structural model	experiment based structural model	structure
Method of structure determination	13C and 15N ssNMR, TEM, STEM, ThT Kinetics	13C and 15N ssNMR, TEM, STEM, ThT Kinetics	cryoEM
Residues assigned in structure	residues 1 - 40	-	residues 1-40
N-terminal order	-	-	-
twist period (nm)	no resolvable twist	85 ± 10 nm between minima and maxima periods	-
width (nm)	7 ± 1 nm	At max period: 11 At min period: 5	7.4 ± 0.4 nm
Mass-per length (kDa/nm)	28 ± 2 kDa/nm	29.1 ± 1.2 kDa/nm	-
β-strand location	residues 12-13, 18-19 and 35-36	-	residues 2-8, 10-13, 15-19 and 32-34
Type of beta sheet structure	in register parallel	in register parallel	in register parallel
Fibril core	residues 28-40	-	residues 13-34
Toxicity	-	-	-

1.2.3. Aβ toxicity

Aβ oligomers are found extracellularly and intracellularly and have been detected in cortex brain sections of both Alzheimer's disease cases and age matched controls. However, oligomers ranging from 45-55 kDa were more frequently detected in Alzheimer's cases, indicating that different oligomer conformations are observed in disease (Bao et al., 2012). It appears that size, hydrophobicity, and conformation of each oligomeric species determines its toxicity (Kayed and Lasagna-Reeves, 2013). Mechanism of toxicity seems to be related to disruption of cell membranes by oligomer incorporation, and NMDAR-dependent long-term potentiation disruption (Kayed and Lasagna-Reeves, 2013).

Cellular toxicity has also been observed after incubation with the distinct Aβ fibril polymorphs. Inhibition of MTT or MTS has been reported for cells incubated with pH 2 or pH 8 $A\beta_{42}$ fibrils (Colvin et al., 2015; Gremer et al., 2017). Direct comparison of the $A\beta_{40}$ fibril polymorphs revealed a decreased neuronal survival after incubation with >10 μM fibrils 3Q compared to 2A (Paravastu et al., 2008). A similar trend was observed for mutant $A\beta_{40}$, where the parallel D23N polymorph bearing parallel β-sheets had a ~10% decrease in neuronal survival compared to the antiparallel D23N $A\beta_{40}$ fibrils.

In vivo, Aβ fibril polymorphism is associated with distinctive clinical presentations of Alzheimer's disease (Qiang et al., 2017). In their study, Qiang et al (2017) amplified $A\beta_{40}$ fibril samples from patients suffering from rapidly progressive Alzheimer's disease (r-AD), posterior cortical atrophy Alzheimer's disease (PCA-AD) and typical progression Alzheimer's disease (t-AD). ssNMR analysis of the brain derived fibrils showed that, although fibrillar variation was inherent within all the samples, a single structure was most prominent in t-AD and PCA-AD, whereas r-AD presented a more pronounced level of $A\beta_{40}$ fibril polymorphism. They attributed this increase in fibril polymorphism to r-AD's disease phenotype, where plaque burden and neurodegeneration occurs earlier in life and increases at a faster pace through ought disease progression, compared to t-AD. In addition, people diagnosed with r-AD have a disease survival rate of less than 3 years after diagnosis (Schmidt et al., 2011; Drummond et al., 2017; Qiang et al., 2017). It is of note that the presence of one of the neurotoxic $A\beta_{40}$ fibril polymorphs present in r-AD is unobserved in the other types of Alzheimer's disease (Qiang et al., 2017).

The variety of these Aβ fibril structures as well as the diverse biological impact these have, observed as cellular toxicity, highlight the fact the seemingly small variations in the physical conditions generate distinct fibril structures that go on to determine disease progression. In the next section a discussion of another neurodegenerative disease where Aβ deposition is observed,

as well as other proteins that interact with Aβ in disease, are discussed in the context of Alzheimer's disease.

1.3. Parkinson's disease and other synucleinopathies

Parkinson's disease, Parkinson's disease with dementia, multiple system atrophy (MSA) and dementia with Lewy Bodies are synucleinopathies. They are defined by the presence of α-synuclein aggregates in the brain. These diseases affect around 5 million people worldwide (Lashuel et al., 2013), with Parkinson's disease being the second most prevalent neurodegenerative disease and only surpassed by Alzheimer's disease.

Parkinson's disease is characterized by neuroaxonal dystrophy and motor impairments like bradykinesia, tremor and rigidity. Clinical symptoms are associated to the loss of dopamine in the nigrostriatal system. Pathology, in the form of α-synuclein aggregation and neuronal loss is mostly observed in the brain, but it can also be distributed through the entire nervous system, including the peripheral and enteric nervous systems (Braak and Del Tredici, 2008).

Lewy bodies are the main intraneuronal lesion in synucleinopathies. They are round inclusions mainly composed predominantly of insoluble aggregated α-synuclein and are commonly observed in the neocortex and brain stem regions in Parkinson's disease. Lewy body accumulation eventually leads to neuronal loss, specifically, dopaminergic neurons in the substantia nigra pars compacta, a movement centre in the brain, hence producing the motor deficiencies observed (Kotzbauer et al., 2001). Like Aβ and tau in Alzheimer's disease, α-synuclein aggregates display a progressive "invasion-like" deposition pattern related to disease progression. In the brain, Lewy bodies are first observed in the dorsal IX/X motor nucleus in the vagus nerve, expanding into the anterior olfactory nucleus and then through the brain stem towards the temporal mesocortex and neocortex (Braak et al., 2003).

1.3.1. α-synuclein

Human α-synuclein protein is encoded by the *SNCA* gene, located on the long arm of chromosome at position 21 (4q21). Mutations and multiplications of the gene are directly related to familial forms of synucleopathies, such as dominant familial parkinsonism, in which the mutations A53T, A30P and E46K have been identified (Lashuel et al., 2013).

The full-length form of α-synuclein (Figure 1.10) is 140 amino acids in length (14.5 kDa), while its common spliced forms have 126 and 112 amino acids, as they lack exon 3 and exon 5 respectively. Its amphipathic N-terminal region, residues 1-60, contains 6 KTKEGV imperfect repeats (Dettmer et al., 2015). The N-terminal region is implicated in membrane binding. Residues 35 to 90 comprise the Non-Amyloid β Component (NAC) domain, a fragment commonly found in senile plaques, and thought to be crucial in the aggregation of α-synuclein. The C-terminal region appears non-structured and is highly dynamic and is thought to be responsible for chaperone activity and contains the sites for the phosphorylation of the protein.

The molecular structure of synuclein bound to an sodium dodecyl sulphate micelle has been determined by solution NMR (Ulmer et al., 2005). It was found the N-terminal region, responsible for lipid binding, is formed by 2 curved antiparallel α-helices that are linked together through residues 38-44, whereas its C-terminal region appeared highly dynamic.

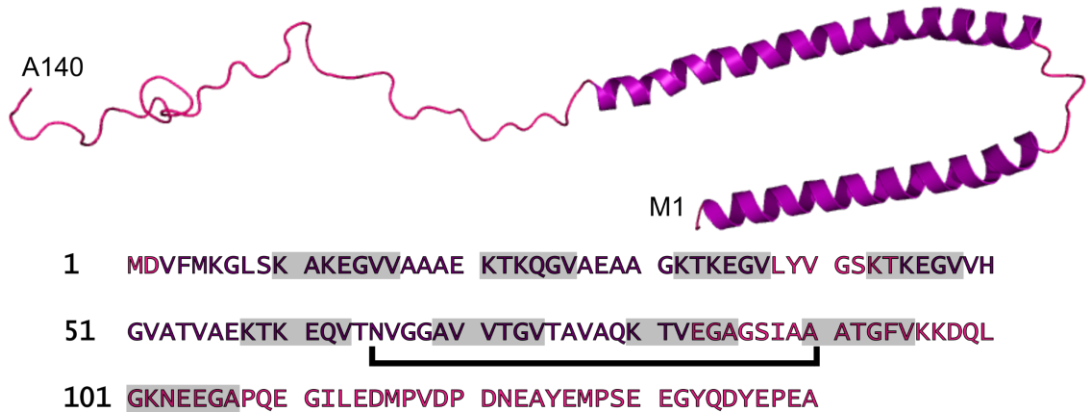

Figure 1.10. Molecular structure of α-synuclein bound to a micelle and protein sequence. *Structure of the micelle-bound form α-synuclein (PDB: 1XQ8), determined by solution NMR, where it arranges into two antiparallel α-helices (in dark purple) that are separated by a 7-residue long linker region that allows it to curve. In contrast, the C-terminal region is highly dynamic. The peptide sequence shows that the helices are restricted to the N-terminal, as the first 6 KTKVEEGV imperfect repeats (highlighted in grey). The NAC region is denoted in the peptide sequence as a black bar between residues 35 and 90, is commonly associated to senile plaques.*

The physiological role for α-synuclein is not fully understood, but it is thought to be involved in the maintenance of a supply of synaptic vesicles throughout mature presynaptic vesicles, as this protein is only detected after synaptic development (Kim et al., 2014). In native aqueous conditions, α-synuclein monomers adopt an unfolded random coiled form which is changed upon binding to phospholipids (into helices) (Lashuel et al., 2013; Beyer, 2006). As with Aβ, α-synuclein is subject to post-translational modifications, more commonly nitration (to residues

Y39, Y125,Y133 and Y136) arising from oxidative stress, lipidation, acylation, ubiquination, and phosphorylation, with the latter two thought to be involved in protein deposition (Kim et al., 2014). Phosphorylation and ubiquination are the main post-translational modifications of the protein in pathological conditions and the presence of these modifications is used to detect α-synuclein in Lewy bodies. In particular, phosphorylation at serine 129 is usually present in α-synuclein in Lewy bodies. Indeed, it has been estimated that 90% of α-synuclein found in dementia with Lewy bodies brains is phosphorylated, with serine 129 one of the most important (Brandel et al., 2015; Beyer, 2006).

1.3.2. α-synuclein fibril structure and polymorphism

As with Aβ, α-synuclein has the capacity to form amyloid fibrils via nucleation dependent assembly. This occurs when nuclei, composed of partially misfolded protein, rich in β-sheets initiate and produce a change in conformation of the non-aggregated form of the protein. Mutations related to early onset Parkinson's disease, like the A53T, have been found to accelerate aggregation compared to WT α-synuclein (Conway et al., 2000; Flagmeier et al., 2016).

A wide variety of fibrillar structures have been described for *in vitro* generated α-synuclein fibrils (Guerrero-Ferreira et al., 2018; Zhao et al., 2020a; Zhao et al., 2020b; Sun et al., 2020), as well as derived from *ex-vivo* synucleopathies (Figure 1.11) (Strohaker et al., 2019; Schweighauser et al., 2020) (Schweighauser et al., 2020). These polymorphs vary in having a different number of protofilament folds, as well as variation in protofilament packing and assembly.

In addition, differences in polymorph structure as well as degree of polymorphism, seems to be correlated with disease type, as different polymorphs have been described for MSA and Parkinson's disease, and a higher degree of polymorphism is observed in the latter (Strohaker et al., 2019).

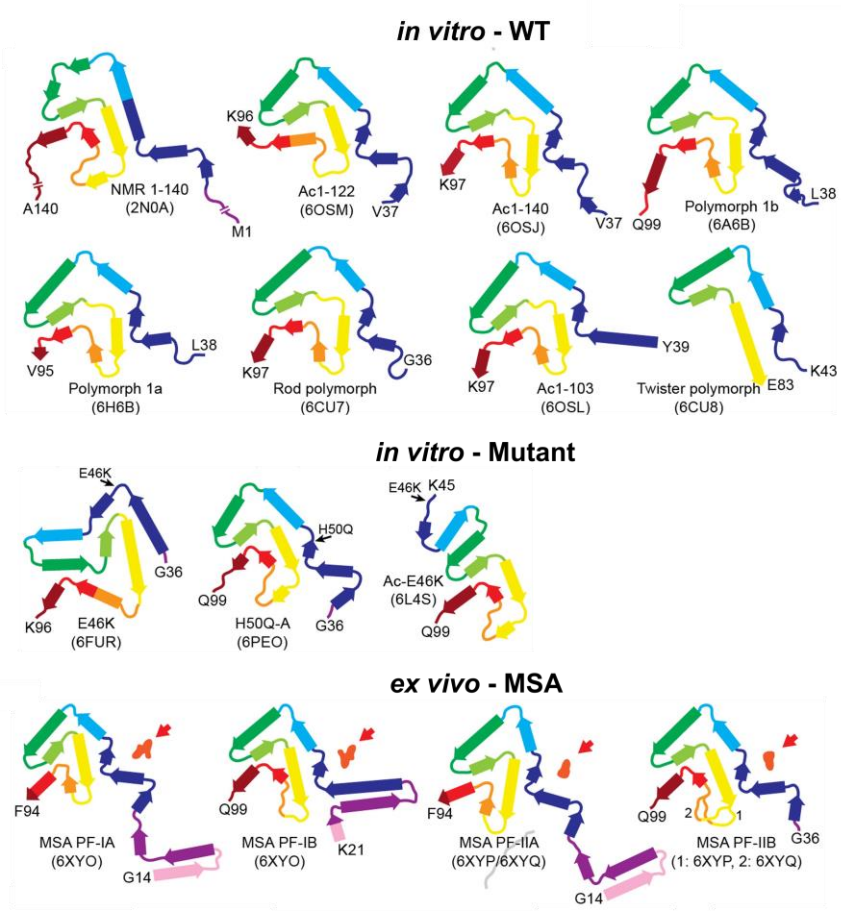

Figure 1.11. Protofilaments of α-synuclein fibril polymorphs.
Various molecular fibril structures have been determined for in vitro generated WT α-synuclein, mutant α-synuclein and ex vivo derived α-synuclein from MSA individuals. Adapted from (Schweighauser et al., 2020).

1.3.3. α-synuclein toxicity

Toxicity of α-synuclein has been studied in a variety of cell models and animal models. Mice models overexpressing mutant and WT α-synuclein develop intracytoplasmic α-synuclein aggregates (Masliah et al., 2001; Giasson et al., 2002; Graham and Sidhu, 2010; Chen, L. et al., 2015). A decreased locomotor activity is observed in mice expressing α-synuclein mutations present in early onset Parkinson's disease (Giasson et al., 2002; Graham and Sidhu, 2010). Mitophagy impairment is also a common feature in these α-synuclein overexpressing mice (Chen, L. et al., 2015). Exogenously added WT α-synuclein fibrils to neuroblastoma cell cultures are reminiscent to prion-like seeding occurs in the formation of Lewy bodies (Pieri et al., 2016).

α-synuclein oligomeric populations have been found to impose different degrees of toxicities in cells (Cremades et al., 2012; Chen, S.W. et al., 2015). Characterisation of two populations of α-synuclein oligomers revealed distinct patterns of cytoplasmic reactive oxygen species in rat

midbrain neuronal cultures. In particular, production of reactive oxygen species, a feature observed in apoptotic cells, was enhanced after incubation with a population of α-synuclein oligomers (160 – 560 kDa) that appear to be more structured, more compact, and contain β-sheets in addition to less solvent-exposed hydrophobic side chains (Cremades et al., 2012).

The distinct defined α-synuclein fibril polymorphs have also been found to possess different toxicities. In their study, Zhao et al (2020) found that 100 nM of WT α-synuclein preformed fibrils induced endogenous α-synuclein aggregation in rat primary cortical neurons after 14 days of incubation concomitant to a 7.5% increase in LDH release, compared to buffer treated neurons. Incubation with 100 nm of phosphoY39 α-synuclein preformed fibrils produced a higher number of α-synuclein aggregates and an increased release of LDH (10%) compared to WT α-synuclein fibrils (Zhao et al., 2020b). Similarly, Tuttle et al (2012) reported a 20% increase in LDH release in neurons, compared to buffer, after an 18-day incubation with WT α-synuclein fibrils.

1.3.4. α-synuclein pathology in Alzheimer's disease

Common characteristics between Alzheimer's disease and synucleinopathies can be delineated. Similarities in histopathological hallmarks and cellular dysfunction have long been observed in these diseases. Furthermore, ~60% of Alzheimer's disease cases (both sporadic and familial) present Lewy body pathology simultaneously to senile plaques and tau protein tangles (Kotzbauer et al., 2001; Hamilton, 2000). In addition, Lewy bodies have also been observed in Down syndrome patients in conjunction to Aβ senile plaques (Kotzbauer et al., 2001; Selkoe, 1999) . It has also been reported that individuals diagnosed with Dementia with Lewy bodies present plaques and neurofibrillary tangles at a ~39-80% frequency, though no correlation has yet been found between these lesions (Kotzbauer et al., 2001). Proteomic analysis of subtypes of Alzheimer's disease patients has also revealed the specific presence of proteins and other Aβ plaque components. Drummond et al. (2017) showed that hippocampal sections taken from rapidly progressive AD patients (r-AD) presented a significantly different proteome from those diagnosed with sporadic AD (s-AD). In particular, the presence of higher levels of α-synuclein were noted in r-AD samples, when compared to s-AD samples, noting a relationship between pathologies but also that differential prognosis occurs by the presence of aggregated α-synuclein.

A multicentre study by Irwin et al. (2017) found that increasing levels of neurofibrillary tangles and senile plaques were associated with a higher α-synuclein pathology score and a shorter interval from motor symptoms to dementia in Lewy body spectrum disorder patients. Neuropathological assessment of post-mortem Alzheimer's disease brain sections has revealed that the mean age at death is significantly different between those presenting Lewy body

pathologies and those who don't present Lewy body deposition. In addition, sleep behaviour patterns, as well as delusions and hallucinations have been reported to be more severe in AD patients who present Lewy body pathology (Irwin et al., 2017).

In vitro cell and mice model reports have described the relationship of Aβ and α-synuclein. An MTT reduction decrease, and hence decrease in cell viability, was reported in neuroblastoma cells overexpressing α-synuclein upon exposure to fibrils and protofibrils of $A\beta_{42}$ (10 μM monomer equivalent), compared to the untreated mutant cells (Hunya et al., 2008). Co-overexpression of α-synuclein and Aβ in a bigenic mouse model has also revealed the exacerbated presence of Aβ aggregates as well as increased neurodegeneration, compared to the single mutants (Masliah et al., 2001). The Dementia and Lewy bodies and Alzheimer's disease transgenic mice, a modified 3X transgenic Alzheimer's disease mice (that expresses APP gene bearing the Swedish mutation and the human tau gene bearing the P301L mutation) that was modified to also express mutant human α-synuclein (A53T), presents accelerated cognitive decline in comparison to the 3X transgenic Alzheimer's disease mice. This suggests that α-synuclein, Aβ and tau proteins might interact, promoting the acceleration and/or enhancement of degenerative pathologies and cognitive decline (Kim et al., 2014; Clinton et al., 2010).

In vitro biochemical experiments have also reported the synergism between α-synuclein and Aβ.

The NAC region often observed in Aβ plaques, was found to be heterologously seeded, or cross-seeded, by fibrils of $A\beta_{40}$ by turbidity analysis at pH 7.4 in the presence of 100 mM NaCl and 10% DMSO. The aggregation kinetics of the NAC region was considerably altered by the presence of 25% (v/v) $A\beta_{40}$ fibrils, as a reduction in the lag time was observed (Han et al., 1995). Later reports showed that fibril formation occurs at a faster pace in the presence preformed fibrils of synthetic α-synuclein, $A\beta_{40}$ and $A\beta_{42}$ as well as with the presence of oligomers of the same molecules, showing the cross seeding effect between α-synuclein, $A\beta_{40}$ and $A\beta_{42}$ (Ono et al., 2012).

1.4. Project aims

Given the evidence stated here, a relationship between Aβ and α-synuclein pathology is observed in Alzheimer's disease. The heterogeneity of the disease also points that both severity in neurodegeneration, as well as cognitive decline, can be influenced by the occurrence of fibril polymorphism.

Thus, the aim of this thesis project is to study α-synuclein's aggregation by Aβ fibril structures.

Firstly, the production of defined fibrillar Aβ structures will be performed. This will involve the production of $A\beta_{40}$ and $A\beta_{42}$ peptides, followed by the production of each Aβ fibril polymorph in their specific condition. Characterisation of the fibril polymorphs will be done through spectroscopy methods.

The second focus of this thesis is to characterise the interaction between Aβ fibrils and α-synuclein by in vitro biochemical analysis. Specifically, the aggregation of α-synuclein is studied in the presence of the well-defined fibrillar structures of Aβ, in a variety of physical conditions. The mechanism and kinetics of α-synuclein aggregation will also be studied.

Lastly, the third focus is to understand the involvement of the distinct Aβ fibril polymorphs in the generation of α-synuclein aggregation in cells. Lewy body-like formation will be studied in a neuroblastoma cell model that overexpresses α-synuclein. The involvement of acidic organelles will be studied.

2. Materials and Methods

2.1. $A\beta_{40}$ and $A\beta_{42}$ expression and purification

In order to produce amyloid fibril polymorphs of $A\beta_{40}$ and $A\beta_{42}$, used in the analysis of the interaction with α-synuclein, the Aβ peptide was expressed and purified

2.1.1. Expression of $A\beta_{40}$ and $A\beta_{42}$ in *Escherichia coli*

The transformation of Escherichia coli (E.coli) BL21 DE3 was done with the use of the pET-Sac-Aβ(Met1-40) or the pET-Sac-Aβ(Met1-42) plasmids (provided by Dr Sara Linse), encompassing the Methionine-Aβ residues 1-40 ($A\beta_{40}$) and Methionine-Aβ residues 1-42 ($A\beta_{42}$) respectively. The ATG (Methionine) codon is inserted in the beginning of the sequence as a facilitator of expression of the protein in E. coli. For the transformation, 50 µl of cells were incubated for 30 minutes on ice with 1.5µl of the vector. Cells were then heat shocked at 42°C for 45 seconds and left 10 minutes to recover. After this 450µl of lysogeny broth (LB) media was added and left incubating for 30 minutes at 37°C and shaking. These cells were then plated in a LB-agar media plate containing carbenicillin at a final concentration of 100µg/mL and incubated at 37°C overnight.

A single colony from each overnight plate were inoculated into autoclaved LB 100 mL cultures containing 100 µg/mL carbenicillin and left incubating at 37°C with shaking at 200 rpm until they reached OD600 ≥1. Subsequently 500 µl of each culture was inoculated into 500 mL LB media containing 100 µg/mL carbenicillin and were left growing until reaching OD600 ≥ 0.5. Induction was then performed by adding 0.5 mL of isopropyl β-D-1-thiogalactopyranoside (IPTG) at a final concentration of 1 mM. Cells were allowed to grow an additional 4 hours past induction or until reaching cell plateau. A total of 5.5 L of induced culture was centrifuged for 15 minutes at 6000 rpm at 4°C (Beckman Coulter JLA 8.1000 Rotor). Cell pellets were then retrieved and stored at -20°C until needed.

2.1.2. Inclusion body isolation

2.1.2.1 Inclusion body isolation of $A\beta_{40}$

Inclusion body isolation was done following a series of centrifugation and sonication cycles as described before (Walsh et al., 2009). First, cell pellets were thawed on ice and subsequently

resuspended and homogenized in 12.5 mL of 10 mM Tris, 1 mM ethylenediaminetetraacetic acid (EDTA), pH 8.5, 1mM phenylmethylsulfonyl fluoride (PMSF) and 15 μg/mL DNase by mechanical stirring at 4°C for 30 minutes. The pellet solution was then pulled through a 1 ½ syringe, and sonicated for 30 seconds at 22% amplitude (4 watts) at 4°C. This solution was centrifuged for 15 minutes at 18000 rpm and 4°C (Beckman Coulter, JLA-25.50 rotor) and separated into supernatant and pellet. The homogenization, sonication and centrifugation steps were repeated, saving the supernatant fraction (S2) for later analysis. After this, the pellet was homogenized by mechanical stirring in 8M urea, 10mM Tris, 1mM EDTA, pH 8.5 and sonicated as before. This mixture containing the Aβ peptides were centrifuged for 30 minutes at 18000 rpm and 4°C (Beckman Coulter, JLA-25.50 rotor) and separated into supernatant, containing the inclusion body isolate (IC), and the pellet. An aliquot of each was saved for analysis and the IC saved for purification.

2.1.2.2 Inclusion body isolation of $A\beta_{42}$

Inclusion body isolation as performed as described in (Gremer et al., 2017). First, to lyse the cells and recover inclusion bodies, the cell pellet was resuspended in 20 mL of 10 mM Tris.HCl, 1 mM EDTA, pH 8.0 and sonicated for 2 minutes on ice at 50% duty cycle until the lysate appeared homogenous. The lysate was then centrifuged for 25 minutes at 18000 rpm at 4˚C using a JLA-25.50 rotor. The supernatant was removed, and the pellet was resuspended in 10 mM Tris.HCl, 1 mM EDTA, pH 8.0 sonicated and centrifuged as described above. This sonication and centrifugation steps were repeated another three times. After the last supernatant was removed, the remaining pellet was resuspended in 15 mL of 8 M urea or 7 mM NaOH in 10 mM Tris.HCl, 1 mM EDTA, pH 8.0 and was sonicated as described above, until the solution became clear. The solution was then diluted with 10 mL of 10 mM Tris.HCl, 1 mM EDTA, pH 8.0 and filtered through 0.22 μm Durapore non-sterile hydrophilic polyvinylidene fluoride (PVDF) filters (Merck). The solution recovered after filtering was kept at 4°C until further purification.

2.1.3. Anion exchange chromatography of $A\beta_{40}$

Protein purification was done as described in (Walsh et al., 2009), subjected to two rounds of "batch" anion exchange chromatography with the use of a Buchner funnel. First, 25 mL of Q Sepharose Fast Flow resin (GE healthcare) was equilibrated with 100 mL 10 mM Tris, 1 mM EDTA, pH 8.5. The protein sample was then added to the resin and left rocking for 30 minutes at 4°C and subsequently air-filtered and recovered to go through resin passes. The fractions were separated, and aliquots were kept for analysis at each step.

The first fraction recovered consisted of the protein sample that was let to flow through (FT). The resin was subsequently washed with 50 mL 10 mM Tris, 1 mM EDTA, pH 8.5 followed by 50 mL 25 mM, 10 mM Tris, 1 mM EDTA, pH 8.5. The peptide was then eluted from the resin with 125 mM NaCl in 10 mM Tris, 1 mM EDTA, pH 8.5, followed by 250 mM NaCl in 10 mM Tris, 1 mM EDTA, pH 8.5 in the last elution step. Finally, the resin was washed with 1 M NaCl, 10 mM Tris, 1 mM EDTA, pH 8.5 followed by 8 M urea, 1 M NaCl in 10 mM Tris, 1 mM EDTA, pH 8.5. The collected FT fraction was re-purified in the same manner. The collected aliquots were analysed by Tris-Tricine SDS-PAGE.

2.1.4. Dialysis and lyophilisation

After the two steps of batch anion-exchange the eluted fractions were dialysed into 50 mM ammonium bicarbonate. The eluted protein fractions were placed in equilibrated snake-skin tubing and dipped inside 50 mM ammonium bicarbonate and changed 4 times during the course of the two-day dialysis period. After this time, the protein was collected in 50 mL falcon tubes and snap frozen in dry ice covered in 70% Et-OH. Lyophilisation was then performed in a Heto Powerdry PL300 for the course of 2 days.

2.1.5. Size exclusion chromatography for $A\beta_{40}$ purification

The lyophilised protein was re-purified by size exclusion chromatography. A Superdex 75 16/60 column (GE Healthcare) was connected to an AKTA prime plus chromatograph using a 5 mL loop and equilibrated with 1 column volume of 50 mM ammonium bicarbonate. The peptide was then solubilised in 50 mM Tris, 7 M guanidine HCl, pH 8.5 and centrifuged for 10 minutes at 14000 rpm at 4°C (Eppendorf 5418 rotor). The supernatant was then injected into the chromatograph and run for 180 minutes at a 2 mL/min flow, collecting 2 mL fractions.

The fractions containing the $A\beta_{40}$ peptide were snap frozen in dry ice covered in 70% Et-OH and subsequently lyophilized as mentioned before for 48 h. The lyophilised pure protein was stored at -20°C until use.

Monomeric protein concentration was determined by solubilising one aliquot in 50 mM Tris, 7 M guanidine, pH 8.5 and analysing the absorbance at 280 nm wavelength using a quartz cuvette with 10 mm path length and an using and extinction coefficient 1490 M-1cm-1 (Stewart et al., 2016). To validate protein purity, protein aliquots were also assigned for molecular mass

determination by electrospray ionisation mass spectrometry at the mass spectrometry facility at the Faculty of Biological Science at the University of Leeds.

2.1.6. High performance liquid chromatography (HPLC) for $A\beta_{42}$ purification

The $A\beta_{42}$ peptide was purified from the filtered cell lysate crude by preparative mass directed HPLC by Dr Martin Walko. For this, a Kinetex EVO (21.2 x 250 mm) C18 column was used and run on an increasing 10-60% gradient of acetonitrile in water + 0.1% ammonia (v/v). For each purification run, 0.5 mL of crude lysate was injected into the column and allowed to run at a flow rate of 20 ml/min over 20 minutes. Fractions containing the $A\beta_{42}$ peptide were collected with the use of the mass directed chromatography software Masshunter by ChemStation (Agilent) and an Agilent 6120 Quadropole Liquid chromatography-mass spectrometry, which separates the eluents at a defined m/z. Fractions containing the purified peptide were combined and lyophilised as mentioned before.

2.2. Aβ monomer fluorescent labelling and fibril formation

SEC purified $A\beta_{40}$ or $A\beta_{42}$ was solubilised in fresh cold 25 mM sodium phosphate pH 7.5 at 0.5 mg/mL final concentration and mixed with ATTO-594 in a 3.5 X molar excess fashion. This was left rotating on a roller at 4°C for 16 h before quenching the reaction with 3.5 mM Tris. The peptide was then purified by analytical SEC. For this, an analytical Superdex 75 10/300 GL SEC column (500 µl injection) in 50 mM ammonium bicarbonate pH 8.0. Fractions corresponding to the monomer where pooled and snap frozen in 70% EtOH dry ice and lyophilised as mentioned in section 2.1.4. Fluorescently labelled monomer was kept at -20°C until used. To generate fluorescently labelled fibrils, 1% labelled monomer was added to the reactions mentioned in Section 2.3.

2.3. $A\beta_{40}$ and $A\beta_{42}$ fibril preparation

2.3.1. 2A and 3Q $A\beta_{40}$ fibril seeding

2A and 3Q fibrils were prepared by solubilising SEC purified lyophilised $A\beta_{40}$ peptide in 25 mM sodium phosphate pH 7.5 to a 0.9 mg/mL concentration and seeding with 2A and 3Q seeds (kindly provided by Dr Robert Tycko) in a 5% (v/v) ratio, respectively. The fibrils were then left growing quiescently overnight at room temperature and one cycle of sonication consisting of 5 seconds at 22% amplitude (4 watts) followed by 45 seconds off sonication was performed the day after. 2A and 3Q fibrils were then stored at 4°C until used.

To prepare new seeds, 2A and 3Q fibrils (0.9mg /mL, monomer equivalent) were subjected to three cycles of sonication consisting of 5 seconds at 22% amplitude (4 watts) followed by 45 seconds off sonication. Seeds were stored at -20°C until needed.

2.3.2. *de novo* $A\beta_{40}$ fibril generation

Unseeded *de novo* $A\beta_{40}$ fibrils were formed by solubilising the SEC purified and lyophilised $A\beta_{40}$ peptide to a final concentration of 0.9 mg/mL in 25 mM sodium phosphate pH 7.5. This was then plated onto a 3881 Corning 96-well plate and incubated for 16 h at 37°C and 600 rpm shaking. ThT fluorescence was monitored described in 2.7.1. After this time, fibrils were collected and stored at 4°C until needed.

2.3.3. $A\beta_{42}$ fibril generation at pH 2 and pH 8

Fibrils of $A\beta_{42}$ were generated as described in (Gremer et al., 2017), at pH 2, and as done in (Colvin et al., 2015), at pH 8. For the formation of $A\beta_{42}$ fibrils at pH 2 lyophilised $A\beta_{42}$ monomer was solubilised in 30% (v/v) acetonitrile, 0.1% trifluoroacetic acid (TFA) in water at a 120.5 µM concentration and was left undisturbed at room temperature. In contrast, for the formation of fibrils at pH 8, the lyophilised $A\beta_{42}$ monomer was solubilised in 20 mM sodium phosphate, 0.2 mM EDTA, 0.02% (v/v) NaN_3 at a 50 µM final concentration. The monomer solution was maintained in quiescent conditions at room temperature. Kinetics of fibril formation was followed by ThT fluorescence as described in section 2.8.1 and negative stain electron micrographs were taken for both fibrils after 24 h and 8 weeks of incubation. Fibrils were kept at room temperature until used.

2.4. Fibril yields

Insoluble fraction formation was determined after ThT fluorescence kinetic assays. After collection of samples, a small aliquot of the whole sample was taken and saved for later analysis. Samples were then centrifuged at 14000 rpm for 35 minutes in a bench centrifuge (Eppendorf 5418 rotor) at room temperature. Fractions were consecutively separated into supernatant and the pellet for later analysis. The pellet was resuspended with fresh buffer in an equal volume as the supernatant before SDS-PAGE.

2.5. Sodium dodecyl sulphate-polyacrylamide gel electrophoresis (SDS-PAGE)

For SDS-PAGE, an equal volume of 2 X sample buffer (50 mM Tris-HCl pH 6.8, 100 mM DTT, 2% (w/v) SDS, 0.1 % (w/v) bromophenol blue, 10% (v/v) glycerol) was added to the samples. Samples were then denatured at 100°C for 5 minutes before loading into a 15% (v/v) acrylamide Tris-Tricine buffered gel. Gels were run in Tris-Tricine SDS buffer (National diagnostic) at 30 mA for 30 minutes, then at 60 mA at a constant 200 V for 50 minutes, in a Biorad power gel chamber. Precision plus protein standard (Biorad, USA) was used as a size marker in all gels. Gels were stained in InstantBlue (Expedeon) and imaged with a transilluminator (Ingenius, Syngene). Intensity of stained protein bands was quantified in ImageJ using the gel analyser plugin.

2.6. Negative staining Transmission Electron Microscopy (TEM) of fibrils

Imaging by negative staining TEM was done to validate fibril formation. For this, 10 uL aliquots of each fibril sample were adsorbed for 40 seconds on to carbon coated glow discharged copper grids. They were then washed twice with water and subsequently stained with 2% uranyl acetate for 40 seconds. Grids were left to dry at room temperature and stored until used. Imaging was done in a JEOL 1400 electron microscope operating at 100 kV. Micrographs were taken at 5000 X - 15000 X magnification and captured with an AMT 2k CCD camera (AMT Corp., MA) in the Astbury BioStructure laboratory at the University of Leeds.

2.7. Fluorescence polarization assays of Aβ fibrils and α-synuclein

Alexafluor 488 labelled monomeric α-synuclein (kindly provided by Dr Matt Jackson) was solubilised at a final concentration of 0.05 μM and incubated under quiescent conditions in the presence of 25 μM monomeric α-synuclein and increasing concentrations of α-synuclein seed or Aβ fibril polymorphs (0-5 μM, monomer equivalent). Samples were incubated at 25°C in a Corning 3881 96-well black microplate with transparent bottom (Corning) and the assay was performed in a FLUOstar Optima plate reader (BMG LABTECH) in the Facility of Biomolecular interactions at the University of Leeds. To measure fluorescence polarization, excitation and emission wavelengths were set at 492 and 520 nm, respectively.

2.8. Thioflavin T (ThT) fluorescence assays

2.8.1 Aβ fibril formation

For *de novo* $A\beta_{40}$ fibrils, pH 2 $A\beta_{42}$ and pH 8 $A\beta_{42}$ fibril formation, aliquots of the individual monomers were prepared in the previously specified buffer adding ThT to a final concentration of 10 μM. ThT fluorescence was set up at 480 nm for emission and 440 nm for excitation in a Clariostar BMG Labtech. *de novo* $A\beta_{40}$ fibrils were grown at 37°C and 600 rpm, whereas pH 8 and pH 2 $A\beta_{42}$ fibrils were grown quiescently at room temperature.

2.8.2 Cross-seeding of α-synuclein monomer by Aβ fibrils

2.8.1.1 Cross-seeding at pH 7.5

Monomeric SEC purified α-synuclein (kindly provided by Dr Matt Jackson, Mike Davies and Sabine Ulamec) was solubilised to a final concentration of 70 μM in 0.015 mM ThT, 25 mM sodium phosphate pH 7.5. It was then seeded with the fibril polymorphs of $A\beta_{40}$, $A\beta_{42}$ or α-synuclein seed (kindly provided by Mike Davies) at 1%, 5% or 20% final concentration in triplicates on a Corning 3881 96-well black microplate with transparent bottom (Corning). The plate was sealed with adhesive film to avoid evaporation and inserted into a Clariostar or Fluostar OMEGA fluorescence plate reader (BMG Labtech). Kinetics experiments were performed under constant 600 rpm shaking and kept at 37°C. Fluorescence emission was read with bottom optics for >60 h, and ThT fluorescence was set up using a 440 ± 10 nm filter for excitation and a 470 ± 10 nm filter for emission wavelength.

2.8.1.2 Cross-seeding at pH 4.5

For analysis of cross-seeding at pH 4.5, monomeric SEC purified α-synuclein was solubilised in 0.0.15 mM ThT, 20 mM ammonium acetate, 20 mM NaCl pH 4.5. Fibril seeding concentration, plate and plate reader set up was done as described in section 2.8.1.1.

2.9. Curcumin binding assay

To assess structural heterogeneity of fibrils, a curcumin binding assay was set up following (Strohaker et al., 2019). Cross-seeded fibrils, formed by 70 μM α-synuclein cross-seeded with 20% (v/v) Aβ fibrils, were prepared without ThT as mentioned in section 2.8.1.2.

A 10 mM curcumin stock was done in DMSO which was then used to prepare 1 mM curcumin in 20 mM ammonium acetate, 20 mM NaCl pH 4.5. Samples were then prepared by following a 1:6 protein dye ratio and then loaded in triplicate on to a black clear bottomed 96 well plate in the Clariostar and fluorescent emission spectra was measured between 485 and 700 nm. The data was analysed using Graphpad Prism 6.1.

2.10. Cell culture

2.10.1 Recovery of cells from frozen stocks and maintaining

Frozen SH-SY5Y-GFP-α-synuclein cells were retrieved from liquid nitrogen storage and quick-thawed by placing cryovials in a water bath at 37°C. Cells were then resuspended in full media composed of DMEM culture medium (Gibco), supplemented with 10% FBS (Sigma-Aldrich), 1% (v/v) GlutaMAX (Gibco), 20 units/ml penicillin, 20 mg/ml streptomycin (Penn-Strep, Gibco) and grown in 75 cm^2 cell culture flasks. Cells were incubated at 37°C, 5% CO_2. After 24 h, medium was replaced with fresh full media. To maintain, cells were passaged using a 0.25% Trypsin-EDTA solution (Sigma-Aldrich) when they reached 80% confluency.

2.10.2 Cell stock maintenance (freezing)

Cryo-storage of cells was done to preserve cell lines. Cells were trypsinised, resuspended in full media and centrifuged at 100 xg for 5 minutes. The supernatant was decanted, and cells were

resuspended in cold freezing medium composed of full media supplemented with 10% (v/v) dimethyl sulfoxide (DMSO). Cryovials were filled with 1 ml of cell solution and then placed in Styrofoam containers to be frozen overnight at -80°C. Long-term storage of cells was kept in liquid nitrogen.

2.11. $A\beta_{40}$ and $A\beta_{42}$ fibril polymorph cross-seeding α-synuclein in cells

SH-SY5Y cells tagged with GFP-α-synuclein were plated in individual FluoroDishes (World Precision Instruments) at 100 000 cells per well and cultured as above mentioned. After 16 h, the cells were incubated with 1 μM 2A $A\beta_{40}$, 3Q $A\beta_{40}$, *de novo* $A\beta_{40}$, pH 2 $A\beta_{42}$ or pH 8 $A\beta_{42}$ fibrils for the course of 6 days. The buffer in which fibrils were made was used as a negative control and 1 μM α-synuclein seeds (provided by Mike Davies) were used as a positive control in the imaging experiments.

2.11.1 Cell permeabilisation for insoluble GFP puncta formation analysis

After the recombinant amyloid beta fibrils exposition, cells were first rinsed with Dulbecco's PBS (Sigma) twice, and then washed with 0.2% (w/v) saponin in PBS by quiescently leaving for ten minutes at room temperature. This step disrupts the cell membrane of cells and allow soluble α-synuclein-GFP to be washed away. Cells were then rinsed by doing two PBS washes and subsequently fixed with 4% formaldehyde in PBS. After ten minutes, cells were rinsed twice with PBS and stained for nuclei using 10 μg/mL Hoechst stain. Confocal fluorescent microscopy was then performed with the use of a LSM880 or LSM700 upright microscopes (Zeiss). Z-stacking was done on tiles of 4x4 images taken at a 40X objective per glass dish, accounting for at least 50 cells per individual tile. Threshold and gain settings were determined per individual experiment. For each experiment, preliminary manual counting was done. Images were then processed with the Fiji software and data was analysed using GraphPad Prism Version 6.01 software.

2.12. Cellular viability assays after incubation with $A\beta_{40}$ and $A\beta_{42}$ fibrils

For cell viability assays, cells were plated in 96-well plates at 10 000 cells per well and kept at 37°C and 5% CO_2. After 16 h, cells were then incubated with 1, 2, and 10 μM (monomer equivalent) 2A, 3Q and *de novo* $A\beta_{40}$ fibrils, pH 2 or pH 8 $A\beta_{42}$ fibrils for 48 h. After exposure to Aβ fibrils cellular viability was assessed. Unless otherwise stated data analysis of cell viability data was done with GraphPad Prism Version 6.01 software.

2.12.1 ATP assay

For ATP quantification in cells, the ATPLite (Perkin Elmer) kit was used following the manufacturer's specifications. The ATPLite is a luminescence assay based on the firefly luciferase enzyme and D-luciferin production of light by the presence of ATP in the media.

Following incubation of the cells with fibrils, 50 μL of the kit's lysis buffer was added to cells in 100 μL of media and shaken at 600 rpm for 5 minutes at room temperature. The substrate reaction mix containing firefly luciferase enzyme and D-luciferin was then added to the cells. Media was transferred to a white bottomed 96-well plate and luminescence was measured in a FluoStar Optima (BMG Labtech) plate reader in the Facility of Biomolecular interactions at the University of Leeds.

2.12.2 LDH assay

The Pierce LDH Cytotoxicity Assay Kit (Thermo Scientific) was used to measure LDH release, a sign of plasma membrane damage in cells, following manufacturer's instructions.

After fibril incubation, 50 μL of media were transferred to a black clear-bottomed 96-well plate (Prod. No. 3631, Corning) and mixed with the reaction mixture. This was kept at room temperature for 30 minutes and reaction was subsequently stopped by adding the kit's stop solution. Absorbance was measured at 490 and 680 nm for the LDH activity assay on a Fluostar OMEGA fluorescence plate reader plate reader.

2.12.3 3-(4,5-dimethylthiazol-2-yl)-2,5-diphenyltetrazolium bromide (MTT) reduction assay

After exposure to Aβ fibrils, MTT in PBS was added to each well at 0.5 mg/mL final concentration. The plates were then incubated for two and a half hours at 37°C and 5% CO_2. Cell media was then removed from wells and 100 μL of dimethyl sulfoxide was added and incubated

for 10 minutes at 37°C. Absorbance was measured at 570 nm and 650 nm in a Clariostar (BMG Labtech) plate reader.

2.13. Live cell imaging of after $A\beta_{40}$ and $A\beta_{42}$ fibrils incubation

For the analysis of colocalization between fibrils and lysosomes SH-SY5Y cells tagged with GFP-α-synuclein were plated in individual FluoroDishes (World Precision Instruments) at 100 000 cells per well and cultured as mentioned in section 2.8.1.1. The cells were then incubated with 1 µM fluorescently labelled 2A $A\beta_{40}$, 3Q $A\beta_{40}$, *de novo* $A\beta_{40}$, pH 2 $A\beta_{42}$ or pH 8 $A\beta_{42}$ fibrils (some kindly provided by Maddie Brown) for the course of 3 and 6 days. After this time, the cells were washed with PBS and incubated with warm phenol free full media. Deep red lysotracker (Thermo Fisher) and Hoechst stain was added to the media to a final concentration of and 10 µM, respectively. Imaging was then done in an LSM700 upright microscope (Zeiss). Z-stacking images taken at a 40 X objective per glass dish, accounting for at least 15 cells per image. Threshold and gain settings were determined per individual experiment. Images were then processed with the Fiji software and data was analysed using GraphPad Prism Version 6.01 software.

2.14. Cell fractionation

2.14.1 Sequential detergent fractionation of cells incubated with Aβ fibrils

To observe differences in α-synuclein levels in cells, soluble and insoluble cell fractionation was done following a modified protocol of PHF's retrieval (Goedert et al., 1992).

SH-SY5Y cells tagged with GFP- α-synuclein were plated at 100 000 cells per well in 6-well plates (Thermo Fisher) and incubated for 6 days with $A\beta_{40}$ and $A\beta_{42}$ fibril polymorphs. Cells were then lysed and re-suspended in 1% triton, PBS with cOmplete™, EDTA-free protease inhibitor cocktail. They were then sonicated at 40% amplitude for 10 sec (1 sec on, 2 sec off) at 4°C and centrifuged for 10 minutes at 16 000 x g at 4°C in a bench top centrifuge (5418, Eppendorf). The supernatant was collected, brought up to 1% (v/v) sarkosyl and left rotating for 1 h at room temperature. The samples were then ultracentrifuged for 1 h at 100 000 x g at 4°C using a

Beckmann Coulter Optima Ultracentrifuge, equipped with a TLA100 rotor. Supernatant and pellet were separated, and the pellet was re-suspended in 1/3 of the sample supernatant volume. Total protein concentration was then measured using the DC protein concentration kit (Biorad) following the manufacturer's instructions. Samples were all normalised before running SDS-PAGE as described in section 2.5.

2.14.2 Subcellular fractionation and lysosome isolation

Lysosome isolation was done as described in (Davidson et al., 1990). For this, SH-SY5Y cells tagged with GFP- α-synuclein were plated and allowed to grow on 175 cm^2 flasks until 100% confluent as established on section 2.9.2. These cells ($3x10^7$ cells/mL) were then trypsinised and resuspended in homogenisation buffer consisting of 10 mM triethanolamine, 10 mM acetic acid, 5 mM EDTA, 25 mM sucrose, pH 7.4. Lysing was done by subjecting cells to 10 passages through a 10 µm steel ball-bearing homogeniser. Cells were then centrifuged at 400 x g at 4°C on a bench top centrifuge (5418 R, Eppendorf) for 10 minutes and the supernatant collected. The supernatant was then brought to 9 mL with 27 % Percoll solution in homogenisation buffer. This mixture was then ultracentrifuged at 23 000 rpm for 1 h at 4°C on an Avanti J-HC centrifuge using a 70.1 Ti Fixed angle rotor (Beckman Coulter). Then, 500 µL fractions were pooled from the ultracentrifuged cell lysate and assayed for alkaline phosphatase and α-N-acetylgalactosaminidase (NAGA) enzyme activities.

Once assayed, fractions positive for NAGA were collected and ultracentrifuged at 214 000 x g for 1 h at 4°C using a Beckmann Coulter Optima Ultracentrifuge, equipped with a TLA 110 rotor.

2.14.2.1 α-N-acetylgalactosaminidase enzyme (NAGA) assay

To isolate lysosomes after cell fractionation by ultracentrifugation, the detection of the NAGA enzyme, a lysosomal glycosidase, was done by the addition of substrate (2,4-dinitrophenyl-*N*-acetyl-α-D-galactosaminide). First, 2 mM 2,4-dinitrophenyl-*N*-acetyl-α-D-galactosaminide was prepared in 100 mM citric acid, 0.2% (v/v) triton, pH 4.5. A 5 µL aliquot was taken from the cell fractions and placed in a clear bottom 96-well plate. Next, 100 µL of substrate was added to the wells and the plate was incubated at 37°C for 30 minutes. The reaction was quenched with 100 µL of 200 mM glycine pH 10.3 and absorbance was measured at 405 nm in a Clariostar plate reader (BMG Labtech)(Robbins, 1979; Morten et al., 2007).

2.14.2.2 Alkaline phosphatase assay

As a control for the NAGA assay, an alkaline phosphatase assay was set up and done in parallel for the cell fractions collected after ultracentrifugation. Alkaline phosphatase is a membrane bound glycoprotein (Morten et al., 2007), and so in this assay acts as a marker of the cell membrane. For this, 5 mM 4-nitrophenylphosphate substrate was prepared in 5 mM magnesium chloride, 10 mM triethanolamine, 10 mM acetic acid, 1 mM EDTA pH 7.4 and kept on ice until needed. A 5 µL aliquot was taken from the fractions and placed in a 96 well plate. Then, 100 µL of the prepared substrate was added to the wells and the plate was incubated at 37°C for 30 minutes. Absorbance was then measure at 405 nm in a Clariostar plate reader (BMG Labtech) and data was compared to the results from NAGA assay to pool lysosomes after the cell fractionation.

2.15. Western blotting

After separation of soluble and insoluble fractions of cells that had been incubated with Aβ fibrils, SDS-PAGE and immunoblotting were done to detect α-synuclein levels. First, gels were transferred to a methanol activated PVDF membrane (0.45 µm pore size, Amersham, GE Healthcare) on a Biorad semi-dry transfer blotter for 1 h at 12 V. The membrane was consecutively fixed with 4% formaldehyde and then blocked for 1 h at room temperature in 5% (w/v) milk, 20 mM Tris.HCl, 150 mM NaCl pH 7.2, 0.1% (v/v) tween (TBS-T). Primary antibody stocks were done in 5% (w/v) milk TBS-T. The antibodies probed were the anti-aggregated α-synuclein antibody clone 5G4 (1:2000, Merck) and the anti-GAPDH antibody (1:1000, Proteintech group Inc.). Following blocking, membranes were left incubating at 4°C and rotating for 16 h, in the primary antibody stock solution previously made. Anti-mouse HRP or anti-rabbit HRP secondary antibodies were made in TBS-T (1:2000, Cell signalling technology). The membrane was washed twice in TBS-T and then left incubating for 1 h at room temperature in secondary antibody. After this time, the membrane was washed twice in TBS-T and twice in TBS and chemiluminescence was detected using the SupersSignal West Pico PLUS substrate (Thermo Fisher) following the manufacturer's instructions.

2.16. Lysosomal degradation

Fibrils, synuclein monomer were mixed together keeping a 20% (v/v) seeding concentration in PCR tubes. Consecutively, lysosomal isolate (0.09 units) were added into the mixture and kept at

37°C. Aliquots of 10 μL were taken after 4 h and 16 h of incubation and analysed by SDS-PAGE. Densitometry analysis was done using ImageJ and Graphpad Prism 6.1.

2.17. Statistical analysis

Statistical analysis was performed using Graphpad Prism 6.1. Where appropriate, ANOVA was subjected to post-hoc Tukey's or Holm-Sidak's test to compare every mean of a sample to every other mean. p values <0.05, <0.01, <0.001 and <0.0001 are indicated by (*), (**), (***) and (****) respectively. Lack of significance was indicated in the text when p>0.05.

3. Aβ$_{40}$ and Aβ$_{42}$ fibril polymorph formation

3.1. Introduction

Distinct molecular structures have been defined for i*n vitro* generated fibrils of both 40 and 42 residue Aβ peptides. In this work I focused on the 2A and 3Q polymorphs of Aβ$_{40}$ and fibril forms of Aβ$_{42}$ generated at pH 2 and pH 8, herein called pH 2 and pH 8 Aβ$_{42}$ fibrils, respectively. These fibrils have been comprehensively characterised (Colvin et al., 2015; Gremer et al., 2017; Paravastu et al., 2008; Petkova et al., 2005), and are known to have distinct molecular structures, making them good models to examine how fibril polymorphism affects the interaction with α-synuclein and its aggregation.

The 2A and 3Q fibril polymorphs of the Aβ$_{40}$ peptide are used in this study as they present a distinct two-fold striated ribbon structure and three-fold twisted fibrillar forms respectively. (Figure 3.1, A and B). They were initially formed from synthetic Aβ$_{40}$ peptide under different conditions: the 2A under agitation, and quiescently for the 3Q. The fibril structural model for both fibril types was generated from chemical shifts from solid state nuclear magnetic resonance (ssNMR), TEM and scanning transmission electron microscopy (STEM) data. All of these revealed that they a have an unstructured N-terminal, an in register parallel β-sheet structure and 5 nm or 8 nm widths for the 2A and 3Q, respectively (Paravastu et al., 2008; Petkova et al., 2005).

A third Aβ$_{40}$ fibril polymorph was used in this study. This *de novo* fibril preparation is formed under agitative conditions, and has also been noted to have different ^{13}C-^{13}C dipolar assisted rotational rationale ssNMR spectrum to the one observed for the 2A and 3Q, specifically for residues I31 and V24 (Madine et al., 2012). However, unseeded fibril preparations are known to contain a mixture of fibril structures (Petkova et al., 2005; Stewart et al., 2017).

Differences in structures have also been observed for fibrils of Aβ$_{42}$. My work focused on the fibrils formed at pH 2 and pH 8 (Figure 3.1, C and D), and whose structures were determined by cryogenic electron microscopy (cryoEM) and ssNMR, respectively. These *in vitro* generated fibrils have distinct morphologies: Aβ$_{42}$ pH 2 fibrils are formed by staggered protofilaments that have an LS shaped arrangement (Figure 3.1 C), whereas pH 8 fibrils are formed as a dimer from two S-shaped monomers with the hydrophobic residues hidden in the fibril core (Figure 3.1 D).

Both pH 2 and pH 8 fibrils were formed from recombinant peptide and, as the Aβ$_{40}$ fibrils described before, present an in register parallel β-sheet structure and different to the previously

described fibrils (Colvin et al., 2016; Gremer et al., 2017). Apart from their distinctive shape, the pH 2 structure differs from the pH 8 in presenting a structured N-terminal region.

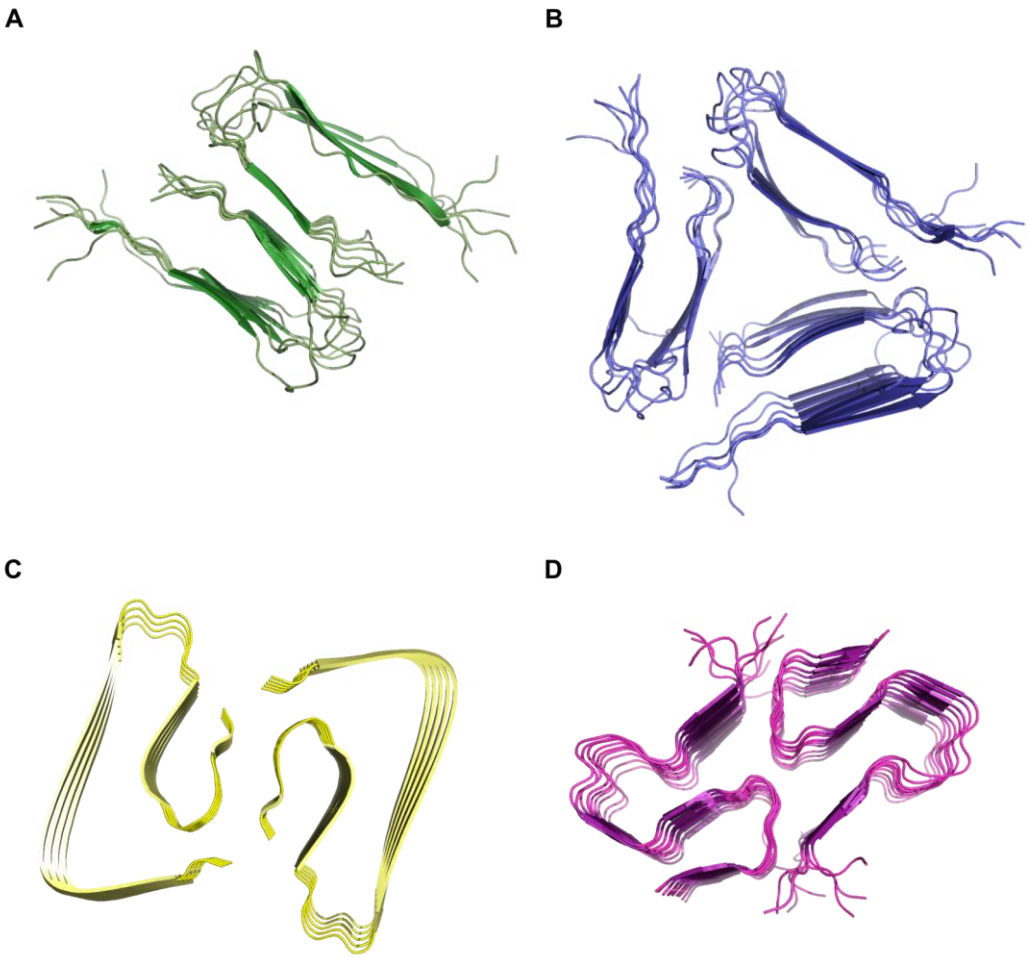

Figure 3.1. $A\beta_{40}$ and $A\beta_{42}$ fibril polymorphs.
Molecular fibril structures of the 2A (PDB 2LMN/2LMO) (A), 3Q (PDB 2LMP/2LMQ) (B) $A\beta_{40}$ fibrils, and pH 2 (PDB 5OQV) (C) and pH 8 (PDB 5KK3) (D) $A\beta_{42}$ fibrils. All of these fibrils were prepared under distinct physical conditions and present different structural properties.

3.2. Expression of Aβ40 and Aβ42 peptides

The first step in the investigation of the interactions between Aβ fibril polymorphs and α-synuclein was the formation of the fibrils. This begins with the production of the Aβ peptides, followed by fibril formation and the characterisation of the fibrils.

The method used for the production of both Aβ peptides was bacterial expression. This requires the introduction of a methionine (Met) at their N-termini for the promotion of expression and increase in protein yield. Methionine-Aβ peptides have been used extensively, and it is known that the Met residue does not significantly alter the aggregation kinetics of either $A\beta_{40}$ or $A\beta_{42}$ when compared to their synthetic counterpart that doesn't contain the Met residue. In addition, no significant differences have been observed in regards their toxic effect to hippocampal rat neurons (Walsh et al., 2009). In addition, the ^{13}C-^{13}C dipolar assisted rotational rationale ssNMR spectra signals from 2A and 3Q $A\beta_{40}$ fibrils prepared Methionine-$A\beta_{40}$ peptide coincides to the ones originally reported, implying this residue does not alter the overall fibrillar structure (residues 10-40) (Stewart et al., 2017).

E. coli BL21 DE3 cells were transformed with plasmids encoding either the 40 or 42 residue Aβ peptide, bearing a Met residue at the N-terminal. Cells were cultured and expression of the peptides was induced with IPTG. SDS-PAGE of aliquots taken before and after induction with IPTG showed that the $A\beta_{40}$ and $A\beta_{42}$ (Figure 3.2 A and B) were indeed expressed in the cells after 4 h of induction.

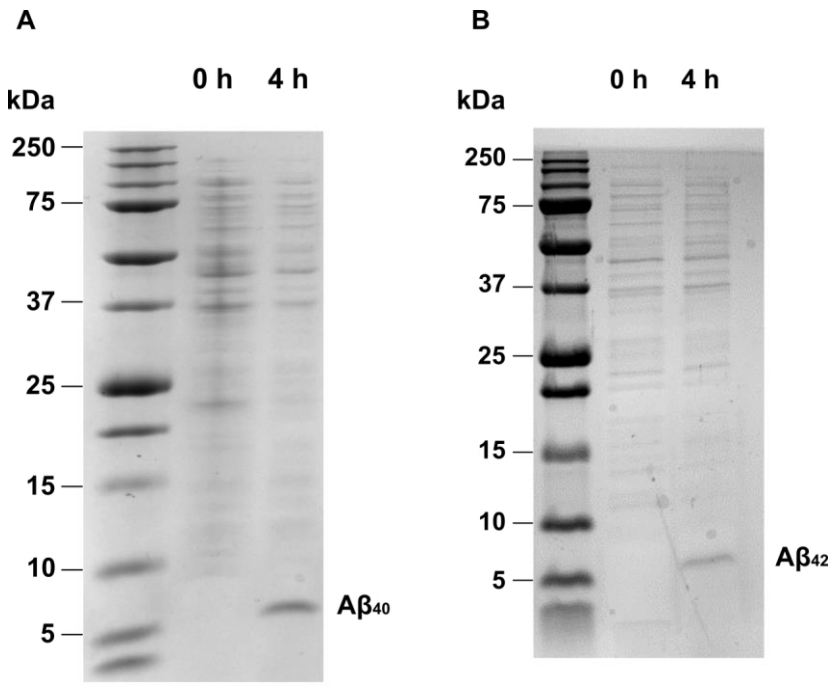

Figure 3.2. $A\beta_{40}$ and $A\beta_{42}$ peptide expression
BL21 DE3 E. coli cells were transformed with the A) pET Sac Met-$A\beta_{40}$ plasmid or B) pET Sac Met-$A\beta_{42}$ plasmid and grown in LB media for the production of $A\beta_{40}$ or $A\beta_{42}$ respectively. Cells were induced with 0.1 M IPTG for 4 h before harvesting. Samples were taken before and after induction and resolved by SDS-PAGE on a 15% Tris-Tricine gel.

3.3. Purification of Aβ40

The presence of contaminants, soluble aggregates or pre-aggregated forms of both Aβ40 and Aβ42 peptides can change the aggregation kinetics, or ultimately alter their fibrillar morphology rendering a distinct uncharacterized form unsuitable for the purpose of this study (Hellstrand et al., 2010; Meisl et al., 2016). It is therefore necessary to ensure the samples used to prepare fibrils are pure. Figure 3.3 summarizes the different steps in the methods used to purify the Aβ40 and Aβ42 peptides. Both protocols, anion exchange chromatography followed by SEC for Aβ40, and HPLC for Aβ42, have successfully purified these peptides for the production of fibrils and its structural analysis (Finder et al., 2010; Hoarau et al., 2016; Walsh et al., 2009).

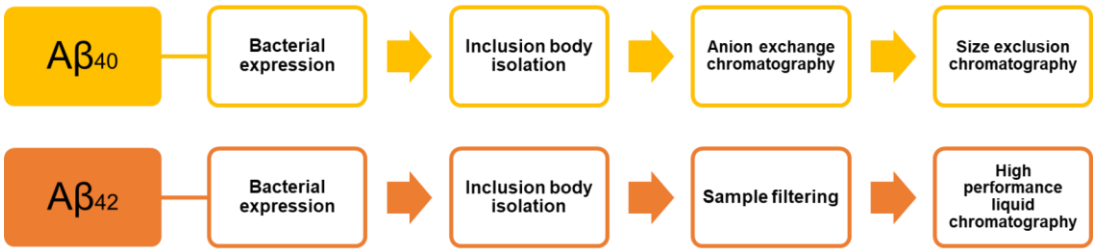

Figure 3.3. Expression and purification of Aβ40 and Aβ42 workflow
Two different approaches were taken: anion exchange chromatography and SEC to purify Aβ40, and HPLC for Aβ42 purification.

3.3.1 Inclusion body isolation and anion exchange chromatography of Aβ40

Aβ forms insoluble aggregates in inclusion bodies in bacterial expression systems (Meisl et al., 2016; Walsh et al., 2009). To purify the Aβ peptides form inclusion bodies centrifugation-sonication cycles were performed. This method is known to remove nucleic acids and proteins weakly associated to inclusion bodies (Hoarau et al., 2016). Inclusion bodies were homogenized in 8 M urea and solubilisation was followed by a sonication and centrifugation step.

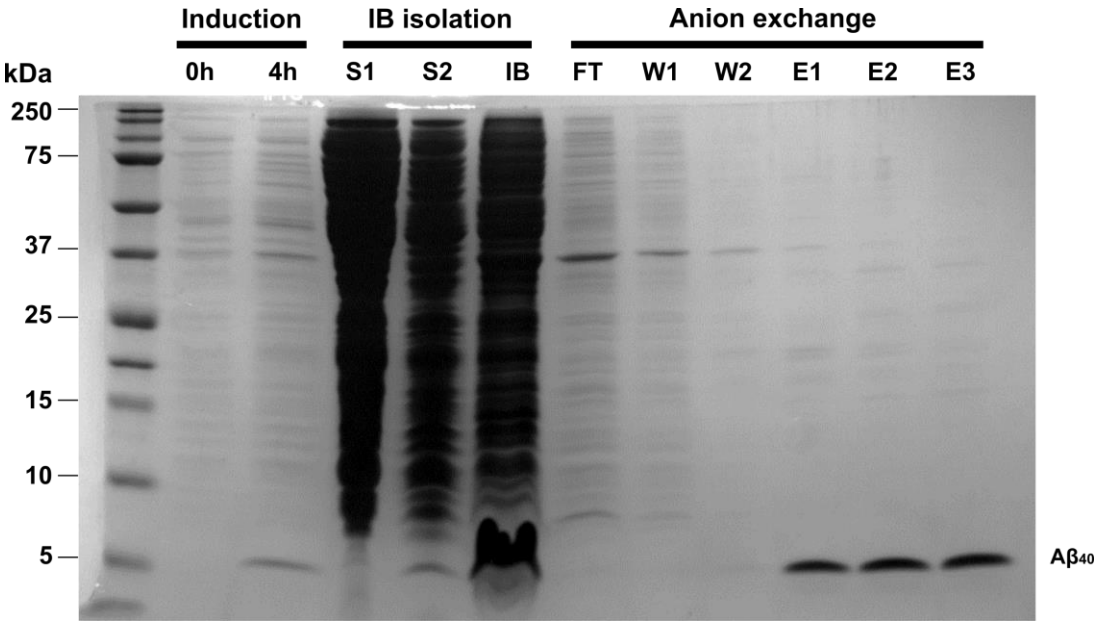

Figure 3.4. SDS-PAGE gel of induction, inclusion body isolation and anion-exchange batch purification of $A\beta_{40}$.
Purification by anion exchange was done by harvesting cells by centrifugation after 4 h of induction with IPTG. The isolation of inclusion bodies was performed by a sonication and centrifugation cycle of the cell pellet. Supernatants from this process were collected (S1 and S2). Inclusion bodies were homogenized in 8 M urea, followed by sonication and centrifugation (IB). This last sample was added to Q-Sepharose resin, and anion exchange was run in batch mode, where fractions for the flow through (FT), wash 1 and 2 (W1 and W2) and elution (E1, E2, E3) were collected. The calculated molecular weight of the $A\beta_{40}$ peptide with an N-terminal Met residue is 4461.05 Da and corresponds to a band at ~5 kDa in the 15% Tris-tricine gel.

After inclusion body solubilisation, the next step of purification of $A\beta_{40}$ was batch anion exchange chromatography. For this, the Q-Sepharose resin and the homogenized inclusion body solution were mixed in a Buchner funnel, allowed to equilibrate, and elution of the peptide off the resin was done with the addition of 125 mM NaCl in the buffer, before the system was washed and regenerated for the purification of the flow through. SDS-PAGE analysis of aliquots taken at different points during this process showed that $A\beta_{40}$ was eluted at this NaCl concentration, but that anion exchange alone was not effective in eliminating all impurities (lanes E1 - E3, Figure 3.4), and that an additional purification step is necessary.

3.3.2 Size exclusion chromatography (SEC) of Aβ40

Following the lyophilisation of anion-exchange purified Aβ40, the peptide was subjected to SEC, which has been demonstrated to result in homogeneous monomeric Aβ (Walsh et al., 2009).

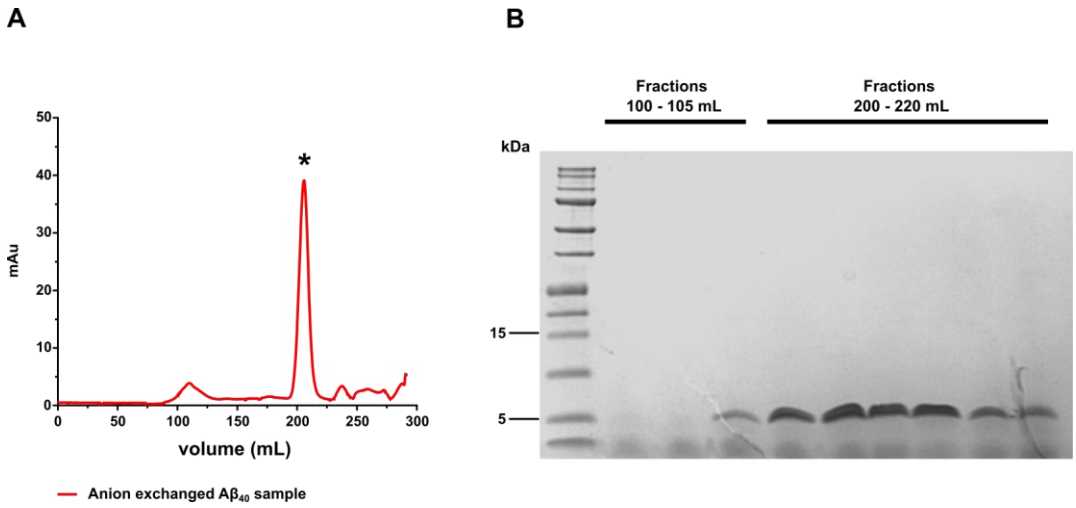

Figure 3.5. Protein purification SEC of Aβ40 peptide.
The elution (E1-E5) fractions collected from the anion exchange batch purification were subjected to SEC. A) After equilibration of a Superdex 75 16/60 column in 50mM ammonium bicarbonate, the peptide sample in 50 mM Tris pH 8.5, 7 M guanidice.HCl was injected into the system. The SEC trace (mAU, absorbance at 280 nm) showed that monomeric Aβ40 eluted in fractions collected around 200-225 mL (*). B) Samples collected from SEC were analysed by SDS-PAGE on a 15% Tris-Tricine gel. Samples collected between 200-225 mL corresponded to monomeric Aβ40 and were revealed as a single band of ~5 kDa demonstrated the efficient purification of Aβ40 through this method.

The SEC trace showed one prominent peak eluting between 200 and 225 mL and a smaller eluting ~100 mL (Figure 3.5 A). Samples of the fractions collected were analysed by SDS-PAGE (Figure 3.5 B), showing a single band at ~5 kDa on the fractions collected between 200-225 mL, corresponding to Aβ40. Mass spectrometry analysis of these samples showed a mass of ~4461 Da (Figure 3.6), consistent with the predicted Met-Aβ40 of 4461.05 Da. Some preparations of the peptide presented very low abundant ion adducts and a possible valine cleavage product, but this did not have an effect on fibril formation. A total of ~2-3 mg/L of Aβ40 were typically obtained using this method of purification.

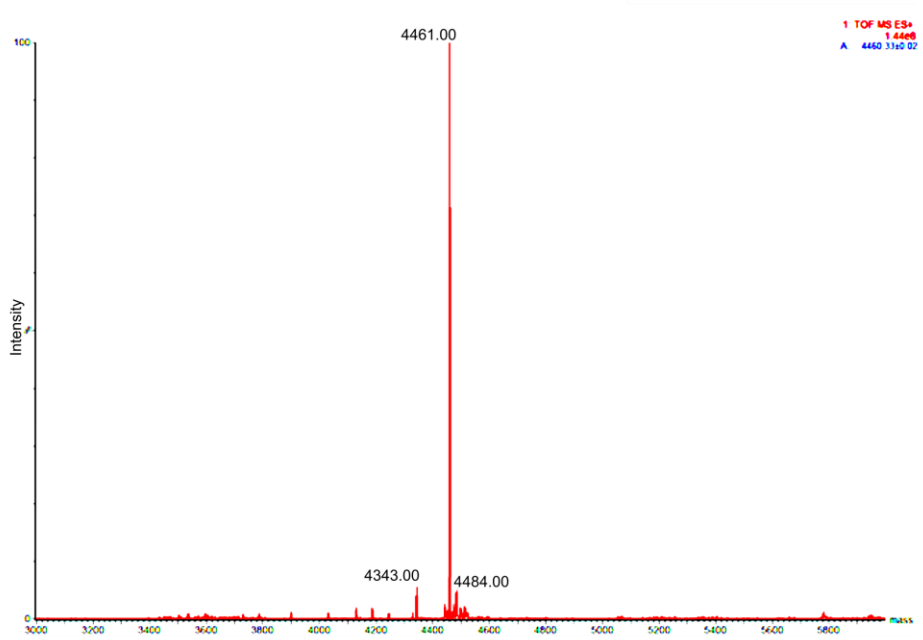

Figure 3.6. Mass spectrometry spectra of purified Aβ$_{40}$ peptide.
Deconvoluted mass spectrometry spectrum of Aβ$_{40}$ after being purified by size exclusion chromatography. Mass spectrometry analysis was done by electrospray ionisation at the Mass spectrometry facility at the University of Leeds. Samples submitted showed a mass ~4461 Da, which corresponds to the expected mass of Met-Aβ$_{40}$ (4461.05 Da). The presence of low abundant metal ion adducts to Met-Aβ$_{40}$ (4484 Da) as well as a possible Met-Aβ$_{40}$ valine cleavage product (4343 Da) were observed.

3.4. Purification of Aβ$_{42}$

For the purification of Aβ$_{42}$ the approach stated by Yoo et al. (2018) was followed. The inclusion body preparation is first filtered through a PVDF membrane before performing preparative HPLC, and typically results in a high yield of peptide (mgs per litre of bacterial culture) and takes less time when compared to the method used for Aβ$_{40}$ purification.

3.4.1 Inclusion body isolation of Aβ$_{42}$

In contrast to the Aβ$_{40}$ cell lysis and inclusion body preparation, this method uses 5 cycles of centrifugation and sonication before filtering: four to remove weakly bound impurities by pelleting and a last one to solubilise inclusion bodies. My initial Aβ$_{42}$ peptide preparations were done by homogenization of inclusion bodies in 8 M urea, but switched to 7 mM sodium hydroxide

in later preparations of the peptide as this concentration was found to be better for the HPLC column (method improved by Dr Martin Walko)

Unfortunately, a slight loss of $A\beta_{42}$ is observed during the 2nd to 4th centrifugation cycles, as the band corresponding to $A\beta_{42}$ is observable in the supernatant fractions (Figure 3.7, S2-S4, ~5kDa). This however did not result in a pronounced decrease in the total yield of protein obtained.

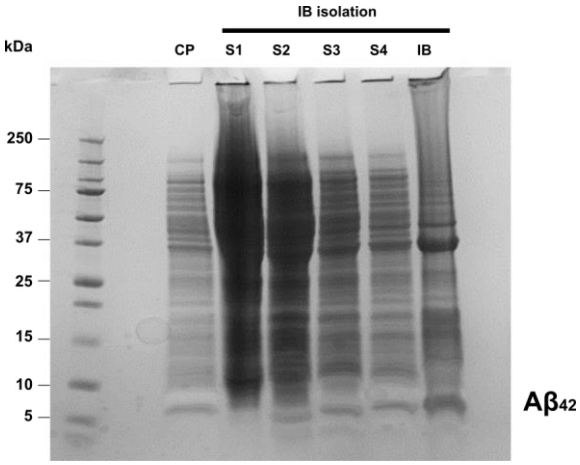

Figure 3.7. Isolation of $A\beta_{42}$ peptide from inclusion bodies.
Induced cells were harvested by centrifugation (CP) and lysed by sonication. Four cycles of sonication and centrifugation were done (S1-S4) to isolate inclusion bodies. Inclusion bodies were then solubilised by the addition of 8 M urea (IB). Samples were analysed by SDS-PAGE on a 15% Tris-Tricine gel.

3.4.2 HPLC purification of $A\beta_{42}$

The solubilized inclusion body solution obtained from the centrifugation-isolation cycles was passed through a hydrophilic PVDF syringe filter before preparative HPLC. For this a C18 column was used and a gradient of 10 - 60% gradient of acetonitrile was run to elute the peptide (method kindly performed by Dr Martin Walko). Three well resolved peaks were observed in the HPLC trace of the filtered inclusion body solution (Figure 3.8, A). A run of the purified peptide resulted in the elution of a single peak at ~ 3.5 minutes (Figure 3.8, B), corresponding to the first peak observed in the HPLC trace of the crude solution. SDS-PAGE analysis of the purified peptide revealed a single band at ~5 kDa, consistent with monomeric $A\beta_{42}$ (Figure 3.9, A).

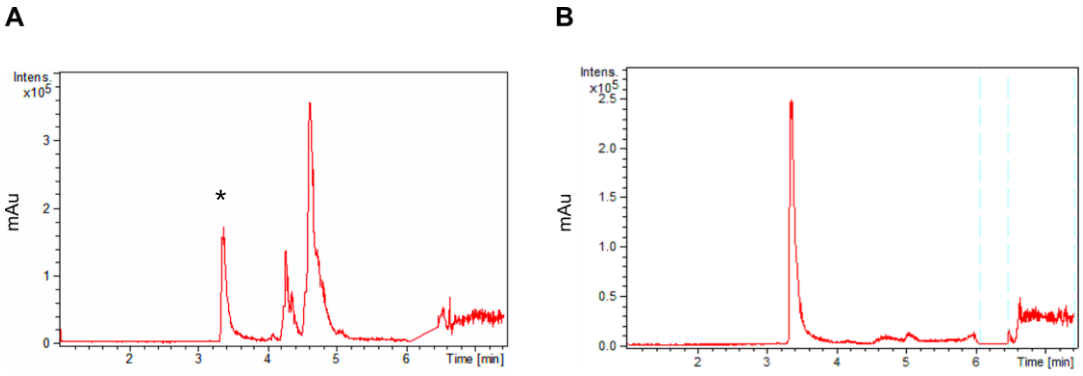

Figure 3.8. HPLC spectra of $A\beta_{42}$ peptide purification.
For purification a Kinetex EVO C18, 21.2x250 mm column using a 10-60% gradient of acetonitrile in water with 0.1% ammonia and run at 20 ml/min over 20 minutes. LC trace (mAU, 210 nm) of IB solution after preparative HPLC (A) and the purified peptide (B) show that the first eluted peak (*) of the IB solution corresponds to $A\beta_{42}$. Samples collected at this time were combined, lyophilised and stored for later use.

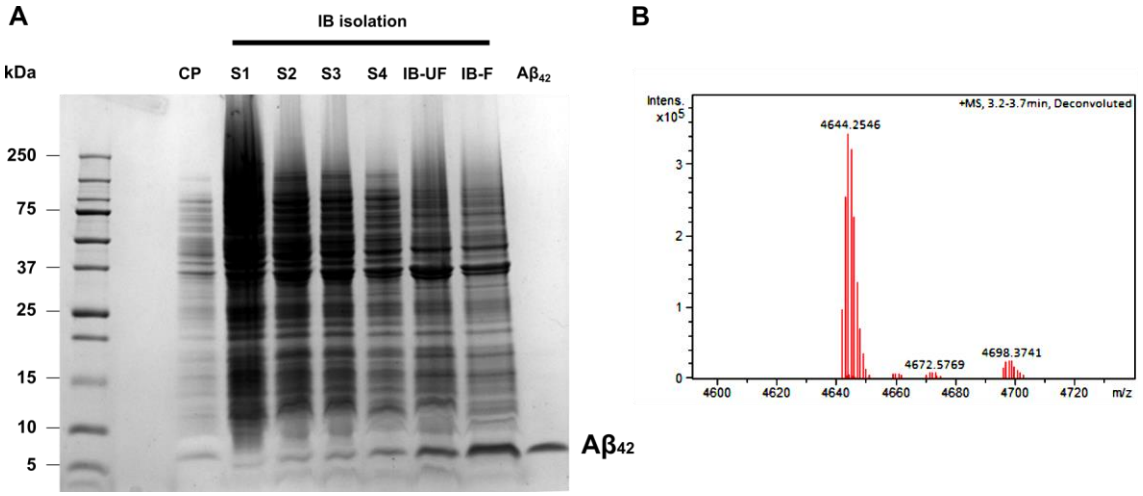

Figure 3.9. SDS-PAGE of HPLC purified $A\beta_{42}$ and high-resolution mass-spectrometry.
Samples collected through the purification process were analysed by SDS-PAGE. Samples correspond to the cell pellet (CP), the inclusion body isolation centrifugation steps (S1-S4), the solubilized insoluble bodies, before (IB-UF) and after (IB-F) being filtered, and the HPLC purified $A\beta_{42}$, which is a single band on the gel of ~5 kDa. B) Deconvoluted mass spectrum of $A\beta_{42}$. Mass spectrometry confirms that the observed mass of $A\beta_{42}$ with an N-terminal methionine corresponds to the expected 4645.29 Da mass. Metal ion adducts were observed to a in low abundance after purification (4672.5 and 4698.3 Da).

Mass spectrometry analysis of the purified peptide showed a mass of ~4644 Da, consistent with the calculated 4645.29 Da Met-Aβ$_{42}$ mass (Figure 3.9, B). Low abundant ion adducts were observed for some Aβ$_{42}$ preparations but did not alter fibril formation. All Aβ$_{42}$ HPLC collected fractions were combined, lyophilised and stored at -20°C until peptide use. A total of ~6.5 mg per litre of bacterial culture of purified peptide were obtained.

3.5. Fibril production

3.5.1 2A and 3Q Aβ$_{40}$ fibril polymorph seeding

Elongation of fibrils from seeds or shorter fibrils is a common method to make amyloid fibrils and bypasses the nucleation step of fibril assembly and allows the intrinsic molecular structure of the seed/fibril to be propagated through generations (Arosio et al., 2015). This is observed by a reduction in the lag time and the more rapid entry into the elongation phase in the aggregation kinetics of amyloidal peptides. Kinetic analysis of the seeding of the Aβ$_{40}$ monomer by 2A and 3Q fibrils by monitoring ThT fluorescence showed an accelerated rate of fibril formation compared to the unseeded monomer (Figure 3.10) and a reduction in the half-times of the seeded reactions compared to the monomer on its own (Table 3.1).

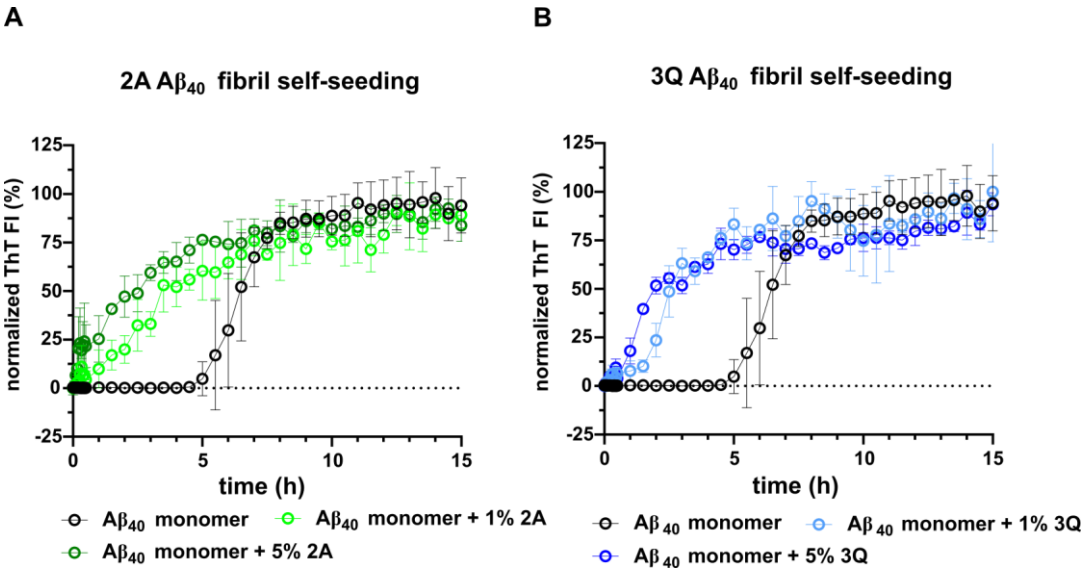

Figure 3.10. 2A and 3Q fibril seeding.
Fibril seeding of the 2A and 3Q Aβ$_{40}$ fibril polymorphs was monitored by ThT fluorescence. For this Aβ$_{40}$ monomer (100 μM) was resuspended in 25 mM sodium phosphate pH 8.5 and seeded at 1 and 5% (v/v) with 2A (A) or 3Q (B) fibrils. The seeding of monomer bypasses the nucleation process and reaches the growth phase at a much faster rate, as well as allowing for the molecular structure of the fibril to be propagated through generations. Experiment done in triplicates (Mean ± S.D.).

Table 3.1. Half times of the kinetic reaction of 2A and 3Q Aβ$_{40}$ fibril seeding.

	Half-time (h)		
	2A	**3Q**	**monomer**
1% seeding	3.97 ± 0.08	2.5 ± 0.13	-
5% seeding	2.97 ± 0.58	2.5 ± 0.19	-
monomer	-	-	6.4 ± 0.86 h

3.5.2 *de novo* Aβ$_{40}$ fibril generation

The unseeded fibril elongation of Aβ$_{40}$, termed herein as *de novo* fibril preparation, was monitored by ThT fluorescence (Figure 3.11). The lag time was calculated following the fitting of the experimental data to a sigmoidal function $y = y_0 + A/(1 + \exp(-k(t - t_{0.5})))$, where the lag time is defined as $t_{lag} = t_{0.5} - 1/2k$ (Arosio et al., 2015). The monomer showed a calculated lag time of 6.2 h at this concentration, and plateau was reached within 10 h of incubation under the conditions before mentioned. The reaction was stopped after 24 h of incubation and fibrils were collected to be analysed by TEM (Figure 3.13).

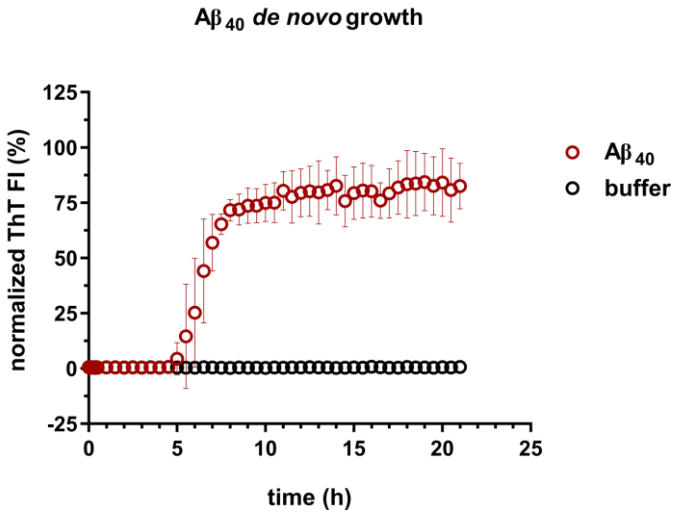

Figure 3.11. ThT kinetic analysis of the unseeded de novo Aβ$_{40}$ fibril generation.
de novo fibril formation (100 μM) exhibited a calculated lag time of ~6 h and plateauing occurred after ~10 h of incubation at 37°C and 600 rpm shaking. Experiment done in triplicates (Mean ± S.D.)

The lag time for the reaction of the unseeded *de novo* $A\beta_{40}$ fibril preparation bearing an exogenous initiating methionine residue depends on the concentration, buffer and temperature in which the fibrils where formed. Reports using similar conditions as this study have been found to be between 20 minutes and 6 h (Walsh et al., 2009; Bunce et al., 2019), consistent to what was observed here.

3.5.3 Characterisation of fibrillation of $A\beta_{40}$

After fibril formation, fibril yields were determined for the fibril preparations. This consisted of the sedimentation of the fibrils by centrifugation, separation of the supernatant and pellet fractions and subsequent SDS-PAGE analysis (Figure 3.12, A). >80% of $A\beta_{40}$ was in the pellet fraction for all of the $A\beta_{40}$ fibril preparations, confirming the formation of insoluble material. Multiple comparison analysis showed no significant difference on insoluble material formation between these fibrils (Figure 3.12, B).

To confirm fibril formation in the 2A, 3Q and *de novo* $A\beta_{40}$ fibril preparations, negative stain TEM imaging was performed (Figure 3.13). Although analysis of fibrils through this method confirmed that fibrils had formed successfully for each of the fibril polymorphs, it was not possible to distinguish the twist observed in the 3Q structure by this technique. However, structural differences have been observed by solid state NMR spectroscopy for fibrils produced by elongation of 2A and 3Q fibrils from seeds (Paravastu et al., 2008; Petkova et al., 2005), as well as by GAG binding analysis between the fibril polymorphs, in which a specific binding sites for GAGs were revealed as well as distinct binding affinities for both the 2A and 3Qs (Madine et al., 2012). ^{13}C-^{13}C dipolar assisted rotational rationale ssNMR spectra obtained for preparations of 2A and 3Q fibrils produced in house have been reported to be consistent with the published structural models (Stewart et al., 2017) .

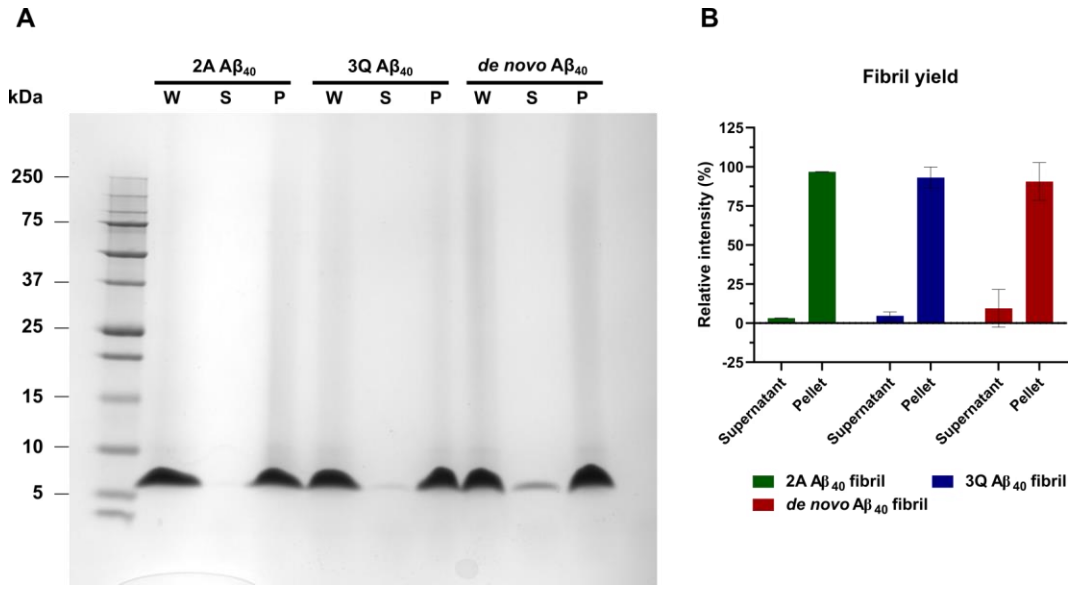

Figure 3.12. Fibril yields of the Aβ$_{40}$ fibril polymorphs.
The Aβ$_{40}$ fibril polymorphs formed were subjected to centrifugation at 14000 rpm (room temperature, Eppendorf 5418 rotor) for 35 minutes and subsequent separation of the pellet and supernatant fractions. A) SDS-PAGE analysis was done in a 15 % Tris-tricine gel for the whole (W), supernatant (S) and pellet (P) samples of the three fibril polymorphs to assess fibril yields. B) Densitometric quantification of the fibril yields showed that for the 3 polymorphs ~81-92% of the sample remained in the pellet, confirming the insoluble fraction formation after seeding with 2A or 3Q seeds, or de novo Aβ$_{40}$ fibril formation.

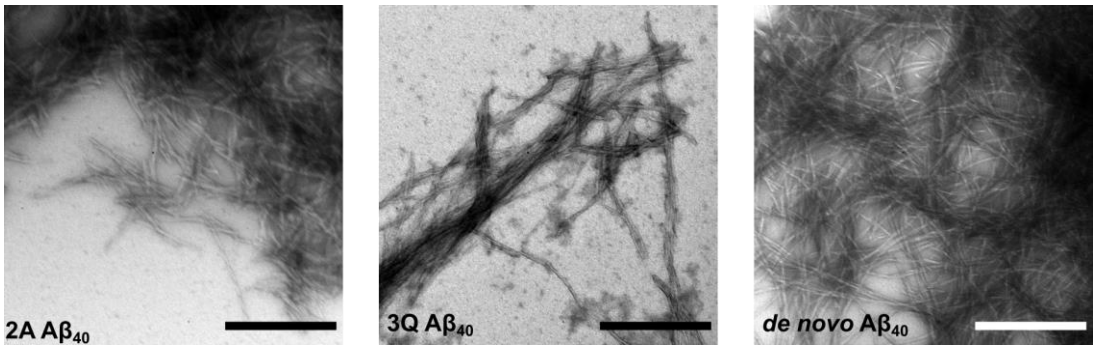

Figure 3.13. Electron micrographs of the Aβ$_{40}$ fibril polymorphs.
Negative stain TEM was performed on each of the fibril preparations. Scale bar is 500 nm.

Assessment of fibril polymorphism has been evaluated by analysis of curcumin dye binding. Heterogeneity of fibrils from brain derived α-synuclein amplifications from Parkinson's disease and MSA patients has been evaluated through curcumin dye binding. Structural differences, observed as emission spectra shifts, between *in vitro* generated fibrils and brain-derived amplifications, has been noted (Lau et al., 2020; Strohaker et al., 2019). Preliminary analysis of $A\beta_{40}$ fibril preparations using this method did not demonstrate spectra that were significantly different between the 2A, 3Q and *de novo* fibril preparations upon binding curcumin (Figure 3.14, A), although minor visual differences can be observed. However, two-way ANOVA of the mean curcumin fluorescence spectra (Tukey corrected) demonstrated statistically significant differences for the three $A\beta_{40}$ polymorphs in their binding capability to curcumin (Figure 3.14, B), proving to be a possible method to discern between the molecular structures of the $A\beta_{40}$ fibrils. Similarly, one-way ANOVA of the raw endpoint ThT fluorescence (Figure 3.15) showed a significant difference of the 2A with 3Q and *de novo fibrils*, but not between *de novo* and 3Q fibrils suggesting differences in available ThT binding sites, and structural morphologies (Table 3.2). Differences in ThT fluorescence intensities have been reported for WT α-synuclein fibrils when compared to its disease associated single point mutation A30P and A53T α-synuclein fibrils, as well as for α-synuclein fibrils cross-seeded with either fibrils from the A30P or A53T (Sidhu et al., 2018).

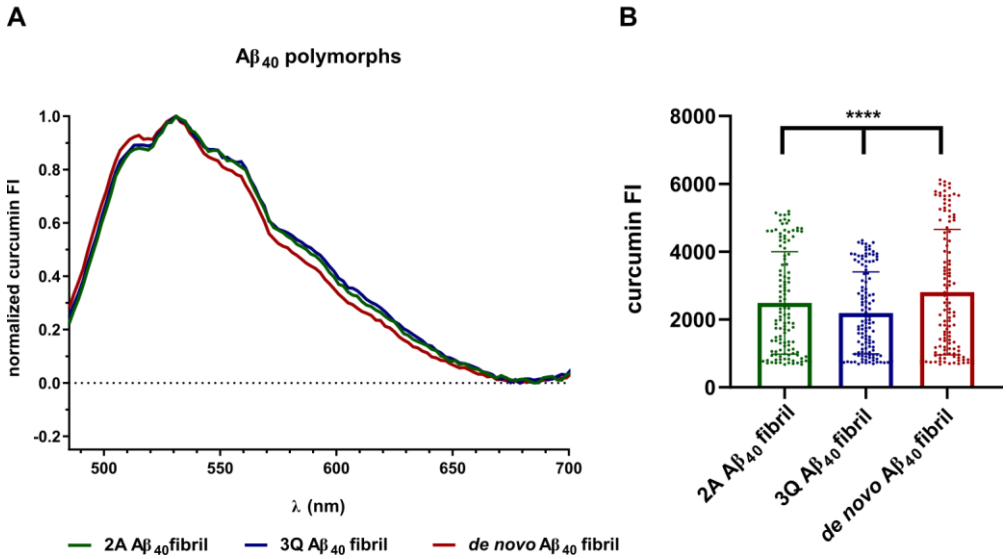

Figure 3.14. Curcumin dye binding to Aβ40 polymorphs.
*Analysis of the fluorescence spectrum of the 2A, 3Q and de novo Aβ40 upon binding to curcumin appeared to be different between the fibril polymorphs, however significance was not reached. B) In comparison, mean curcumin fluorescence intensity revealed to be significantly different between the three fibril polymorphs (Tukey multiple comparisons, **** p<0.0001).*

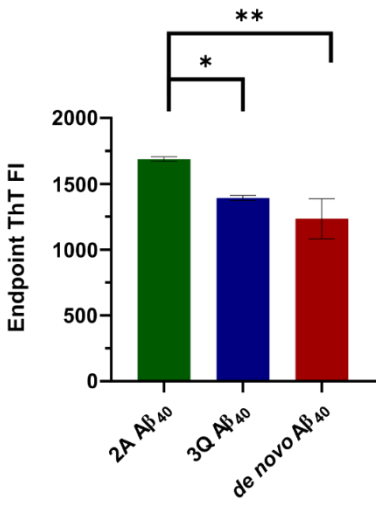

Figure 3.15. Endpoint ThT fluorescence of the Aβ40 polymorphs.
*Endpoint ThT fluorescence intensities of 5% seeded 2A and 3Q fibrils and de novo Aβ40 formed fibrils were significantly different (Tukey multiple comparison test, * p<0.05, ** p<0.005).*

Table 3.2. Significant differences of curcumin and ThT fluorescence observed between the Aβ40 fibril preparations.

	Significant difference	
	Curcumin	**ThT**
2A Aβ40 vs. 3Q Aβ40	Yes	Yes
3Q Aβ40 vs. *de novo* Aβ40	Yes	No
***de novo* Aβ40 vs. 2A Aβ40**	Yes	Yes

3.5.4 Aβ42 fibril generation at pH 2 and pH 8

Aβ42 fibrils used in this study were formed as described in Colvin et al (2016) and Gremer *et al.* (2017), using buffers at pH 2 and pH 8, at room temperature and under quiescent conditions. Fibrillation was followed by ThT fluorescence analysis for 100 h for fibrils formed at pH 2 (Figure 3.16, A), and until plateau occurred for pH 8 fibrils (Figure 3.16, B). Differences were observed in each of the fibril's half-times (Table 3.3) and their calculated lag times were 15.3 h and 0.73 h, for pH 2 and pH 8 fibrils, respectively.

To confirm fibril formation, negative stain TEM imaging was performed for the two Aβ42 fibril preparations (Figure 3.16, C and D). Although some visual differences can be observed between

the fibrils, e.g. rounder-shaped like pH 2 fibrils compared to pH 8 Aβ42 fibrils, analysis of mean ThT fluorescence intensity (Figure 3.17) revealed that the pH 8 showed a significantly higher fluorescence.

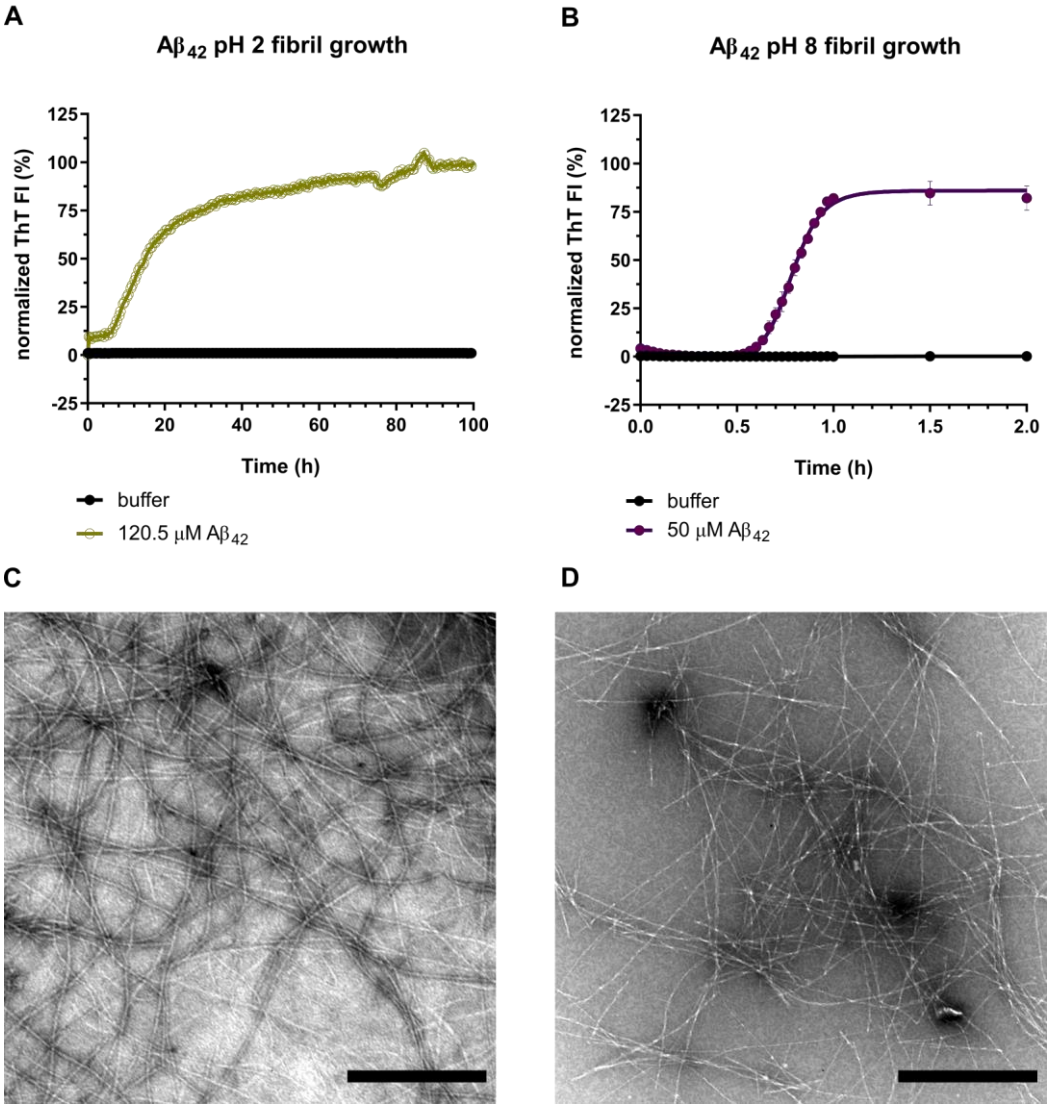

Figure 3.16. Fibrils of Aβ42 grown at pH 2 and pH 8.
Analysis of ThT kinetics of pH 2 (A) and pH 8 (B) fibrils of Aβ42 showed a lag time of 0.73 h for the Aβ42 fibrils formed at pH 8 (50 μM) and 15.36 h for the fibrils formed at pH 2 (120.5 μM). Negative stain TEM of the samples after 24 h of incubation revealed the formation of fibrils (C, pH 2, D pH 8). Scale bar is 500 nm. Experiment done in duplicates (Mean ± S.D.)

Table 3.3. Half times of Aβ42 fibrils formed at pH 2 and pH 8.

	Half time (h)
pH 2 Aβ42 fibril	15.6 ± 0.23
pH 8 Aβ42 fibril	0.78 ± 0.005

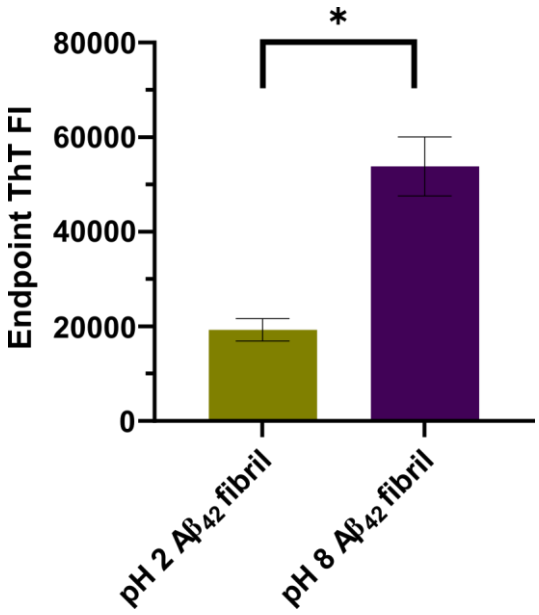

Figure 3.17. Endpoint ThT fluorescence of Aβ$_{42}$ fibrils.
*Endpoint ThT fluorescence intensities of the pH 2 and pH 8 Aβ$_{42}$ formed fibrils were significantly different. Experiment done in duplicates (Mean ± S.D., Tukey multiple comparison test, * p<0.05).*

3.6. Discussion

Here, methods of purification for the Aβ$_{40}$ and Aβ$_{42}$ peptides and fibril preparation were evaluated. The purification protocols used were quick and efficient in the production of both Aβ$_{40}$ and Aβ$_{42}$ peptides. Although both methods are relatively affordable and can be easily scaled up, advantages of HPLC over anion exchange and SEC purification are noted, as the time to purify the peptide decreased from 3 weeks to 1 week and purified peptide yield was double. HPLC has been proposed a cost-effective method of purification that renders high-quality recombinant proteins (Dammers et al., 2015; Warner et al., 2017; Yoo et al., 2018).

After validation of peptide purity by mass spectrometry and SDS-PAGE, fibril formation was performed and verified through fluorescence spectroscopy, biochemical and imaging techniques. ThT fluorescence analysis and fibril yields of the Aβ$_{40}$ and Aβ$_{42}$ fibril polymorphs was consistent with β-sheet and insoluble material formation. Kinetic ThT analysis showed that plateauing occurred within 24 h for all Aβ$_{40}$ or Aβ$_{42}$ fibril growth. However, noted differences in half times and lag times are seen between *de novo* Aβ$_{40}$, pH 8 and pH 2 Aβ$_{42}$ (Tables 3.2 and 3.3), showing 6 h, 0.73 h and 15 h lag times, respectively.

Confirmation of fibrillation after seeded (2A and 3Q $A\beta_{40}$) or *de novo* (*de novo* $A\beta_{40}$, pH 2 $A\beta_{42}$, pH 8 $A\beta_{42}$) fibril formation was done by and TEM imaging, although no specific differences were distinguishable through this technique. The inability to discern the fibril twist present in the 3Q $A\beta_{40}$ fibril preparations has been noted in the past, however it has also been confirmed that the dipolar assisted rotational rationale ssNMR spectra correspond to the ones originally published regardless of this caveat (Stewart et al., 2017).

Nevertheless, variation in curcumin fluorescence was observed between the three $A\beta_{40}$ polymorphs, a dye recently used to observe polymorphism of brain derived in vitro generated α-synuclein fibrils (Strohaker et al., 2019). Differences between 2A's with 3Q's and *de novo*'s mean ThT fluorescence intensity were also noted, but not between 3Q's and *de novo*'s mean ThT fluorescence intensity. In the same manner, marked significant differences in the mean ThT fluorescence intensities were observed between the $A\beta_{42}$ fibrils formed at pH 2 and pH 8. It is known that pH can influence the fluorescent spectra of organic compounds (Hope et al., 2016) and therefore caution should be taken when assessing the two $A\beta_{42}$ fibrils through this method.

ssNMR analysis of the interaction between curcumin and $A\beta_{42}$ fibrils showed that curcumin interacts with residues 12, and 17−21 of the peptide (Masuda et al., 2011). Molecular dynamics simulations and docking of curcumin to $A\beta_{42}$ fibrils (PDB 2MXU) showed that binding occurred through contacts of the aromatic rings of the molecule to residues V12 - F20 of the first and second monomer of the fibril, as well as residues I32 - L34 of the fourth and fifth monomer of the fibril, in a non-disruptive way (Jakubowski et al., 2020). These sites correspond to the most common β-strand locations in the Aβ fibril structures.

Curcumin fluorescence intensity variations between the fibril polymorphs might occur due to differences in the number of β-strands and the position they adopt in the fibril structure of the distinct polymorphs (i.e. exposed in some structures, or hidden within the fibril core and inaccessible to the fluorescent probe/molecule). Differences in ThT fluorescence intensity might be accounted by the same reason, as ThT binds parallel to the fibril axis, between the fibril β-strands (Krebs et al., 2005) and preferentially interacting with channels formed by aromatic residues in the side chains (Biancalana and Koide, 2010). Validation of these results could be done with the use of other structural techniques, as well as other molecular probes. Fibril polymorphism has recently been evaluated with luminescent conjugated oligo- and polythiophenes. These molecules are thought to possess the same binding site as Congo red, but in contrast to it, are known to have a twistable thiophene backbone that upon restriction a different emission profile is observed (Fandrich et al., 2018). This feature can be seen as an optical fingerprint of a specific molecule and proven useful tool for fibril polymorphism characterisation.

Hence, these results suggest the presence of variation in structural conformations, observed through binding site availability for curcumin and ThT, in the $A\beta_{40}$ fibril types, but further investigation is required for the validation of all 5 fibril types.

In the following chapters the Aβ fibril preparations formed here will be used to study their interaction with purified α-synuclein in vitro as well as in cells.

4. Cross-seeding analysis of α-synuclein fibril formation by Aβ fibrils

4.1. Introduction

A growing body of evidence highlights the overlap of pathologies in neurodegenerative diseases. α-synuclein is an intrinsically disordered protein that is involved in the maintenance and supply of synaptic vesicles for neurotransmitter release and synaptic plasticity (Lashuel et al., 2013; Spillantini and Goedert, 2018). Parkinson's disease and other Lewy body diseases are characterised by the deposition of intraneuronal inclusions of misfolded α-synuclein (Spillantini et al., 1997). However, it is known that a region of α-synuclein, encompassing residues 61 - 95, also known as the non-amyloid-β-component, or NAC region, is commonly found in Aβ plaques in Alzheimer's disease (Twohig and Nielsen, 2019; Hurtig et al., 2000; Jensen et al., 1997). This interaction between α-synuclein and Aβ has been further investigated in Alzheimer's disease pathology and Lewy body spectrum disorders. In a retrospective study, Irwin et al. (2017) examined symptoms, onset, genetic and neuropathological features in a cohort of Alzheimer's disease cases with autopsy-confirmed α-synucleinopathy. They found that increasing levels of neurofibrillary tangles, composed of tau tangles, and neuritic Aβ plaques, were associated with a higher degree of α-synuclein pathology, after assessment by immunohistochemistry and assignment of a semiquantitative global cortical score for burden of Lewy bodies and Lewy neurites (Irwin et al., 2017; Hurtig et al., 2000). Assessment of Alzheimer's patients also revealed that the mean age at death occurs at a younger age in those cases who presented Lewy body pathology when compared to those who did not present Lewy body deposition, additionally the presence of Lewy body was associated with having at least one *APOE ε4* allele, a risk factor for Alzheimer's disease (Chung et al., 2015).

Amyloid fibrils can act as seeds that initiate the polymerisation of monomers. Typically, homologous seeding leads to a reduction in the lag-time and half-times of the aggregation reaction when assessed by ThT binding kinetic assays (Arosio et al., 2015). However, the interaction between misfolded proteins of different sequences can occur in disease (Morales et al., 2013). Examples of heterologous seeding, or cross-seeding, between amyloidogenic proteins have been described extensively (Guo et al., 2013; Sarell et al., 2013; Watanabe-Nakayama et al., 2020; Young et al., 2017). Moreover, the cross-talk between α-synuclein and Aβ has been described *in vivo* models (Masliah et al., 2001), where the co-overexpression of human α-synuclein and the APP protein in mice led to the generation of higher order α-synuclein oligomeric species, as well as a higher number of Lewy body-like inclusions in the cortex of mice. *In vitro*, α-synuclein fibrils

are known to act as catalysts of Aβ aggregation at neutral pH (Chia et al., 2017). Cross-seeding of α-synuclein monomer by Aβ fibrils has also been described *in vitro* (Ono et al., 2012). In their study, Ono et al (2012) showed that α-synuclein fibril formation occurs at a faster rate in the presence of preformed fibrils of synthetic α-synuclein, $A\beta_{40}$ or $A\beta_{42}$ when analysing cross-seeding with Thioflavin S (ThS) binding kinetics. In their experiments, the presence of oligomers and fibrils, whether they were from $A\beta_{40}$, $A\beta_{42}$ or α-synuclein, promoted the aggregation of α-synuclein monomer and fibril formation. In addition, they observed that both $A\beta_{40}$ and $A\beta_{42}$ monomer were cross-seeded by fibrillar α-synuclein fibrils and presented a reduced lag-time when compared to the unseeded $A\beta_{40}$ and $A\beta_{42}$ monomers.

Co-aggregation of α-synuclein and Aβ monomers has also been described *in vitro*. In their ThT kinetic binding experiments, Koppen and collaborators (Koppen et al., 2020) observed a reduction in the lag time of α-synuclein's aggregation kinetics in the presence of 1 μM monomeric $A\beta_{42}$ and pyroglutamated Aβ(3-42) monomers compared to un-seeded wild-type (WT) α-synuclein (55 μM) at neutral pH. Fibril formation was confirmed by immuno-gold TEM, but the presence of a specific morphology of fibril was not possible to discern through this method, nor were the presence of co-polymers, or fibrils formed by both Aβ and α-synuclein. Differing evidence of this interaction has been noted by Chia et al. (2017). In their study, they observed that the α-synuclein monomer (0.1 – 1 molar equivalents) acted as an inhibitor of $A\beta_{42}$ aggregation, whereas the α-synuclein seeds accelerated the rate of aggregation of the $A\beta_{42}$ monomer at pH 8. These events are suggested to occur by the inhibition of binding between misfolded monomeric $A\beta_{42}$ to the surface of newly formed fibrils of $A\beta_{42}$ by monomeric α-synuclein and impede the catalysis of formation of new nuclei in its surface, otherwise known as secondary nucleation. No α-synuclein aggregation was observed within the time analysed.

The cross-interaction between Aβ and α-synuclein is emphasised in these previous studies, nonetheless, the molecular mechanism by which the synergistic effect between α-synuclein and Aβ fibrils occurs in pathology has yet to be fully characterised. Moreover, it is still unknown whether different Aβ polymorphs promote α-synuclein aggregation to differing extents. Here, making use of the different fibrillar $A\beta_{40}$ and $A\beta_{42}$ fibril preparations, the effect on α-synuclein aggregation is analysed in *in vitro* biochemical assays.

4.2. Binding of Aβ fibrils and α-synuclein monomer at pH 7.4

An *in vitro* fluorescence polarization assay was set up to analyse the binding of the $A\beta_{40}$ fibril preparations to α-synuclein monomer (kindly provided by Dr Matt Jackson). Fluorescence

polarization is based on the random tumbling of particles in solution and the particles' size. As the fluorescent dye in the labelled molecule is excited, only those particles oriented within the same range of where polarized light was applied will be able to emit polarized light. The larger the particle is, the slower the tumbling it has in solution and the higher the possibility of emitting light with respect of the polarization plane (Montagnaro et al., 2008; Rossi and Taylor, 2011). For this assay, Alexa-488 labelled monomeric α-synuclein and monomeric α-synuclein were incubated with 0.5 - 10 μM (monomer equivalent) $A\beta_{40}$ fibril polymorphs in PBS at pH 7.4. If binding occurs between the small fluorescent α-synuclein monomer and the Aβ fibrils an increase in polarized light, or polarization value, would be apparent.

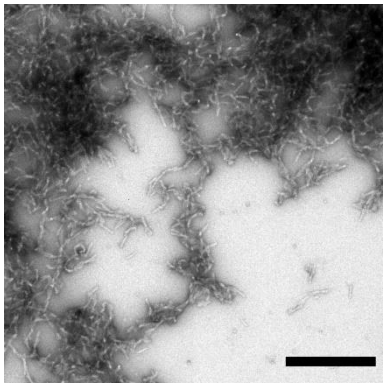

Figure 4.1. α-synuclein short fibrils (seeds).
α-synuclein fibrils (seeds) were formed by 48 h of stirring at 37°C on a heat plate. These method renders fibrils of an average length of 50 nm. Scale bar 500 nm.

After 10 minutes of incubation at room temperature, fluorescence polarization was measured. An increase in fluorescence polarization was observed as the concentration of $A\beta_{40}$ fibril preparations or α-synuclein ~50 nm long short fibrils kindly provided by Mike Davies (Figure 4.1), from here onwards referred as seeds, increased (Figure 4.2). On the other hand, the incubation of the labelled α-synuclein with 0.5 – 5 μM of the monomeric $A\beta_{40}$ did not result in a significant increase of fluorescence polarization signal. These data demonstrate that $A\beta_{40}$ fibrils bind to α-synuclein monomer, but this binding was not significantly different between the $A\beta_{40}$ fibril preparations.

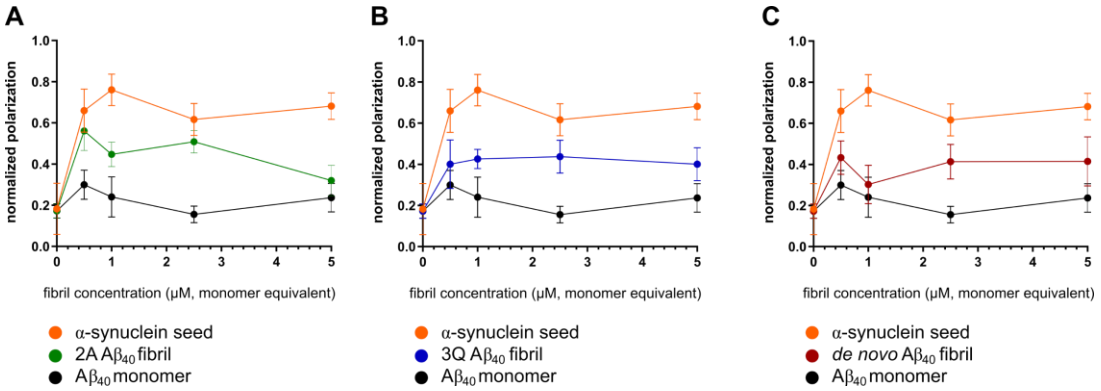

Figure 4.2. Binding of Aß fibril polymorphs with α-synuclein monomer.
Fluorescence polarization assay was set up to analyse binding between the $A\beta_{40}$ fibril preparations and α-synuclein monomer. 20 μM α-synuclein monomer was incubated with 0.05 μM α-synuclein monomer-Alexa 488 and increasing concentrations of either 2A (A), 3Q (B) or de novo $A\beta_{40}$ fibril preparations (C). The α-synuclein short fibril and $A\beta_{40}$ monomer were used as controls. An increase in fluorescence polarization was noted after the addition of $A\beta_{40}$ fibrils at increasing concentrations, suggesting binding to the α-synuclein monomer. In contrast the $A\beta_{40}$ monomer did not present a significant increase in fluorescence polarization. For all fibril polymorphs the experiment was done in duplicates (N= 3, mean ± SEM).

4.3. Analysis of cross-seeding of α-synuclein monomer by $A\beta_{40}$ fibrils at pH 7.5

Previous experiments have shown the cross-seeding of α-synuclein monomer by $A\beta_{40}$ and $A\beta_{42}$ fibrils at pH 7.4 (Ono et al., 2012), a pH present in the cerebrospinal fluid (Messeter and Siesjo, 1971). However, the impact of fibril polymorphism on cross-seeding has not been described to date. To analyse if the extent of cross-seeding is differential between the $A\beta_{40}$ fibril preparations, ThT fluorescence kinetics analysis was performed. For this 1% - 20% (v/v) of the 2A, 3Q or *de novo* $A\beta_{40}$ fibril preparations were added to 70 μM α-synuclein monomer and incubated at 37°C under agitative conditions for a 70h period in 25 mM sodium phosphate (pH 7.5). Unseeded α-synuclein and α-synuclein seeded with α-synuclein seeds at 1% - 20% (v/v) were set up in parallel as controls. The experimental data was fitted to a sigmoidal function $y = y_0 + A/(1 + \exp(-k(t - t_{0.5})))$, where the lag time is defined as $t_{lag} = t_{0.5} - 1/2k$ (Arosio et al., 2015).

Aggregation of α-synuclein monomer occurred in the presence of α-synuclein seeds, observed as an increase in ThT fluorescence intensity, whilst the unseeded monomer did not exhibit in an increase in fluorescence intensity over the timescale analysed (Figure 4.3, A, C and E). α-synuclein's rate of aggregation was increased when the concentration of α-synuclein seeds increased. No lag time was observed in the 20% and 5% (v/v) self-seeded reactions and the calculated half-times (Table 4.1) confirms that aggregation rate is faster for the 20% α-synuclein

seeded sample, followed by the 5% and 1% α-synuclein seeded samples. In marked contrast, the addition of any of the $A\beta_{40}$ polymorphs (Figure 4.3 B, D and F) resulted in no increase in fluorescence intensity and thus it can be concluded there was no aggregation into amyloid, at least over 70 h under these conditions.

After the ThT kinetic assay at pH 7.5, samples were subjected to a sedimentation assay, whereby samples were centrifuged for 35 minutes at 14000 rpm (room temperature, Eppendorf 5418 rotor) and further analysed by SDS-PAGE. The formation of insoluble pelleted material was observed and quantified by densitometry for the unseeded and self-seeded α-synuclein aggregation reactions (Figure 4.4). In the unseeded reaction, α-synuclein remained in the supernatant fractions and less than 5% became insoluble (Figure 4.4 A and B). Contrary to this, the self-seeded reaction showed that the majority of α-synuclein was insoluble and pelleted in the 5% (v/v) and 20% (v/v) self-seeded reactions, although ~20% of the sample could still be observed in the supernatant (Figure 4.4, C and D). The 1% (v/v) self-seeded reaction showed that ~50% of the α-synuclein was insoluble.

Different results were observed for the samples incubated with $A\beta_{40}$ fibrils. SDS-PAGE showed that most of the α-synuclein remained in the supernatant fraction after centrifugation (Figure 4.5 A, C and E). Densitometric quantification of the fibril yields (Figure 4.5 B, D and F) confirmed that < 10% of the α-synuclein was in the pellet fraction for these samples, while the other ~90% was observed in the supernatant fraction. The α-synuclein observed in the pellet could be residual α-synuclein soluble protein in the pellet fraction, as a similar percentage was in the pellet fraction in the unseeded α-synuclein sample.

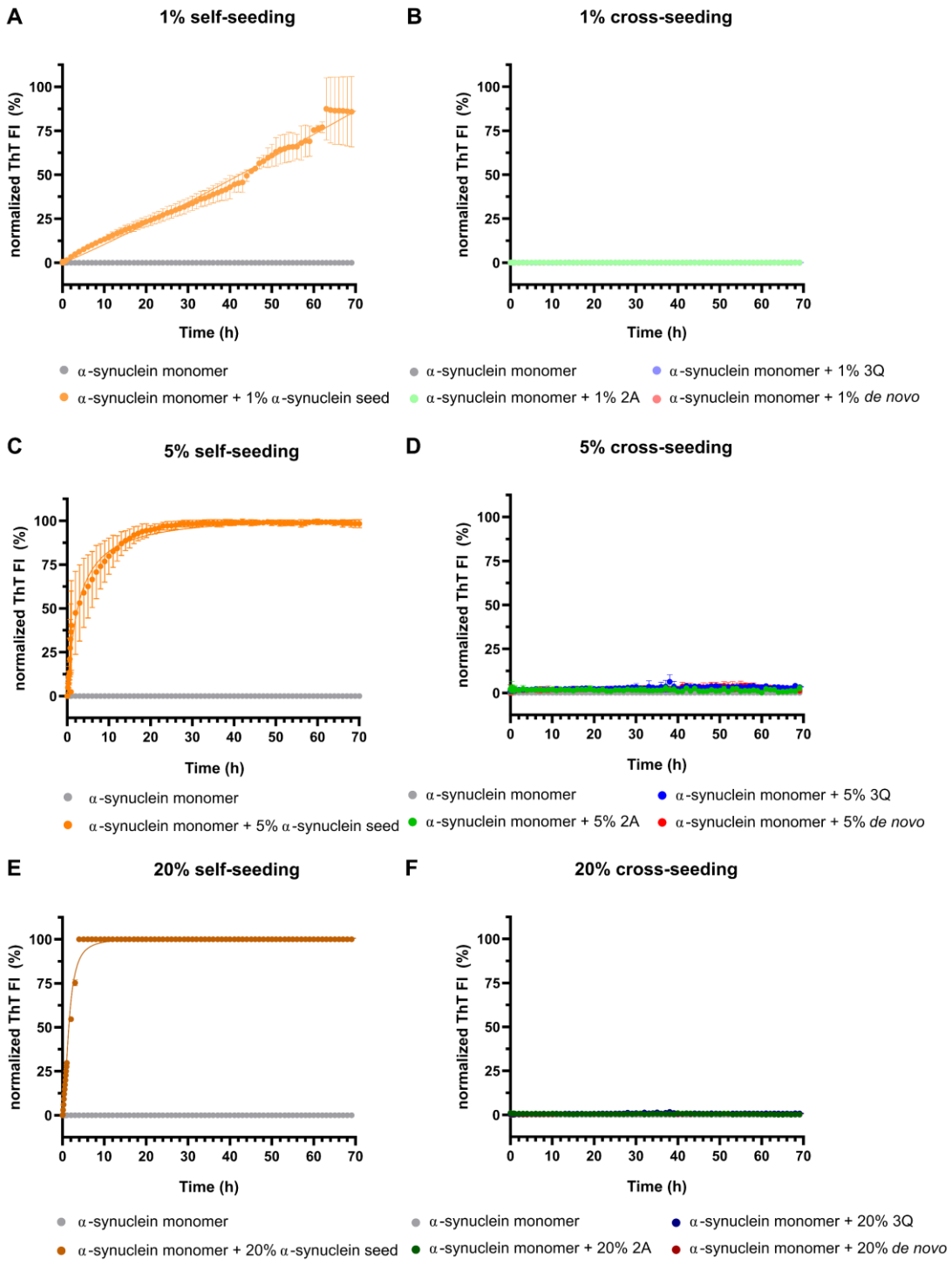

Figure 4.3. Cross-seeding analysis of α-synuclein monomer by $A\beta_{40}$ fibril polymorphs at pH 7.5.

ThT kinetic analysis of the unseeded α-synuclein (70 µM) and 1% (A), 5% (C) and 20% (v/v) (E) α-synuclein seeded reactions was done at pH 7.5 for 70 h. In parallel, ThT kinetics were followed for the α-synuclein cross-seeded with $A\beta_{40}$ polymorphs 2A, 3Q or de novo in a 1% (B), 5% (D) or 20% (F) (v/v) ratio. No increase in fluorescence intensity was observed for the unseeded α-synuclein, whereas adding α-synuclein seed at all concentrations reduced or abolished the lag time. No increase in fluorescence intensity was observed for any of the samples incubated with $A\beta_{40}$ fibrils. The experiment was done at least in duplicates for all conditions (N = 3, Mean ± S.D).

***Table 4.1* .Half-times of the α-synuclein aggregation reaction after adding 1%, 5% or 20% (v/v) α-synuclein seed.**

	Half-time (h)
α-synuclein monomer + 1% α-synuclein seed	39.3 ± 0.7
α-synuclein monomer + 5% α-synuclein seed	2.7 ± 0.1
α-synuclein monomer + 20% α-synuclein seed	1.5

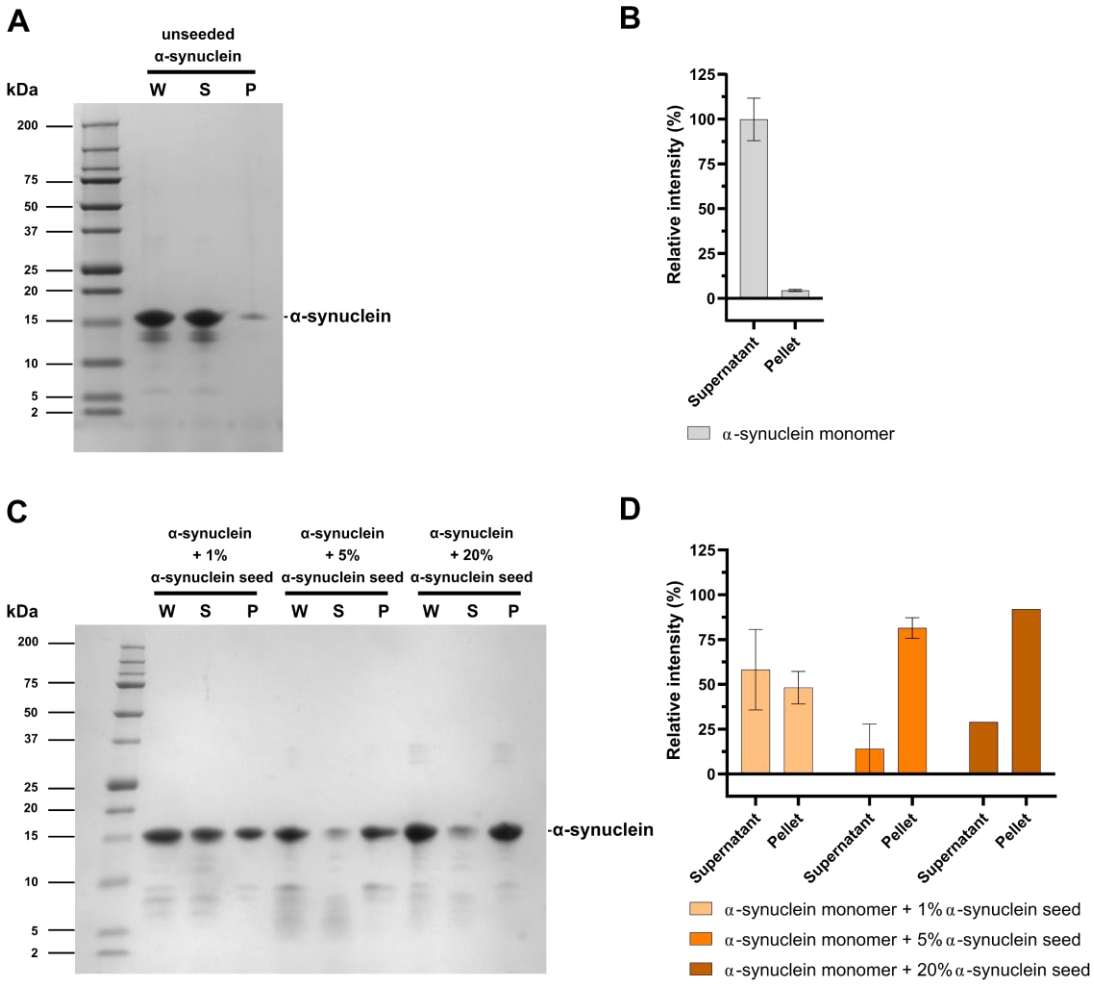

Figure 4.4. Fibril yields and densitometry of unseeded and self-seeded α-synuclein samples from the ThT kinetic assay of self-seeding of at pH 7.5.
After 70 h of incubation, the unseeded α-synuclein monomer (A) and the α-synuclein monomer incubated with 1% (v/v), 5% (v/v) or 20% (v/v) α-synuclein seed (C), were centrifuged and separated into pellet (P) and supernatant (S) fractions, whilst keeping an aliquot of the whole (W) sample. SDS-PAGE analysis was then done using a 15 % Tris-tricine gel. For the unseeded α-synuclein, most of the α-synuclein remained in the supernatant fraction, and a small fraction appeared to pellet. As for the 1%, 5% and 20% (v/v) self-seeded samples, the pellet contained most of the α-synuclein. Densitometric quantification of the fibril yields (B and D) confirmed that ~10% of α-synuclein was seen in the pellet in the unseeded α-synuclein samples. For the 1% self-seeded, half of the sample formed insoluble material, and >80% of the sample was insoluble for the 5% and 20% (v/v) self-seeded. The experiment was done at least in duplicates for all conditions (N = 3, Mean ± S.D).

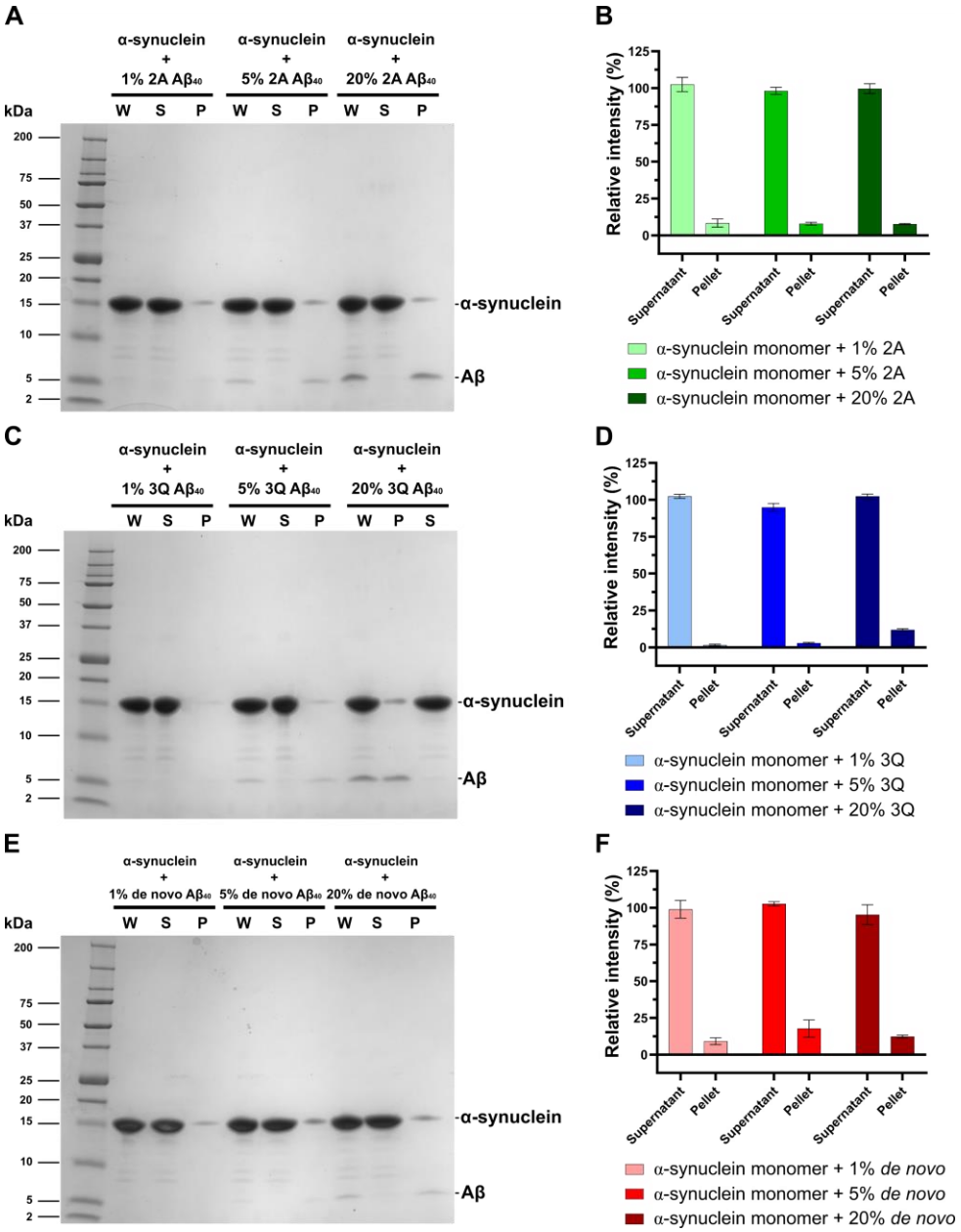

Figure 4.5. Fibril yields and densitometry of samples from the ThT kinetic assay of cross-seeding of α-synuclein monomer by $A\beta_{40}$ fibril preparations at pH 7.5.
After 70 h of incubation, α-synuclein monomer samples incubated with 1% (v/v), 5% (v/v) or 20% (v/v) 2A (A), 3Q (C) or de novo (E) $A\beta_{40}$ fibril preparation were centrifuged and separated into pellet (P) and supernatant (S) fractions, keeping an aliquot of the whole (W) sample. SDS-PAGE analysis was then done in a 15 % Tris-tricine gel. It was observed that most of the α-synuclein remained in the supernatant fraction, while the $A\beta_{40}$ fibril preparations remained insoluble as they were only observed in the pellet fraction after centrifugation. Densitometric quantification of the fibril yields (B, D and F) confirmed that ~80-90% of the α-synuclein in the samples co-incubated with the $A\beta_{40}$ fibrils remained in the soluble fraction in all cross-seeded samples. The experiment was done at least in duplicates for all conditions (N = 3, Mean ± S.D).

Negative stain transmission electron microscopy (TEM) of the samples after ThT kinetic analysis at pH 7.5 showed the presence of fibrils in the α-synuclein seeded sample (Figure 4.6). In contrast, the unseeded α-synuclein sample (Figure 4.6) and the α-synuclein monomer incubated with the different fibril preparations of $A\beta_{40}$ fibrils at different concentrations (Figure 4.7) exhibited large amorphous aggregates. Although it is not possible to confirm through TEM, the presence of fibrillar material in the α-synuclein samples incubated with $A\beta_{40}$ fibrils could be attributed to the $A\beta_{40}$ fibrils, as it was observed that $A\beta_{40}$ remained insoluble in the fibril yields (Figure 4.5). It is also noted that there was an absence of fibrils in the 20% (v/v) *de novo* sample, but this could be due to fibrils not attaching to the grid.

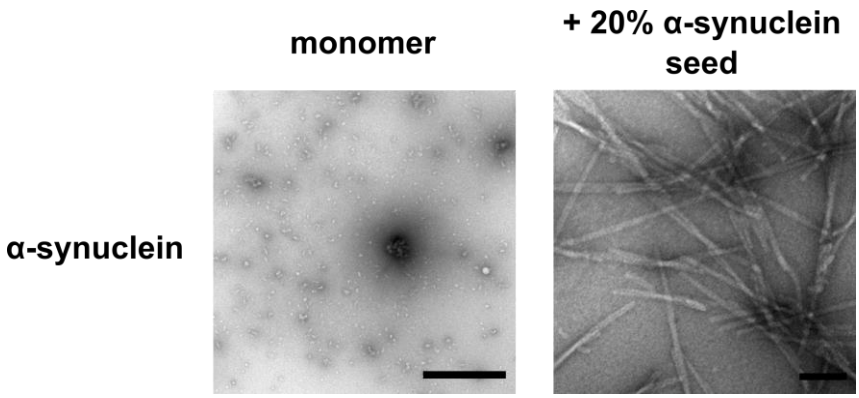

Figure 4.6. Electron microscopy imaging of unseeded α-synuclein monomer and self-seeded α-synuclein after ThT kinetics at pH 7.5.
After 70 h, ThT kinetic reactions were stopped and samples analysed by negative stain TEM. This confirmed the absence of fibrils in the unseeded sample, and the presence of fibrils in the 20% (v/v) self-seeded α-synuclein sample. Scale bar is 500 nm for the monomer and 100 nm for 20% (v/v) self-seeded sample.

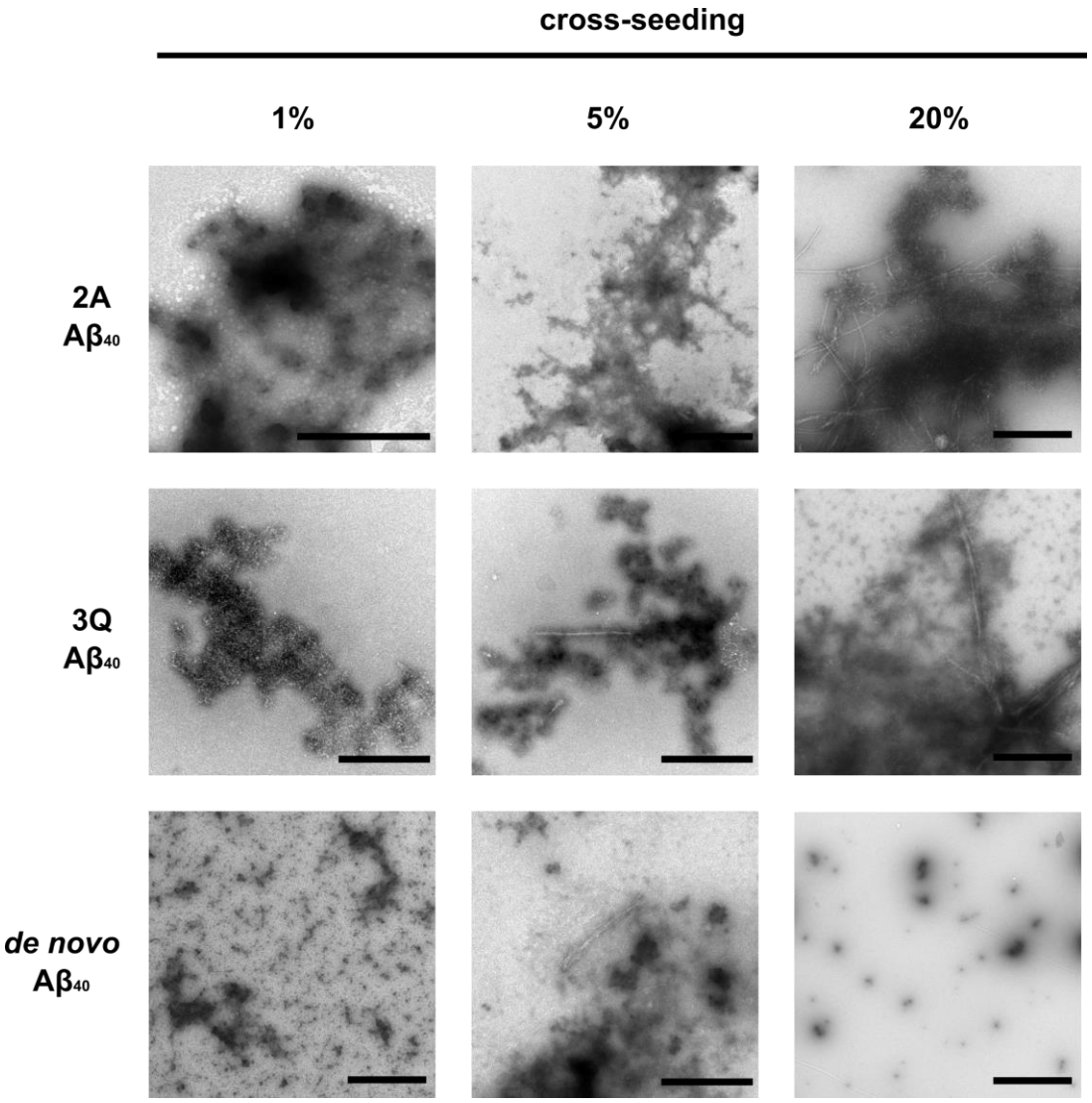

Figure 4.7. Electron microscopy imaging of α-synuclein monomer incubated with $A\beta_{40}$ fibrils after ThT kinetics at pH 7.5.

After 70 h, ThT kinetic reactions were stopped and samples analysed by negative stain TEM. This confirmed the minimal presence of fibrils in the samples after the incubation of α-synuclein with the 2A, 3Q and de novo $A\beta_{40}$ fibrils at 1% (v/v), 5% (v/v) and 20% (v/v) concentration. Scale bar is 500 nm.

As Ono et al (2012) had shown that α-synuclein could be cross-seeded by both $A\beta_{40}$ and $A\beta_{42}$ fibrils, a cross-seeding assay was set up using their experimental conditions. For this, 25 μM synuclein was incubated with at 10% (v/v) $A\beta_{40}$ fibril preparations at pH 7.4 and 37°C, in the presence of ThS, a dibenzothiazole derivative and homologous compound of ThT (Figure 4.8), that is commonly used for histological staining of Aβ plaques (Rodriguez-Rodriguez et al., 2010; Wu et al., 2006). As was observed at pH 7.5 with ThT, no increase in fluorescence intensity was seen after 70h for the unseeded α-synuclein monomer, nor the samples incubated with the $A\beta_{40}$ fibril preparations (Figure 4.9 A). Negative stain TEM showed the presence of amorphous aggregates in the samples, and the area of the grid analysed did not show the presence of any fibrillar material, although the presence of the Aβ fibrils cannot be excluded.

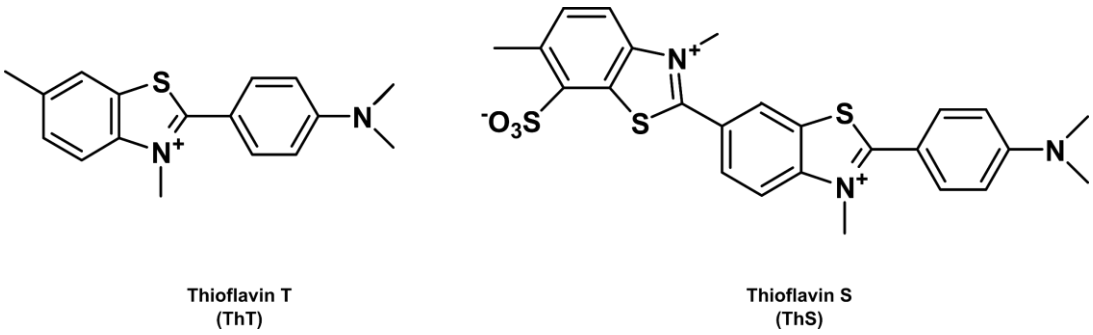

Figure 4.8. Molecular structures of ThT and ThS.
ThT and ThS are widely used amyloid dyes known to bind on the fibril surface, in grooves formed by side chains (adapted from Wu et al., 2006).

It can therefore be concluded that at neutral pH the aggregation of α-synuclein into amyloid fibrils was promoted by the addition of α-synuclein seeds. Conversely, those samples incubated with the $A\beta_{40}$ fibril preparations from this study did not cross-seed the aggregation of α-synuclein into amyloid fibrils by the endpoint of the experiment (70 h). The cross-seeding effect denoted by Ono et al., (2012), where they use synthetic peptide and pH 7.4 in a ThS reaction, could be due to the use of $A\beta_{40}$ fibril polymorphs different to the ones used in this study.

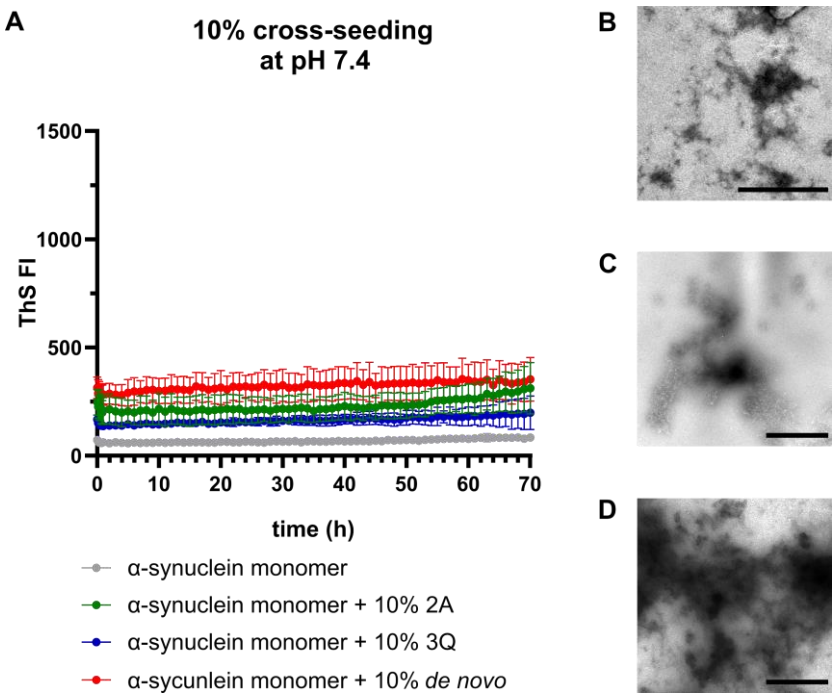

Figure 4.9. Cross-seeding analysis of α-synuclein monomer by Aβ$_{40}$ fibrils at pH 7.4.
ThS kinetic analysis after adding Aβ$_{40}$ polymorphs 2A, 3Q and de novo to 25 μM α-synuclein monomer in a 10% (v/v) cross-seeding ratio at pH 7.4, for 70 h (A). No increase in fluorescence intensity was observed after 70h for the unseeded α-synuclein, nor the samples incubated with Aβ$_{40}$ fibrils at all concentrations (Mean ± S.D). Negative stain TEM of the endpoint sample of the 10% (v/v) 2A (B), 3Q (C) and de novo (D) cross-seeded α-synuclein samples did not show fibrillar material. Scale bar is 500 nm.

4.4. Cross-seeding of α-synuclein monomer by Aβ$_{40}$ fibrils at pH 4.5

The interaction between Aβ$_{40}$ fibrils and the α-synuclein monomer was also examined at pH 4.5, another pH of physiological importance. The lysosome, has a pH of 4.5 in its lumen and contains proteolytic enzymes involved in degradation of proteins, including α-synuclein, which are delivered by the autophagic pathways (Mak et al., 2010). α-synuclein is known to readily aggregate into amyloid fibrils at pH 3 - 6 (Buell et al., 2014; Cho et al., 2009). Large aggregate internalization has been proposed to occur through phagocytosis and further channelled to the endolysosomal pathway in HEK-293 cells (Couceiro et al., 2015). At the same time, Aβ$_{40}$ and Aβ$_{42}$ peptides are suggested to accumulate in lysosomes in differentiated PC12 cells and induce toxicity (Liu, R.Q. et al., 2010).

To determine if cross-seeding occurred between the fibril preparations and α-synuclein at pH 4.5, 1% - 20% (v/v) 2A, 3Q or *de novo* Aβ$_{40}$ fibrils were added to 70 μM α-synuclein monomer and incubated at 37°C under agitative conditions for 50 h. As a control, self-seeded α-synuclein

aggregation was examined using 1% (v/v), 5% (v/v) or 20% (v/v) α-synuclein seed. ThT fluorescence was used to monitor amyloid formation.

An increase of ThT fluorescence was observed for the unseeded α-synuclein reaction after ~30 h and this plateaued after 50 h of incubation under these conditions (Figure 4.10). Incubation with 1% (v/v), 5% (v/v) or 20% (v/v) α-synuclein seed increased the rate of aggregation of α-synuclein; a reduction in the lag time for the 1% seeded (v/v) (Figure 4.10 A) and ablation of the lag time for the 5% (v/v) (Figure 4.10 C) and 20% (v/v) self-seeded (Figure 4.10 E) were observed.

For the α-synuclein samples incubated with 1% (v/v) $A\beta_{40}$ fibrils an increase in ThT fluorescence was observed and plateauing occurred after 50h, but no difference in the rate of aggregation was observed compared to the unseeded α-synuclein (Figure 4.10 B). In contrast the aggregation appeared to occur more quickly for the 5% (v/v) cross-seeded samples (Figure 4.10 D) and a marked reduction in the lag time as well as half time was observed for the 20% (v/v) cross-seeded samples (Figure 4.10 F, Table 4.2).

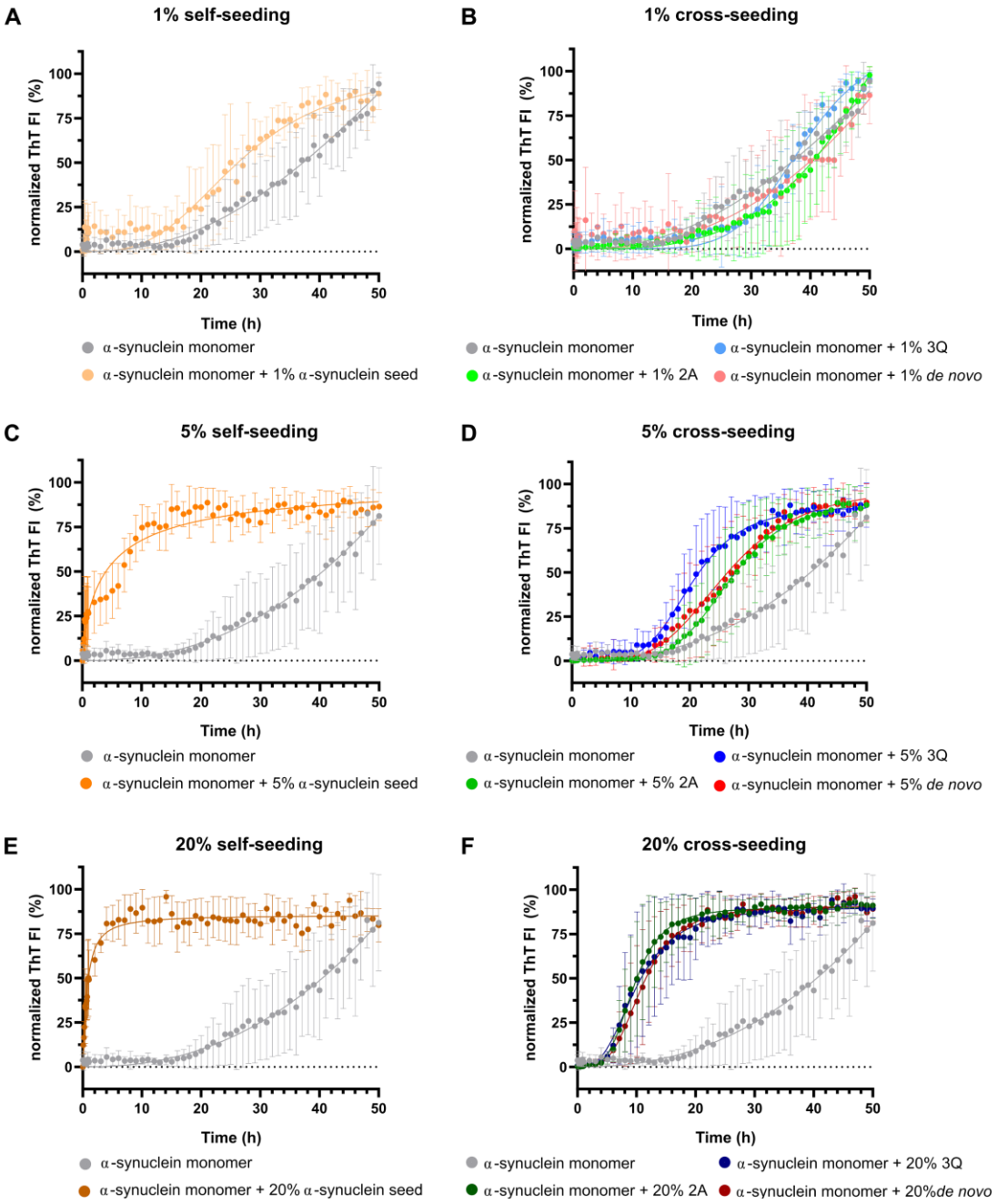

Figure 4.10. Cross-seeding analysis of α-synuclein monomer by $A\beta_{40}$ fibrils at pH 4.5.
ThT kinetic analysis of the unseeded α-synuclein (70 µM) and 1% (v/v) (A), 5% (v/v) (C) and 20% (v/v) (E) α-synuclein seeded reactions was done at pH 4.5 for 50 h. In parallel, ThT kinetics were followed for the α-synuclein cross-seeded with $A\beta_{40}$ polymorphs 2A, 3Q or de novo in a 1% (v/v) (B), 5% (v/v) (D) or 20% (v/v) (F) (v/v) ratio. The unseeded α-synuclein aggregated after ~20h; adding α-synuclein seed at all concentrations reduced or abolished the lag time. ThT kinetics showed an increase in fluorescence intensity after 50h for all the samples incubated with the $A\beta_{40}$ fibril preparations, at all concentrations. No difference in the lag time was observed for the 1% (v/v) cross-seeded samples compared to the unseeded α-synuclein. The lag time was reduced at 5% (v/v) and 20% (v/v) cross-seeding, but no apparent differences were observed between the fibril preparations. The experiment was done at least in duplicates for all conditions (Mean ± S.D).

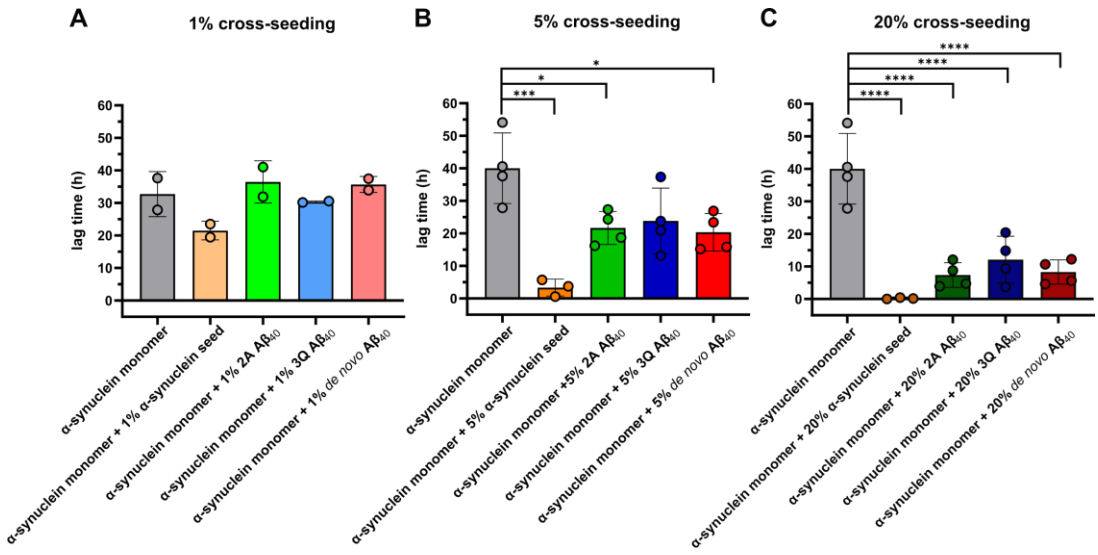

Figure 4.11. Lag time comparison of cross-seeded α-synuclein monomer by $Aβ_{40}$ fibril preparations at pH 4.5.
*No significant difference in lag times was observed for the samples cross-seeded at a 1% (v/v) concentration (A) compared to the unseeded α-synuclein. However, at a 5% (v/v) cross-seeding concentration (B) a reduction in lag time was observed for the samples cross-seeded with 2A and de novo $Aβ_{40}$ as well as samples seeded with α-synuclein seed. A significant reduction in lag time was observed in the 20% (v/v) $Aβ_{40}$ fibril cross-seeded and α-synuclein seeded sample (C). Mean ± S.D. Significance level after ANOVA with Tukey multiple comparison test: * $p<0.05$, *** $p<0.001$, **** $p<0.0001$.*

Table 4.2. Half-times and lag-times of the α-synuclein aggregation reaction after 20% (v/v) α-synuclein seeding and cross-seeding with $Aβ_{40}$ fibrils at pH 4.5.

	Half-time (h)	Lag-time (h)
	Mean ± S.D.	Mean ± S.D.
αsynuclein monomer	43.69 ± 10.5	40.04 ± 9.4
αsynuclein monomer + 20% 2A	10.1 ± 2.66	7.38 ± 3.28
αsynuclein monomer + 20% 3Q	14.9 ± 6.5	12.08 ± 6.23
αsynuclein monomer + 20% *de novo*	10.86 ± 2.9	8.29 ± 3.23
αsynuclein monomer + 20% αsynuclein seed	0.78 ± 0.42	-

ANOVA and multiple comparison of the lag times (Figure 4.11) showed there was no significant difference between the lag time of the unseeded α-synuclein when compared to the samples incubated with 1% (v/v) $Aβ_{40}$ fibril preparations. In contrast a significant decrease in the lag time was observed for the 5% (v/v) 2A and *de novo* cross-seeded samples compared to the un-seeded α-synuclein. Multiple comparisons of the lag times showed that all 20% (v/v) cross-seeded

samples were significantly different from the unseeded α-synuclein reaction (Figure 4.11 C), but the lag times were not significantly different between the $A\beta_{40}$ fibril polymorphs.

After the ThT kinetic analysis at pH 4.5, insoluble material and fibril formation was analysed by SDS-PAGE and negative stain TEM. A shift from soluble to insoluble material could be seen at the endpoint of the samples at pH 4.5. Both the unseeded α-synuclein (Figure 4.12 A), as well as α-synuclein in the samples incubated with the different concentrations of α-synuclein seed (Figure 4.12 C) were pelleted after centrifugation. It was noted that ~85% and ~95% of α-synuclein in the sample was insoluble and observed in the pellet respectively in the unseeded α-synuclein reaction (Figure 4.12 B) and α-synuclein seeded reaction (Figure 4.12 D), respectively. Negative stain TEM of the α-synuclein seeded samples as well as the unseeded samples confirmed the presence of fibrils (Figure 4.13).

Furthermore, α-synuclein in samples that were cross-seeded with $A\beta_{40}$ fibril preparations (Figure 4.14 A, C and E) formed insoluble material that was pelleted after centrifugation. The pellet fraction also contained $A\beta_{40}$ (~5 kDa) from the fibrils that were introduced at the beginning of the experiment. Negative stain TEM (Figure 4.15) demonstrated that this insoluble material was in fact fibrillar material, as mostly fibrils were observed through the whole sample analysed. No discernible differences were noted between the fibrils formed from cross-seeding and self-seeding, mostly because in all samples the fibrils appeared highly clumped. In the same manner, $A\beta_{40}$ fibrils could not be distinguished from α-synuclein fibrils in the cross-seeded samples through this method.

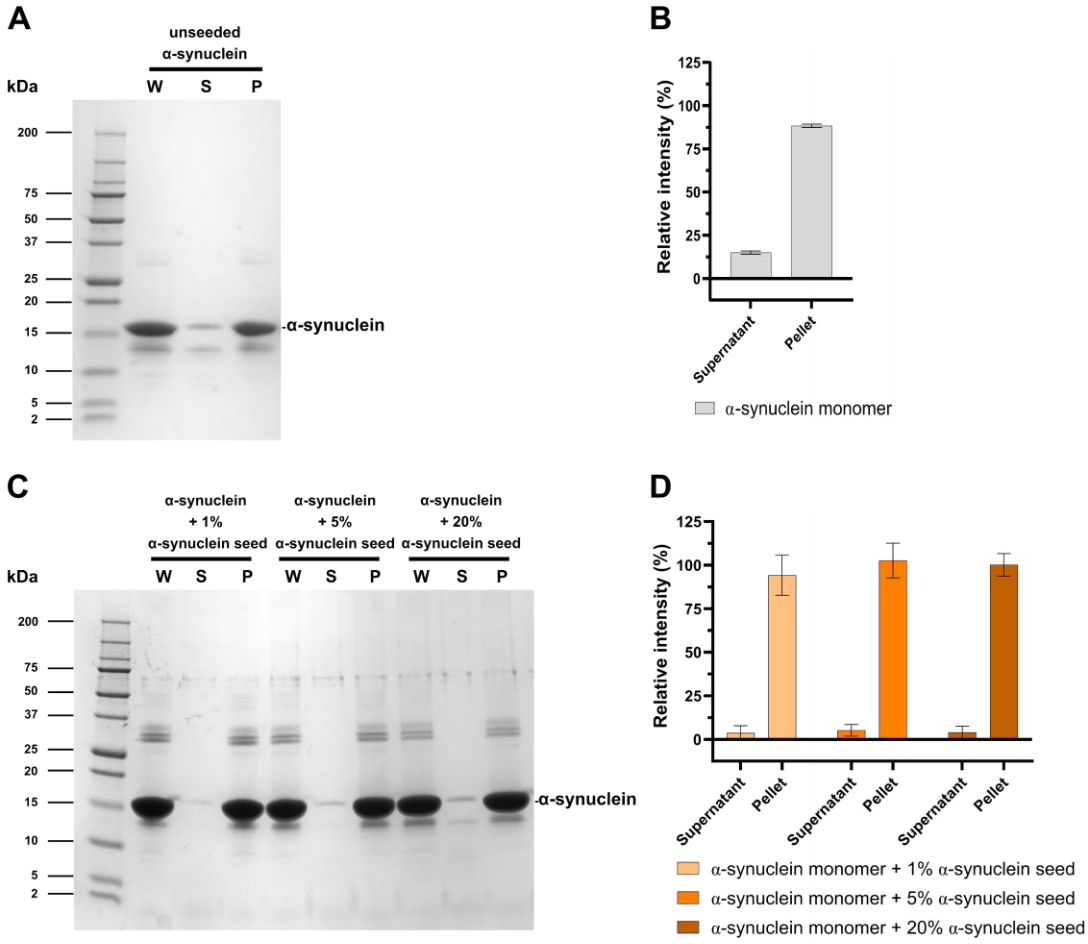

Figure 4.12. Fibril yields of samples from the ThT kinetic of unseeded and self-seeding of α-synuclein at pH 4.5

After 50h of incubation, the unseeded α-synuclein monomer (A) and the α-synuclein monomer incubated with 1% (v/v), 5% (v/v) or 20% (v/v) α-synuclein seed (C), were centrifuged and separated into pellet (P) and supernatant (S) fractions, whilst keeping an aliquot of the whole (W) sample. SDS-PAGE analysis was then performed on a 15 % Tris-tricine gel. Insoluble pelleted α-synuclein was observed on both the unseeded sample (A) and seeded samples (C). Densitometric quantification of the fibril yields (B and D) confirmed the formation of insoluble α-synuclein, as ~90% of the α-synuclein was in the pellet fraction. N=3, Mean ± S.D.

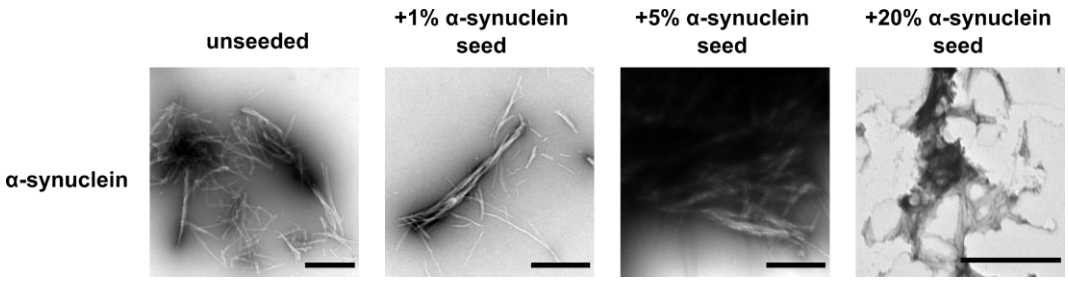

Figure 4.13. Electron microscopy imaging of samples after self-seeding of α-synuclein monomer at pH 4.5.

Negative stain TEM confirmed the presence of fibrils in the unseeded and self-seeded samples after ThT kinetic assays at pH 4.5. Highly clumped fibrils were visible in all samples. Scale bar is 500 nm.

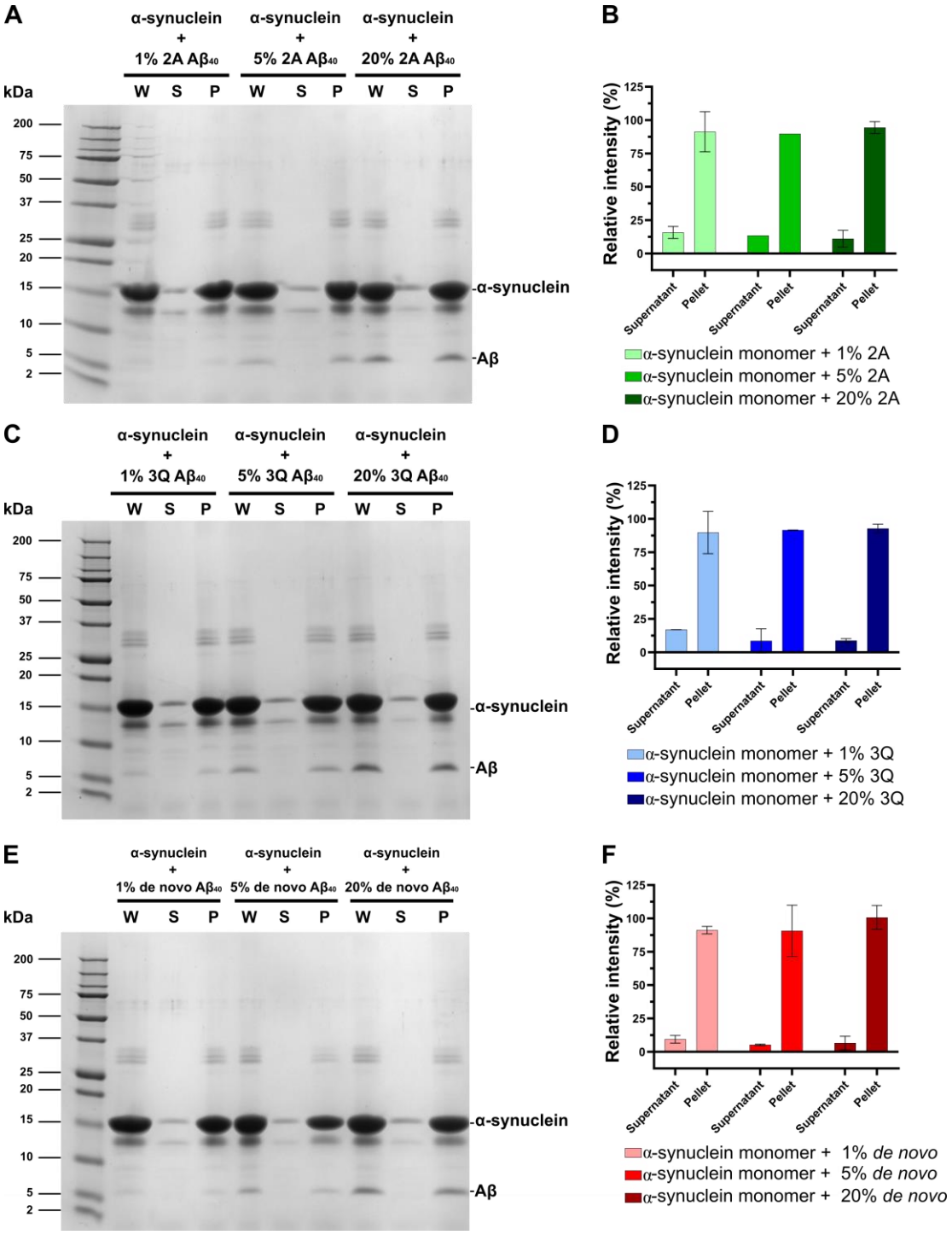

Figure 4.14. Fibril yields of samples from the ThT kinetic assay of cross-seeding of α-synuclein monomer by $Aβ_{40}$ fibril preparations at pH 4.5.

After 50 h of incubation, α-synuclein monomer samples incubated with 1% (v/v), 5% (v/v) or 20% (v/v) 2A (A), 3Q (C) or de novo (E) $Aβ_{40}$ fibril preparations were centrifuged and separated into pellet (P) and supernatant (S) fractions, keeping an aliquot of the whole (W) sample. SDS-PAGE analysis was then done in a 15 % Tris-tricine gel. It was observed that α-synuclein formed insoluble material after incubation with all of the $Aβ_{40}$ fibril preparations and at all concentrations, and the $Aβ_{40}$ fibrils remained insoluble. Densitometric quantification of the α-synuclein fibril yields (D, E and F) confirmed the formation of insoluble material of α-synuclein, as more than 90% of the α-synuclein was in the pellet fraction. N=3, mean ± S.D.

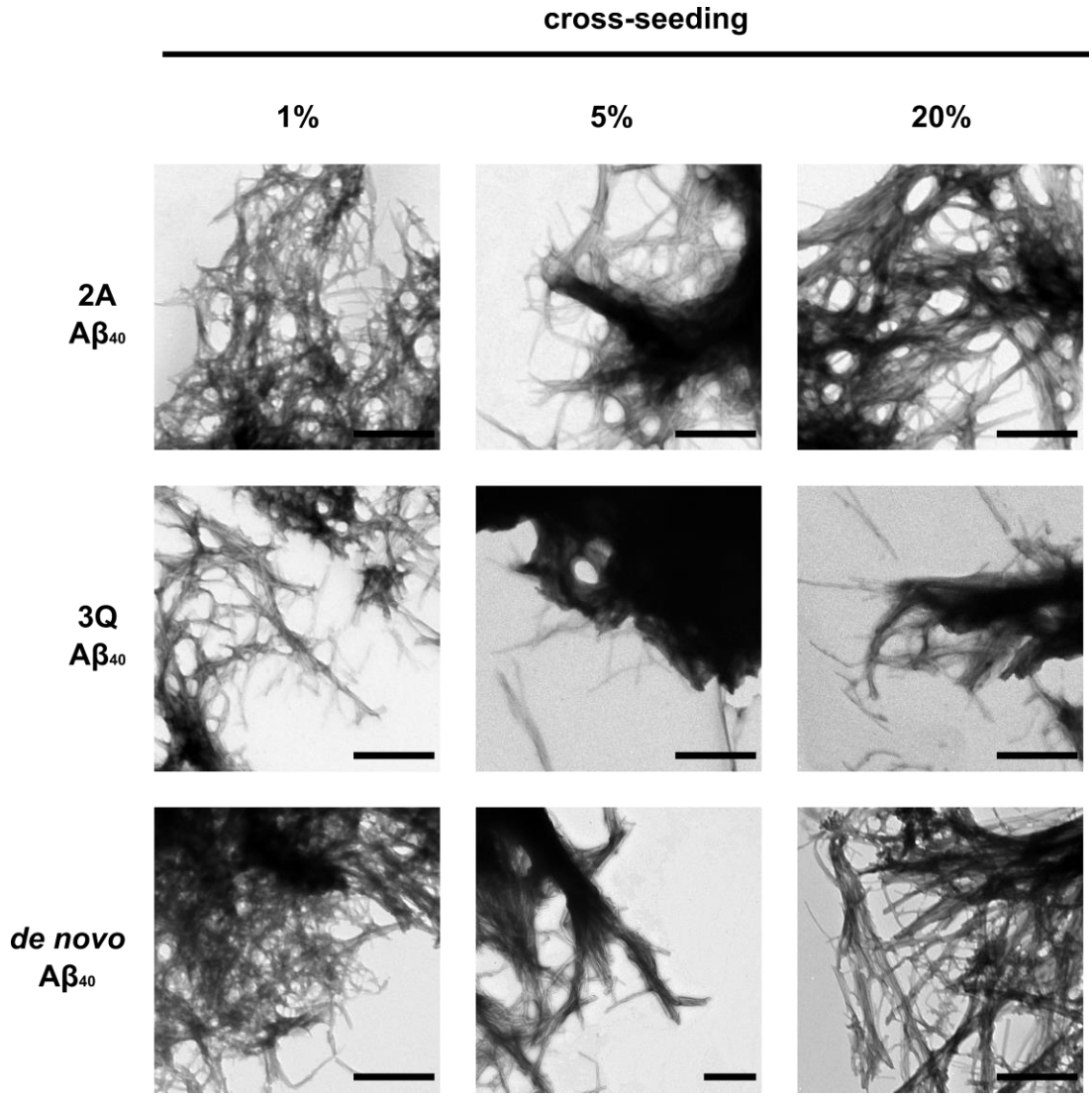

Figure 4.15. Electron microscopy imaging of samples after cross-seeding of α-synuclein monomer by $A\beta_{40}$ fibrils at pH 4.5.
After ThT kinetic reactions were completed, negative stain TEM confirmed the presence of fibrils in the samples after the cross-seeding of α-synuclein by the 2A, 3Q or de novo $A\beta_{40}$ fibrils at 1% (v/v), 5% (v/v) and 20% (v/v) concentration. Scale bar is 500 nm.

Taken together, these results suggest there is a pH dependence in the cross-seeding of α-synuclein by $A\beta_{40}$ fibril preparations. The cross-seeding of α-synuclein aggregation by the presence of $A\beta_{40}$ fibril preparations occurred at pH 4.5, observed as a reduction of the lag time in the ThT fluorescence. Negative stain TEM confirmed that this aggregation resulted in insoluble fibrillar material.

These results show that multiple fibril preparations of $A\beta_{40}$ can cross-seed α-synuclein and form amyloid at pH 4.5, and it is not a phenomenon specific to one fibril type. However cross-seeding is not observed at neutral pH.

4.5. α-synuclein monomer cross-seeding by $A\beta_{42}$ fibrils

The most abundant isoform of Aβ in the brain is $A\beta_{40}$ (Selkoe and Hardy, 2016; Murphy and LeVine, 2010). However, a closer link has been established between the 42-residue peptide, $A\beta_{42}$, and Alzheimer's disease (Meilandt et al., 2020). A shift in the ratio of $A\beta_{40}$:$A\beta_{42}$ as well as an overall increase of $A\beta_{42}$ is observed in plaques of mice models bearing familial mutations of the *PSEN1* gene (Duff et al., 1996; Kovacs et al., 1996). This increase in the deposition of $A\beta_{42}$ compared to $A\beta_{40}$ has also been seen in cases of dementia with Lewy bodies, by immunohistochemistry and immunoblotting analysis on parahippocampal and hippocampal brain sections (Lippa et al., 1999a). More recent reports have established that the CSF ratio of $A\beta_{42}$:$A\beta_{40}$ decreases in Alzheimer's disease , a characteristic believed to be due to a conversion of soluble $A\beta_{42}$ into plaques (Hansson et al., 2019; Niemantsverdriet et al., 2017).

$A\beta_{42}$ has been found to enhance α-synuclein aggregation *in vitro*. In their experiment set up at pH 7.5, Masliah *et al*. (2001) reported that the 24 h incubation of recombinant monomeric human α-synuclein with high concentrations of synthetic monomeric $A\beta_{42}$ generated oligomers and high molecular weight polymers of α-synuclein, observable by western blot. These higher order species were not present in the control unseeded samples nor the ones incubated with $A\beta_{40}$. Moreover, in their ThS fluorescence at pH 7.4 and 37°C, Ono *et al*. (2012) found a 67% increase on the growth rate of α-synuclein by the presence of 10% (v/v) $A\beta_{42}$ fibrils when compared to the α-synuclein samples incubated with $A\beta_{40}$ fibrils and the unseeded α-synuclein. However, to date, no studies have examined the effect of $A\beta_{42}$ fibril polymorphism on the cross seeding of α-synuclein.

Here, by using pH 2 and pH 8 $A\beta_{42}$ fibril preparations (generated as described in Chapter 2), I examine whether $A\beta_{42}$ polymorphs can cross-seed α-synuclein aggregation. A ThT fluorescence assay was performed on α-synuclein monomer incubated with 1 - 20% (v/v) pH 2 and pH 8 $A\beta_{42}$ fibrils, at pH 7.5 and pH 4.5. It was observed that at pH 7.5 there was no increase in fluorescence

intensity after the incubation of the α-synuclein monomer with different concentrations of the $A\beta_{42}$ fibril preparations (Figure 4.16 A, C and E). Contrary to this, at pH 4.5 cross-seeding of the α-synuclein aggregation by the $A\beta_{42}$ fibrils at 20% (v/v) was observed, with a significant reduction in the lag time when compared with the unseeded α-synuclein sample (Figure 4.16 F, Table 4.3).

Multiple comparison ANOVA of the lag times at pH 4.5 did not find significant differences between the samples cross-seeded with 20% (v/v) pH 2 and pH 8 $A\beta_{42}$ fibrils (Table 4.3, Figure 4.17 C). Surprisingly, the incubation of the α-synuclein monomer with 1% (v/v) of either pH 2 or pH 8 $A\beta_{42}$ fibrils appeared to increase the lag time (Figure 4.17 B), although no significant differences to the unseeded α-synuclein's lag time were observed after ANOVA multiple comparisons (Figure 4.17 A).

The presence of insoluble material was analysed by separation into supernatant and pellet fractions by ultracentrifugation, followed by SDS-PAGE and densitometry analysis. It was observed that ~10% of the α-synuclein in the sample was in the insoluble pellet fraction at pH 7.5 after the incubation with pH 2 $A\beta_{42}$ fibrils (Figure 4.18 A and C) and pH 8 $A\beta_{42}$ fibrils (Figure 4.18 B and D). However, at pH 4.5, the formation of insoluble α-synuclein is observed for all samples (Figure 4.19). At pH 4.5, ~50% of the α-synuclein was in the pellet fraction in the samples cross-seeded with 1% pH 2 $A\beta_{42}$ (Figure 4.19 C), and less than 40 % of the α-synuclein was insoluble in those samples incubated with 1% pH 8 $A\beta_{42}$ at pH 4.5 (Figure 4.19 D).

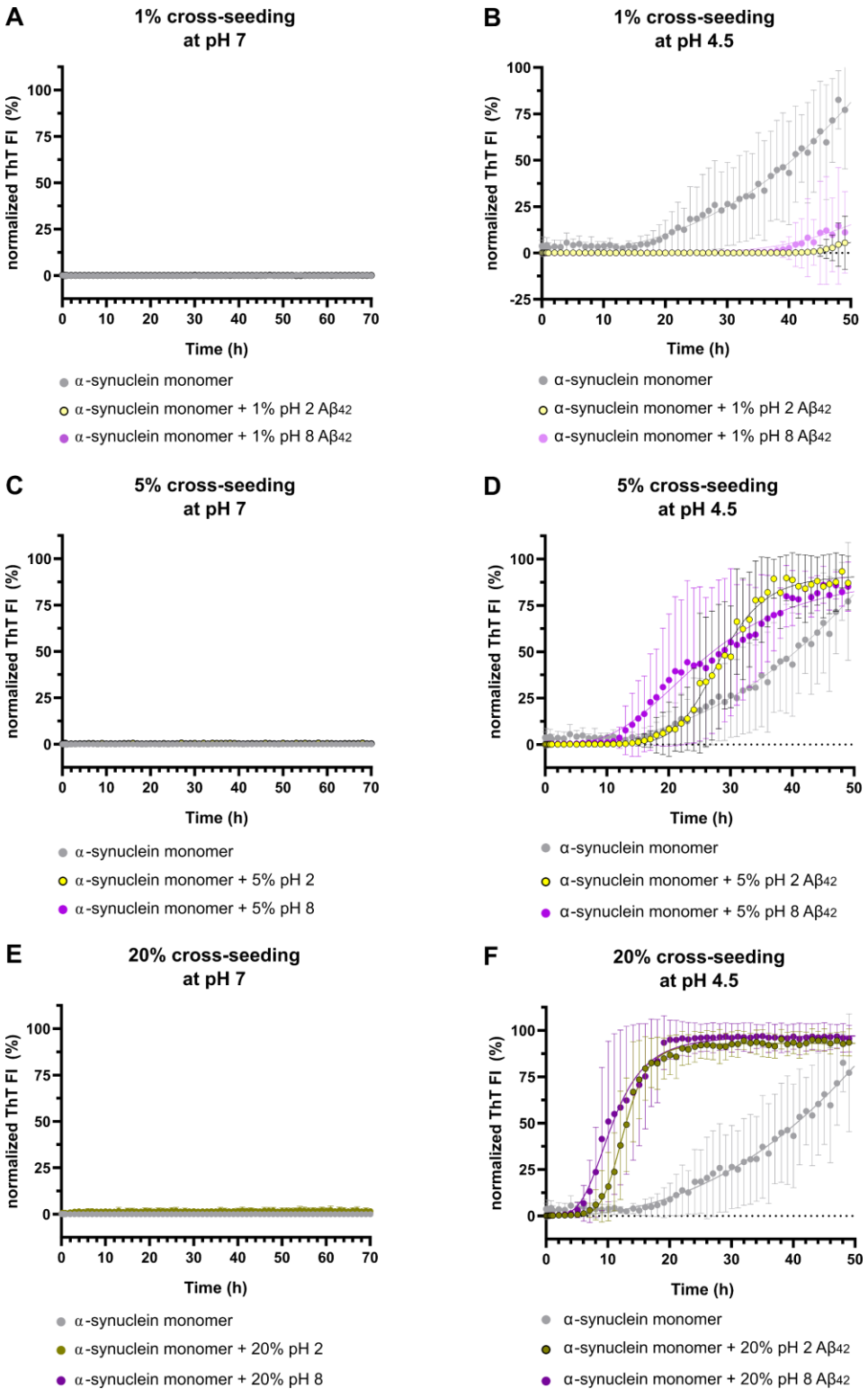

Figure 4.16. Cross-seeding analysis of α-synuclein monomer by $A\beta_{42}$ fibrils at pH 7.5 and 4.5. *ThT kinetic analysis after adding $A\beta_{40}$ polymorphs 2A, 3Q and de novo to 70 μM α-synuclein monomer in a 1%, 5% or 20% (v/v) cross-seeding ratio at pH 7.5 (A, C and E) and pH 4.5 (B, D and F), for 50 h. At pH 7.5, there was no increase in fluorescence intensity after 70 h for the unseeded α-synuclein nor the samples incubated with $A\beta_{42}$ fibril preparations, nor concentration. In contrast, at pH 4.5 the unseeded α-synuclein aggregated after ~20h. ThT kinetics showed an increase in fluorescence intensity for all the samples incubated with the $A\beta_{42}$ fibril preparations, at all concentrations. Mean ± S.D.*

Table 4.3. Half-times and lag-times of the α-synuclein aggregation reaction after 20% (v/v) α-synuclein seeding and cross-seeding with $A\beta_{42}$ fibrils at pH 4.5.

	Half-time (h)	Lag-time (h)
	Mean ± S.D.	Mean ± S.D.
αsynuclein monomer	43.7 ± 10.5	40 ± 9.4
α-synuclein monomer + 20% (v/v) pH 2 $A\beta_{42}$	12.7 ± 1.8	8.7 ± 1.8
α-synuclein monomer + 20% (v/v) pH 8 $A\beta_{42}$	11.8 ± 3.6	7.6 ± 4

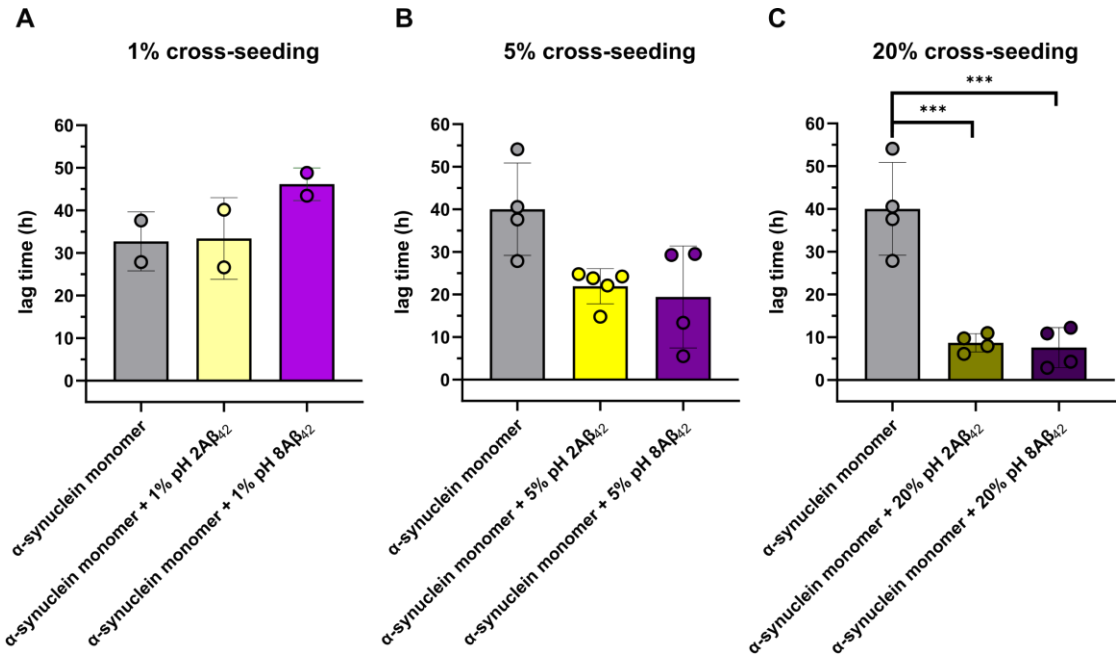

Figure 4.17. Lag time comparison of cross-seeded α-synuclein monomer by $A\beta_{42}$ fibril preparations at pH 4.5.
*No significant difference in lag times was observed for the samples cross-seeded at a 1% (v/v) and 5% (v/v) concentration (A and B) compared to the unseeded α-synuclein. However, at a 20% (v/v) cross-seeding concentration (C) a reduction in lag time was observed for the samples cross-seeded with both pH 2 and pH 8. Mean ± S.D. Significance level after ANOVA with Tukey multiple comparison test: *** $p<0.001$.*

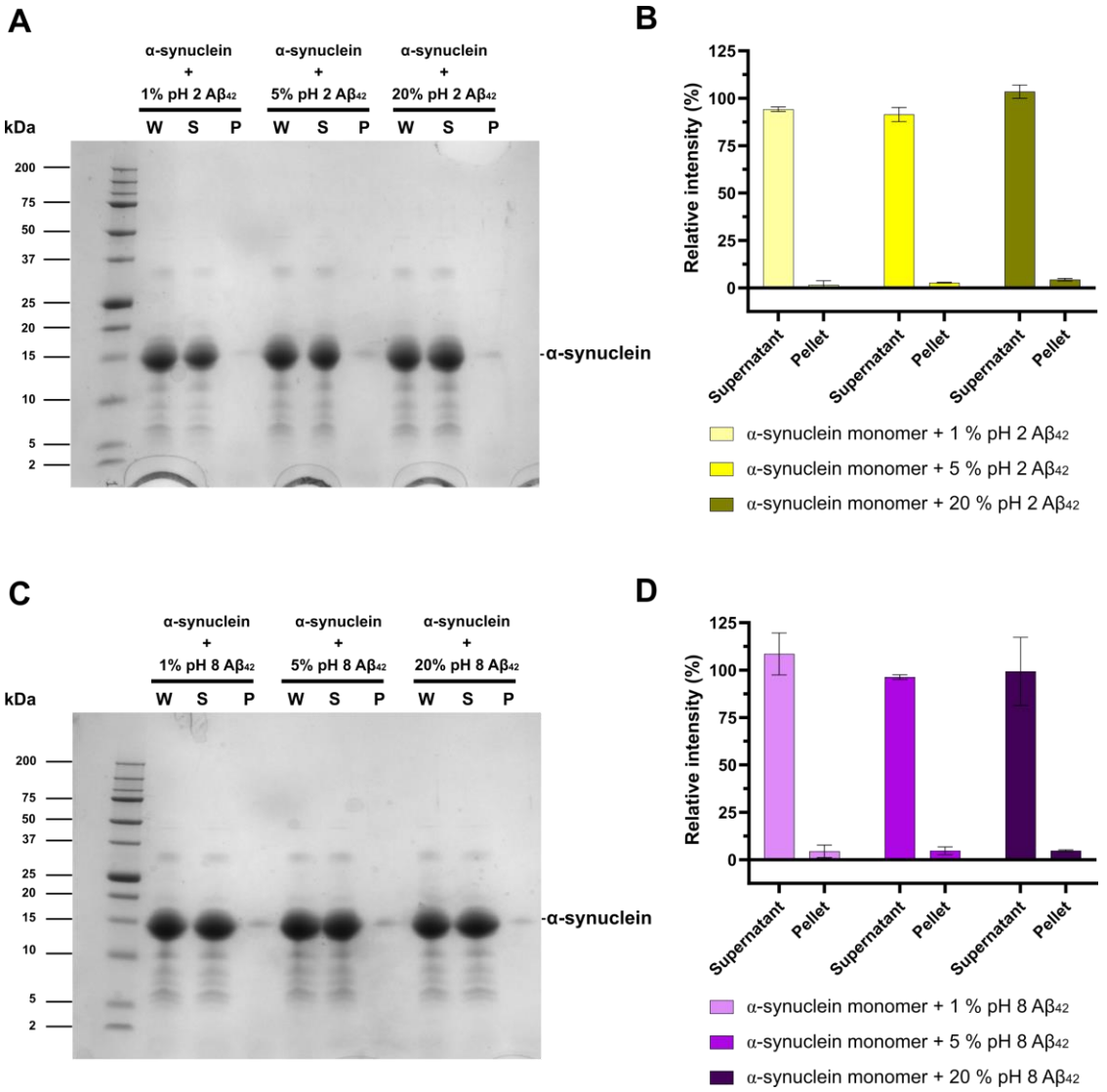

Figure 4.18. Fibril yields of samples from the ThT kinetic assay of cross-seeding of α-synuclein monomer by $A\beta_{42}$ fibril preparations at pH 7.5.

After 70 h of incubation, α-synuclein monomer samples incubated with 1%, 5% or 20% (v/v) pH 2 (A) and pH 8 (C) $A\beta_{42}$ fibrils were centrifuged and separated into pellet (P) and supernatant (S) fractions, keeping an aliquot of the whole (W) sample. SDS-PAGE analysis was then done in a 15 % Tris-tricine gel. It was observed that α-synuclein remains in the supernatant fraction. Densitometric quantification of the fibril yields (B and D) confirmed that ~5-10% of the sample remained in the pellet fraction after incubation with the $A\beta_{42}$ fibrils. N= 3, mean ± S.D.

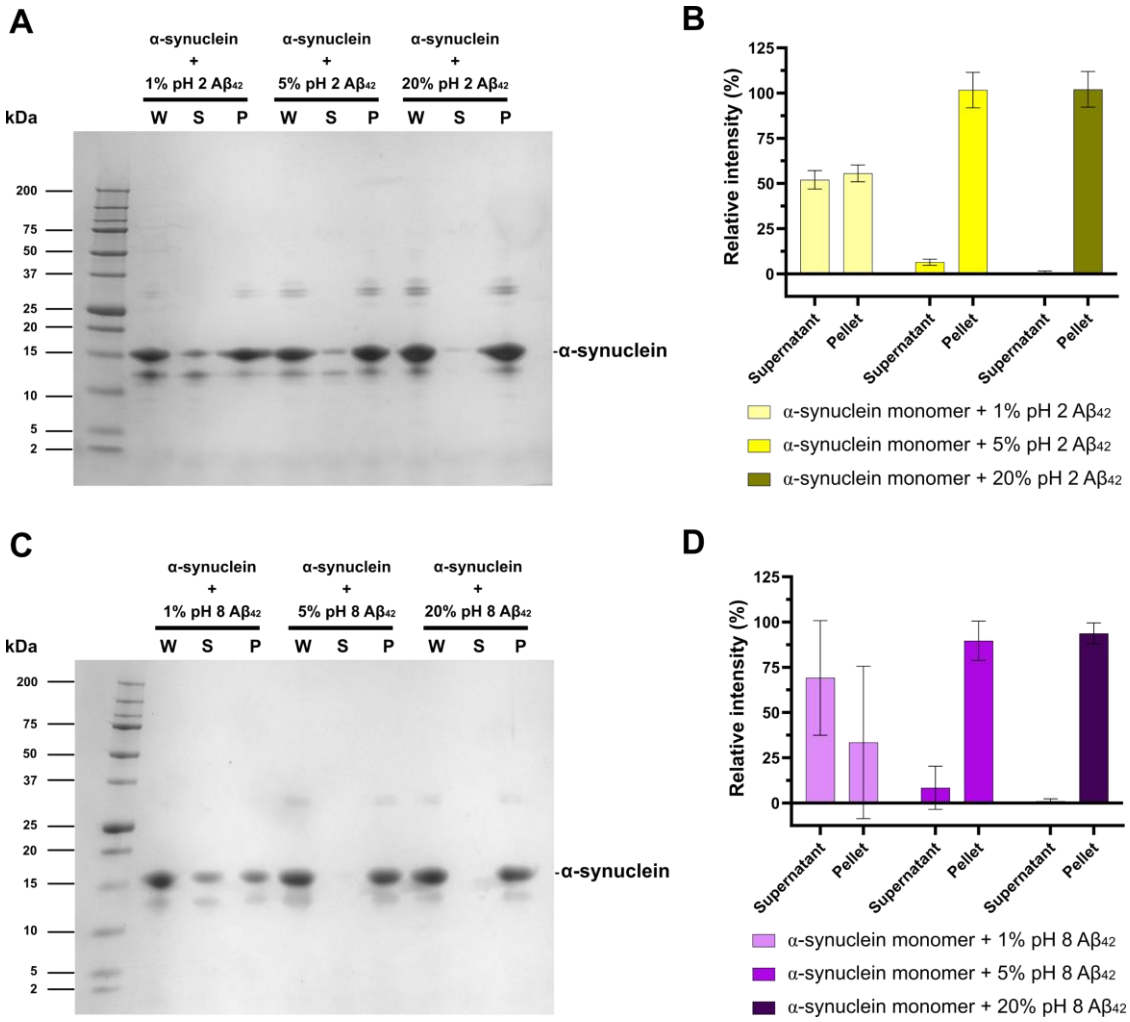

Figure 4.19. Fibril yields of samples from ThT kinetic assay of cross-seeding of α-synuclein cross-seeding by $A\beta_{42}$ fibril preparations at pH 4.5.

After 50 h of incubation, α-synuclein monomer samples incubated with 1%, 5% or 20% (v/v) pH 2 (A) $A\beta_{42}$ or pH (C) 8 $A\beta_{42}$ fibrils were centrifuged and separated into pellet (P) and supernatant (S) fractions, keeping an aliquot of the whole (W) sample. SDS-PAGE analysis was then done in a 15 % Tris-tricine gel. For both $A\beta_{42}$ cross-seedings, it was observed that ~70% of α-synuclein remained in the supernatant fraction in the 1% (v/v) cross-seeded sample, whereas at 5% (v/v) and 20% (v/v) cross-seeding <80% of the α-synuclein remained in the pellet. Higher molecular weight structures resistant to SDS were also visualized between 25 and 37 kDa in the insoluble fraction. N=3, mean ± S.D.

Negative stain TEM confirmed the presence of fibrils in the α-synuclein samples incubated with 5% and 20% (v/v) $A\beta_{42}$ fibrils at pH 4.5 (Figure 4.20). These were highly clumped and formed networks of highly condensed insoluble material, whereas amorphous condensed material was observed in the α-synuclein samples incubated with 1% (v/v) $A\beta_{42}$ fibrils.

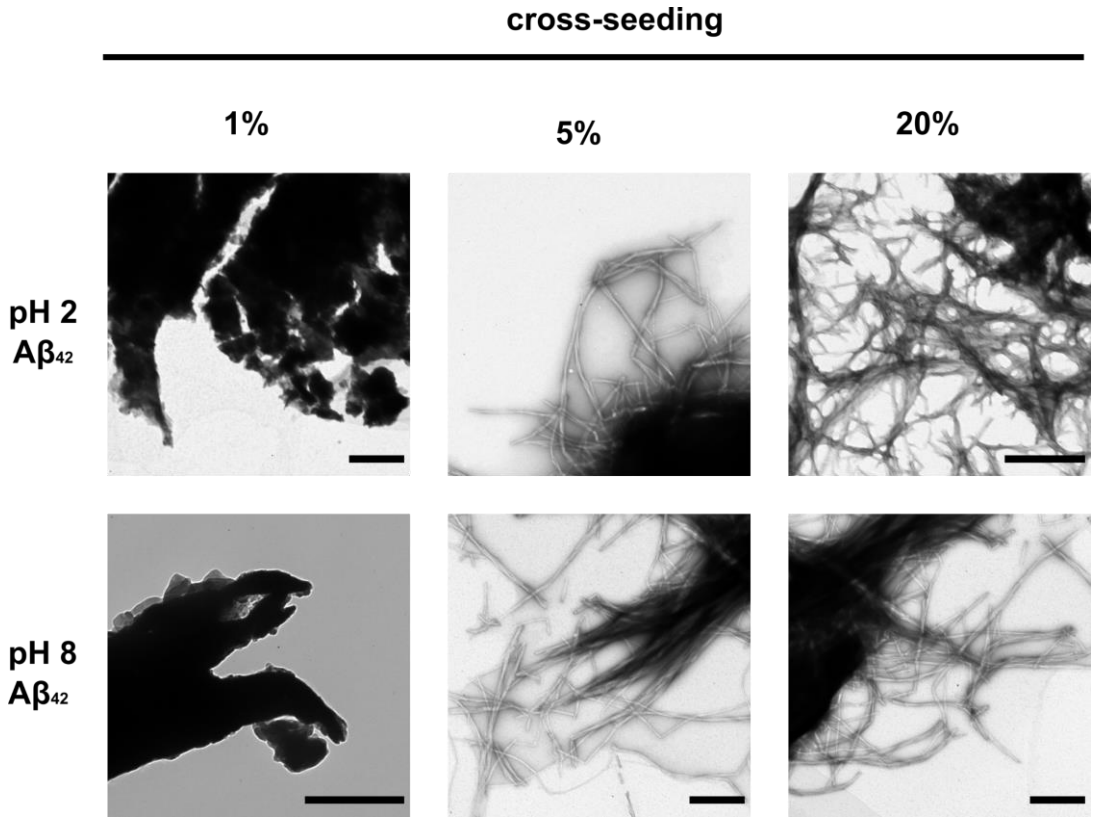

Figure 4.20. Figure 4.20. Electron microscopy imaging of samples after cross-seeding of α-synuclein monomer by $A\beta_{42}$ fibrils at pH 4.5.
After ThT kinetic reactions were stopped, negative stain TEM confirmed the presence of fibrils in the samples after the cross-seeding of α-synuclein by the pH 2 and pH 8 $A\beta_{40}$ fibrils at 5% and 20% (v/v) concentrations. Some amorphous material was also observed in the samples incubated with 1% $A\beta_{42}$ fibrils. Scale bar is 500 nm.

In summary, as observed for $A\beta_{40}$ fibril preparations, an acidic pH of 4.5 promoted the cross-seeding of α-synuclein by two very structurally different fibrils of $A\beta_{42}$. α-synuclein's aggregation after cross-seeding was confirmed to be fibrillar material.

4.6. Molecular mechanism of aggregation of α-synuclein monomer by Aβ fibrils

The aggregation of a misfolded peptide and fibril formation is a nucleation dependent polymerisation process that can occur through different molecular mechanisms (Chiti and Dobson, 2017; Linse, 2017). The main events taking place in the amyloid assembly cascade are primary nucleation of the monomers, occurring in solution or on the surface of another material; elongation of the fibrils through addition of monomers to fibril ends; surfaced catalysed secondary nucleation of monomers by pre-formed fibrils of the same species and fibril fragmentation, which leads to further elongation of fibrils by monomer addition to fibril ends (Figure 4.21) (Chiti and Dobson, 2017).

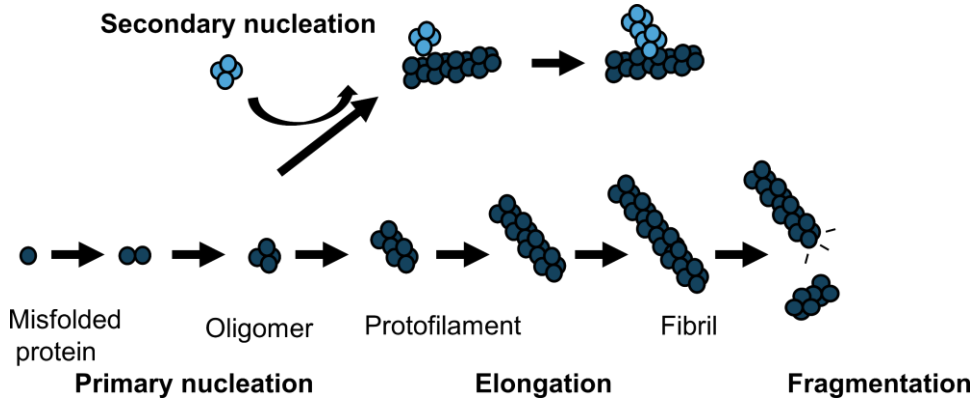

Figure 4.21. Mechanism of amyloid formation.
Amyloid formation is a nucleation dependent polymerisation reaction that begins with the misfolding of a protein or peptide. Nucleation of the misfolded monomers is followed by fibril formation. Fibrillation can occur through elongation of fibrils by misfolded monomer addition to fibril ends. In turn, a fibril can break into smaller aggregates and the surfaces of preformed fibrils can catalyse the fibril formation reaction in a process known as secondary nucleation.

To investigate the mechanisms of amyloid formation an $A\beta_{40}$ self-seeded assay was set up with the use of fragmented and unfragmented 2A, 3Q or *de novo* $A\beta_{40}$ fibril preparations. For this, fibrils were generated as described in Chapter 2, and then subjected to fibril fragmentation by sonication, prior to the self-seeding of the $A\beta_{40}$ monomer in a ThT binding kinetics analysis (Figure 4.22). Fragmentation of the fibrils occurs after sonication and this in consequence generates a higher number of fibril ends, whilst keeping the same surface area along the fibril axis. If the mechanism of aggregation were to be dominated by elongation, the lag time and half-times would diminish in the sonicated fibril samples as compared to the unsonicated samples.

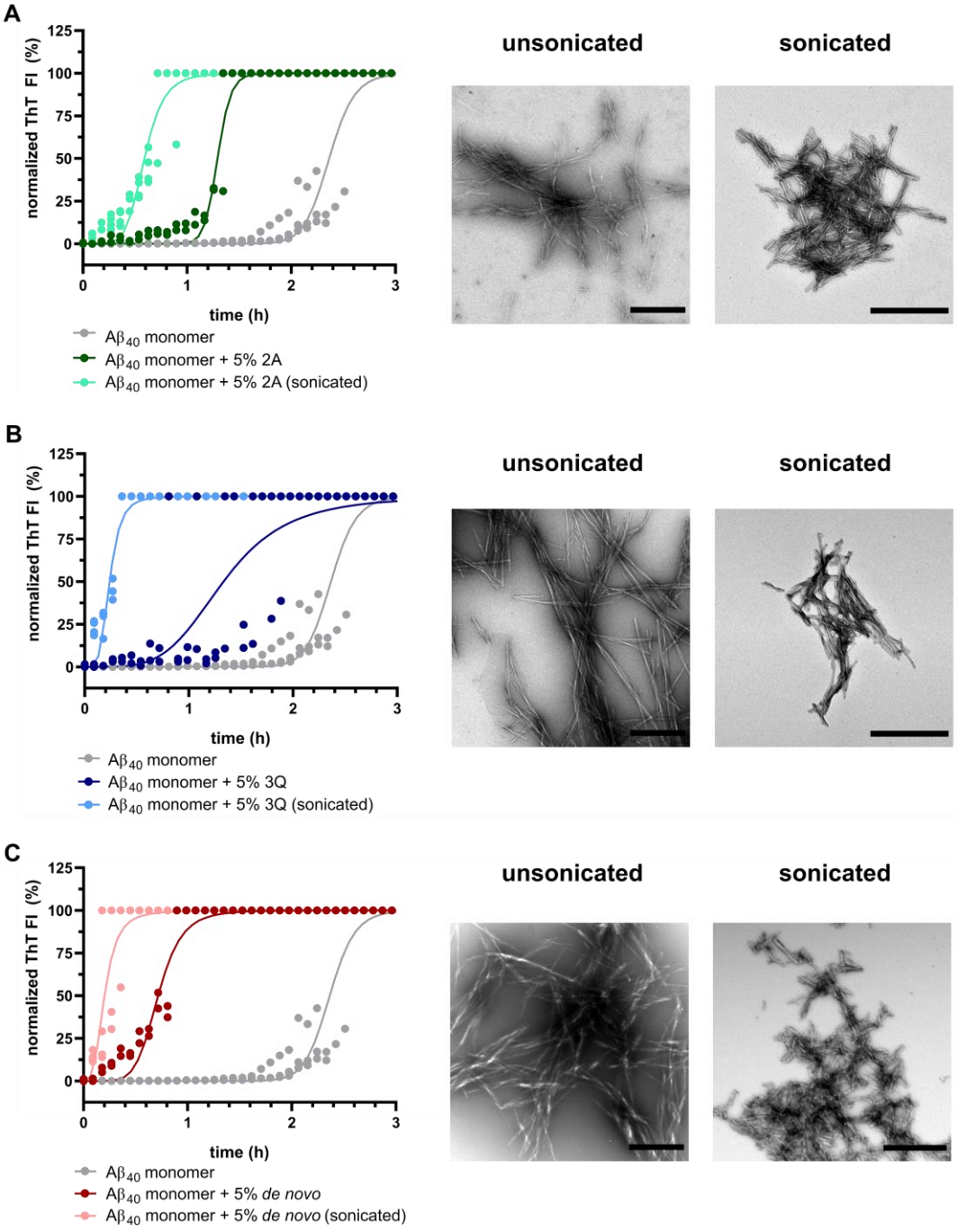

Figure 4.22. Assessment of aggregation of Aβ$_{40}$ by seeding with sonicated and unsonicated fibril preparations.

Fibril aggregation of Aβ$_{40}$ by seeding with Aβ$_{40}$ fibril preparations was monitored by ThT binding kinetics. Aβ$_{40}$ monomer was resuspended in 25 mM sodium phosphate pH 8.5 and seeded at 5% (v/v) with sonicated or unsonicated 2A (A) or 3Q (B) or de novo (C) fibrils. The seeding of monomer bypasses the nucleation process and reaches the growth phase at a much earlier than the unseeded monomer, whilst the fragmented fibrils have more ends available and thus the aggregation of Aβ$_{40}$ is more rapid. Negative stain TEM of the sonicated fibrils before seeding of the Aβ$_{40}$ monomer confirms this method is effective in fragmenting the fibrils. Experiment done at least in duplicates for all conditions (N=1, mean).

Table 4.4. Comparison of half-times of Aβ$_{40}$ self-seeding reactions using 5 % (v/v) unsonicated or sonicated fibrils.

	Half-time	
	- sonication	**+ sonication**
	Mean ± SEM	Mean ± SEM
Aβ$_{40}$ monomer	2.3 ± 0.2	-
Aβ$_{40}$ monomer + 5% 2A	1.3	0.59
Aβ$_{40}$ monomer + 5% 3Q	1.4	0.24
Aβ$_{40}$ monomer + 5% *de novo*	0.7	0.2

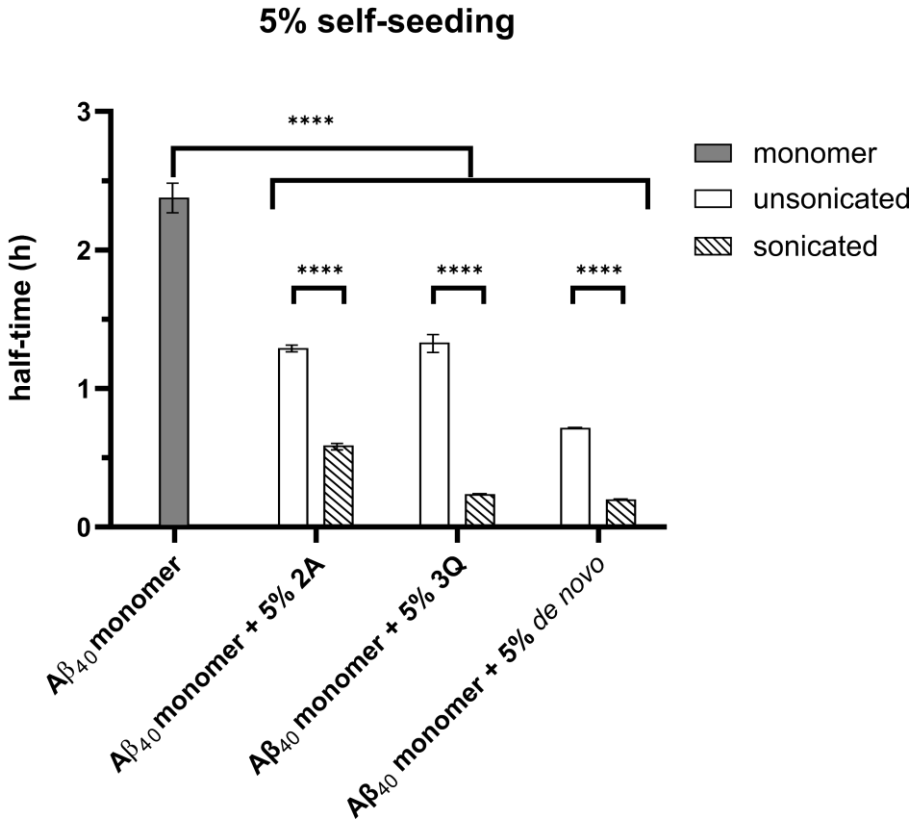

Figure 4.23. Half-time comparison of 5% (v/v) self-seeded Aβ$_{40}$ by sonicated and unsonicated Aβ$_{40}$ fibrils.
*Significant differences were observed between the half time of the unseeded Aβ$_{40}$ and the self-seeded Aβ$_{40}$ with sonicated and unsonicated fibrils. Likewise, significant differences in the half-times were seen between unsonicated and sonicated fibrils in the self-seeding of Aβ$_{40}$ with the 2A, 3Q and de novo Aβ$_{40}$ fibril preparations. Mean ± SEM, significance level after ANOVA with Sidak's multiple comparison test **** p< 0.0001*

.

In controls, $A\beta_{40}$ was first resuspended in 25 mM sodium phosphate pH 7.5 at 200 μM and then incubated with either 5% (v/v) sonicated or unsonicated fibrils. Negative stain TEM confirmed that sonication reduced the length of the $A\beta_{40}$ fibrils (Figure 4.22). ThT kinetic analysis showed a significant reduction in the half-time (Table 4.4, Figure 4.23) in the seeded reactions, compared to the unsonicated reactions. It was also observed that indeed sonication of the $A\beta_{40}$ fibrils significantly reduced the half-times of the reactions compared to the unsonicated fibrils (Figure 4.23). This is consistent with the sonicated fibrils having an increased number of ends onto which monomeric $A\beta_{40}$ can bind to and extend the fibrils.

To identify the mechanism of cross-seeding of α-synuclein by $A\beta_{40}$ and $A\beta_{42}$ fibrils a cross-seeding assay using fragmented and unfragmented Aβ fibrils was performed. As observed in the self-seeded assay, this set up would determine whether the mechanism of fibril formation was governed by elongation, i.e. unfolded α-synuclein adding on to fibril ends of Aβ, or surfaced catalysed secondary nucleation by α-synuclein monomer binding to Aβ's fibril surface. If cross-seeding were to be dominated by an elongation mechanism a reduction in the lag time would be observed in the reactions that contained fragmented fibrils, when compared to the samples that contained unfragmented fibrils. To do this, 70 μM α-synuclein was cross-seeded with 5% (v/v) or 20% (v/v) sonicated (fragmented) 2A, 3Q, de *novo* $A\beta_{40}$ fibrils or pH 2 $A\beta_{42}$ fibrils at pH 4.5 and compared with α-synuclein samples cross-seeded with unsonicated fibrils (Figure 4.24).

It was observed that there was no reduction in the lag times of the α-synuclein samples that were cross-seeded with sonicated 2A, *de novo* $A\beta_{40}$ fibril or pH 2 $A\beta_{42}$ fibrils, compared to the reactions performed with unsonicated fibrils (Figure 4.24 A, C and D, Table 4.5). This was also observed in the samples incubated with 5% (v/v) 3Q $A\beta_{40}$ fibrils (Figure 4.24 B). In contrast, the 20% (v/v) 3Q cross-seeded samples showed a reduction in the lag time (~7 h) when sonicated 3Q fibrils were used compared with unsonicated fibrils (Figure 4.25 B, Table 4.5). Previous analysis of the lag time of the α-synuclein sample cross-seeded by 20% (v/v) 3Q fibrils showed to be variable (12.1 h ± 6.2 h) (Table 4.2), suggesting that these fibrils could be clumping differently to the other Aβ fibrils and therefore interacting differently with α-synuclein.

These results indicate that at pH 4.5, the aggregation of α-synuclein monomer by pH 2 $A\beta_{42}$ fibrils, and 2A and *de novo* $A\beta_{40}$ fibrils, likely occurs via heterogeneous secondary nucleation. Further investigation regarding the mechanism of aggregation is required for the cross-seeding of α-synuclein monomer by 3Q $A\beta_{40}$ fibrils. Clumping of the 3Q fibrils, prior the cross-seeding assay, might account for the significant reduction in the lag time after sonication when compared to

unsonicated 3Q cross-seeded samples, as there was no further reduction in the lag time when compared to the other the α-synuclein samples cross-seeded with sonicated $A\beta_{40}$ and $A\beta_{42}$ fibrils.

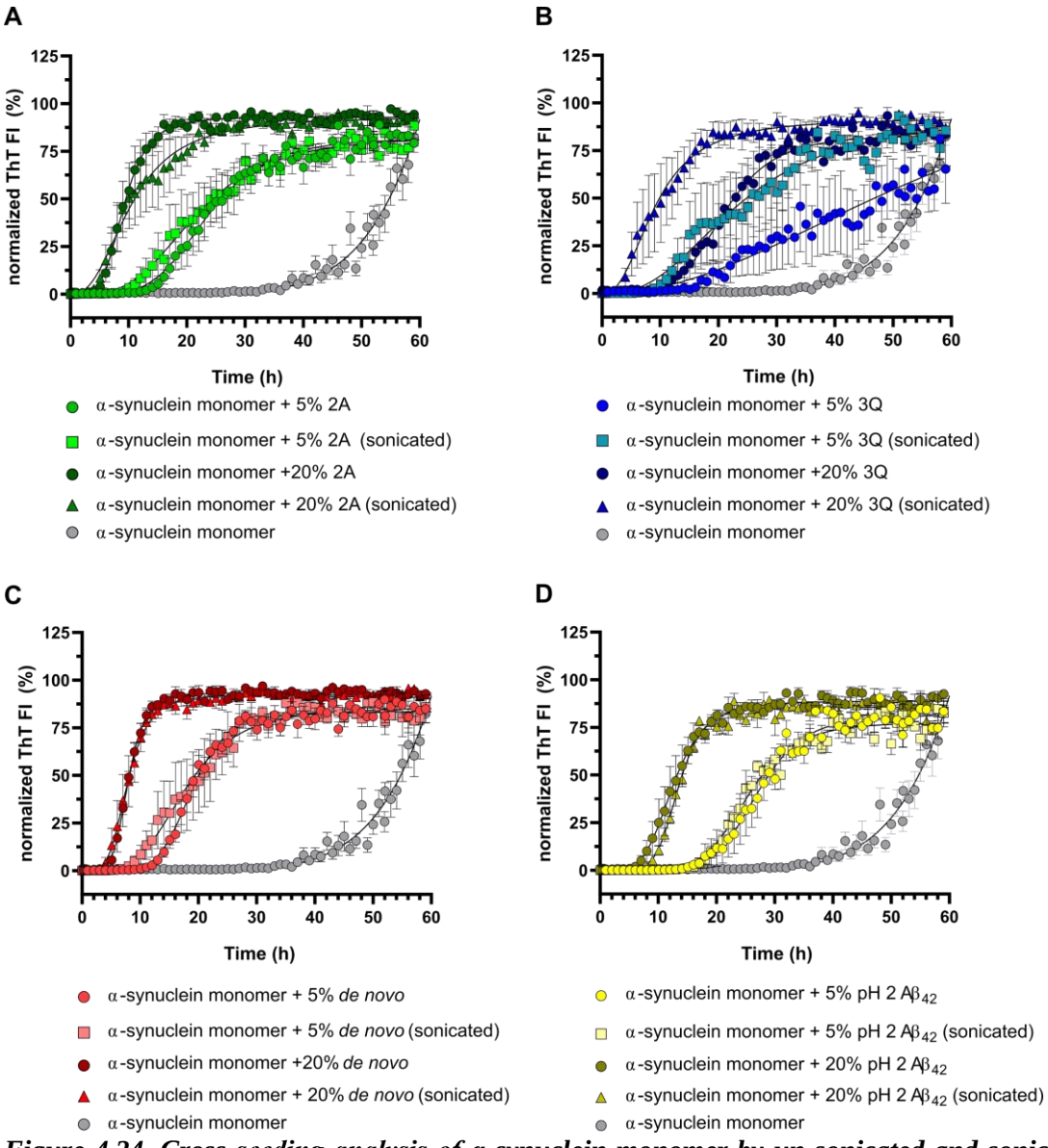

Figure 4.24. Cross-seeding analysis of α-synuclein monomer by un-sonicated and sonicated $A\beta_{40}$ and $A\beta_{42}$ fibrils at pH 4.5.

ThT kinetic analysis of $A\beta_{40}$ fibril preparations 2A (A), 3Q (B) and de novo (C) and pH 2 $A\beta_{42}$ were added to 70 μM α-synuclein monomer in a 5% (v/v) or 20% (v/v) seeding ratio at pH 4.5, after undergoing three sonication cycles. In parallel, un-sonicated fibrils were incubated with α-synuclein at the same ratio and ThT binding kinetics were followed for 60 h. ThT kinetics showed no difference in the rate of aggregation after sonication of the 2A (A), de novo (C) $A\beta_{40}$ fibrils and pH 2 (D) $A\beta_{42}$ fibrils. However, the aggregation rate appeared to heighten with the use of sonicated 3Q (B) fibrils. Mean ± S.D.

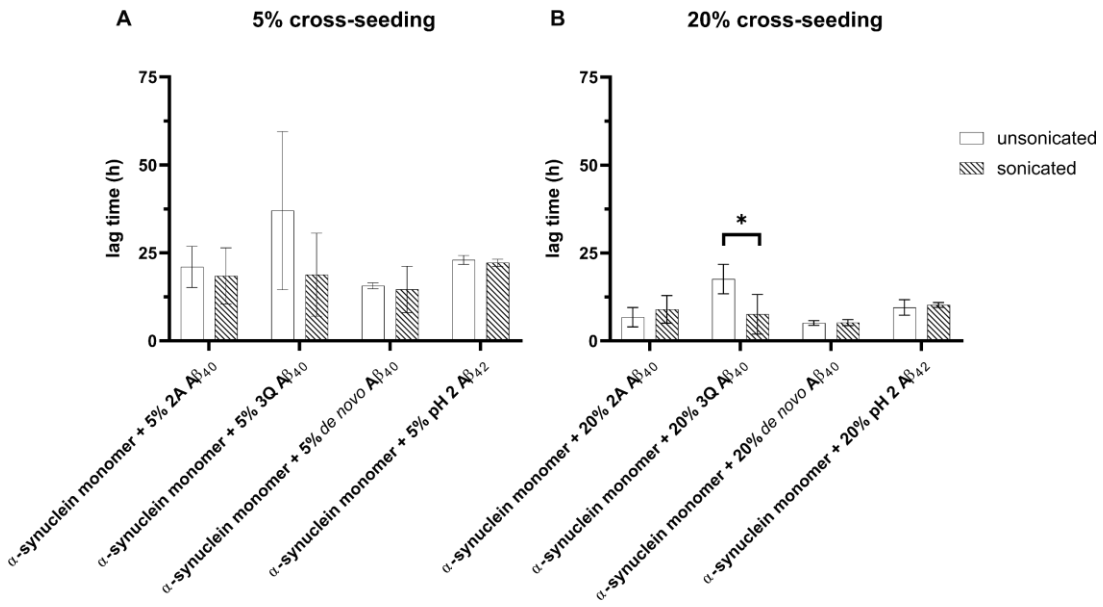

Figure 4.25. Lag time comparison of cross-seeded α-synuclein monomer by sonicated and unsonicated $A\beta_{40}$ and $A\beta_{42}$ fibrils.
*No significant differences in lag times were observed for the samples cross-seeded at a 5% (v/v) cross-seeding concentration with sonicated and unsonicated fibrils (A). The same trend happened at 20% cross-seeding, apart from the samples cross-seeded with 3Q fibrils, were sonication appeared to significantly reduce the lag time compared to the samples incubated with unsonicated 3Q fibrils (B). Mean ± S.D. Significance level after ANOVA with Tukey multiple comparison test: * p=0.0499.*

Table 4.5. Comparison of lag times of α-synuclein cross-seeding by unsonicated or sonicated $A\beta_{40}$ and $A\beta_{42}$ fibrils at pH 4.5.

		Lag times (h)	
		- sonication	+ sonication
		Mean ± S.D.	Mean ± S.D.
5% (v/v)	α-synuclein monomer + 5% 2A $A\beta_{40}$	21 ± 4.2	18.4 ± 5.7
	α-synuclein monomer + 5% 3Q $A\beta_{40}$	37 ± 15.9	18.8 ± 8.3
	α-synuclein monomer + 5% *de novo* $A\beta_{40}$	15.7 ± 0.6	14.6 ± 4.7
	α-synuclein monomer + 5% pH 2 $A\beta_{42}$	23 ± 0.9	22.2 ± 0.7
20% (v/v)	α-synuclein monomer + 20% 2A $A\beta_{40}$	6.7 ± 1.9	8.97 ± 2.8
	α-synuclein monomer + 20% 3Q $A\beta_{40}$	17.6 ± 3	7.6 ± 4
	α-synuclein monomer + 20% *de novo* $A\beta_{40}$	5.1 ± 0.5	5.2 ± 0.6
	α-synuclein monomer + 20% pH 2 $A\beta_{42}$	9.5 ± 1.6	10.2 ± 0.5

4.7. Polymorphism characterisation of cross-seeded α-synuclein fibrils

To evaluate fibril polymorphism in the cross-seeded derived α-synuclein fibrils, a curcumin dye binding assay was performed, as described by Störharker *et al*. 2019. Curcumin (Figure 4.26) is a polyphenol present in turmeric commonly studied for its biological and pharmacological effects, including ROS decrease, apoptosis attenuation and autophagy recovery in cell models of Parkinson's disease (Hassan et al., 2019). It has recently come to attention as a dye capable of distinguishing heterogeneity in brain deposits composed of either WT, E22G or E22Q $A\beta_{40}$ in mice models of familial Alzheimer's diseases and cerebral amyloid angiopathy (Condello et al., 2018), as well as fibrillar structural diversity of brain derived *in vitro* generated α-synuclein fibrils from Parkinson's disease and MSA (Lau et al., 2020; Strohaker et al., 2019).

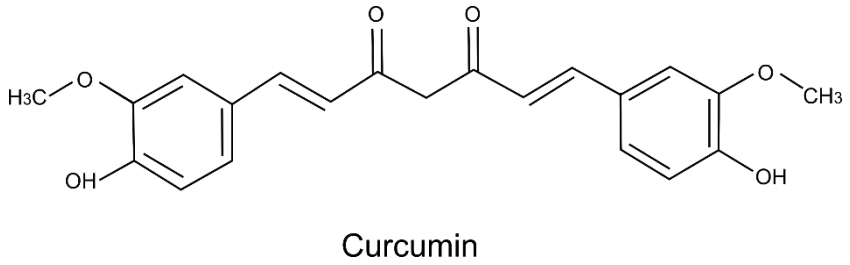

Figure 4.26. Curcumin molecular structure.
Chemically known as diferuloylmethane, curcumin is a polyphenol derived from the Curcuma longa plant studied for its effects on cellular viability, inflammation and antioxidant actions.

For this assay, cross-seeded fibrils were grown by incubating α-synuclein monomer with 20% (v/v) 2A, 3Q or *de novo* $A\beta_{40}$ fibrils, or pH 2 or pH 8 $A\beta_{42}$ fibrils, at pH 4.5 in the absence of ThT. Fibrils were then incubated with curcumin dye at a 1:6 protein to dye molar ratio and the fluorescent emission spectra of the fibril-dye mixture were subsequently measured.

The samples containing α-synuclein fibrils after the cross-seeding with $A\beta_{40}$ at pH 4.5 had a different emission spectrum to the spectrum of the individual $A\beta_{40}$ fibrils, as the spectrum of the $A\beta_{40}$ fibrils appeared to be red-shifted compared with the cross-seeded α-synuclein fibrils (Figure 4.27, A). However, minimal changes in the spectra shape were observed between the samples of α-synuclein cross-seeded by the different $A\beta_{40}$ fibril preparations. A 4 nm difference in the emission λ_{max} was observed between α-synuclein cross-seeded fibrils by 2A $A\beta_{40}$ fibrils, compared to the 3Q and *de novo* $A\beta_{40}$ cross-seeded fibrils. In addition, a higher normalized fluorescence intensity was observed at specific wavelengths (between 550-650 nm) for the 3Q α-synuclein cross-seeded sample compared to the others.

A similar trend can be observed with samples of α-synuclein fibrils obtained after the cross-seeding with 20% (v/v) pH 2 or pH 8 $A\beta_{42}$ in acidic conditions. A maximal peak at ~510 nm was observed for the α-synuclein cross-seeded fibrils compared to ~535 nm maximal peak observed for the individual $A\beta_{42}$ fibrils (Figure 4.27, B). As with the α-synuclein fibrils cross-seeded by $A\beta_{40}$, a 4 nm difference in the λ_{max} was observed between the α-synuclein fibrils cross-seeded by either 20% (v/v) pH 2 or pH 8 $A\beta_{42}$ fibril preparations at pH 4.5 (Figure 4.28).

Analysis of the curcumin fluorescence intensity showed that there were significant differences between the samples of α-synuclein fibrils cross-seeded with 20% (v/v) 2A, 3Q and *de novo* $A\beta_{40}$ (Figure 4.29). In contrast, no differences in the fluorescence intensities were observed between the α-synuclein fibrils cross-seeded by $A\beta_{42}$ were observed (Figure 4.29). In particular, the 2A derived α-synuclein fibrils showed a higher mean curcumin fluorescence intensity, compared to the rest of the fibrils, whereas the 3Q derived α-synuclein fibrils, showed a more uniform lower total fluorescence compared to the other cross-seeded fibrils.

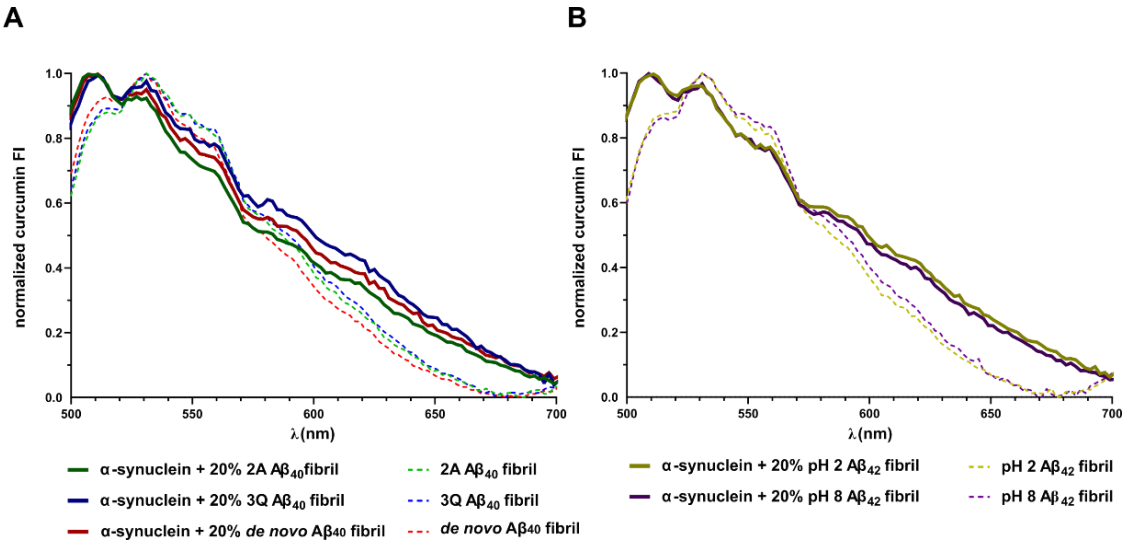

Figure 4.27. Curcumin dye binding to fibrils of α-synuclein after cross-seeding with 20% (v/v) $A\beta_{40}$ and $A\beta_{42}$ preparations at pH 4.5.
A) A fluorescence maximal peak at 510 nm is observed for the α-synuclein fibrils after cross-seeding by 2A, 3Q and de novo $A\beta_{40}$ compared to the maximal peak obtained for the individual $A\beta_{40}$, at 535 nm. ANOVA of the fluorescence spectra appeared to be different between the cross-seeded fibrils by the $A\beta_{40}$ fibril preparations between 560 and 620 nm ($p < 0.05$). B) The maximal fluorescence peak for cross-seeded α-synuclein fibrils by pH 2 and pH 8 $A\beta_{42}$ fibrils and the individual $A\beta_{42}$ fibrils were 510 and 535 nm, respectively. No significant differences were observed between the cross-seeded fibrils curcumin spectra.

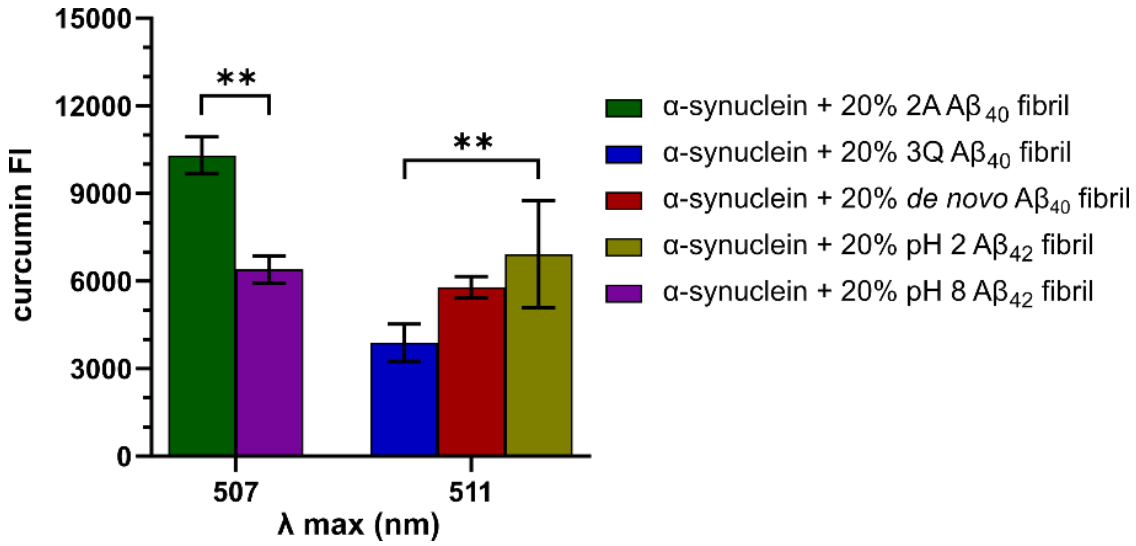

Figure 4.28. Curcumin λ_{max} fluorescence intensity of α-synuclein fibrils after cross-seeding by 20% (v/v) $A\beta_{40}$ or $A\beta_{42}$ fibril preparations at pH 4.5

*Two different λ_{max} were observed between the α-synuclein cross-seeded fibrils: 507 nm, for 2A $A\beta_{40}$ and pH 8 $A\beta_{42}$ cross-seeded α-synuclein fibrils and 511 nm for 3Q, de novo $A\beta_{40}$ and pH 2 $A\beta_{42}$ cross-seeded fibrils. ANOVA of the mean curcumin λ_{max} fluorescence intensity was significantly different between 2A $A\beta_{40}$ and pH 8 $A\beta_{42}$ cross-seeded α-synuclein fibrils. Significant differences were also observed between 3Q $A\beta_{40}$ and pH 2 $A\beta_{42}$ cross-seeded α-synuclein fibrils but not de novo $A\beta_{40}$ and pH 2 $A\beta_{42}$ cross-seeded α-synuclein fibrils. (Tukey multiple comparisons, ** $p<0.01$).*

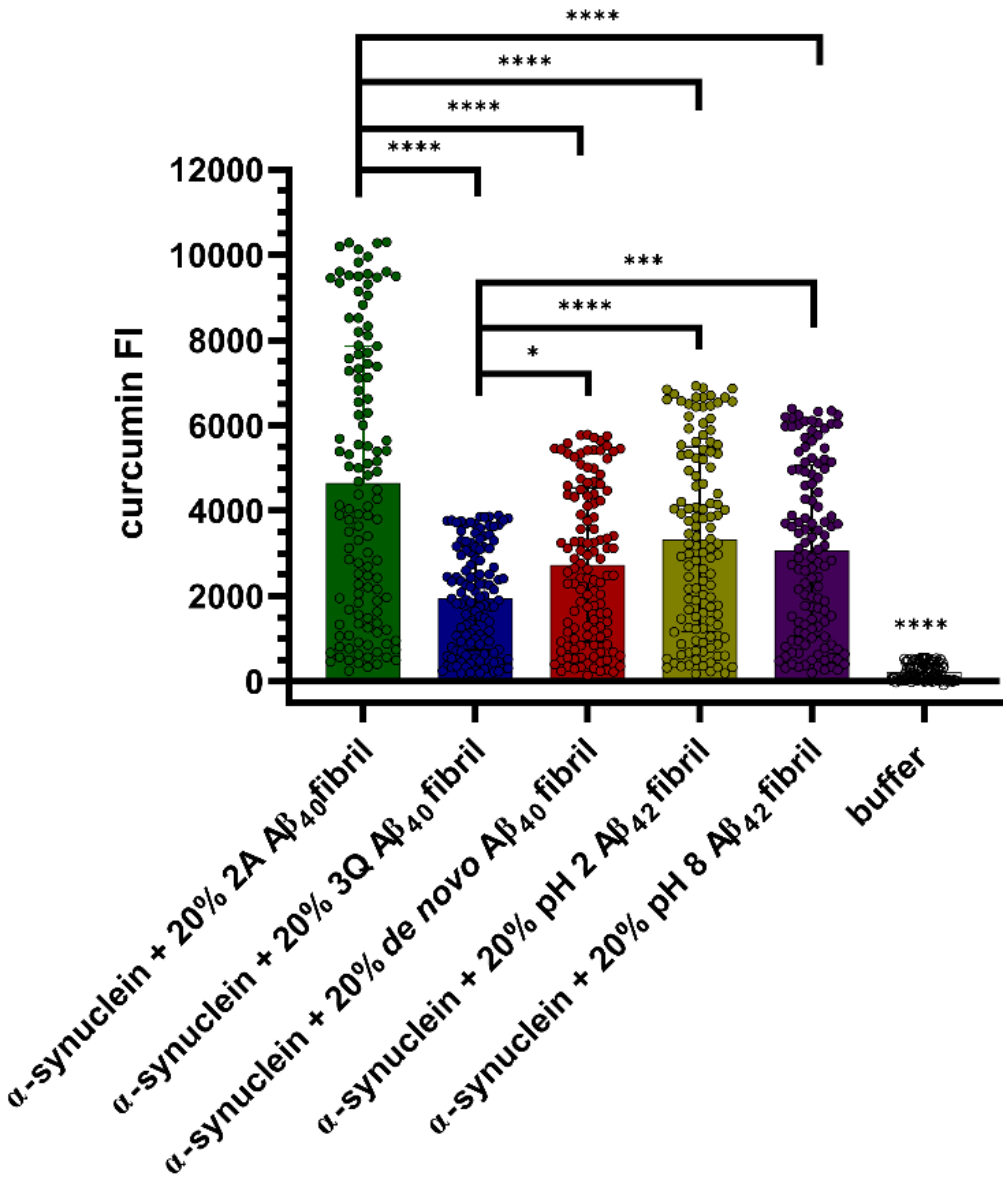

Figure 4.29. Mean curcumin fluorescence intensity of α-synuclein fibrils after cross-seeding by 20% (v/v) $A\beta_{40}$ or $A\beta_{42}$ fibril preparations at pH 4.5
*ANOVA of the mean curcumin fluorescence intensity revealed to be significantly different between the buffer and all of the Aβ derived α-synuclein fibrils. Significant differences were also observed between the α-synuclein fibrils formed after cross-seeding with 20% 2A, 3Q or de novo $A\beta_{40}$ fibrils. The mean curcumin intensity between the synuclein fibrils formed after cross-seeding with 20% pH 2 or pH 8 $A\beta_{42}$ was not significantly different. (Tukey multiple comparisons, * $p<0.05$, *** $p<0.005$, **** $p<0.0001$).*

It is possible that the difference in curcumin fluorescence intensity of the cross-seeded α-synuclein fibrils comes from the Aβ fibrils themselves, as they represent 20% of the whole sample analysed. However, if indeed the change came solely from the Aβ fibrils, the same curcumin fluorescence intensities would be observed for the Aβ fibrils and the α-synuclein samples cross-seeded with the Aβ fibrils. As discussed in Chapter 3, the *de novo* fibrils $A\beta_{40}$ fibrils showed a higher curcumin fluorescence intensity than the 2A fibrils, and the 2A fibrils showed a higher

curcumin fluorescence intensity than the 3Q fibrils. This is not observed in the cross-seeded fibrils: the α-synuclein fibrils cross-seeded by the 2A $A\beta_{40}$ fibrils show the highest curcumin fluorescence intensity, followed by the *de novo* cross-seeded and 3Q cross-seeded fibrils. In contrast to the individual $A\beta_{42}$, no differences in overall curcumin fluorescence intensities were seen between the pH 2 and pH 8 $A\beta_{42}$ cross-seeded α-synuclein fibrils.

Together these results indicate that the α-synuclein fibrils formed after cross-seeding with Aβ fibrils might be different to each other, as different binding of curcumin by the fibrils, observed as the difference of curcumin fluorescence intensities, could be occurring due to different structural morphologies. It is to be noted that curcumin dye binding of self-seeded α-synuclein fibrils would be required to confirm if these could be classified as a different polymorph. Unfortunately, this experiment was not completed due to the closure of the lab during the COVID-19 lockdown.

4.8. Discussion

A pH dependent mechanism of cross-seeding of α-synuclein by Aβ fibrils has been detailed here. Two pHs were studied, pH 7.5 and pH 4.5, as conditions in which binding of the Aβ fibrils to α-synuclein and cross-seeding of α-synuclein by Aβ may occur *in vivo*. It was demonstrated that cross-seeding of α-synuclein from Aβ fibrils may occur through a secondary nucleation mechanism, as shown by ThT kinetic analysis using fragmented fibrils. Moreover, the fibrils generated via cross-seeding might present different structural morphologies as observed by curcumin fluorescence analysis.

Previous studies have shown that at pH 7.4, the cross-seeding of α-synuclein by Aβ fibrils can occur (Ono et al., 2012). Under their conditions, 10% (v/v) cross-seeding ratio, pH 7.4 and 37°C, Ono et al (2012) observed an acceleration in the aggregation of α-synuclein after the addition of fibrils of $A\beta_{40}$ and $A\beta_{42}$ as well as cross-linked oligomers. Here, binding between the $A\beta_{40}$ fibrils and the α-synuclein monomer was observed using a fluorescence polarisation assay at pH 7.5. Binding has also been shown to occur between α-synuclein monomer and fibrils of $A\beta_{42}$ at pH 8, and the inhibition of self-proliferation of $A\beta_{42}$ fibrils in the presence of α-synuclein monomer has been attributed to the association of the α-synuclein monomer to the surfaces of early formed $A\beta_{42}$ fibrils and the inhibition of self-seeded secondary nucleation of $A\beta_{42}$ in ThT kinetic binding assays (Chia et al., 2017).

However, in the present study, kinetic analysis of the aggregation of α-synuclein at pH 7.5 by ThT and at pH 7.4 by ThS binding (as reported in (Ono et al., 2012)), showed that that neither

the unseeded α-synuclein monomer nor the α-synuclein incubated with Aβ fibrils aggregated into amyloid fibrils after 70 h. At this pH, only the α-synuclein fibril seeds were able to reduce the lag time and accelerate the aggregation of α-synuclein monomer into fibrils. α-Synuclein aggregation *in vitro* is known to be dependent on physical and solution conditions such as temperature, agitation state, pH and ionic strength, and is induced by the presence of cofactors such as lipids (Gaspar et al., 2017; Meisl et al., 2016). This dependence is due to α-synuclein's sequence domains, rich in basic residues at the N-terminal region and rich in acidic residues at the C-terminal region, and a high net charge at neutral pH (pI 4.7) (Gaspar et al., 2017; Uversky et al., 2001). At neutral pH, α-synuclein has been determined to adopt a closed conformation, as a result of stabilisation of transient long-range interactions. In particular, its C-terminal conformation seems to remain extended, flexible, and with a higher probability to be close to the NAC region, whilst the interactions between C-terminal and the N-terminal are weaker than what is observed under acidic pH (Cho et al., 2009). This closed conformation, and reduced interactions between the aggregation-prone regions and the N-terminal have been suggested to hinder the aggregation of α-synuclein at neutral pH (Cho et al., 2009; Doherty et al., 2020). At neutral pH ThT binding kinetics show that α-synuclein's aggregation is slower than at acidic pH (Doherty et al., 2020), and it has also been reported to not aggregate at all after 90 h (Grey et al., 2011).

Although it was not possible to replicate Ono et al. (2012) findings, it cannot be excluded that their cross-seeding effect could be happening due to the nature of the Aβ fibrils used. Even though no mention of fibril polymorphism is stated, their Aβ fibril preparation differs (synthetic peptide was solubilized in 10 mM sodium phosphate buffer or 20 mM Tris buffer, and then subjected to sonication) from the method used to form the $A\beta_{40}$ and $A\beta_{40}$ preparations used in this study (described in Chapter 2). In the same manner, while no fibrillar aggregation of α-synuclein was seen due to the presence of Aβ fibrils in this study, this feature cannot be ruled out from the scenario, and a longer incubation time may be needed to observe both the aggregation of the unseeded α-synuclein monomer, and the effect of fibrils $A\beta_{40}$ and $A\beta_{42}$ preparations on α-synuclein at pH 7.5.

At acid and mildly acidic pH's, like pH 4.5 present in lysosomes, α-synuclein is known to adopt an ensemble of natively unfolded conformations characterized by a rigid and compact C-terminal region, that has a higher probability of NAC-C-terminal interactions (Cho et al., 2009), with a higher propensity and faster rate of aggregation than at neutral pH (Doherty et al., 2020). In this study it was observed that at pH 4.5 α-synuclein's aggregation started after ~40 h, whereas no fibril formation was detected at pH 7.5 after 70 h. pH 4.5 also proved to be a favourable condition for the cross-seeding between α-synuclein and a high concentration of $A\beta_{40}$ and $A\beta_{42}$ fibrils (20 % v/v) to occur, as the α-synuclein lag times decreased to ~7 - 12 h.

Unseeded aggregation of α-synuclein at acidic pH is thought to be driven by secondary nucleation processes (Buell et al., 2014; Gaspar et al., 2017; Peduzzo et al., 2020). In their study, Gaspar et al (2017) found that at pH's lower than 6, α-synuclein monomer associated and dissociated more readily to immobilized α-synuclein fibrils, whereas at pH's higher than 6 this association and dissociation occurred more slowly as observed using a quartz-crystal microbalance with dissipation assay. They attributed this difference to the mechanism of association occurring: secondary surface binding being favoured at pH < 6, observed as an increase in frequency after addition of the monomer to the immobilized fibrils, as well as a high frequency after washing, a sign that most of the mass added could dissociate from the fibrils. At pH > 6 elongation mechanisms dominated α-synuclein's aggregation, seen as less sharp and smaller increase in frequency before and after washing, indicating a less transient association between fibril and monomer (elongation at the fibril ends). Confirmation of their results was done by dSTORM imaging, where they visualized fluorescently labelled α-synuclein seeds and α-synuclein monomer at the fibril ends or on their surfaces of fibrils, at pH 8.8 and 5.5, respectively (Gaspar et al., 2017; Pinotsi et al., 2014).

In the present study, the association between the α-synuclein monomer, and its increase of fibrillation due to the cross-seeding by the 2A, *de novo* $A\beta_{40}$ and pH 2 $A\beta_{42}$ fibrils was found to be driven by an heterogenous secondary nucleation at pH 4.5, detected as a lack of further reduction of the lag time after fragmentation of the Aβ fibrils prior to the ThT kinetics binding assay of α-synuclein cross-seeding. Heterogeneous nucleation mechanisms of interaction have been reported between α-synuclein fibrils and $A\beta_{42}$ monomers, the opposite of what was studied here, as α-synuclein fibrils (1-10% v/v) where found to increase the rate of aggregation of $A\beta_{42}$ (Chia et al., 2017). Further investigation to determine the mechanism of interaction of the 3Q fibrils with α-synuclein monomers is needed, as it was observed that there was a reduction in the lag time of α-synuclein aggregation with the fragmented 3Q fibrils when compared to the unfragmented 3Q fibrils. Nonetheless, the lag time observed was not different to the other lag times using sonicated fibrils, suggesting that the 3Q fibrils are possibly densely clumping and impeding α-synuclein to bind to the fibril surface. It can be therefore concluded that at pH 4.5 a higher concentration of α-synuclein monomer might preferentially bind to the surface of the Aβ fibrils, providing a higher chance for the α-synuclein monomers to form nuclei and consequently aggregate into fibrillar material.

As there were no significant differences between the lag times and half times of α-synuclein aggregation at pH 4.5 after cross-seeding with $A\beta_{40}$ and $A\beta_{42}$ fibrils it could be speculated that the associations between the α-synuclein monomer and the fibrils could be occurring in the same region of the Aβ fibril structures. Solvent exposure of the N-terminal region of Aβ is observed in

all the fibril morphologies of $A\beta_{40}$ and $A\beta_{42}$ (Petkova et al., 2005; Paravastu et al., 2008; Colvin et al., 2016; Gremer et al., 2017). In particular the 2A and 3Q $A\beta_{40}$ fibril structure, as well as and pH 2 $A\beta_{42}$ structures present a solvent exposed N-terminal and a buried C-terminal: residues 29-40 or 42, and the highly hydrophobic region 30-36, can be found in the core of the fibril structures (Gremer et al., 2017). This is in contrast with the pH 8 $A\beta_{42}$ fibril structure, where part of the C-terminal region is solvent exposed, apart from residues 29-38 which are buried in the fibril core, leaving its last β-sheet solvent exposed. The highly hydrophobic KVLFF region (residues 16-22) of Aβ is located in middle of the Aβ sequence and could be an area where association with α-synuclein could occur. In isolation, $A\beta_{16-22}$ is known to aggregate faster than $A\beta_{40}$ and can cross-seed $A\beta_{40}$ through surface catalysed nucleation (Bunce et al., 2019).

The determination of which α-synuclein region is interacting with the Aβ fibrils is more complicated. Evidence of what is observed on Aβ plaques from Alzheimer's disease cases show that the NAC region of α-synuclein (residues 61–95) is commonly associated with Aβ plaques (Ueda et al., 1993) and is known to self-aggregate (Giasson et al., 2001; Iwai et al., 1995). However, evidence on α-synuclein membrane binding might come as an alternative explanation of where interactions with Aβ fibrils might occur. In this regard, the N-terminal region of α-synuclein has been implicated in vesicle and membrane binding (Fusco et al., 2016; Maltsev et al., 2012), in particular residues 1-12 were found to associate to DOPE:DOPS:DOPC vesicles in MD simulations . In addition, α-synuclein is known to aggregate in the presence of lipids. At low lipid to α-synuclein ratios primary nucleation can occur on the vesicle surfaces on which α-synuclein is bound (Galvagnion et al., 2015). The precise site in α-synuclein binds to Aβ fibrils remains to be clarified, for example using α-synuclein variants or cross-seeding mass-spectrometry experiments.

Finally, fibril polymorphism was assessed by curcumin binding of the α-synuclein fibrils obtained after cross-seeding with $A\beta_{40}$ or $A\beta_{42}$ fibrils. This method has been previously used to distinguish between strains of brain derived α-synuclein fibrils by comparing the spectral shape and fluorescence intensities between the α-synuclein fibrils (Lau et al., 2020; Strohaker et al., 2019). In this study no significant differences were observed in the spectra shape of the α-synuclein fibrils formed at pH 4.5 by cross-seeding with 20% (v/v) 2A, 3Q and *de novo* $A\beta_{40,}$ or pH 2 and pH 8 $A\beta_{42}$ fibrils. This minimal difference in spectral shape has been observed for *in vitro* generated fibrils of α-synuclein, but principle component analysis revealed different fibril populations for these (Strohaker et al., 2019). In the present study clear differences in curcumin fluorescence intensities were observed. The curcumin fluorescence intensities of the α-synuclein fibrils formed by incubation with 20% (v/v) $A\beta_{40}$ preparations were significantly different between them. This suggests that these α-synuclein fibrils bind to curcumin differently and this

might be related to distinct fibril structural arrangements. A comparison with the unseeded α-synuclein fibrils would allow a better understanding of this interaction and determine if the structural arrangement of cross-seeded α-synuclein fibrils changed when cross-seeded with the different $A\beta_{40}$ or $A\beta_{42}$ fibril polymorphs.

Given the results shown here, it would be interesting to determine in more detail cross-seeded α-synuclein fibrils differ from each other, as well from unseeded α-synuclein fibrils by other structural techniques. CryoEM and ssNMR have been used in the past to determine the structure of full-length α-synuclein fibrils formed at pH 7-9 (Tuttle et al., 2016a; Li et al., 2018; Guerrero-Ferreira et al., 2019; Guerrero-Ferreira et al., 2018). It would be interesting to see if the change in pH, as well as the fact that the fibrils were secondary nucleated by $A\beta_{40}$ or $A\beta_{42}$ affect the structure of α-synuclein fibrils.

In the next chapter the analysis of the cross-seeding of α-synuclein by the distinct Aβ fibril preparations is analysed in cells. The assessment of α-synuclein inclusion formation after the incubation with Aβ fibrils is performed using a SH-SY5Y cell model that overexpresses GFP-α-synuclein. Analysis of α-synuclein aggregate formation and the involvement of lysosomes is also evaluated.

5. Cross-seeding of α-synuclein by Aβ$_{40}$ and Aβ$_{42}$ fibrils in a cellular model

5.1. Introduction

Lewy bodies are cytosolic insoluble aggregates, made of an array of proteins and cellular components (Forno, 1996), but are mainly characterised by the presence of α-synuclein fibrils and filaments (Spillantini et al., 1997). They exhibit strong α-synuclein staining in the core and surrounding halo, as well as strong ubiquitin staining in their halo (Spillantini et al., 1998).

Parkinson's disease, dementia with Lewy bodies, Parkinson's disease with dementia and MSA, are characterised by the presence of Lewy bodies (Lashuel et al., 2013). Differences in α-synuclein aggregate distribution can reflect different pathologies. Individuals with dementia with Lewy bodies appear to have a higher burden of α-synuclein in the cortex, compared to Parkinson's disease patients, as well as presenting with a different sequence over time of motor and dementia symptoms, which reflects a worsening of prognosis with the increase in burden of Lewy bodies (McKeith, 2007).

Lewy bodies are also known to accumulate in up to 60% of individuals with Alzheimer's disease (Hamilton, 2000; Jellinger, 2003). In the case of Alzheimer's disease, a higher density of Lewy bodies is observed in the amygdala compared to those observed in the cortex (Jellinger, 2003). Co-occurrence of both α-synuclein and Aβ pathology is observed in Down syndrome (Lippa et al., 1999b). As discussed previously (Chapter 1), there is an overproduction of Aβ protein due to the triplication of chromosome 21 that encompasses the APP gene. In addition to neuritic plaques, these individuals normally present co-existing Lewy body pathology, a hallmark not observed in unaffected people (Ballard et al., 2011; Margallo-Lana et al., 2004). Proteomic analysis of hippocampal brain sections diagnosed with subtypes of Alzheimer's disease individuals showed that rapidly progressive Alzheimer's disease individuals had a significantly different proteome from those diagnosed with sporadic Alzheimer's disease, who displayed lower levels of α-synuclein, whilst showing the same levels of tau, ApoE and ubiquitin between both groups (Drummond et al., 2017).

Immunohistochemistry analysis of brain cortex sections has also revealed differences Aβ isoform distribution related to the presence of Lewy bodies. An increased ratio of Aβ$_{40}$ deposition has been observed in brain cortex tissue of cases of Alzheimer's disease, whereas dementia with Lewy bodies individuals present a higher concentration of Aβ$_{42}$ (Lippa et al., 1999a).

Having demonstrated that α-synuclein fibrillar aggregation can occur via cross-seeding with Aβ at pH 4.5 *in vitro* (Chapter 4, Section 4.4 and 4.5), the analysis of α-synuclein cross-seeding was investigated in a cellular model for α-synuclein aggregation. First, the effect of the different Aβ fibril preparations, as well as the cross-seeded and self-seeded α-synuclein fibrils, on cell viability was analysed. The association of the Aβ fibril preparations with cells over expressing α-synuclein was then analysed, to evaluate their effect on the cross-seeding of α-synuclein. Lastly, the involvement of acidic organelles on the cross-seeding effect was investigated through cellular and biochemical assays.

5.2. Development of a cellular model for α-synuclein seeding

Insoluble α-synuclein aggregate formation has been widely studied on cells overexpressing WT and mutant α-synuclein (Hasegawa et al., 2004), primary neurons (Volpicelli-Daley et al., 2014; Mahul-Mellier et al., 2020), as well as neuroblastoma cell lines (Luk et al., 2009). This has been primarily done by incubation with preformed α-synuclein fibrils with the cells over a set period of time. Specifically, the generation of α-synuclein positive puncta is known to occur in neuroblastoma cells overexpressing human WT α-synuclein, after the incubation with *in vitro* generated α-synuclein fibrils (Luk et al., 2009).

To study the cross-seeding effect of Aβ fibril preparations in cells a GFP-α-synuclein cell line developed in the Hewitt lab was used. This cell line stably expresses GFP-α-synuclein and was generated by initially cloning the α-synuclein sequence into a pAcGFP1 vector (Figure 5.1 A) and transfecting it into SH-SY5Y neuroblastoma cells to generate a stably transfected cell line. These SH-SY5Y-GFP-α-synuclein cells express GFP and human WT α-synuclein through a CMV enhancer and promoter. The predicted expressed protein consists of GFP linked to the N-terminal region of α-synuclein by a short spacer sequence (Figure 5.1 B) and has a predicted molecular weight of 42.53 kDa.

First, a self-seeded experiment using human WT α-synuclein 50 nm long fibrils (kindly provided by Mike Davies), known as seeds, was set up, in order to test whether insoluble GFP-α-synuclein aggregates were formed after a 6-day incubation with pre-formed α-synuclein short fibrils. Cells incubated with the fibril buffer were analysed in parallel. The initial experimental system did not include any washing steps before fixing with formaldehyde, prior to imaging.

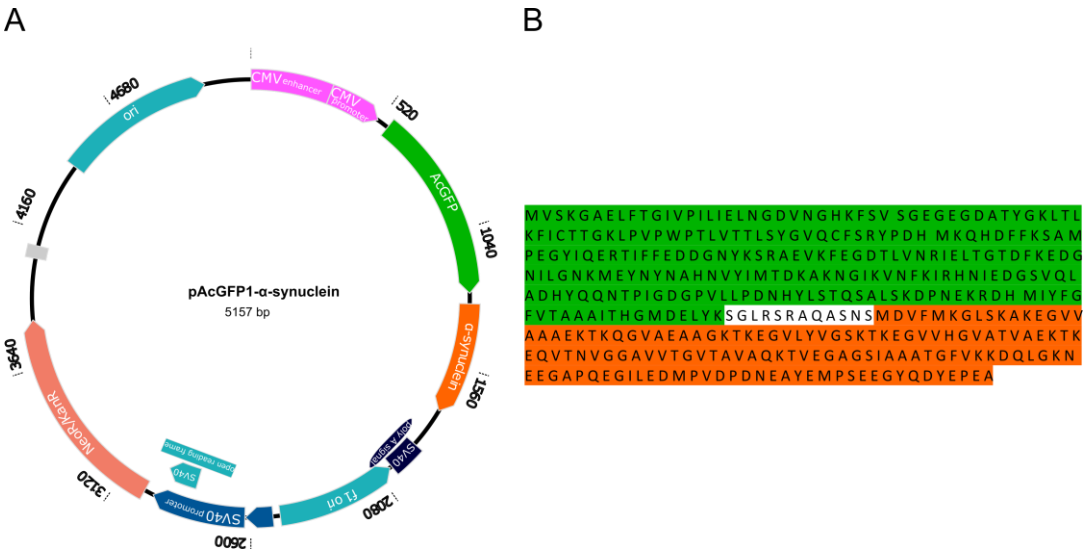

Figure 5.1. GFP-α-synuclein vector and predicted protein sequence.
Representation of the GFP-α-synuclein plasmid (A). The AcGFP is at N-terminus of α-synuclein and there is a short linker sequence between both genes. The predicted protein sequence of AcGFP-α-synuclein (B), shows the AcGFP protein sequence in green, the short linker region and the α-synuclein protein sequence in orange.

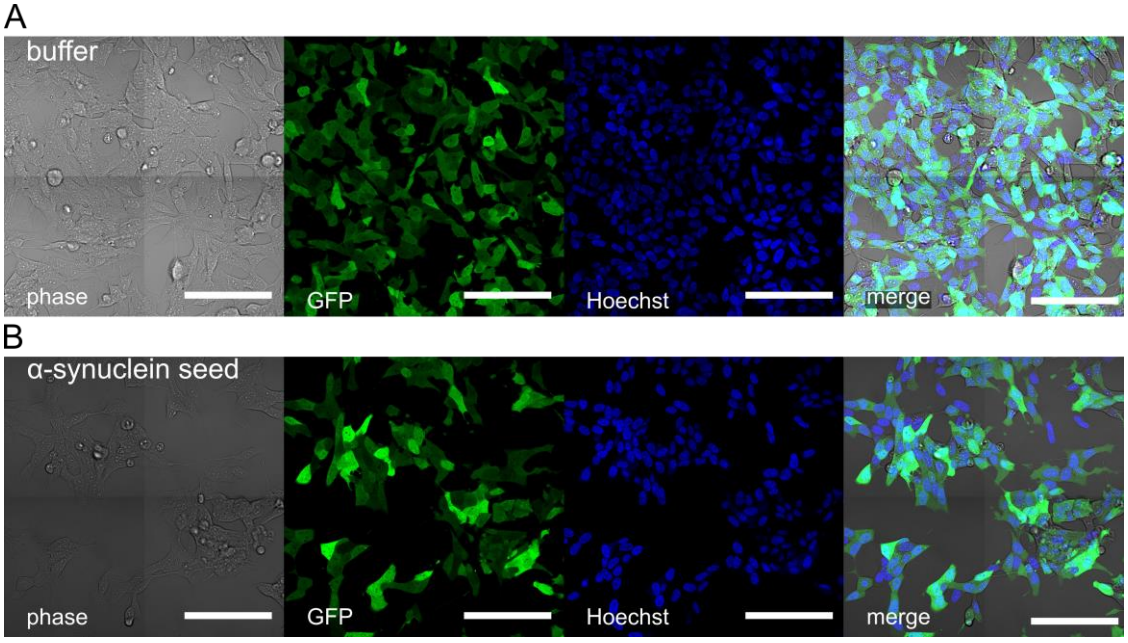

Figure 5.2. Analysis of GFP-α-synuclein insoluble aggregate formation in unpermeabilised SH-SY5Y-GFP-α-synuclein cells.
After a 6-day incubation with fibril buffer (A) or α-synuclein seeds (B) (1 µM, monomer equivalent) the cells were fixed and analysed by confocal imaging. Unpermeabilised cells did not show significant differences in GFP-α-synuclein. Scale bar 100 µm.

In this experimental set up, it was not possible to observe differences in levels of GFP-α-synuclein, nor any distinctive GFP-α-synuclein puncta, when comparing the buffer treated cells and α-synuclein seeded cells up (Figure 5.2 A and B). The high levels of soluble GFP-α-synuclein may be masking any insoluble puncta when imaged by fluorescence microscopy. It was therefore decided include a mild detergent wash prior to fixation and imaging. This step was done by subjecting the cells to a wash with *Quillaja* bark saponin, from here onwards referred as saponin. Saponin is a plant derived glycoside and biosurfactant that forms a 1:1 complex with membrane sterols, such as cholesterol, that leads to the formation of pores on the membrane and cell lysis (Jamur and Oliver, 2010; Augustin et al., 2011). Saponin is also known to disassociate proteins, facilitating their unfolding (Piotrowski et al., 2012). This experimental set up relies on the property of saponin to remove soluble protein and soluble aggregates from the samples in order to visualize saponin resistant GFP-α-synuclein aggregates. After this, the cells were fixed with formaldehyde, stained with the nuclear dye Hoechst and imaged by confocal microscopy. GFP puncta formation was quantified by using the Fiji software's particle analysis plugin. Cells were incubated with either α-synuclein monomer or buffer were analysed in parallel.

It was observed that incubation with α-synuclein seeds (Figure 5.3 C) resulted in a greater number of GFP puncta in the cells when compared to cells incubated with either buffer or α-synuclein monomer (Figure 5.3, A and B). Quantification of puncta number confirmed that this difference was significant between the α-synuclein seeded and the other two samples (Figure 5.4). These data therefore demonstrate that SH-SY5Y-GFP-α-synuclein cells are an appropriate cellular model to study α-synuclein aggregation.

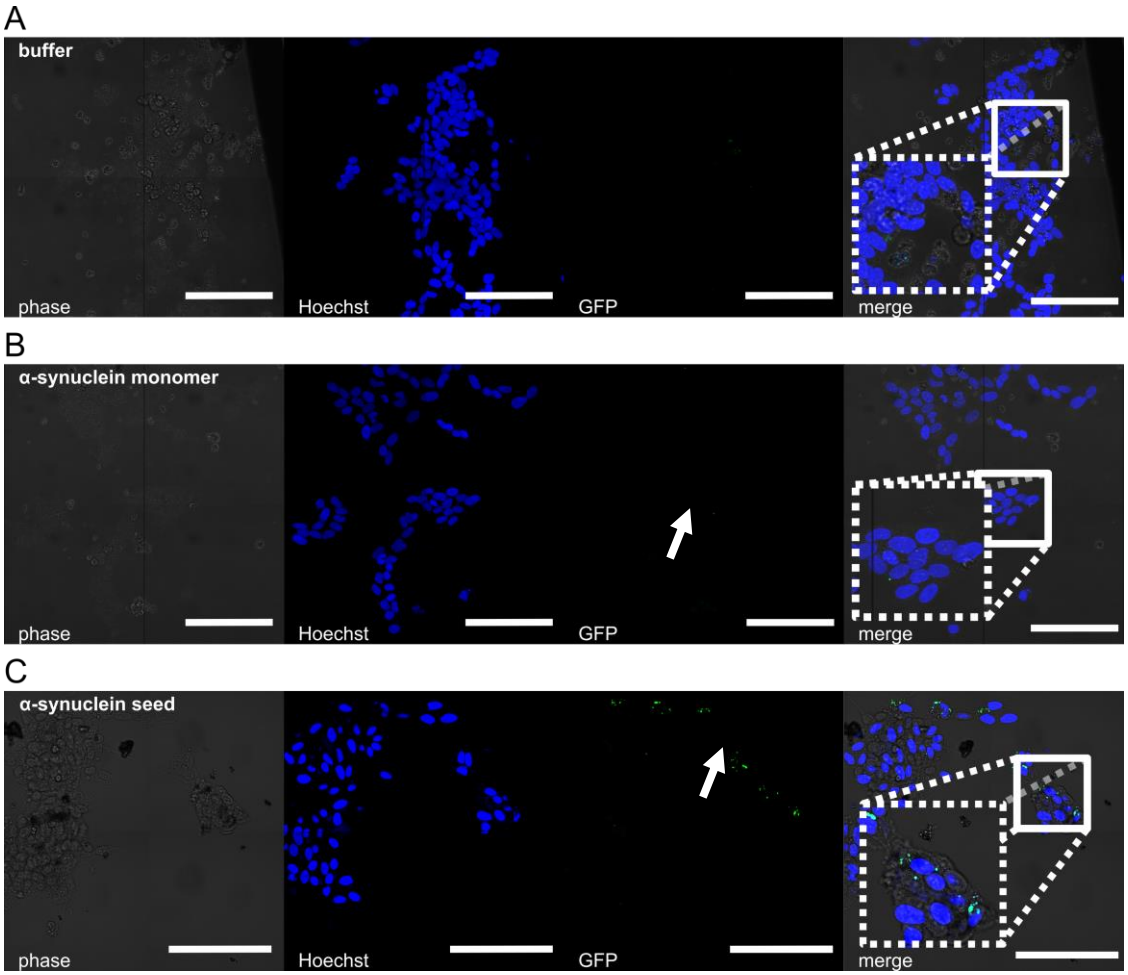

Figure 5.3. Insoluble GFP puncta formation in SH-SY5Y-GFP-synuclein cells after incubation with α-synuclein seeds.

After incubating the cells with fibril buffer (A), 1 µM synuclein monomer (B) or 1 µM (monomer equivalent) α-synuclein monomer seeds (C) for 6 days, cells were permeabilised with 0.2% saponin to remove soluble material and fixed with 4% formaldehyde. Hoechst staining was performed to visualize nuclei. Imaging was performed with a confocal LSM880 or LSM700 microscope, using 2X2 tiles and doing z-stack at 40X magnification. Incubation of the cells with α-synuclein seed resulted in the increased formation of insoluble GFP (arrows) when compared to the buffer treated control. In contrast, incubation with the α-synuclein monomer did not result in the formation of insoluble GFP puncta numbers different to the buffer treated cells. Scale bar is 100 µm.

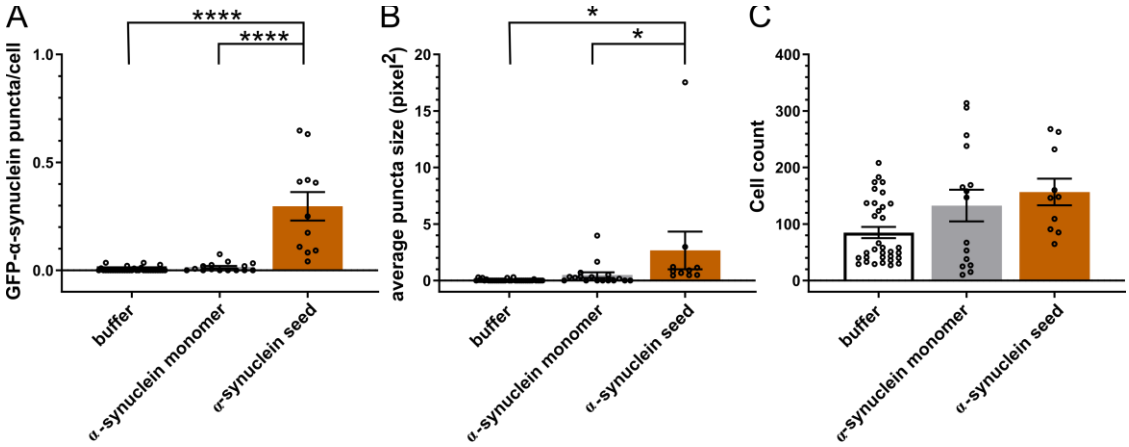

Figure 5.4. Quantification of insoluble GFP puncta, average area of puncta and cell number in SH-SY5Y-GFP-synuclein cells after incubation with buffer, α-synuclein monomer or α-synuclein seeds.

*After imaging, GFP puncta (A), puncta average size (B) and cell number by nuclei count (C) quantification was performed. A) Incubation with 1 μM α-synuclein for 6 days resulted in a significantly higher number of GFP puncta visualized in cells, compared to what was observed in the α-synuclein monomer and buffer treated cells. B) The average size of puncta observed was significantly larger in cells incubated with α-synuclein seeds than with monomer or buffer. C) On average, the same number of cells per field were imaged in the samples analysed. N=3. Mean ± S.E. Significance level after ANOVA with Tukey multiple comparison test: * $p<0.05$, **** $p < 0.0001$.*

5.3. Cellular toxicity of $A\beta_{40}$ and $A\beta_{42}$ fibril preparations

Next the effect of the Aβ fibril polymorphs on the viability of SH-SY5Y-GFP-α-synuclein cells was analysed. Firstly, cellular viability was analysed after incubation of the $A\beta_{40}$ and $A\beta_{42}$ fibril preparations with the cells for a period of 48 h. A differential effect of the 2A and 3Q $A\beta_{40}$ fibril polymorphs has been reported in cortex neurons from rats after a 48 h incubation. Over 50% neuronal death was observed after the incubation with 10 - 75 μM 2A fibrils (Petkova et al., 2005), and more than 80% neuronal death was seen after incubation with 10 - 75 μM 3Q fibril preparations (Paravastu et al., 2008). Cellular toxicity has also been assessed after incubation with the pH 2 or pH 8 $A\beta_{42}$ fibrils. Gremer et al. (2017) reported a >50% decrease in MTT reduction after incubation with 0.1 – 3 μM monomer equivalent of fibrils in PC12 cells. A decrease of 20 - 60% of 3-(4,5-dimethylthiazol-2-yl)-5-(3-carboxymethoxyphenyl)-2-(4-sulfophenyl)-2H-tetrazolium (MTS) reduction was observed after the 24 h incubation with 0.01 μM (monomer equivalent) pH 8 $A\beta_{42}$ fibrils in SH-SY5Y cells (Cohen et al., 2015). Here, cell viability assays performed after the incubation with 0.5 – 3 μM (monomer equivalent) of 2A, 3Q and *de novo* $A\beta_{40}$, as well as pH 2 and pH 8 $A\beta_{42}$ fibril preparations.

Cellular ATP quantification (Figure 5.5 A) was performed with a commercial assay that uses D-luciferin as the substrate for the firefly luciferase enzyme. The enzyme adenylates the substrate

via ATP hydrolysis, and the substrate is then oxidised, generating oxyluciferin, inorganic pyrophosphates (PPi) as well as a luminescent signal. This luminescent signal is proportional to the number of viable cells at the time analysed (Teow et al., 2019). It was observed that a 48 h incubation with 0.5 – 3 μM $A\beta_{40}$ fibril preparations (Figure 5.5 B), or 0.5 – 1 μM (monomer equivalent) $A\beta_{40}$ fibril preparations (Figure 5.5 C) did not have any significant effect on ATP levels. ATP levels at these fibril concentrations were comparable to buffer treated cells. In contrast, incubation with 3 μM (monomer equivalent) pH 8 $A\beta_{42}$ fibrils resulted in a decrease of ~20% cellular ATP compared to the buffer treated cells (Figure 5.5 C). No significant difference in cellular ATP, compared to the buffer treated cells, was observed after incubating with 3 μM (monomer equivalent) pH 2 $A\beta_{42}$ fibrils.

In parallel, a lactate dehydrogenase (LDH) release assay (Figure 5.6 A) was used to quantify the degree of membrane damage after incubation with the fibril preparation. LDH is a stable cytoplasmic enzyme found in all cells that is released into culture media when the plasma membrane has been damaged. The assay is based on the production of NADH after the reduction of lactate into pyruvate by LDH catalysis. The NADHs produced are used to reduce a 2-p-iodophenyl-3-p-nitrophenyl tetrazolium chloride (INT), a tetrazolium salt, into formazan crystals via diaphorase catalysis. Formazan crystals can then be dissolved, and absorbance can be measured. In this case, the amount of formazan produced will be proportional to the amount of LDH present in the media (Parhamifar et al., 2013; Kumar et al., 2018a). After the incubation with 0.5 – 3 μM $A\beta_{40}$ or $A\beta_{42}$ fibril preparations no significant increase in LDH was detected in the culture media (Figure 5.6 B and C), compared to the buffer treated cells.

Finally, cellular metabolism was measured using a 3-(4,5-dimethylthiazol-2-yl)-2,5-diphenyltetrazolium bromide (MTT) reduction assay. The MTT assay depends on the reduction of MTT into formazan crystals by the action of cellular NADases located in the mitochondria of viable cells (Figure 5.7 A). This assay can be used to measure the growth rate of cells and a linear relationship between cell activity and absorbance is noted (Mahajan et al., 2012; Kumar et al., 2018b). As before, cells were incubated with 0.5 – 3 μM $A\beta_{40}$ and $A\beta_{42}$ fibril preparations for 48 h. There was no decrease in MTT reduction after incubation with $A\beta_{40}$ fibril preparations at any of the concentration (Figure 5.7 B). However, a ≥50 % decrease in reduction of MTT was observed after incubation with either pH 8 or pH $A\beta_{42}$ fibrils at all concentrations tested (Figure 5.7 C). A further decrease in MTT reduction was seen with after incubation with 3 μM pH 8 fibrils, compared to the pH 2 $A\beta_{42}$ fibril treated cells.

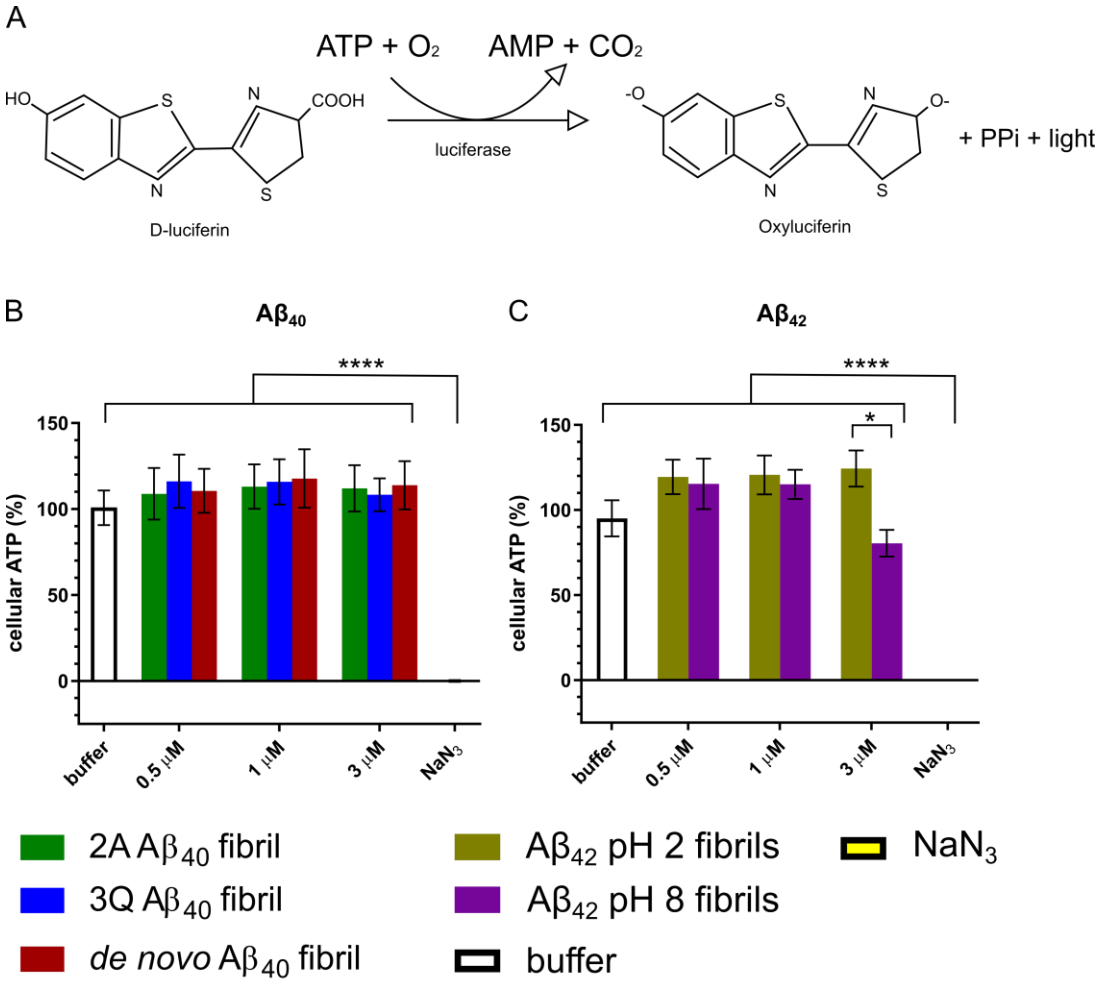

Figure 5.5. ATP cellular viability assay after 48 h incubation with $A\beta_{40}$ and $A\beta_{42}$ fibril preparation. The ATP assay reaction (A) is based on the reaction of the D-luciferin substrate with the luciferase enzyme via ATP hydrolysis.

*The enzyme luciferase can act on the substrate and turn it into oxyluciferin, inorganic pyrophosphate phosphate (PPi) and light. The amount of light produced is proportional to the amount of ATP present in the cell media after cell lysing. SHSY5Y-α-synuclein-GFP cells were incubated with 0.5, 1 and 3 μM (monomer equivalent) 2A, 3Q and de novo $A\beta_{40}$ fibrils preparations (B) and pH 2 and pH 8 $A\beta_{42}$ fibrils (C) for 48 h and subjected to viability assays. Cells incubated with the fibril buffer or 2% (w/v) NaN_3 were incubated and analysed in parallel. Cellular ATP levels did not significantly decrease after the incubation with any concentration of the $A\beta_{40}$ the fibril preparations compared to the buffer treated cells. The same was observed after the incubation with 0.5 or 1 μM of either $A\beta_{42}$ fibril preparation, when compared to the buffer treated cells. However, at 3 μM, a ~20% decrease in cellular ATP levels was observed in cells incubated with pH 8 fibrils, but not pH 2 fibrils. Incubation with NaN_3 killed the cells observed as null ATP levels. ATP levels were calculated after normalising against buffer treated cells (100%) and NaN_3 treated cells (0%). Error bars represent one S.E. over three independent experiments containing at least 3 replicates each. Significance level after Two-way ANOVA with Tukey multiple comparison test: * $p<0.05$, **** $p<0.0001$.*

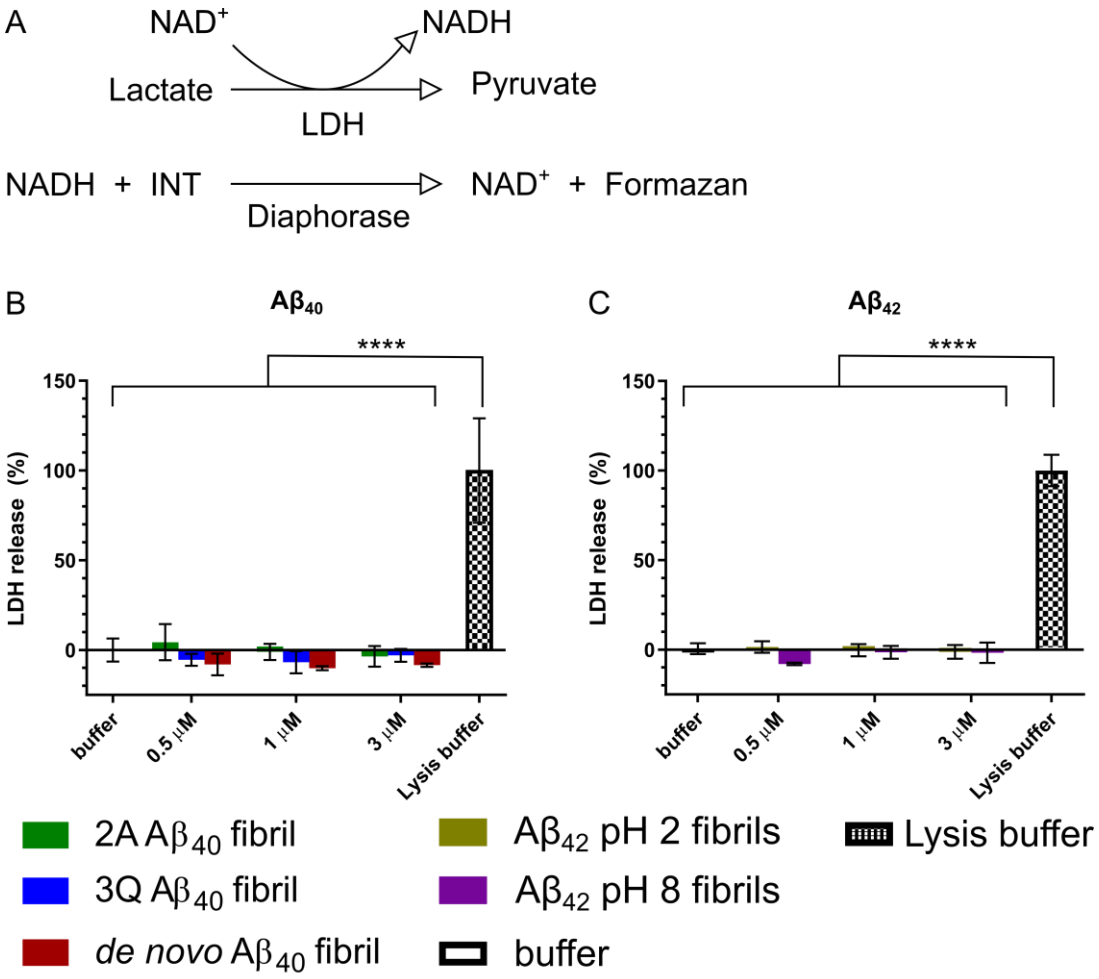

Figure 5.6. LDH cellular viability assay after 48 h incubation with $A\beta_{40}$ and $A\beta_{42}$ fibril preparation.

*The LDH assay (A) is based on the production of NADH after the reduction of lactate into pyruvate via LDH catalysis. 2-p-iodophenyl-3-p-nitrophenyl tetrazolium chloride (INT), a tetrazolium salt, is then reduced by diaphorase into formazan crystals via NADH hydrolysis. SHSY5Y-α-synuclein-GFP cells were incubated with 0.5, 1 and 3 μM (monomer equivalent) 2A, 3Q and de novo $A\beta_{40}$ fibrils preparations (B) and pH 2 and pH 8 $A\beta_{42}$ fibrils (C) for 48 h and subjected to viability assays. LDH release was not significatively increased after the incubation with the $A\beta_{40}$ nor $A\beta_{42}$ fibril preparations, implying there was no disruption to cell membranes at the timepoint analysed. Maximum LDH release was observed by lysing the cell 20 minutes prior performing the assay with the kit's lysis buffer. LDH levels were calculated after normalising against lysed cells (100%) and buffer treated cells (0%). Error bars represent one S.E. over three independent experiments containing at least 3 replicates each. Significance level after Two-way ANOVA with Tukey multiple comparison test: * $p<0.05$, **** $p<0.0001$.*

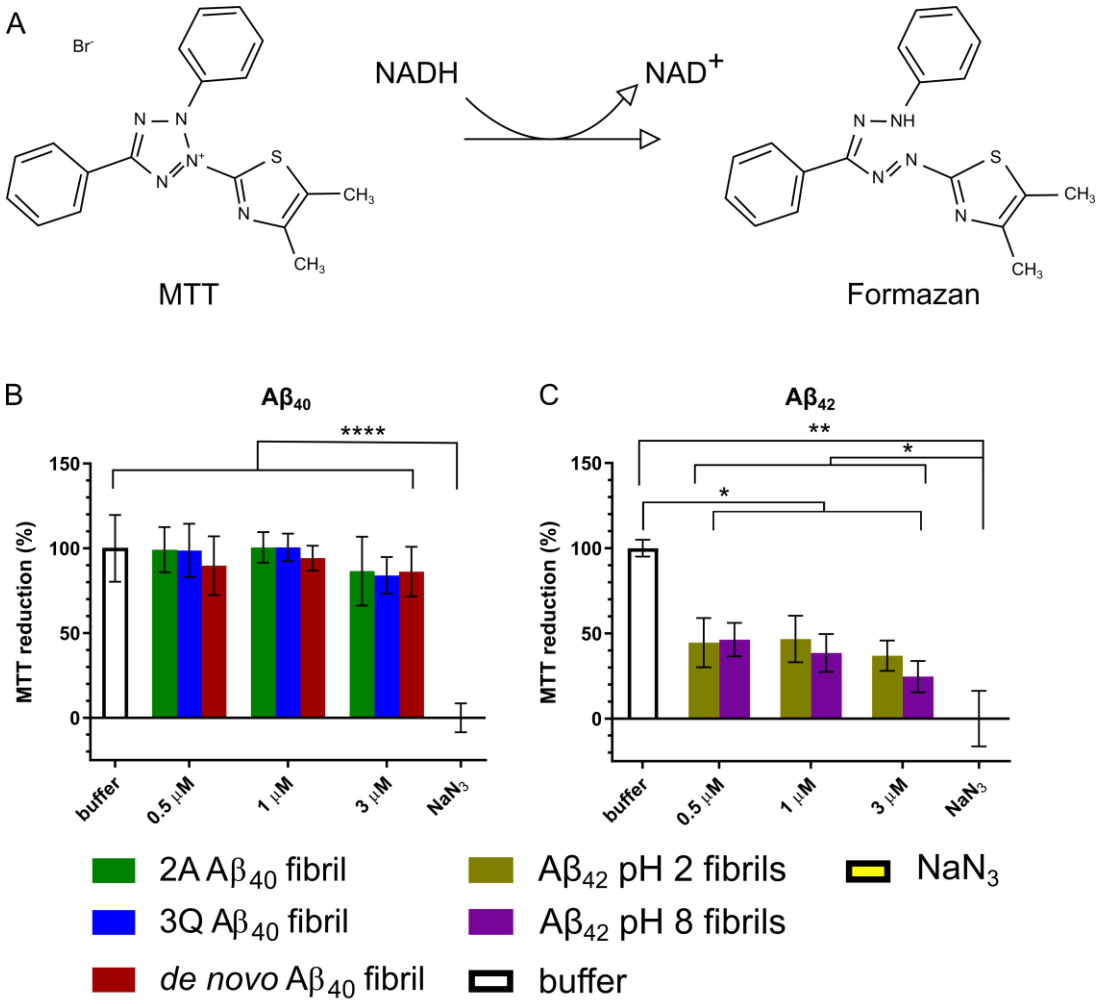

Figure 5.7. MTT cellular viability assay after 48 h incubation with Aβ$_{40}$ and Aβ$_{42}$ fibril preparation.
*Reduction of MTT (A) is analysed by a colorimetric assay in which MTT is reduced into formazan crystals by NADase catalysis and NADH hydrolysis. Incubation with Aβ$_{40}$ fibril preparations did not decrease MTT reduction by the cells compared to the buffer treated cells. Incubation with 2% (w/v) NaN$_3$ killed the cells. In contrast, MTT reduction was significantly affected after the incubation with Aβ$_{42}$ fibril preparations (C), compared to the buffer treated cells. A decrease in ~50% MTT reduction was observed at all concentrations with the pH 2 treated cells whereas a 50 – 75% decrease was seen for the pH 8 treated cells. MTT levels were calculated after normalising buffer treated cells (100%) and NaN$_3$ treated cells (0%). Error bars represent one S.E. over three independent experiments containing at least 3 replicates each. Significance level after Two-way ANOVA with Tukey multiple comparison test: * p<0.05, ** p<0.01, **** p<0.0001.*

These results indicate that there is differential toxicity observed in the cells depending on the Aβ fibril preparation used. Noticeably, no significant viability decrease was observed in Aβ$_{40}$ fibril treated cells compared to the buffer control treated cells. In contrast, cells incubated with Aβ$_{42}$ fibrils showed a decrease in cellular ATP at 3 μM fibril concentration, whilst a >50% decrease in MTT reduction was seen at all fibril concentrations.

These data therefore demonstrate that $A\beta_{40}$ fibrils are not toxic under the experimental parameters used, but $A\beta_{42}$ fibril may be toxic to SHSY5Y-α-synuclein-GFP cells. However, even though no decrease in viability was observed after incubation with $A\beta_{40}$ fibrils preparations longer assay time frames might reveal a toxic effect in the cells.

5.4. Cellular toxicity cross-seeding derived α-synuclein fibrils

Evidence of the differential effect of α-synuclein fibrils have on cell viability has been observed previously. Yonetani, et al. (2009) found that A30P α-synuclein fibrils exhibited a decrease on cellular MTT reduction compared to WT α-synuclein fibrils. They also observed that cross-seeded WT α-synuclein fibrils formed in the presence of A30P fibrils and mutant A30P α-synuclein fibrils formed in the presence of WT fibrils, decreased MTT reduction more than WT α-synuclein fibrils.

Cell viability assays were performed to analyse whether fibrils generated by cross-seeding with 20% (v/v) $A\beta_{40}$ fibril preparations were more toxic than those produced in the absence of cross-seeding. For this, SH-SY5Y-GFP-α-synuclein cells were incubated with 0.5 – 5 μM cross-seeded fibril preparations, unseeded α-synuclein fibrils, or 20% (v/v) seeded α-synuclein fibrils from the ThT binding kinetic experiments (Chapter 4, Section 4.4), although grown in the absence of ThT. As controls, buffer or NaN_3 treated cells were analysed in parallel. After a 48 h incubation, cellular viability was assessed using the previously described ATP, MTT and LDH assays. No decrease in cellular ATP (Figure 5.8 A), nor an increase in LDH release (Figure 5.8 B) was observed with either of the α-synuclein fibrils, compared to the buffer treated cells. However, MTT reduction (Figure 5.8 C) decreased after the incubation with 0.5 - 5 μM cross-seeded α-synuclein fibrils compared to the buffer treated cells. In addition, cells incubated with self-seeded α-synuclein fibrils, but not unseeded α-synuclein fibrils presented this decrease in MTT reduction. Inhibition of MTT reduction was not differential between the α-synuclein cross-seeded fibrils, nor the α-synuclein seeded or unseeded fibrils as significance difference was not reached after two-way ANOVA and Tukey post hoc test.

These results indicate that the cell viability may be unaffected after incubation with the unseeded α-synuclein fibrils, self-seeded α-synuclein fibrils as well as cross-seeded α-synuclein fibrils.

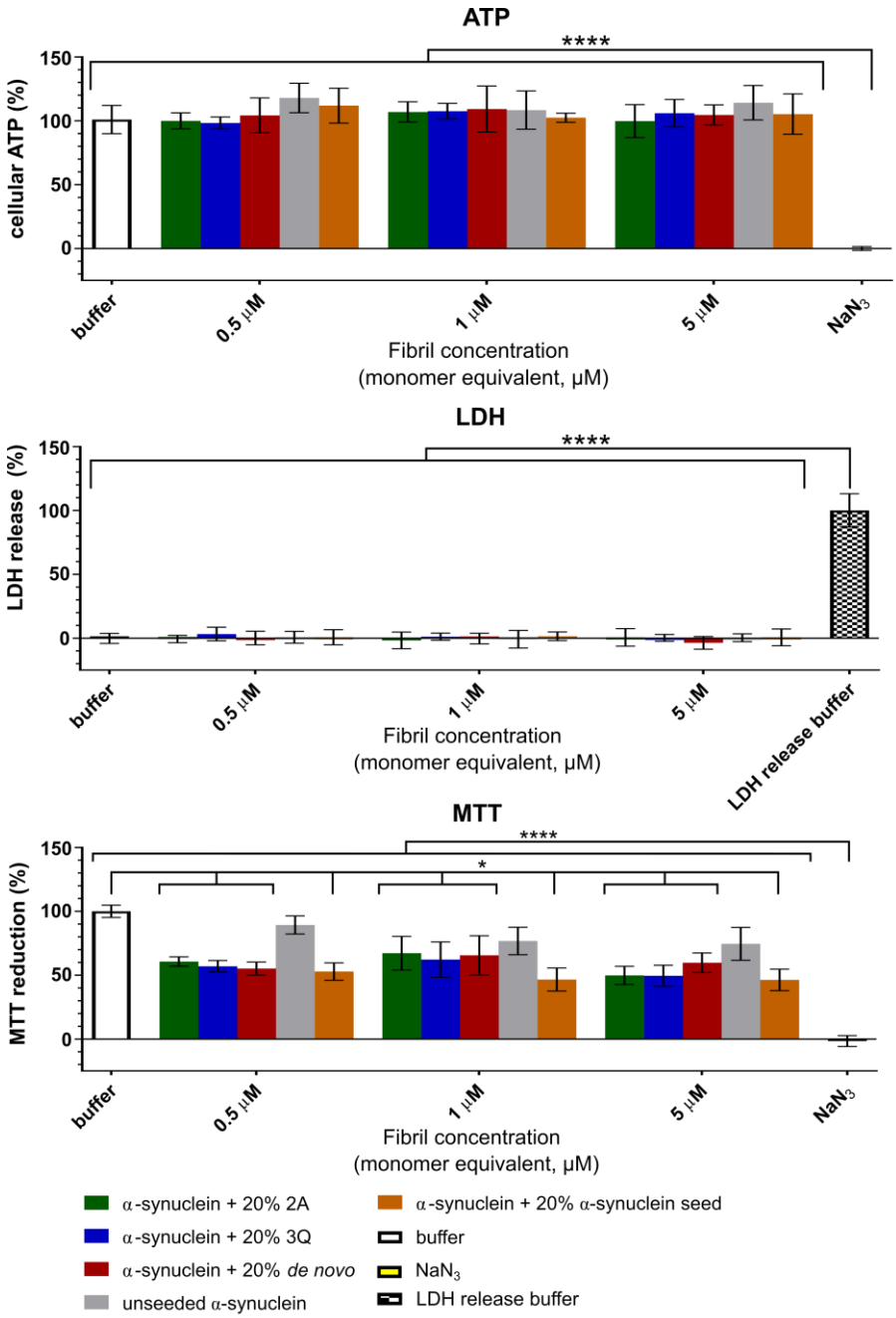

Figure 5.8. Cellular viability assays after 48 h incubation with the α-synuclein cross-seeded fibrils. SHSY5Y-α-synuclein-GFP cells were incubated with α-synuclein fibrils generated after the cross-seeding of α-synuclein with 20% (v/v) Aβ$_{40}$ fibrils preparations for 48 h.
*Cells incubated with the fibril buffer, the unseeded α-synuclein fibrils, the 20% (v/v) seeded α-synuclein fibrils, or 2% (w/v) NaN_3 were analysed in parallel as controls. Cellular ATP levels (A) were not significantly decreased after incubation with either α-synuclein fibrils when compared to the buffer treated cells. LDH release (B) was not increased after incubation with either of the α-synuclein fibrils, implying there was no disruption to cell membranes at the timepoint analysed. In contrast, MTT reduction was inhibited upon incubation with the cross-seeded α-synuclein fibrils and α-synuclein fibrils. ATP and MTT levels were calculated after normalising against buffer treated cells (100%) and NaN_3 treated cells (0%). LDH levels were calculated after normalising against lysed cells (100%). Error bars represent one S.D. over 3 independent experiments containing at least 2 replicates each. Significance level after Two-way ANOVA with Tukey multiple comparison test: * $p<0.05$, ** $p<0.01$, **** $p<0.0001$.*

5.5. Insoluble GFP-α-synuclein puncta formation in cells after incubation with $A\beta_{40}$ and $A\beta_{42}$ fibril preparations

In the next series of experiments, the ability of Aβ fibrils to promote α-synuclein aggregation was analysed using the SH-SY5Y-GFP-α-synuclein cells. To analyse cross-seeding of α-synuclein by the different Aβ fibril polymorphs a 6-day seeding experiment was performed using 1 μM fibrils (monomer equivalent). The experimental procedure included the saponin permeabilization wash before fixing the cells in order to visualize the GFP-α-synuclein insoluble puncta.

Confocal fluorescent imaging of the permeabilised SH-SY5Y-GFP-α-synuclein cells was performed on cells incubated with either $A\beta_{40}$ or $A\beta_{42}$ fibrils. A differential formation of insoluble GFP puncta was observed to occur between the $A\beta_{40}$ fibril incubations (Figure 5.9). Incubation with $A\beta_{42}$ fibril preparations (Figure 5.10) also showed the presence of GFP puncta, although not as prominent as that observed for $A\beta_{40}$ fibril incubated cells. Quantification and ANOVA multiple comparisons of the GFP puncta number (Figure 5.11 A) revealed a significant difference between cells incubated with *de novo* $A\beta_{40}$ fibrils compared to cells incubated with $A\beta_{42}$ pH 8 fibrils. A distinguishable difference in GFP puncta size was also observed after incubation with $A\beta_{40}$ and $A\beta_{42}$ incubated fibril preparations (Figure 5.11 B). *de novo* derived GFP puncta were significantly larger than puncta derived from 2A $A\beta_{40}$, 3Q $A\beta_{40}$, pH 2 $A\beta_{42}$ and pH 8 $A\beta_{42}$ incubations.

In summary, these results show that some Aβ fibril preparations generate a greater number of GFP-α-synuclein puncta and that these puncta are larger. Specifically, *de novo* $A\beta_{40}$ fibrils, known to contain a mixture of fibril polymorphs, generate the most GFP-α-synuclein puncta as well as the larger puncta, when compared to the rest of the $A\beta_{40}$ and $A\beta_{42}$ fibril preparations. In comparison, the 2A $A\beta_{40}$ fibrils were the least efficient in generating GFP-α-synuclein puncta, as well as were seen to produce the smaller puncta in size.

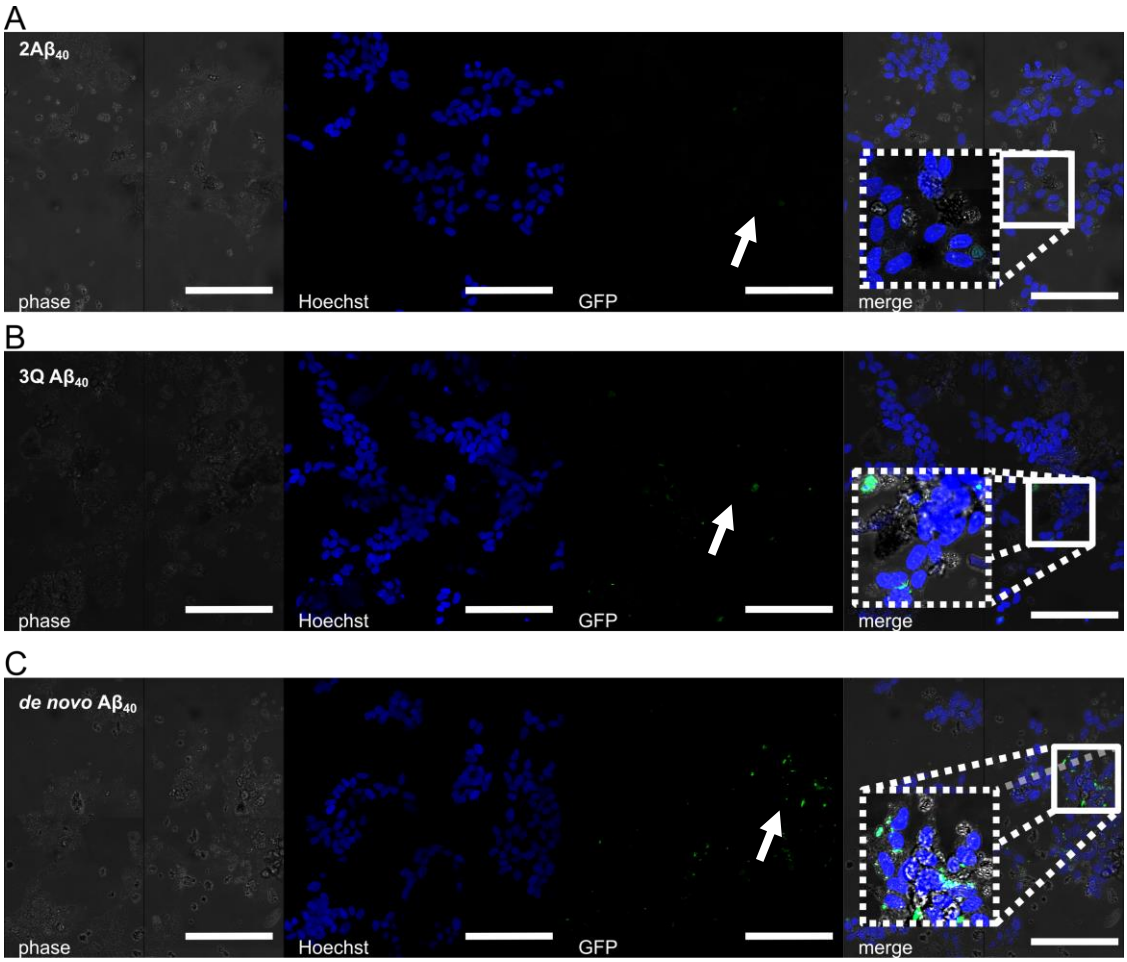

Figure 5.9. Insoluble GFP puncta formation in SH-SY5Y-GFP-synuclein cells after incubation with $A\beta_{40}$ fibril preparations.
After incubating the cells with 1µM 2A (A), 3Q (B), or de novo (C) $A\beta_{40}$ fibril preparations for 6 days, they were permeabilised with 0.2% saponin to remove soluble material and fixed with 4% formaldehyde. Hoechst staining was performed to visualize nuclei. Imaging was done in a confocal LSM880 or LSM700 microscope, at 40X magnification using 2X2 tiles and doing z-stack. Differential formation of GFP insoluble puncta (arrows) was observed between the $A\beta_{40}$ polymorphs, being the de novo treated cells the ones that presented a higher number of puncta compared to the 2A and 3Q treated cells. Scale bar is 100 µm.

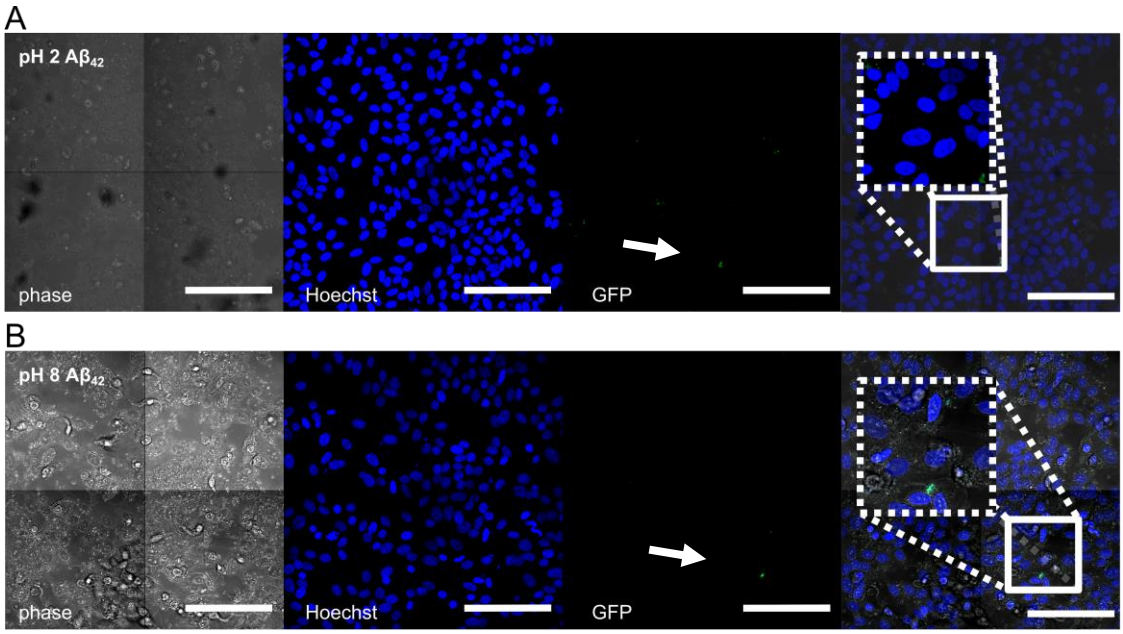

Figure 5.10. Insoluble GFP puncta formation in SH-SY5Y-GFP-synuclein cells after incubation with $A\beta_{42}$ fibril preparations.

After incubating the cells with 1 µM pH 2 (A) and pH 8 (B) $A\beta_{42}$ fibril preparations for 6 days, they were permeabilised with 0.2% saponin to remove soluble material and fixed with 4% formaldehyde. Hoechst staining was performed to visualize nuclei. Imaging was done in a confocal LSM880 or LSM700 microscope at 40X magnification, using 2X2 tiles and doing z-stack. Slight formation of GFP insoluble puncta (arrows) was observed after incubation with the $A\beta_{42}$ fibrils. Scale bar is 100 µm.

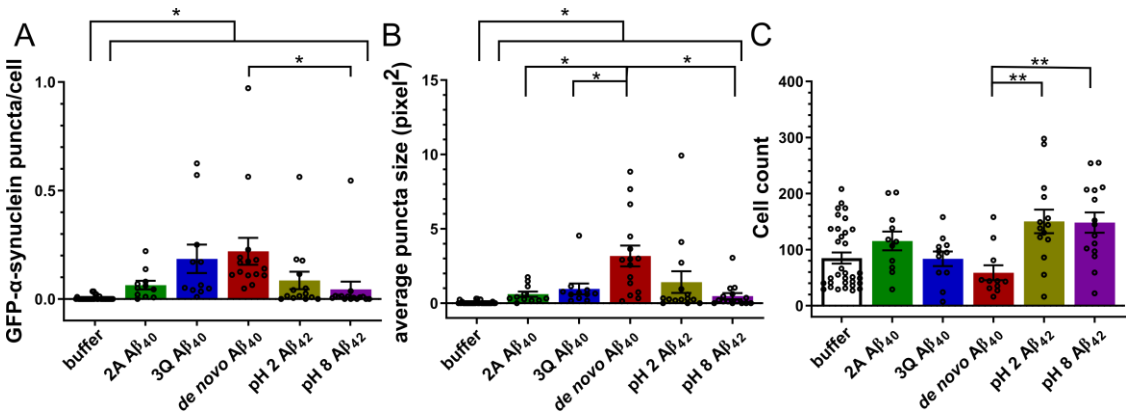

Figure 5.11. Quantification of insoluble GFP-puncta, average area of puncta and cell number in SH-SY5Y-GFP-synuclein cells after incubation with $A\beta_{40}$ and $A\beta_{42}$ fibril preparations.
*After imaging, GFP puncta (A), particle average size (B) and cell number by nuclei count (C) quantification was performed. A) Incubation with 1 μM de novo $A\beta_{40}$ for 6 days resulted in a higher number of GFP puncta visualized in cells, and significantly higher to what was observed in pH 8 $A\beta_{42}$ treated cells. B) The average size of puncta observed was significantly larger in cells incubated with de novo $A\beta_{40}$ fibril preparations. C) On average, the same number of cells per field were imaged in the samples incubated with 2A, 3Q and de novo $A\beta_{40}$ fibril preparations. A significant difference in the number of cells per field was observed between the de novo $A\beta_{40}$ fibril and pH 2 and pH 8 $A\beta_{42}$ fibrils. Error bars represent one S.E. over 3 independent experiments containing at least 3 replicates each. Significance level after Two-way ANOVA with Tukey multiple comparison test: * $p<0.05$, ** $p < 0.01$.*

A complementary approach was used to the imaging experiments to analyse the formation of insoluble α-synuclein in cells incubated with the $A\beta_{40}$ fibrils. For this a sequential detergent fractionation by ultracentrifugation was performed. This method is based on a paired helical filament retrieval from brain tissue for electron microscopy visualization (Goedert et al., 1992). This technique uses N-lauryl sarcosine, also known as sarkosyl, and ultracentrifugation to separate soluble material from insoluble material. Sarkosyl is an anionic mild detergent used for cell lysis. Its capability to selectively disrupt the inner cell membrane of *E. coli* has been documented before (Wroblewski et al., 1978) and its use in cellular fractionation for α-synuclein analysis has been documented for brain tissue and neuronal cell cultures (Guo et al., 2013; Yancopoulou et al., 2005). Variations of this technique, using different detergents, such as Triton X-100 and Nonidet, have also been used to separate insoluble material (Sanderson et al., 2020; Henderson et al., 2017).

To obtain soluble and insoluble fractions cell lysates were subjected to a 1% (w/v) sarkosyl incubation. This was followed by an ultracentrifugation step and subsequent separation of the samples into into soluble, or the supernatant, and pellet, or insoluble, fractions. SDS-PAGE of the fractionated samples (Figure 5.12 A) showed the effective separation into soluble and insoluble cell fractions, as the initially inoculated $A\beta_{40}$ fibril preparations and α-synuclein seeds were only

visible insoluble cell fraction. Probing western blots with an α-synuclein specific antibody (Figure 5.12 B) showed the extensive presence of GFP-α-synuclein in the soluble material of all samples, confirming the need for a detergent wash before fixing for visualization of aggregates using confocal imaging. In contrast, the insoluble cell fraction revealed the differential presence of GFP-α-synuclein between the $A\beta_{40}$ incubated cell samples, and no GFP-α-synuclein was observed in this fraction from buffer incubated cells. The WT α-synuclein seed (100 μM) was analysed as a positive control for α-synuclein the blot. Glyceraldehyde 3-phosphate dehydrogenase (GAPDH) immunoblotting (Figure 5.12 C) of the same cell fractions analysed for the α-synuclein blot was performed as a loading control. GAPDH, is a "housekeeping" enzyme that catalyses the oxidative phosphorylation of glyceraldehyde-3-phosphate during glycolysis (Sikand et al., 2012). No differences in loading could be noted in the soluble cell fractions. Minimal GAPDH was observed in all the insoluble cell fractions, demonstrating the removal of soluble proteins from these fractions.

This analysis confirmed that the formation of insoluble GFP-α-synuclein material is promoted in the presence of Aβ fibrils and α-synuclein seeds in the SH-SY5Y-GFP-α-synuclein cell line. Through this method, the 3Q $A\beta_{40}$ fibrils generated the highest amount of insoluble GFP-α-synuclein material followed by *de novo* Aβ fibrils and α-synuclein seeds. 2A $A\beta_{40}$ fibrils generated the least amount of insoluble GFP-α-synuclein material. No insoluble GFP-α-synuclein was observed in the buffer treated sample. It is to be noted that α-synuclein seeds were the likely source of insoluble full length α-synuclein present in these cells.

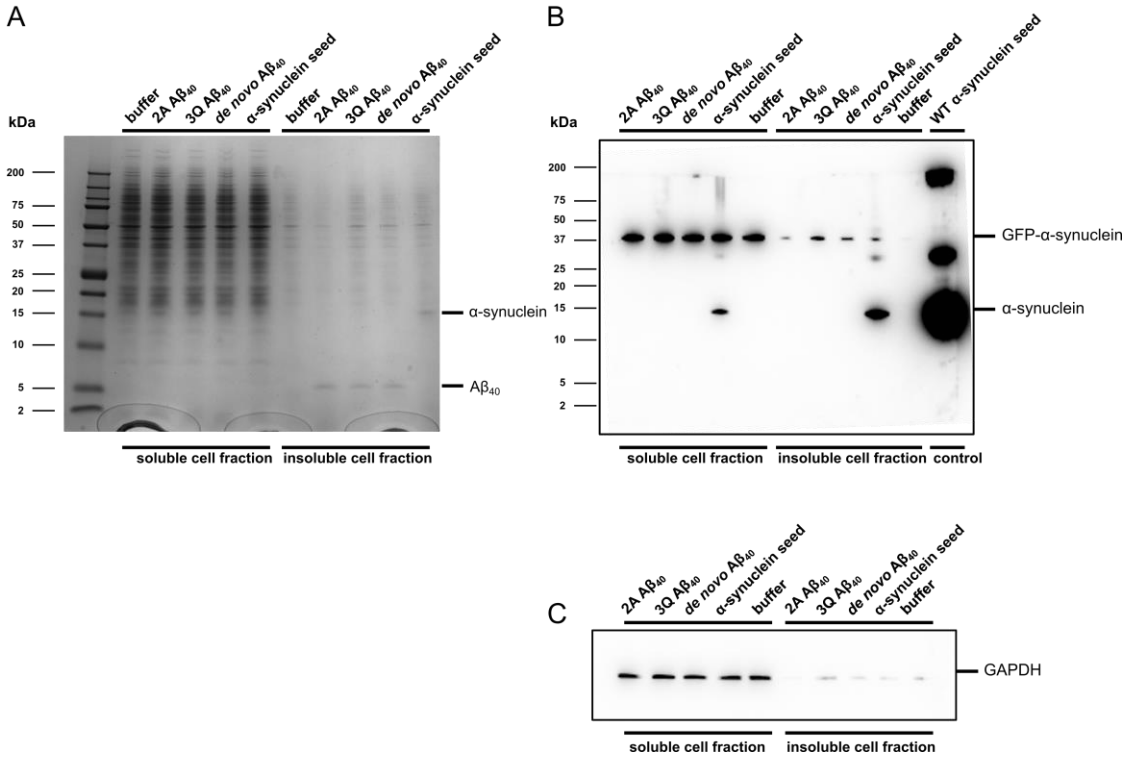

Figure 5.12. Sequential detergent fractionation of SH-SY5Y-GFP-α-synuclein cells after a 6-day incubation with Aβ40 fibril preparations or α-synuclein seeds.
Fractionation into soluble and insoluble material of cells incubated with 1 μM (monomer equivalent) Aβ40 fibril preparations or α-synuclein seeds was done via 1% Sarkosyl incubation and ultracentrifugation. A) SDS-PAGE of the samples displayed the separation into soluble and insoluble cell fractions, showing the initially inoculated Aβ40 fibril preparations and α-synuclein seeds only in the insoluble material. B) Immunoblotting against α-synuclein showed the presence of GFP-α-synuclein in the soluble material of all samples. The insoluble cell fraction showed the differential presence of GFP-α-synuclein between the samples. There was noted absence of GFP-α-synuclein in buffer incubated cells. The WT-α-synuclein seed was analysed (control) as a positive control for the blot. C) Immunoblotting against GAPDH (samples ran in the same order as α-synuclein blot) was done as a control of loading and insoluble fraction separation. No differences in loading could be noted in the soluble cell fractions. Minimal soluble remnants were observed in all the insoluble cell fractions.

5.6. Lysosomal co-localization with Aβ fluorescent fibrils

The results from the experiments described above are consistent with the cross-seeding of α-synuclein aggregation in cells after incubation with Aβ fibril preparations. It has here been shown that α-synuclein is cross-seeded by both $A\beta_{40}$ and $A\beta_{42}$ fibril preparations at pH 4.5 (Chapter 4). For this reason, I investigated whether Aβ fibrils can be internalised by SH-SY5Y-GFP-α-synuclein cells and trafficked to lysosomes, an organelle with a luminal pH of 4.5.

Fibril internalization was first analysed with the SH-SY5Y-GFP-α-synuclein cells. It has been here shown that α-synuclein fibrils, $A\beta_{40}$ and pH 2 $A\beta_{42}$ fibrils after a 6-day incubation generate saponin resistant GFP-α-synuclein puncta. Fibril internalization was therefore evaluated using 1 μM fibrils (monomer equivalent) on a time course seeding experiment with a 24 h, 72 h and 6 days of incubation timepoints. Association of Aβ fibrils to cells was examined with the use of fluorescently labelled-ATTO 594 (Exc. 603, Em. 626) $A\beta_{40}$ and $A\beta_{42}$ fibril preparations (kindly provided by Maddie Brown). These fibrils were prepared by labelling $A\beta_{40}$ or $A\beta_{42}$ monomer via an overnight primary amine labelling N-hydroxysuccinimide ester reaction, followed by gel filtration and lyophilisation. Labelled monomer and unlabelled monomers were then resuspended and mixed in a 1:100 ratio, respectively. Fibril generation was then performed as described in Chapter 3 and fibrils were later imaged by negative stain EM to verify fibril formation (Figure 5.13).

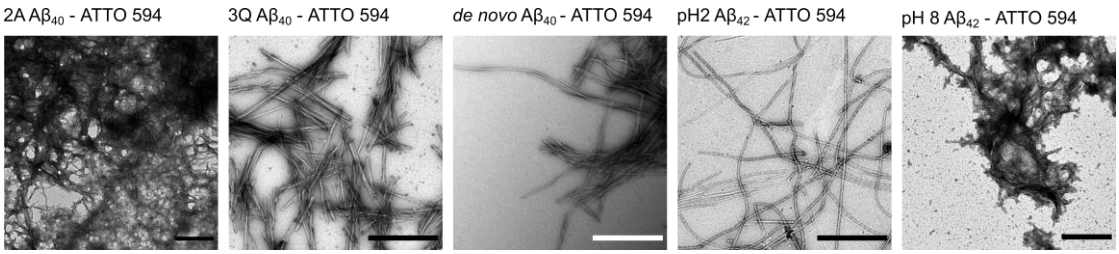

Figure 5.13. Fluorescently labelled $A\beta_{40}$ and $A\beta_{42}$ fibrils.
Negative stain EM was performed on each of the fibril preparations after labelling with ATTO-594 in an NHS ester-primary amine reaction. Some fibrils appeared more clumped than others. Scale bar is 500 nm.

Fluorescently labelled $A\beta_{40}$ fibrils (1 μM, monomer equivalent) were then incubated with the cells in the culture media. At the endpoint of the experiments, cells were thoroughly washed with PBS to remove non-cell associated fibrils and media was then replaced with phenol-free full media prior to live cell imaging by confocal microcsopy.

Almost no $A\beta_{40}$ fibril association with the cells was observed after a 24 h incubation, with either of the $A\beta_{40}$ fibril preparations (Figure 5.14). Fibril association with the cells was observed at 72 h and then at 6 days of incubation (Figure 5.14). Fluorescently labelled fibril puncta quantification (Figure 5.15) was performed after imaging. Quantification confirmed that an increased number of red puncta were associated to the cells at 6 days, compared to 72 h and 24 h. It is to be noted that no red fluorescence was observed on buffer treated cells at any time point.

It was also observed that through all the time points, intensity of expressed GFP-α-synuclein appeared the same between the cells incubated with fibril buffer compared to the cells incubated with $A\beta_{40}$ fibril preparations.

Analysis of fibril colocalization with lysosomes was performed next. To do this, the fluorescently labelled ATTO-594 $A\beta_{40}$ fibrils (1 μM, monomer equivalent) were incubated in the cells for 6 days in full media. Live cell imaging was done at the endpoint of the experiments by performing a wash to remove non-cell associated fibrils before replacing with phenol-free full media. The cells were incubated with the deep red lysotracker probe, a pH sensitive probe that stains acidic compartments and is used to visualize lysosomes. Nuclei were stained with Hoechst dye prior imaging.

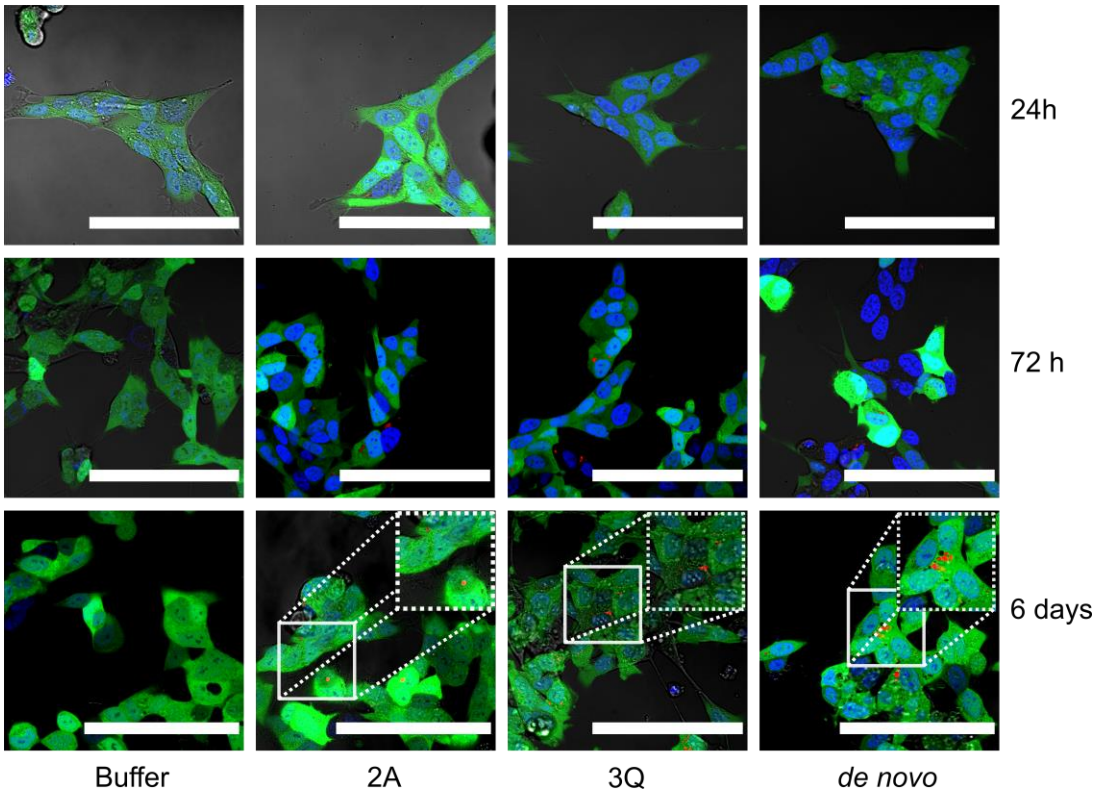

Figure 5.14. SH-SY5Y-GFP-α-synuclein cell seeding with fluorescently labelled 2A, 3Q and de novo $A\beta_{40}$ fibrils.
After incubating the cells with fibril buffer, 1 μM (monomer equivalent), fluorescently labelled 2A, 3Q or de novo $A\beta_{40}$ fibril preparations for 24 h, 72 h and 6 days, the cells were washed and media was replaced with phenol-free full media.. Hoechst staining was performed to visualize nuclei. Imaging was done in a confocal LSM880 or LSM700 microscope, at 40X magnification. Merged images shows GFP in green, nuclei in blue, and fibrils in red. A 6-3 day incubation with the $A\beta_{40}$ fibril preparations showed a heightened presence of red puncta on the cells, compared to what was observe after a 24 h incubation, where almost no red puncta were seen. Scale bar is 100 μm.

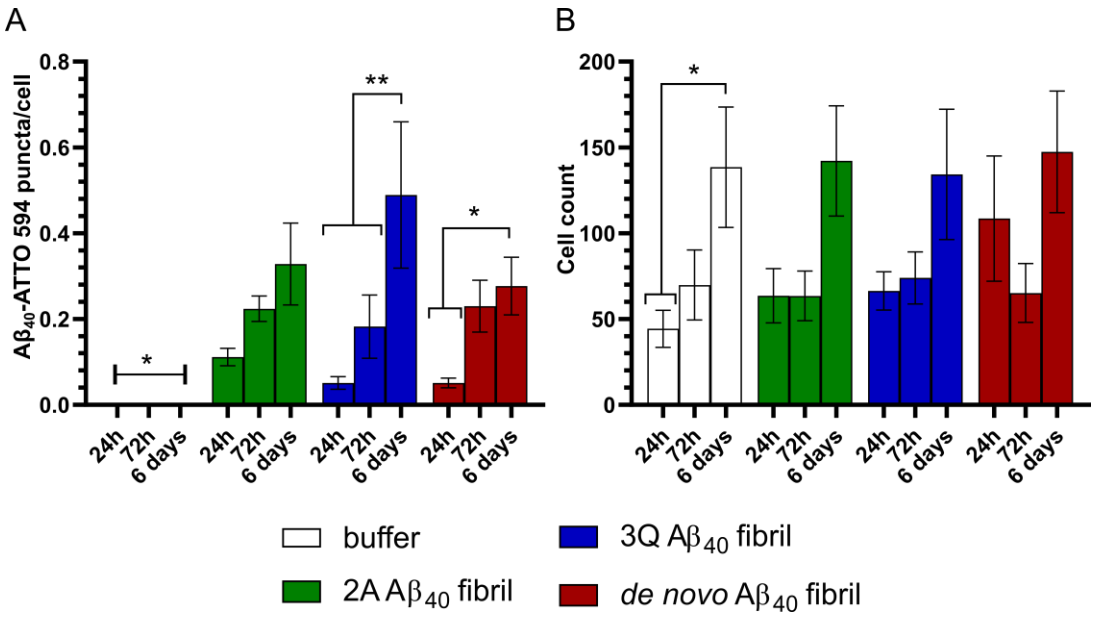

Figure 5.15. Quantification of fluorescently labelled Aβ₄₀ fibril in SH-SY5Y-GFP-α-synuclein cells.

*After imaging, red fibril puncta (A) and cell number by nuclei count (B) quantification was performed. A) Incubation for 6 days resulted in a significantly higher number of red puncta visualized in cells, compared to what was observed at 24 h and 72 h for the 2A treated and 3Q treated cells. No red fluorescence, and therefore no red puncta were observed on cells incubated in fibril buffer at any time point. B) No significant differences in cell numbers, or Hoechst count, were observed between the samples analysed. It is to be noted an increased number of cells were counted at 6 days for the 2A treated cells, compared to what was quantified at 24 h and 72 h. Puncta count was performed with the particle analyser on Fiji software, adjusting the threshold at the same settings for all the samples, per individual experiment. Error bars represent one S.E. over 3 independent experiments containing at least 3 replicates each. Significance level after Two-way ANOVA with Tukey multiple comparison test: * $p<0.05$, ** $p < 0.01$.*

An absence of red fluorescence was observed in cells incubated with buffer (Figure 5.16), and no colocalization of red puncta and lysosomes, observed as green puncta in this case, was seen. In contrast, fibril and lysosome colocalization was observed for the samples incubated with the 2A (Figure 5.17), 3Q (Figure 5.18) and *de novo* (Figure 5.19) fluorecent fibril preparations. These results suggest that $A\beta_{40}$ fibril preparations associate with the cells and are internalized . They are then trafficked into lysosomes pathway where they they will be exposed to the acidic pH of this organelle's lumen. Crucially, α-synuclein is delivered to lysosomes by chaperone mediated autophagy through the lysosome-associated membrane protein 2 (LAMP2) as well as through macroautophagy (Mak et al., 2010), thus these data suggest Aβ fibrils and α-synuclein may intersect in lysosomes.

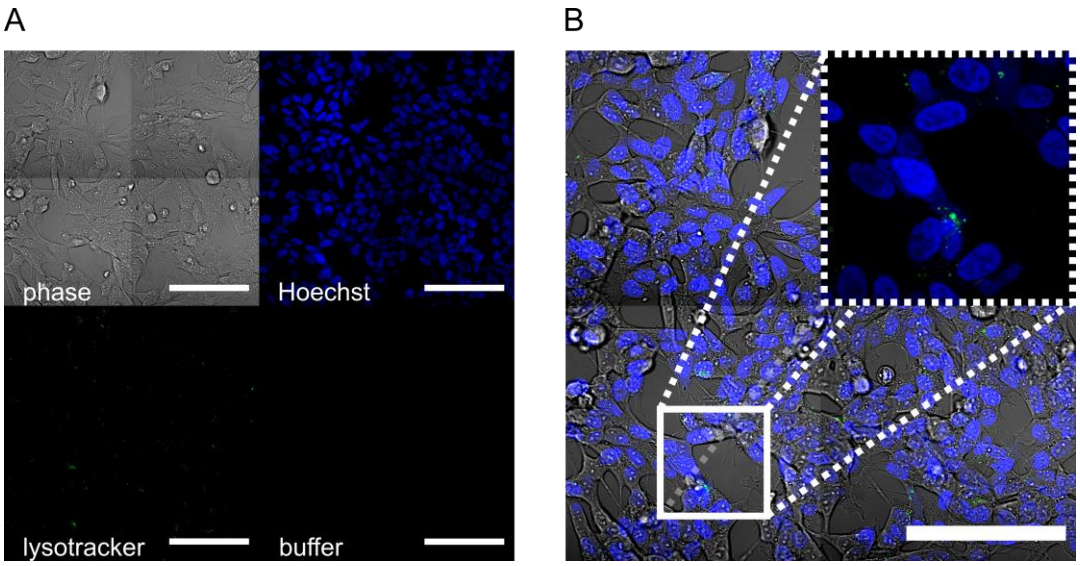

Figure 5.16. Fibril colocalization with lysosomes: Buffer control.
Fibril colocalization was analysed using by using the lysosomal probe lysotracker and fluorescently labelled fibrils or buffer. Cells were plated and incubated with fibril buffer for 6 days before imaging. Live cell imaging after this period was done on a confocal LSM 880 or LSM 700 microscope, using 2X2 tiles. Hoechst staining was added before imaging to visualize nuclei. A) Montage showing the cells on the phase, nuclei stained by Hoecsht, lysotracker and red fluorescence. B) Merge of the channels and zoom imaged, the lysosomes are observed as green puncta. Scale bar is 100 µm.

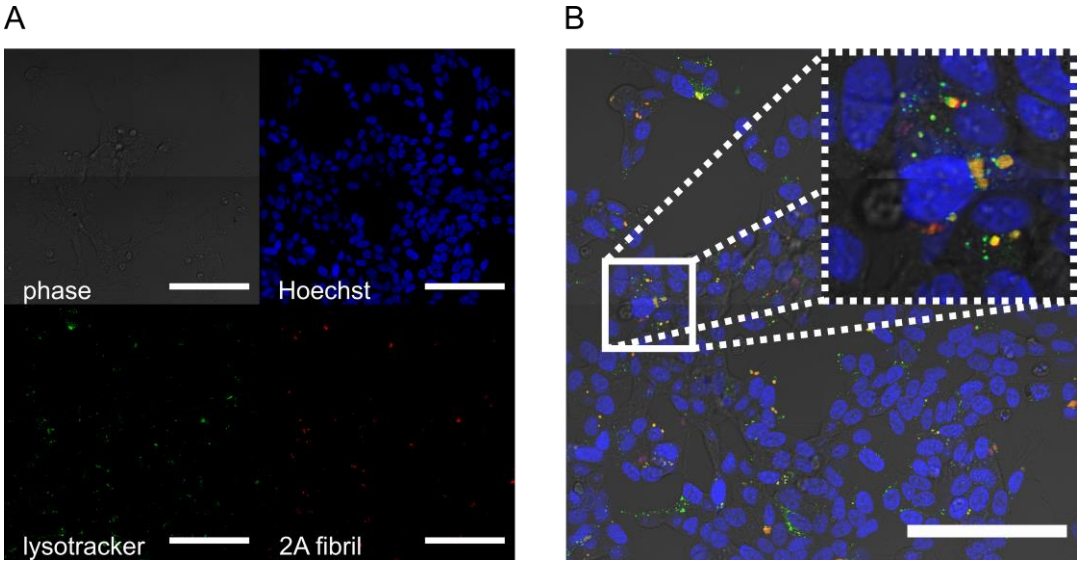

Figure 5.17. Fibril colocalization with lysosomes: 2A.
Fibril colocalization was analysed using by using the lysosomal probe lysotracker and fluorescently labelled fibrils. Cells were plated and incubated with 1 µM (monomer equivalent) 2A fluorescently labelled fibrils for 6 days before imaging. Live cell imaging after this period in a confocal LSM 880 or LSM 700 microscope, using 2X2 tiles. Hoechst staining was added before imaging to visualize nuclei. A) Montage showing the cells on the phase, nuclei stained by Hoecsht, lysotracker and red fluorescence. B) Merge of the channels and zoom imaged, the lysosomes are observed as green puncta, and fibrils as red puncta and colocalization of both is denoted as yellow puncta. Scale bar is 100 µm.

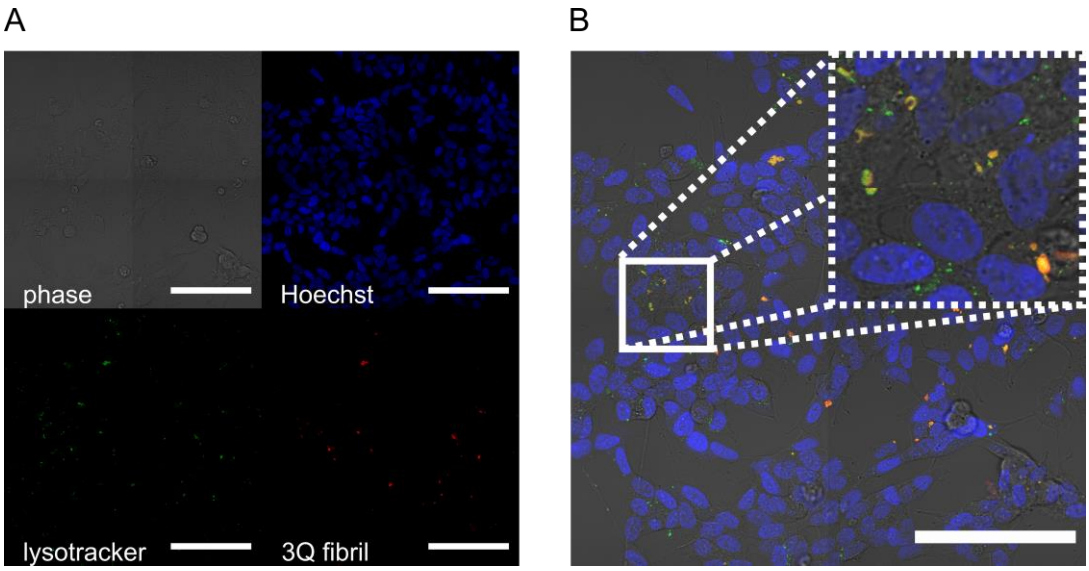

Figure 5.18. Fibril colocalization with lysosomes: 3Q.
Fibril colocalization was analysed using by using the lysosomal probe lysotracker and fluorescently labelled fibrils. Cells were plated and incubated with 1 µM (monomer equivalent) 3Q fluorescently labelled fibrils for 6 days before imaging. Live cell imaging after this period in a confocal LSM 880 or LSM 700 microscope, using 2X2 tiles. Hoechst staining was added before imaging to visualize nuclei. A) Montage showing the cells on the phase, nuclei stained by Hoecsht, lysotracker and red fluorescence. B) Merge of the channels and zoom imaged, the lysosomes are observed as green puncta, and fibrils as red puncta and colocalization of both is denoted as yellow puncta. Scale bar is 100 µm.

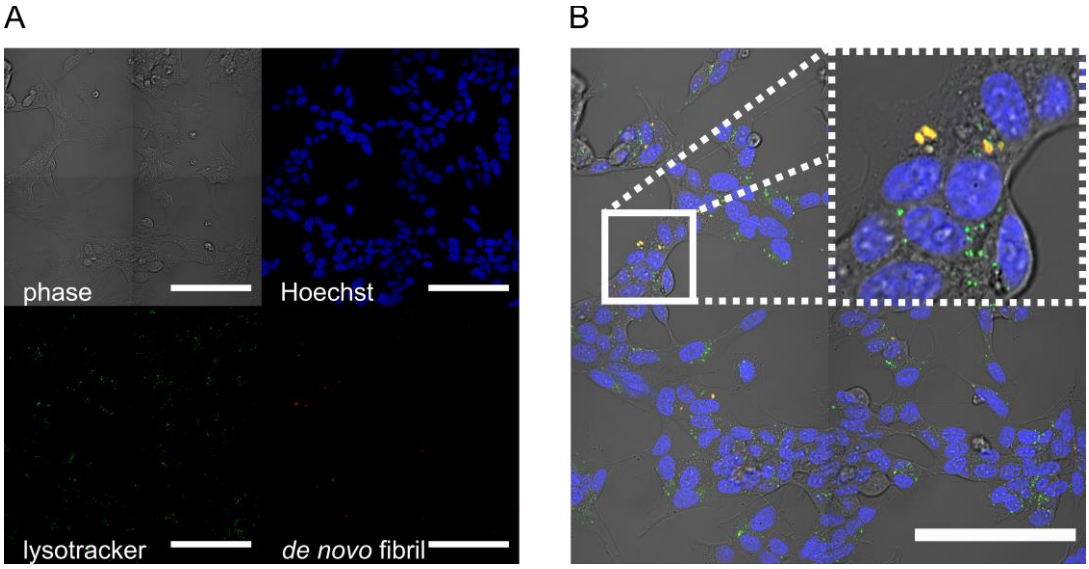

Figure 5.19. Fibril colocalization with lysosomes: de novo.
Fibril colocalization was analysed using by using the lysosomal probe lysotracker and fluorescently labelled fibrils. Cells were plated and incubated with 1 µM (monomer equivalent) de novo fluorescently labelled fibrils for 6 days before imaging. Live cell imaging after this period in a confocal LSM 880 or LSM 700 microscope, using 2X2 tiles. Hoechst staining was added before imaging to visualize nuclei. A) Montage showing the cells on the phase, nuclei stained by Hoecsht, lysotracker and red fluorescence. B) Merge of the channels and zoom imaged, the lysosomes are observed as green puncta, and fibrils as red puncta and colocalization of both is denoted as yellow puncta. Scale bar is 100 µm.

5.7. Cross-seeding of α-synuclein by Aβ in the presence of lysosomes

Lysosomes, due to their acidic pH, and accessibility to Aβ fibrils and α-synuclein via the endocytic (Jin et al., 2016) and autophagy pathways (Mak et al., 2010) respectively, may be a site for cross seeding of α-synuclein. However, the lysosome is a degradative organelle, enriched in proteases, that could potentially degrade Aβ fibrils and α-synuclein (Mak et al., 2010; Wolfe et al., 2013). Therefore, to evaluate whether cross-seeding of α-synuclein can occur in lysosomes an *in vitro* biochemical experiment was set up, where α-synuclein monomer was cross-seeded by Aβ fibrils in the presence of lysosomal fractions extracted from the SH-SY5Y-GFP-α-synuclein.

Lysosomal isolation was performed by fractionating homogenates of the SH-SY5Y-GFP-α-synuclein cells to a Percoll gradient by ultracentrifugation (Morten et al., 2007). Fractions were then pooled and analysed for alkaline phosphatase and α-N-acetylgalactosaminidase (NAGA) activities, markers for the plasma membrane and lysosomes respectively (Figure 5.20). The fractions 18 - 20, most enriched for NAGA, were ultracentrifuged again to remove the Percoll and to pellet the lysosomes. NAGA and alkaline phosphatase activities are reported as a percent of the total activity observed in all the fractions.

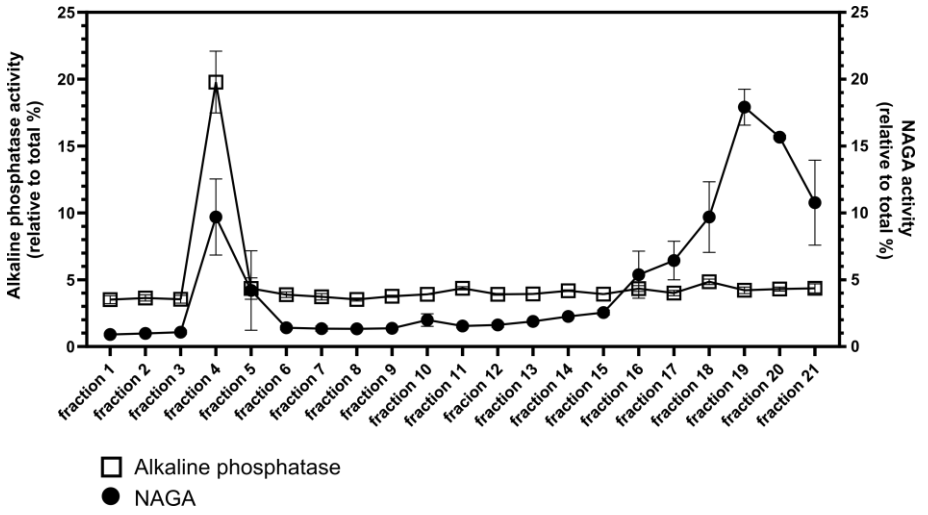

Figure 5.20. Percoll gradient fractionation of SH-SY5Y-GFP-α-synuclein cells.
Lysosomal isolation was performed by fractionation on a Percoll gradient. Cells were subjected to mechanical homogenization and centrifugation of the cell homogenate. The supernatant, containing the post-nuclear fraction, was then ultracentrifuged on a 27% Percoll gradient. Twenty-one fractions were collected from the gradient (1 top, 21 bottom) and assayed for alkaline phosphatase and NAGA activities, a plasma membrane and lysosome marker, respectively. Fractions 18-20 were retained, and ultracentrifuged again to pellet Percoll and concentrate lysosomes. Error bars represent one S.E. over 2 independent experiments.

The proteolytic activity of the extracted lysosomes was then tested on the α-synuclein monomer. For this the α-synuclein monomer was incubated with lysosome fractions equivalent to 0, 2.5, 5, 12 and 20 NAGA units (% of total) at pH 4.5 and 37°C for 10 h. The NAGA enzyme, a lysosomal exo-glycosidase and a lysosomal marker (Casey et al., 2007; Morten et al., 2007). SDS-PAGE showed that indeed after 10 h the α-synuclein monomer was degraded by the proteases present in the lysosomal fraction (Figure 5.21 A). The proteolytic products produced were proportional to the measured NAGA activity for the lysosomal fraction. A significant decrease (>50 %) in intensity relative to the α-synuclein monomer was observed for the samples incubated with lysosome fractions above 5 NAGA units (Figure 5.21 B), although cleavage products (<10 kDa) are visible in all the samples analysed containing lysosomes.

A lysosomal fraction equivalent to 3.5 NAGA activity (% of total), corresponding to less than 50% α-synuclein monomer degradation after 10 h, was used to do a time course experiment to evaluate the cross-seeding α-synuclein by Aβ fibrils. The assumption is that if α-synuclein fibrils are formed, they will be more resistant to proteolysis by lysosomal enzymes than the monomeric proteins (McGlinchey and Lee, 2015; Jung et al., 2017).

As in Chapter 4 (Section 4.4), α-synuclein was incubated in the presence of 20% (v/v) 2A, 3Q and *de novo* $A\beta_{40}$ fibrils and pH 2 $A\beta_{42}$, at 37°C and pH 4.5. SDS-PAGE analysis of the samples was done after 4 h, 16 h and 24 h of incubation. An increase of cleavage products (<10 kDa) was observed after 4 h of cross-seeding incubation (Figure 5.22 A), although no significant differences were seen in the intensity of the band relative to the α-synuclein monomer for self-seeded and cross-seeded samples (Figure 5.22 D). In contrast, a significant increase in the band intensity relative to the synuclein monomer is observed for the samples incubated with 2A $A\beta_{40}$ and α-synuclein seed after 16 h of incubation (Figure 5.22 B and D). After 24 h of incubation, the cross-seeded as well as the self-seeded samples show an increased band intensity relative to the α-synuclein monomer (Figure 5.22 C and D). No significant differences in band intensity (relative to the α-synuclein monomer) were observed between the cross-seeded samples nor with the synuclein α-seeded sample.

These results show that the α-synuclein monomer is degraded in the presence of lysosomal proteases (3.5 NAGA units, % of total). In contrast there is a reduction in the degradation of α-synuclein in the presence of α-synuclein seeds and Aβ. This is observed as a reduction in proteolytic products of α-synuclein and an increased level of intact α-synuclein at the 24 h endpoint.

These data suggest that α-synuclein is more resistant to lysosomal proteolysis at pH 4.5 in the presence of either α-synuclein seeds or Aβ fibril preparations and may reflect the formation of protease resistant α-synuclein fibrils.

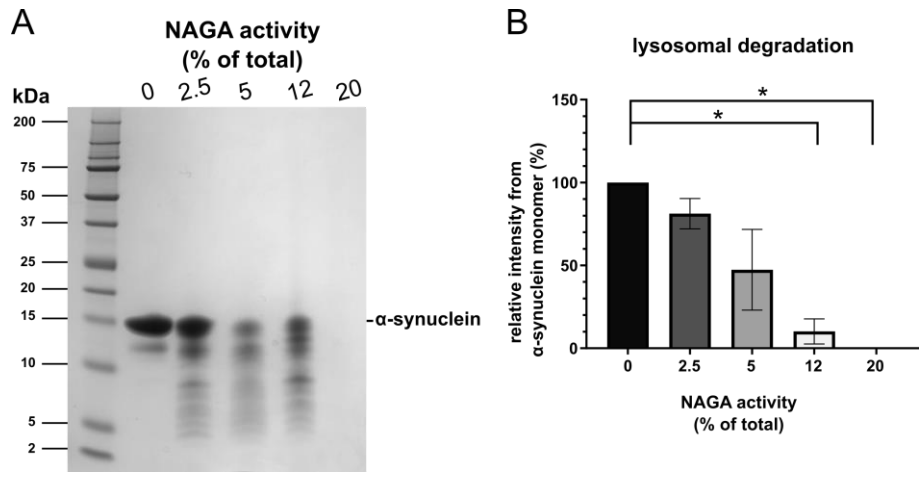

Figure 5.21. In vitro degradation of α-synuclein monomer by lysosomes.
*α-synuclein was degraded after being incubated for 10 h at 37°C and pH 4.5 with increasing concentrations of lysosomes (A). Quantification of full length α-synuclein (B) showed there was a significant decrease of intensity relative to the α-synuclein monomer in the samples incubated with lysosomal fractions with the highest NAGA activity (% of total). Error bars represent one S.E. over 2 independent experiments. Significance level after One-way ANOVA with Tukey multiple comparison test: * $p<0.05$, ** $p < 0.01$.*

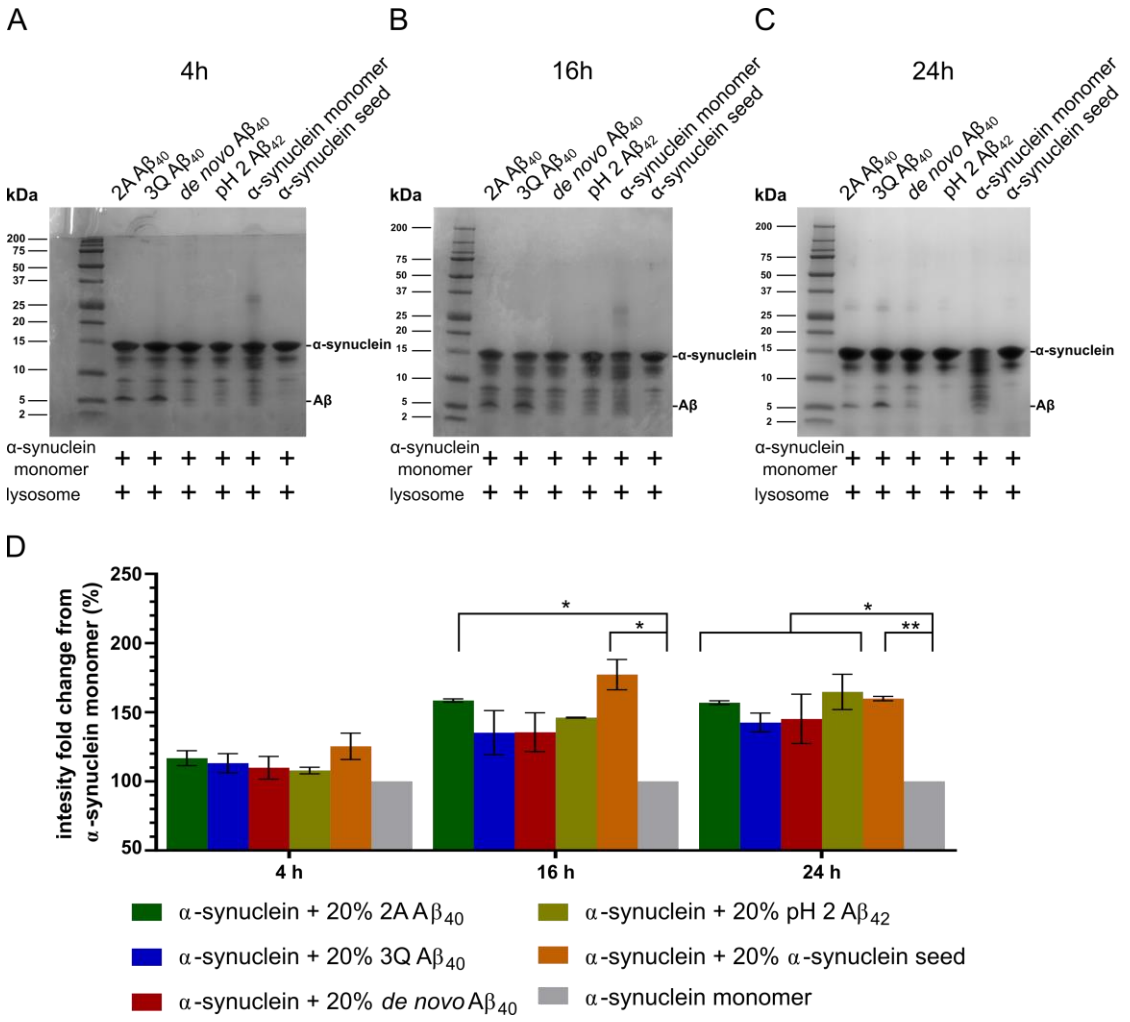

Figure 5.22. Lysosomal degradation of α-synuclein monomer in the presence or absence of Aβ fibril preparations or α-synuclein seeds.
*Quantification showed there was a significant decrease of intensity relative to the α-synuclein monomer in the samples incubated with lysosomal fractions after 16 and 24 h of incubation. No significant differences in relative intensity were observed between the Aβ cross-seeded and self-seeded α-synuclein samples. Error bars represent one S.E. over 2 independent experiments. Significance level after One-way ANOVA with Tukey multiple comparison test: * $p<0.05$, ** $p < 0.01$.*

5.8. Discussion

Alzheimer's disease is a heterogeneous disease. Subtypes of the disease have been described depending on the rate of cognitive decline, rate of plaque formation, cerebrospinal fluid biomarkers as well as profile of the neuropathological lesions observed (Schmidt et al., 2011). This highlights that the mechanisms leading to neurodegeneration in the human brain are complex. Although commonly associated to Parkinson's diseases, Lewy bodies and α-synuclein aggregation presence has been observed in other dementia related disease such as Alzheimer's

disease (Hamilton, 2000; Margallo-Lana et al., 2004; Lippa et al., 1999a; Forno, 1996; McKeith, 2007). Having observed that synergism contributing to fibril aggregation occurs between Aβ fibrils and α-synuclein *in vitro* (Chapter 4), the mechanism of α-synuclein cross-seeding by Aβ fibrils in cells was investigated here.

The effect of Aβ fibrils on the cell line was analysed first. Fibrillar structures have been reported to provoke neuronal death. In their study, Petkova et al. (2005) showed that when exposing rat embryonic primary cells to agitated and quiescent forms of $A\beta_{40}$ fibrils at different concentrations for a period of 24 – 48 h, cell death occurred, being more notably observed in cultures exposed for 48 h to the highest concentration of 3Q $A\beta_{40}$. MTT reduction inhibition was also reported in PC12 cells (Gremer et al., 2017) and SH-SY5Y cells (Colvin et al., 2016) after the incubation with pH 2 and pH 8 $A\beta_{42}$ fibrils, respectively. Moreover, cell toxicity of α-synuclein fibrils has been previously reported (Tuttle et al., 2016b; Boyer et al., 2020; Zhao et al., 2020b). Analysis of neuronal cell viability after long incubations with nanomolar concentrations of different α-synuclein fibril polymorphs has revealed a 7.5 – 20% increase in LDH release (Tuttle et al., 2016b; Zhao et al., 2020b).

Here, cell toxicity assessment revealed that when quantified by MTT reduction, LDH release and ATP levels, no significant reduction in viability occurred after incubation with the distinct $A\beta_{40}$ fibril polymorphs. In contrast, $A\beta_{42}$ fibrils, as well as the distinctly generated α-synuclein fibrils, had an impact on MTT metabolism without affecting ATP levels or LDH release after 6 days of incubation. This inhibitory effect on MTT reduction without rendering cell death has been noted for both Aβ fibrils (Ronicke et al., 2008; Kreutzmann et al., 2010) and β2-microglobulin fibrils (Jakhria et al., 2014). In their viability experiments, Kreutzmann et al. (2010) found that a 24 h incubation with 10 μM Aβ fibrils decreased the ability of murine primary hippocampal cultures to reduce MTT, without rendering an increase in LDH release. Co-incubation with minocycline, a synthetic tetracycline that is believed to exert neuroprotective effect, was initially thought to be shielding of Aβ's detrimental effect, as the inhibitory effect on MTT reduction was recovered. However, it was found that this same outcome was seen in the sole presence of nanomolar concentrations of cholesterol, a regulator of MTT formazan-containing vesicles (Liu, Y. et al., 1998), as 100 nM cholesterol inhibited MTT reduction and minocycline induced recovery of MTT reduction. These results suggest that formazan exocytosis is accelerated in the presence of both Aβ and cholesterol, whilst minocycline delays MTT-formazan externalisation (Kreutzmann et al., 2010). A similar result was observed in the case of β2-microglobulin fibrils, where β2-microglobulin fibrils heightened secretion of MTT-formazan while inhibition of endocytosis of the remaining MTT by cells occurred, as intracellular trafficking is altered by the presence of fibrils (Jakhria et al., 2014). Therefore, inhibition of MTT reduction may represent an early step

in Aβ and α-synuclein triggered toxicity, and an early marker of disruption to endosomal trafficking. The possibility of further interactions of the $A\beta_{40}$, $A\beta_{42}$ fibrils and of the α-synuclein fibrils with the cells is not excluded in this study. In addition, cellular toxicity to the peptides used might require longer exposure times as well as higher concentrations. The results presented by Tuttle et al. (2012) highlight the importance of long fibril incubation times to assess viability, as even in the presence of 500 nM α-synuclein fibrils, no significant increase in LDH release is observed in neurons, compared to the buffer treated cells, for the first 14 days of fibril incubation (Tuttle et al., 2016b).

The formation of detergent insoluble α-synuclein-GFP puncta in the SH-SY5Y-GFP-α-synuclein cell line occurred after the incubation with the different $A\beta_{40}$ and $A\beta_{42}$ fibrillar preparations. Quantification of the puncta after each treatment showed that the *de novo* $A\beta_{40}$ fibril preparation seemed to form the greatest number of GFP-α-synuclein puncta when compared to the rest of the fibril polymorphs. Multiple comparisons analysis (ANOVA) between all the fibril preparations treatments only suggested significant difference with the pH 8 $A\beta_{42}$ fibril incubated cells. GFP-α-synuclein puncta size was also significantly larger in cells incubated with *de novo* $A\beta_{40}$, compared to the rest of the fibril preparations. Future work requires the use of an untagged α-synuclein cell line or neuronal analysis to confirm the results shown here. This will have to go in hand to longer incubation times and with immune-based assays to visualize α-synuclein forms and its interactors.

Even though no significant differences were observed in the lag times of the α-synuclein cross-seeding by Aβ fibrils (Chapter 4, Section 4.4), the effect in cells showed *de novo* and 3Q $A\beta_{40}$ fibrils were more efficient in the generation of GFP-α-synuclein aggregates. This suggests a strain dependent propagation of the $A\beta_{40}$ polymorphs upon the interaction with the cells. α-synuclein strain formation has been previously reported in oligodendrocytes (Peng et al., 2018). Glial α-synuclein inclusions are seen most commonly in MSA, and not Parkinson's disease, which reflects that the formation of distinct pathological α-synuclein strain can also wind up in the presentation of different pathologies. In this study, *de novo* $A\beta_{40}$ fibrils may be acting as a different strain capable of cross-seeding α-synuclein in cells. It is however yet to be determined if the detergent insoluble puncta formed have a differential pathological consequence.

Fibril internalization analysis showed that the Aβ fibrils are internalised and trafficked to lysosomes. This organelle, due to its acidic pH, represents a potential site for cross-seeding of α-synuclein by Aβ fibrils, as depicted in Chapter 4, where pH 4.5 was favourable for α-synuclein cross-seeding to occur. Notably increased resistance of α-synuclein to lysosomal proteases was observed in the presence of Aβ fibril preparations, suggesting that fibrils may be formed that are resistant to the proteases in lysosomal fractions. Evidence points that α-synuclein gets delivered

to lysosomes through chaperone mediated autophagy and through the autophagosome pathway (Hoffmann et al., 2019; Mak et al., 2010). In addition, Aβ assortment to lysosomes occurs through the endo-lysosomal pathway (Nixon, 2017), and intracellularly produced Aβ gets trafficked to lysosomes and accumulates in autophagic vacuoles (Ihara et al., 2012). It is therefore possible that intersection of both protein entities occurs in this organelle (Figure 5.23).

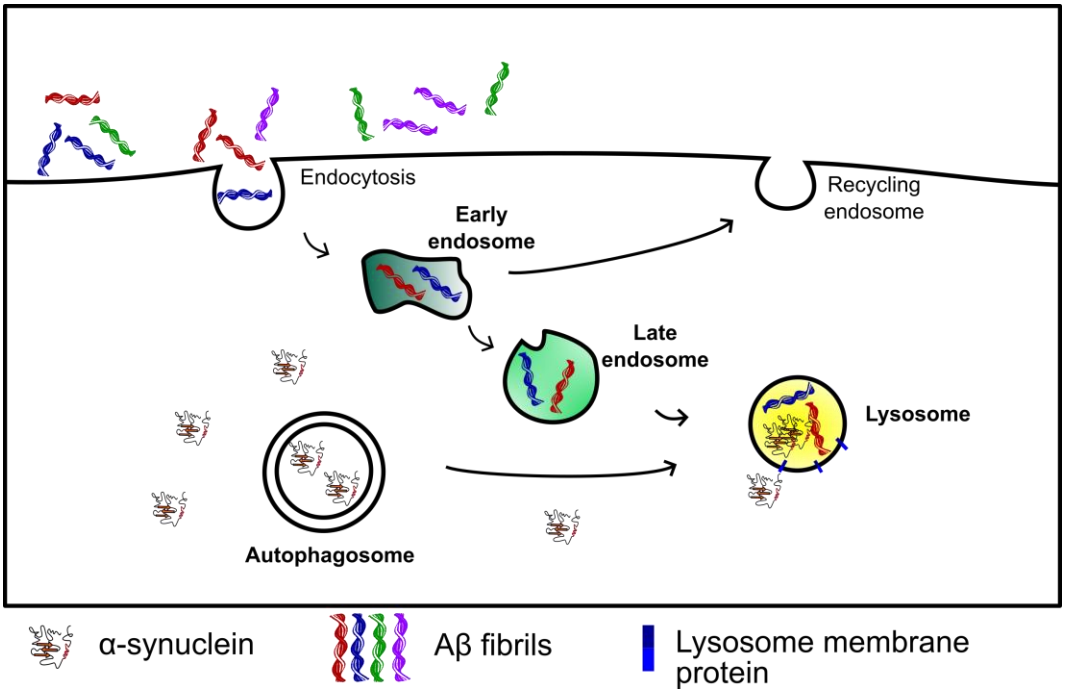

Figure 5.23. Cellular model of α-synuclein cross-seeding by Aβ fibrils.
Aβ fibril internalization can occur through endocytosis, where fibrils get delivered to lysosomes. Furthermore, α-synuclein is trafficked to lysosomes through autophagy via autophagosome fusion or chaperone mediated autophagy via lysosome membrane proteins.

Structurally, it has recently been shown that Lewy bodies and neurites are widely composed of membranes, disrupted organelles and vesicles (Shahmoradian et al., 2019). In their ultrastructural analysis of Lewy body pathology in Parkinson's disease, Shahmoradian et al. (2019) showed by correlated light electron microscopy that there was a minimal presence of α-synuclein fibrils in Lewy bodies and an overshadowing incidence of disrupted mitochondria, lysosomes and other cellular debris. They suggested that Lewy body formation and organelle crowding is the cells process to deal with problems derived from α-synuclein association to lipid membranes and highlighted the fact that a driver for pathogenesis in Parkinson's disease might be impaired organelle trafficking. It is therefore plausible that GFP-α-synuclein puncta present defective

organelle crowding before permeabilization. Future work could include mitochondria chasing in conjunction to α-synuclein tracking to verify these puncta's resemblance to Lewy bodies *in vivo*.

An important feature of Alzheimer's disease is disruption and function loss of the endolysosomal-autophagy pathway. The endolysosomal-autophagy pathway clears cellular debris, such as defective organelles and misfolded protein aggregates, as well as recycle cellular material (Lehtonen et al., 2019). iPSC Parkinson's disease cell models show damage vesicular trafficking components at the early secretory pathway as well as reduced lysosomal function by account of disruption of hydrolase trafficking and maturation (Mazzulli et al., 2016). Specifically, expression of α-synuclein rendered a decline in lysosomal cathepsin B activity, in addition to decreased activity of glucocerebrosidase and β-galactosidase in acidic compartments. This dysfunction was found to be reversible after α-synuclein expression abolishment (Mazzulli et al., 2016). It could therefore be possible that α-synuclein cross-seeding by Aβ fibrils acts as mechanism that contributes towards the dysfunction of this pathway by inducing lysosomal damage and ultimately leads to the progression of Alzheimer's disease.

The results shown here suggest that that interactions between α-synuclein and Aβ fibrils may occur in the lysosomes (Figure 5.23), which have a pH that promotes cross-seeding of α-synuclein by Aβ fibrils *in vitro* (Chapter 4). In cells, incubation with Aβ fibrils leads to the formation of Lewy body like inclusions, observed as GFP-α-synuclein puncta in the cell line used. Further characterisation of these aggregates is required for the better understanding of cross-seeding of α-synuclein in cells, such as prevention of acidification of lysosomes, by bafilomycin A1 exposure, an inhibitor of vacuolar H+ATPase, which controls pH in lysosomes (Redmann et al., 2017), while incubating with Aβ fibrils is done in the SHSY5Y-GFP-α-synuclein cell line could be used to test whether lysosomes are the site for the generation of GFP-α-synuclein puncta. These results put in evidence the importance of α-synuclein-Aβ interactions in the development of Alzheimer's disease.

6. Conclusions and future perspectives

The formation of insoluble protein aggregates and their pathological impact in neurodegenerative diseases can be studied using *in vitro* and *in vivo* models. In human disease, the mechanisms that trigger the production of abnormal protein conformations, seeding and/or generation of amyloid fibrils are still a matter of discussion. As described in the introduction, Alzheimer's disease features the deposition of proteins in their insoluble state in the brain and progressive cognitive decline with disease evolution. However, Alzheimer's disease complexity is demonstrated through the various disease subtypes and clinical symptomatology, such as Lewy body presentation and α-synuclein aggregation in a subset of cases (Hamilton, 2000; Kotzbauer et al., 2001; Jellinger, 2003; Drummond et al., 2017). Here, the investigation of α-synuclein aggregation by Aβ fibrils was performed. Specifically, the effect of Aβ fibril polymorphism on α-synuclein aggregation into amyloid fibrils and intracellular aggregates was explored.

To study the mechanism that governs the interaction between α-synuclein monomers and Aβ fibrils and the involvement of fibril polymorphism, well-defined Aβ structures (Colvin et al., 2016; Gremer et al., 2017; Madine et al., 2012; Paravastu et al., 2008; Petkova et al., 2005) with distinct architectures were chosen. This is described in Chapter 3, where differences in binding site availability for curcumin and ThT of the Aβ preparations (Section 3.5.3) was suggestive of the distinct molecular conformations these fibrils possess.

In Chapter 4, the pH dependent mechanism of α-synuclein aggregation by cross-seeding with $A\beta_{40}$ and $A\beta_{42}$ fibrils was characterised. It was observed that whilst α-synuclein binding to $A\beta_{40}$ fibrils occurs can occur at pH 7.5 (Section 4.2), no fibrillar aggregation is detected (Section 4.3). At pH 7.5 α-synuclein fibril formation was only observed after the incubation with α-synuclein seeds, a mechanism known as α-synuclein self-seeding. The switch to pH 4.5, another physiological pH, showed the cross-seeding of α-synuclein by both $A\beta_{40}$ fibrils (Section 4.4) and $A\beta_{42}$ fibril preparations (Section 4.5). In contrast to neutral pH, at pH 4.5 an 80 – 70% decrease in the lag time of α-synuclein aggregation was observed in the samples incubated with 20% (v/v) of both $A\beta_{40}$ and $A\beta_{42}$ fibrils, compared to unseeded α-synuclein.

In their study, Han et al. (1995) reported a 30% decrease in the lag time of the NAC α-synuclein fragment, when in the presence of 25% (v/v) $A\beta_{40}$ fibrils. Their investigation was performed at pH 7.4 in the presence of 100 mM NaCl, with the use Aβ fibrils generated by stirring but with undetermined structures. It is known that ionic strength, as well as pH, affects the kinetics of α-synuclein aggregation *in vitro* (Doherty et al., 2020). Low pH and low salt promote α-synuclein aggregation, due to an increase in electrostatic interactions between the side chains (Buell et al.,

2014). However, the intracellular concentration of Na^+ ions is reported to be within 10 - 15 mM range and at a concentration of ~140 mM in the extracellular environment of mammalian cells. Tight control and homeostasis of the Na+ ions is kept by Na1/K1-ATPase pump, with little Na^+ concentration variation occurring (Madelin et al., 2014). Hence, α-synuclein cross-seeding by Aβ in the cell might be driven by a pH dependency mechanism, rather than through ionic strength variation, although occurrence of α-synuclein cross-seeding by Aβ could also be taking place extracellularly.

Nonetheless, no significant differences in the lag times were observed between the cross-seeded reactions for the different Aβ preparations at pH 4.5. The results shown here imply that there is not a significant effect of Aβ polymorphism on α-synuclein cross-seeding at pH 4.5. The effect polymorphism on α-synuclein cross-seeding can't be discarded, as *ex vivo* derived (Lu et al., 2013) and *ex vivo* extracted (Kollmer et al., 2019) Aβ fibrils are significantly different from the *in vitro* generated ones in this study and might interact differently with α-synuclein.

Evidence of the mechanism of the biochemical *in vitro* cross-seeding process was shown in Section 4.6. This was probed with the use of fragmented Aβ fibrils on the cross-seeding of α-synuclein at pH 4.5. No significant decrease in the lag time was observed in the samples cross-seeded with fragmented fibrils compared to unfragmented, indicating that the mechanism of aggregation was governed by secondary nucleation of α-synuclein, rather than the elongation of the Aβ fibrils at their ends. Characterisation of the cross-seeded fibrils was also done by curcumin binding (Section 4.7). Curcumin fluorescence intensity was significantly different between the α-synuclein cross-seeded fibrils, demonstrating different binding affinities to curcumin by the cross-seeded α-synuclein fibrils, denoting distinct fibril structural arrangements. Further investigation to resolve how these α-synuclein cross-seeded fibrils differ from unseeded α-synuclein fibrils is needed, for example by using cryoEM to determine their molecular structures (Iadanza et al., 2018).

Additionally, insights into the effect of Aβ polymorphism on cellular α-synuclein aggregation was described in Chapter 5. The generation of insoluble GFP-α-synuclein puncta were observed after the incubation with α-synuclein seeds (Section 5.2), a feature that was not observed after the incubation with the fibril buffer or α-synuclein monomer. Exogenous addition of α-synuclein seeds is known to generate insoluble puncta in cell lines and neuronal models of Parkinson's disease, reminiscent of Lewy body inclusion formation (Hasegawa et al., 2004; Lashuel et al., 2013; Luk et al., 2009).

Cellular viability assays performed on the cell line after incubation with the Aβ fibril polymorphs (Section 5.3) or the α-synuclein fibrils cross-seeded by Aβ (Section 5.4) revealed no significant

decrease in cellular ATP nor increase of LDH release. However, incubation with $A\beta_{42}$ fibrils and α-synuclein fibrils revealed inhibition of MTT reduction. This inhibitory effect on MTT reduction without rendering cell death has been noted and accounted to alterations in intracellular trafficking by the presence of fibrils (Jakhria et al., 2014). Therefore, decrease in MTT reduction may be an early step in Aβ and α-synuclein triggered toxicity, and an early marker of disruption to endosomal trafficking. Longer fibril incubation times might provide a better picture of toxicity for these fibrils, but it may be an early indicator of disruption to endosomal trafficking.

Cross-seeding of α-synuclein by Aβ fibrils in cells was addressed in Chapter 5 (Section 5.5). The differential formation of GFP-α-synuclein insoluble puncta was observed after incubation with the Aβ fibril preparations. It was noted that *de novo* $A\beta_{40}$ generated the most puncta with the largest size, whilst the 2A $A\beta_{40}$ fibril preparations generated the least and smallest GFP-α-synuclein puncta. Biochemical analysis of cell fractionation into soluble and insoluble fractions revealed that indeed the 2A $A\beta_{40}$ generated the least amount of sarkosyl-insoluble GFP-α-synuclein compared to the 3Q and *de novo* samples. These results show that Aβ fibril polymorphs to different degrees, drive α-synuclein aggregation in cells into inclusions that are reminiscent of Lewy-bodies. Limitations of this study, however, are the use of a GFP-α-synuclein cell line. Future work would need to include the use of an untagged α-synuclein overexpressing cell line, or neuronal cell cultures to evaluate the impact of Aβ fibrils on α-synuclein aggregation.

It should be emphasized that whilst the cellular assay revealed differences in the extent of GFP-α-synuclein inclusion formation for cells incubated with the different Aβ fibril preparations, no differences were observed for cross seeding reactions performed with purified Aβ fibrils and α-synuclein. This may reflect differences in how the fibril polymorphs interact with cells, such as the extent of their uptake or their resistance to lysosomal degradation. The role of Aβ fibril polymorphism could in future studies be explored using fibrils obtained from patients with different presentations of Alzheimer's disease.

Lastly, it was shown that Aβ fibrils colocalize to lysosomes (Section 5.5). As it is known that α-synuclein gets trafficked to the endo-lysosomal pathway via autophagy (Klucken et al., 2012; Jackson and Hewitt, 2016), these results reveal an intracellular site where Aβ fibrils and α-synuclein can interact, cross-seed, and ultimately lead to α-synuclein aggregate formation. SDS-PAGE analysis of α-synuclein cross-seeding by Aβ fibril preparations in the presence of lysosomal fractions (Section 5.6) revealed that cleavage of α-synuclein was significatively reduced when it was incubated with α-synuclein seeds and Aβ fibril preparations. This suggests that α-synuclein fibrils produced by cross seeding would exhibits some degree of resistance to degradation by lysosomal proteases.

Crucially, other studies have highlighted a role for lysosomes in Alzheimer's disease. Autophagic vacuoles, or membrane bound vacuoles that contain cell components destined for lysosomal degradation, are commonly found in dystrophic swellings and neurites in Alzheimer's disease brain sections (Nixon, 2017), indicating a disruption to the lysosomal degradation pathway. Rab5, a GTPase involved in endosomal sorting and membrane fusion (Nixon, 2017), is known to be overactivated in endosomes in Alzheimer's disease, contributing to an increase in the rate of endocytosis as well as enlargement of early endosomes (Hu, Y.B. et al., 2015; Nixon, 2017). Lysosomal pH dysregulation is also a characteristic of Alzheimer's disease. Lysosomes normally degrade material delivered by endocytic and autophagic routes, whose enzymes activity depend on the strict control of pH (Hu, Y.B. et al., 2015). Lysosomal proteolysis disruption has been observed in familial Alzheimer's disease mouse models bearing presenilin mutations, where impairment of acidification of lysosomes and maturation of autophagosomes occurs (Lee et al., 2015). This is due to the disruption of the physiological function of presenilin as an endoplasmic reticulum co-chaperone that enables the maturation and targeting of the proton pump v-ATPase V0a1 subunit to lysosomes (Lee et al., 2010). A reduction in lysosomal proteolysis would be predicted to increase the concentrations of both Aβ fibrils and α-synuclein in lysosomes, thus promoting cross-seeding reactions.

Future work regarding the pH requirement of the cross-seeding of α-synuclein by Aβ fibrils is required to determine if cross-seeding could occur in other parts of the endolysosomal pathway. This would include biochemical analysis of the kinetics at pH 5.5 and 6.5, which correspond to the pH in late and early endosomes, respectively. Nevertheless, the results shown in this thesis pose the lysosome as a potential site of cross-seeding of α-synuclein by Aβ fibrils (Figure 6.1A), where α-synuclein delivery to the lysosome occurs by chaperone mediated autophagy or macroautophagy via the autophagosome pathway (Mak et al., 2010) and Aβ through the endocytic pathway (Jin et al., 2016). It is in this environment, at pH 4.5 where α-synuclein aggregation is accelerated by Aβ fibrils through a secondary nucleation mechanism (Figure 6.1 B).

Association of Lewy bodies to autophagosomes and endolysosomes has been detected in Parkinson's disease brain sections (Shahmoradian et al., 2019) and primary hippocampal murine neurons incubated with α-synuclein fibrils (Mahul-Mellier et al., 2020). This points at the potential failure of the protein degradation machinery and consequent α-synuclein accumulation and Lewy body formation.

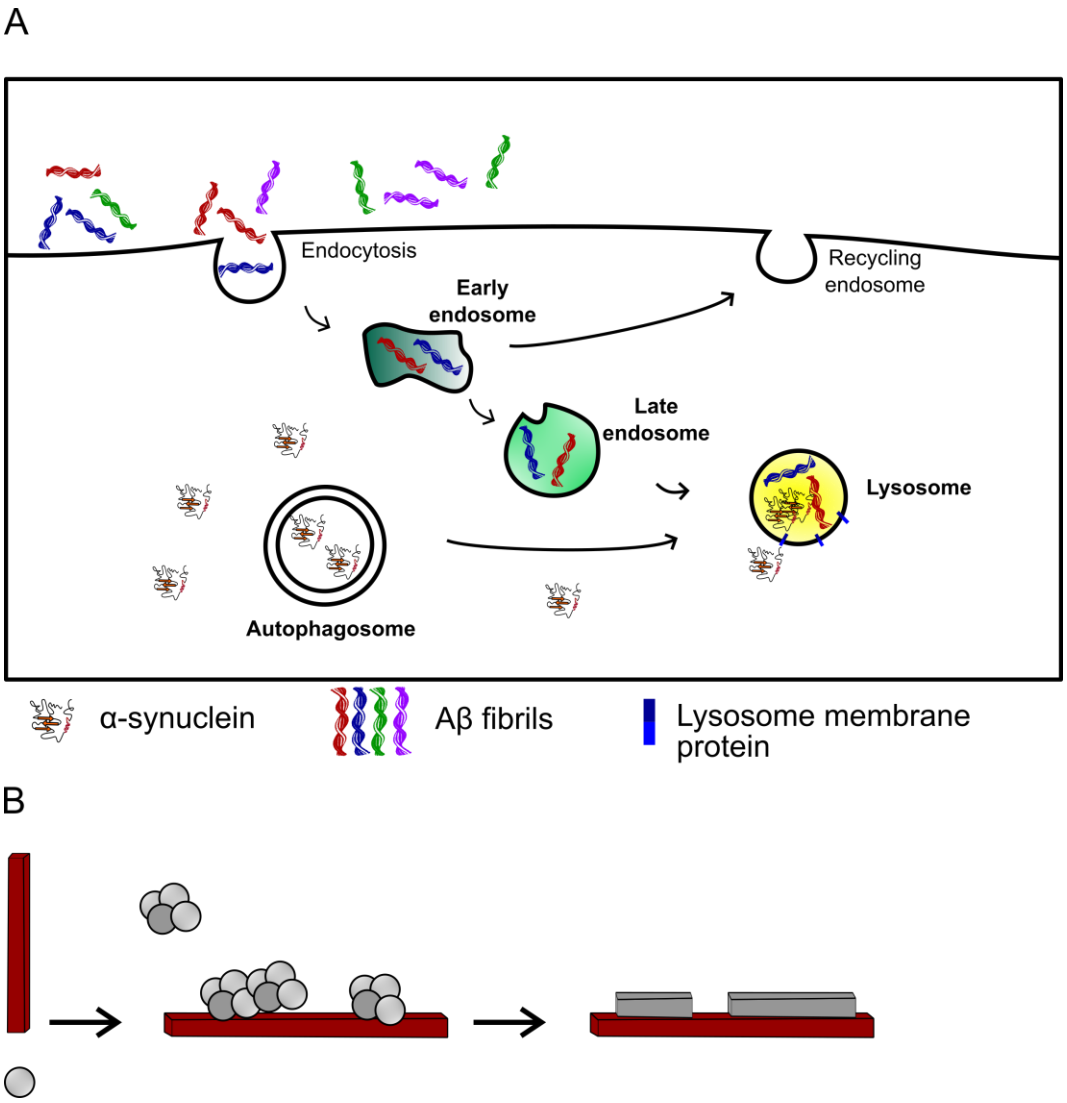

Figure 6.1. Model of α-synuclein cross-seeding by Aβ fibrils.
Schematic diagrams of cellular cross-seeding of α-synuclein (A), in which α-synuclein is delivered to the lysosome through the endocytic pathway. In contrast, α-synuclein gets trafficked to lysosomes via autophagosome fusion or chaperone mediated autophagy. At pH 4.5, cross-seeding of α-synuclein by Aβ fibrils occurs through a surface catalysed secondary nucleation (B) mechanism. Adapted from (Hoffmann et al., 2019) and (Tornquist et al., 2018)

The understanding of the degenerative process in Alzheimer's disease and the synucleopathies, and the development of therapeutics is still a focus of research. However, targeting of this Aβ-α-synuclein interaction might prove a novel therapeutic avenue for Alzheimer's disease. This could initially be tested by altering acidification of lysosomes to analyse the extent of cross-seeding and insoluble puncta formation to get a better understanding of Aβ polymorphism differences, but also confirming the importance of a specific acidic pH. Modulation of endocytosis of fibrils by dynasore, a dynamin inhibitor and modulator of clathrin-dependent endocytosis (Jakhria et al., 2014) or genistein, general tyrosine kinase inhibitor and modulator of caveolar (clathrin-

independent) endocytosis (Mayor and Pagano, 2007), could determine if the distinct Aβ fibril polymorphs are endocytosed through different pathways or present different rates of endocytosis that determine the extent of α-synuclein cross-seeding and Lewy body-like formation in cells.

In summary this project highlights the importance of studying interactions between Aβ and α-synuclein in Alzheimer's disease and proposes new avenues for therapeutic targets.

References

Adamcik, J. and Mezzenga, R. 2018. Amyloid Polymorphism in the Protein Folding and Aggregation Energy Landscape. *Angew Chem Int Ed Engl.* **57**(28), pp.8370-8382.

Arber, C., Toombs, J., Lovejoy, C., Ryan, N.S., Paterson, R.W., Willumsen, N., Gkanatsiou, E., Portelius, E., Blennow, K., Heslegrave, A., Schott, J.M., Hardy, J., Lashley, T., Fox, N.C., Zetterberg, H. and Wray, S. 2019. Familial Alzheimer's disease patient-derived neurons reveal distinct mutation-specific effects on amyloid beta. *Mol Psychiatry.*

Arosio, P., Knowles, T.P. and Linse, S. 2015. On the lag phase in amyloid fibril formation. *Phys Chem Chem Phys.* **17**(12), pp.7606-7618.

Augustin, J.M., Kuzina, V., Andersen, S.B. and Bak, S. 2011. Molecular activities, biosynthesis and evolution of triterpenoid saponins. *Phytochemistry.* **72**(6), pp.435-457.

Bai, X.C., Yan, C., Yang, G., Lu, P., Ma, D., Sun, L., Zhou, R., Scheres, S.H.W. and Shi, Y. 2015. An atomic structure of human gamma-secretase. *Nature.* **525**(7568), pp.212-217.

Ballard, C., Gauthier, S., Corbett, A., Brayne, C., Aarsland, D. and Jones, E. 2011. Alzheimer's disease. *Lancet.* **377**(9770), pp.1019-1031.

Ballard, C., Mobley, W., Hardy, J., Williams, G. and Corbett, A. 2016. Dementia in Down's syndrome. *Lancet Neurol.* **15**(6), pp.622-636.

Bao, F., Wicklund, L., Lacor, P.N., Klein, W.L., Nordberg, A. and Marutle, A. 2012. Different beta-amyloid oligomer assemblies in Alzheimer brains correlate with age of disease onset and impaired cholinergic activity. *Neurobiol Aging.* **33**(4), pp.825 e821-813.

Barnham, K.J., McKinstry, W.J., Multhaup, G., Galatis, D., Morton, C.J., Curtain, C.C., Williamson, N.A., White, A.R., Hinds, M.G., Norton, R.S., Beyreuther, K., Masters, C.L., Parker, M.W. and Cappai, R. 2003. Structure of the Alzheimer's disease amyloid

precursor protein copper binding domain. A regulator of neuronal copper homeostasis. *J Biol Chem.* **278**(19), pp.17401-17407.

Bateman, R.J., Munsell, L.Y., Morris, J.C., Swarm, R., Yarasheski, K.E. and Holtzman, D.M. 2006. Human amyloid-beta synthesis and clearance rates as measured in cerebrospinal fluid in vivo. *Nat Med.* **12**(7), pp.856-861.

Beyer, K. 2006. Alpha-synuclein structure, posttranslational modification and alternative splicing as aggregation enhancers. *Acta Neuropathol.* **112**(3), pp.237-251.

Biancalana, M. and Koide, S. 2010. Molecular mechanism of Thioflavin-T binding to amyloid fibrils. *Biochim Biophys Acta.* **1804**(7), pp.1405-1412.

Boyer, D.R., Li, B., Sun, C., Fan, W., Zhou, K., Hughes, M.P., Sawaya, M.R., Jiang, L. and Eisenberg, D.S. 2020. The alpha-synuclein hereditary mutation E46K unlocks a more stable, pathogenic fibril structure. *Proc Natl Acad Sci U S A.* **117**(7), pp.3592-3602.

Braak, H. and Braak, E. 1991. Neuropathological stageing of Alzheimer-related changes. *Acta Neuropathol.* **82**(4), pp.239-259.

Braak, H. and Del Tredici, K. 2008. Invited Article: Nervous system pathology in sporadic Parkinson disease. *Neurology.* **70**(20), pp.1916-1925.

Braak, H., Del Tredici, K., Rub, U., de Vos, R.A., Jansen Steur, E.N. and Braak, E. 2003. Staging of brain pathology related to sporadic Parkinson's disease. *Neurobiol Aging.* **24**(2), pp.197-211.

Brandel, J.P., Corbille, A.G., Derkinderen, P. and Haik, S. 2015. [Is Parkinson's disease a prion disease?]. *Rev Neurol (Paris).* **171**(12), pp.812-824.

Buell, A.K., Galvagnion, C., Gaspar, R., Sparr, E., Vendruscolo, M., Knowles, T.P., Linse, S. and Dobson, C.M. 2014. Solution conditions determine the relative importance of nucleation and growth processes in alpha-synuclein aggregation. *Proc Natl Acad Sci U S A.* **111**(21), pp.7671-7676.

Bunce, S.J., Wang, Y., Stewart, K.L., Ashcroft, A.E., Radford, S.E., Hall, C.K. and Wilson, A.J. 2019. Molecular insights into the surface-catalyzed secondary nucleation of

amyloid-beta40 (Abeta40) by the peptide fragment Abeta16-22. *Sci Adv.* **5**(6), peaav8216.

Casey, T.M., Meade, J.L. and Hewitt, E.W. 2007. Organelle proteomics: identification of the exocytic machinery associated with the natural killer cell secretory lysosome. *Mol Cell Proteomics.* **6**(5), pp.767-780.

Chavez-Gutierrez, L., Bammens, L., Benilova, I., Vandersteen, A., Benurwar, M., Borgers, M., Lismont, S., Zhou, L., Van Cleynenbreugel, S., Esselmann, H., Wiltfang, J., Serneels, L., Karran, E., Gijsen, H., Schymkowitz, J., Rousseau, F., Broersen, K. and De Strooper, B. 2012. The mechanism of gamma-Secretase dysfunction in familial Alzheimer disease. *EMBO J.* **31**(10), pp.2261-2274.

Chen, L., Xie, Z., Turkson, S. and Zhuang, X. 2015. A53T human alpha-synuclein overexpression in transgenic mice induces pervasive mitochondria macroautophagy defects preceding dopamine neuron degeneration. *J Neurosci.* **35**(3), pp.890-905.

Chen, S.W., Drakulic, S., Deas, E., Ouberai, M., Aprile, F.A., Arranz, R., Ness, S., Roodveldt, C., Guilliams, T., De-Genst, E.J., Klenerman, D., Wood, N.W., Knowles, T.P., Alfonso, C., Rivas, G., Abramov, A.Y., Valpuesta, J.M., Dobson, C.M. and Cremades, N. 2015. Structural characterization of toxic oligomers that are kinetically trapped during alpha-synuclein fibril formation. *Proc Natl Acad Sci U S A.* **112**(16), pp.E1994-2003.

Chia, S., Flagmeier, P., Habchi, J., Lattanzi, V., Linse, S., Dobson, C.M., Knowles, T.P.J. and Vendruscolo, M. 2017. Monomeric and fibrillar alpha-synuclein exert opposite effects on the catalytic cycle that promotes the proliferation of Abeta42 aggregates. *Proc Natl Acad Sci U S A.* **114**(30), pp.8005-8010.

Chiti, F. and Dobson, C.M. 2017. Protein Misfolding, Amyloid Formation, and Human Disease: A Summary of Progress Over the Last Decade. *Annu Rev Biochem.* **86**, pp.27-68.

Cho, M.K., Nodet, G., Kim, H.Y., Jensen, M.R., Bernado, P., Fernandez, C.O., Becker, S., Blackledge, M. and Zweckstetter, M. 2009. Structural characterization of alpha-synuclein in an aggregation prone state. *Protein Sci.* **18**(9), pp.1840-1846.

Chow, V.W., Mattson, M.P., Wong, P.C. and Gleichmann, M. 2010. An overview of APP processing enzymes and products. *Neuromolecular Med.* **12**(1), pp.1-12.

Chung, E.J., Babulal, G.M., Monsell, S.E., Cairns, N.J., Roe, C.M. and Morris, J.C. 2015. Clinical Features of Alzheimer Disease With and Without Lewy Bodies. *JAMA Neurol.* **72**(7), pp.789-796.

Clinton, L.K., Blurton-Jones, M., Myczek, K., Trojanowski, J.Q. and LaFerla, F.M. 2010. Synergistic Interactions between Abeta, tau, and alpha-synuclein: acceleration of neuropathology and cognitive decline. *J Neurosci.* **30**(21), pp.7281-7289.

Cohen, S.I.A., Arosio, P., Presto, J., Kurudenkandy, F.R., Biverstal, H., Dolfe, L., Dunning, C., Yang, X., Frohm, B., Vendruscolo, M., Johansson, J., Dobson, C.M., Fisahn, A., Knowles, T.P.J. and Linse, S. 2015. A molecular chaperone breaks the catalytic cycle that generates toxic Abeta oligomers. *Nat Struct Mol Biol.* **22**(3), pp.207-213.

Colvin, M.T., Silvers, R., Frohm, B., Su, Y., Linse, S. and Griffin, R.G. 2015. High resolution structural characterization of Abeta42 amyloid fibrils by magic angle spinning NMR. *J Am Chem Soc.* **137**(23), pp.7509-7518.

Colvin, M.T., Silvers, R., Ni, Q.Z., Can, T.V., Sergeyev, I., Rosay, M., Donovan, K.J., Michael, B., Wall, J., Linse, S. and Griffin, R.G. 2016. Atomic Resolution Structure of Monomorphic Abeta42 Amyloid Fibrils. *J Am Chem Soc.* **138**(30), pp.9663-9674.

Condello, C., Lemmin, T., Stohr, J., Nick, M., Wu, Y., Maxwell, A.M., Watts, J.C., Caro, C.D., Oehler, A., Keene, C.D., Bird, T.D., van Duinen, S.G., Lannfelt, L., Ingelsson, M., Graff, C., Giles, K., DeGrado, W.F. and Prusiner, S.B. 2018. Structural heterogeneity and intersubject variability of Abeta in familial and sporadic Alzheimer's disease. *Proc Natl Acad Sci U S A.* **115**(4), pp.E782-E791.

Conway, K.A., Lee, S.J., Rochet, J.C., Ding, T.T., Williamson, R.E. and Lansbury, P.T., Jr. 2000. Acceleration of oligomerization, not fibrillization, is a shared property of both alpha-synuclein mutations linked to early-onset Parkinson's disease: implications for pathogenesis and therapy. *Proc Natl Acad Sci U S A.* **97**(2), pp.571-576.

Corder, E.H., Saunders, A.M., Strittmatter, W.J., Schmechel, D.E., Gaskell, P.C., Small, G.W., Roses, A.D., Haines, J.L. and Pericak-Vance, M.A. 1993. Gene dose of apolipoprotein E type 4 allele and the risk of Alzheimer's disease in late onset families. *Science.* **261**(5123), pp.921-923.

Couceiro, J.R., Gallardo, R., De Smet, F., De Baets, G., Baatsen, P., Annaert, W., Roose, K., Saelens, X., Schymkowitz, J. and Rousseau, F. 2015. Sequence-dependent internalization of aggregating peptides. *J Biol Chem.* **290**(1), pp.242-258.

Cremades, N., Cohen, S.I., Deas, E., Abramov, A.Y., Chen, A.Y., Orte, A., Sandal, M., Clarke, R.W., Dunne, P., Aprile, F.A., Bertoncini, C.W., Wood, N.W., Knowles, T.P., Dobson, C.M. and Klenerman, D. 2012. Direct observation of the interconversion of normal and toxic forms of alpha-synuclein. *Cell.* **149**(5), pp.1048-1059.

Dammers, C., Gremer, L., Neudecker, P., Demuth, H.U., Schwarten, M. and Willbold, D. 2015. Purification and Characterization of Recombinant N-Terminally Pyroglutamate-Modified Amyloid-beta Variants and Structural Analysis by Solution NMR Spectroscopy. *PLoS One.* **10**(10), pe0139710.

Davidson, H.W., West, M.A. and Watts, C. 1990. Endocytosis, intracellular trafficking, and processing of membrane IgG and monovalent antigen/membrane IgG complexes in B lymphocytes. *J Immunol.* **144**(11), pp.4101-4109.

Dettmer, U., Newman, A.J., von Saucken, V.E., Bartels, T. and Selkoe, D. 2015. KTKEGV repeat motifs are key mediators of normal alpha-synuclein tetramerization: Their mutation causes excess monomers and neurotoxicity. *Proc Natl Acad Sci U S A.* **112**(31), pp.9596-9601.

DeTure, M.A. and Dickson, D.W. 2019. The neuropathological diagnosis of Alzheimer's disease. *Mol Neurodegener.* **14**(1), p32.

Doherty, C.P.A., Ulamec, S.M., Maya-Martinez, R., Good, S.C., Makepeace, J., Khan, G.N., van Oosten-Hawle, P., Radford, S.E. and Brockwell, D.J. 2020. A short motif in the N-terminal region of alpha-synuclein is critical for both aggregation and function. *Nat Struct Mol Biol.* **27**(3), pp.249-259.

Drummond, E., Nayak, S., Faustin, A., Pires, G., Hickman, R.A., Askenazi, M., Cohen, M., Haldiman, T., Kim, C., Han, X., Shao, Y., Safar, J.G., Ueberheide, B. and Wisniewski, T. 2017. Proteomic differences in amyloid plaques in rapidly progressive and sporadic Alzheimer's disease. *Acta Neuropathol.* **133**(6), pp.933-954.

Duff, K., Eckman, C., Zehr, C., Yu, X., Prada, C.M., Perez-tur, J., Hutton, M., Buee, L., Harigaya, Y., Yager, D., Morgan, D., Gordon, M.N., Holcomb, L., Refolo, L., Zenk, B., Hardy, J. and Younkin, S. 1996. Increased amyloid-beta42(43) in brains of mice expressing mutant presenilin 1. *Nature.* **383**(6602), pp.710-713.

Fandrich, M., Nystrom, S., Nilsson, K.P.R., Bockmann, A., LeVine, H., 3rd and Hammarstrom, P. 2018. Amyloid fibril polymorphism: a challenge for molecular imaging and therapy. *J Intern Med.* **283**(3), pp.218-237.

Finder, V.H., Vodopivec, I., Nitsch, R.M. and Glockshuber, R. 2010. The recombinant amyloid-beta peptide Abeta1-42 aggregates faster and is more neurotoxic than synthetic Abeta1-42. *J Mol Biol.* **396**(1), pp.9-18.

Flagmeier, P., Meisl, G., Vendruscolo, M., Knowles, T.P., Dobson, C.M., Buell, A.K. and Galvagnion, C. 2016. Mutations associated with familial Parkinson's disease alter the initiation and amplification steps of alpha-synuclein aggregation. *Proc Natl Acad Sci U S A.* **113**(37), pp.10328-10333.

Forno, L.S. 1996. Neuropathology of Parkinson's disease. *J Neuropathol Exp Neurol.* **55**(3), pp.259-272.

Fusco, G., De Simone, A., Arosio, P., Vendruscolo, M., Veglia, G. and Dobson, C.M. 2016. Structural Ensembles of Membrane-bound alpha-Synuclein Reveal the Molecular Determinants of Synaptic Vesicle Affinity. *Sci Rep.* **6**, p27125.

Galvagnion, C., Buell, A.K., Meisl, G., Michaels, T.C., Vendruscolo, M., Knowles, T.P. and Dobson, C.M. 2015. Lipid vesicles trigger alpha-synuclein aggregation by stimulating primary nucleation. *Nat Chem Biol.* **11**(3), pp.229-234.

Gaspar, R., Meisl, G., Buell, A.K., Young, L., Kaminski, C.F., Knowles, T.P.J., Sparr, E. and Linse, S. 2017. Secondary nucleation of monomers on fibril surface dominates alpha-

synuclein aggregation and provides autocatalytic amyloid amplification. *Q Rev Biophys.* **50**, pe6.

Gessel, M.M., Bernstein, S., Kemper, M., Teplow, D.B. and Bowers, M.T. 2012. Familial Alzheimer's disease mutations differentially alter amyloid beta-protein oligomerization. *ACS Chem Neurosci.* **3**(11), pp.909-918.

Giasson, B.I., Duda, J.E., Quinn, S.M., Zhang, B., Trojanowski, J.Q. and Lee, V.M. 2002. Neuronal alpha-synucleinopathy with severe movement disorder in mice expressing A53T human alpha-synuclein. *Neuron.* **34**(4), pp.521-533.

Giasson, B.I., Murray, I.V., Trojanowski, J.Q. and Lee, V.M. 2001. A hydrophobic stretch of 12 amino acid residues in the middle of alpha-synuclein is essential for filament assembly. *J Biol Chem.* **276**(4), pp.2380-2386.

Goedert, M., Spillantini, M.G., Cairns, N.J. and Crowther, R.A. 1992. Tau proteins of Alzheimer paired helical filaments: abnormal phosphorylation of all six brain isoforms. *Neuron.* **8**(1), pp.159-168.

Graham, D.R. and Sidhu, A. 2010. Mice expressing the A53T mutant form of human alpha-synuclein exhibit hyperactivity and reduced anxiety-like behavior. *J Neurosci Res.* **88**(8), pp.1777-1783.

Gremer, L., Scholzel, D., Schenk, C., Reinartz, E., Labahn, J., Ravelli, R.B.G., Tusche, M., Lopez-Iglesias, C., Hoyer, W., Heise, H., Willbold, D. and Schroder, G.F. 2017. Fibril structure of amyloid-beta(1-42) by cryo-electron microscopy. *Science.* **358**(6359), pp.116-119.

Grey, M., Linse, S., Nilsson, H., Brundin, P. and Sparr, E. 2011. Membrane interaction of alpha-synuclein in different aggregation states. *J Parkinsons Dis.* **1**(4), pp.359-371.

Guerrero-Ferreira, R., Taylor, N.M., Arteni, A.A., Kumari, P., Mona, D., Ringler, P., Britschgi, M., Lauer, M.E., Makky, A., Verasdonck, J., Riek, R., Melki, R., Meier, B.H., Bockmann, A., Bousset, L. and Stahlberg, H. 2019. Two new polymorphic structures of human full-length alpha-synuclein fibrils solved by cryo-electron microscopy. *Elife.* **8**.

Guerrero-Ferreira, R., Taylor, N.M., Mona, D., Ringler, P., Lauer, M.E., Riek, R., Britschgi, M. and Stahlberg, H. 2018. Cryo-EM structure of alpha-synuclein fibrils. *Elife.* **7**.

Guo, J.L., Covell, D.J., Daniels, J.P., Iba, M., Stieber, A., Zhang, B., Riddle, D.M., Kwong, L.K., Xu, Y., Trojanowski, J.Q. and Lee, V.M. 2013. Distinct alpha-synuclein strains differentially promote tau inclusions in neurons. *Cell.* **154**(1), pp.103-117.

Hamilton, R.L. 2000. Lewy bodies in Alzheimer's disease: a neuropathological review of 145 cases using alpha-synuclein immunohistochemistry. *Brain Pathol.* **10**(3), pp.378-384.

Han, H., Weinreb, P.H. and Lansbury, P.T., Jr. 1995. The core Alzheimer's peptide NAC forms amyloid fibrils which seed and are seeded by beta-amyloid: is NAC a common trigger or target in neurodegenerative disease? *Chem Biol.* **2**(3), pp.163-169.

Hansson, O., Lehmann, S., Otto, M., Zetterberg, H. and Lewczuk, P. 2019. Advantages and disadvantages of the use of the CSF Amyloid beta (Abeta) 42/40 ratio in the diagnosis of Alzheimer's Disease. *Alzheimers Res Ther.* **11**(1), p34.

Hasegawa, T., Matsuzaki, M., Takeda, A., Kikuchi, A., Akita, H., Perry, G., Smith, M.A. and Itoyama, Y. 2004. Accelerated alpha-synuclein aggregation after differentiation of SH-SY5Y neuroblastoma cells. *Brain Res.* **1013**(1), pp.51-59.

Hassan, F.U., Rehman, M.S., Khan, M.S., Ali, M.A., Javed, A., Nawaz, A. and Yang, C. 2019. Curcumin as an Alternative Epigenetic Modulator: Mechanism of Action and Potential Effects. *Front Genet.* **10**, p514.

Hatami, A., Monjazeb, S., Milton, S. and Glabe, C.G. 2017. Familial Alzheimer's Disease Mutations within the Amyloid Precursor Protein Alter the Aggregation and Conformation of the Amyloid-beta Peptide. *J Biol Chem.* **292**(8), pp.3172-3185.

Hellstrand, E., Boland, B., Walsh, D.M. and Linse, S. 2010. Amyloid beta-protein aggregation produces highly reproducible kinetic data and occurs by a two-phase process. *ACS Chem Neurosci.* **1**(1), pp.13-18.

Henderson, M.X., Chung, C.H., Riddle, D.M., Zhang, B., Gathagan, R.J., Seeholzer, S.H., Trojanowski, J.Q. and Lee, V.M.Y. 2017. Unbiased Proteomics of Early Lewy Body Formation Model Implicates Active Microtubule Affinity-Regulating Kinases (MARKs) in Synucleinopathies. *J Neurosci.* **37**(24), pp.5870-5884.

Hoarau, M., Malbert, Y., Irague, R., Hureau, C., Faller, P., Gras, E., Andre, I. and Remaud-Simeon, M. 2016. A Robust and Efficient Production and Purification Procedure of Recombinant Alzheimers Disease Methionine-Modified Amyloid-beta Peptides. *PLoS One.* **11**(8), pe0161209.

Hoffmann, A.C., Minakaki, G., Menges, S., Salvi, R., Savitskiy, S., Kazman, A., Vicente Miranda, H., Mielenz, D., Klucken, J., Winkler, J. and Xiang, W. 2019. Extracellular aggregated alpha synuclein primarily triggers lysosomal dysfunction in neural cells prevented by trehalose. *Sci Rep.* **9**(1), p544.

Holtta, M., Hansson, O., Andreasson, U., Hertze, J., Minthon, L., Nagga, K., Andreasen, N., Zetterberg, H. and Blennow, K. 2013. Evaluating amyloid-beta oligomers in cerebrospinal fluid as a biomarker for Alzheimer's disease. *PLoS One.* **8**(6), pe66381.

Hope, C.K., Billingsley, K., de Josselin de Jong, E. and Higham, S.M. 2016. A Preliminary Study of the Effects of pH upon Fluorescence in Suspensions of Prevotella intermedia. *PLoS One.* **11**(7), pe0158835.

Hou, L., Shao, H., Zhang, Y., Li, H., Menon, N.K., Neuhaus, E.B., Brewer, J.M., Byeon, I.J., Ray, D.G., Vitek, M.P., Iwashita, T., Makula, R.A., Przybyla, A.B. and Zagorski, M.G. 2004. Solution NMR studies of the A beta(1-40) and A beta(1-42) peptides establish that the Met35 oxidation state affects the mechanism of amyloid formation. *J Am Chem Soc.* **126**(7), pp.1992-2005.

Hu, Y.B., Dammer, E.B., Ren, R.J. and Wang, G. 2015. The endosomal-lysosomal system: from acidification and cargo sorting to neurodegeneration. *Transl Neurodegener.* **4**, p18.

Hu, Z.W., Vugmeyster, L., Au, D.F., Ostrovsky, D., Sun, Y. and Qiang, W. 2019. Molecular structure of an N-terminal phosphorylated beta-amyloid fibril. *Proc Natl Acad Sci U S A.* **116**(23), pp.11253-11258.

Hunya, A., Foldi, I., Szegedi, V., Soos, K., Zarandi, M., Szabo, A., Zadori, D., Penke, B. and Datki, Z.L. 2008. Differences between normal and alpha-synuclein overexpressing SH-SY5Y neuroblastoma cells after Abeta(1-42) and NAC treatment. *Brain Res Bull.* **75**(5), pp.648-654.

Hurtig, H.I., Trojanowski, J.Q., Galvin, J., Ewbank, D., Schmidt, M.L., Lee, V.M., Clark, C.M., Glosser, G., Stern, M.B., Gollomp, S.M. and Arnold, S.E. 2000. Alpha-synuclein cortical Lewy bodies correlate with dementia in Parkinson's disease. *Neurology.* **54**(10), pp.1916-1921.

Iadanza, M.G., Jackson, M.P., Hewitt, E.W., Ranson, N.A. and Radford, S.E. 2018. A new era for understanding amyloid structures and disease. *Nat Rev Mol Cell Biol.* **19**(12), pp.755-773.

Ihara, Y., Morishima-Kawashima, M. and Nixon, R. 2012. The ubiquitin-proteasome system and the autophagic-lysosomal system in Alzheimer disease. *Cold Spring Harb Perspect Med.* **2**(8).

Irwin, D.J., Grossman, M., Weintraub, D., Hurtig, H.I., Duda, J.E., Xie, S.X., Lee, E.B., Van Deerlin, V.M., Lopez, O.L., Kofler, J.K., Nelson, P.T., Jicha, G.A., Woltjer, R., Quinn, J.F., Kaye, J., Leverenz, J.B., Tsuang, D., Longfellow, K., Yearout, D., Kukull, W., Keene, C.D., Montine, T.J., Zabetian, C.P. and Trojanowski, J.Q. 2017. Neuropathological and genetic correlates of survival and dementia onset in synucleinopathies: a retrospective analysis. *Lancet Neurol.* **16**(1), pp.55-65.

Iwai, A., Yoshimoto, M., Masliah, E. and Saitoh, T. 1995. Non-A beta component of Alzheimer's disease amyloid (NAC) is amyloidogenic. *Biochemistry.* **34**(32), pp.10139-10145.

Jackson, M.P. and Hewitt, E.W. 2016. Cellular proteostasis: degradation of misfolded proteins by lysosomes. *Essays Biochem.* **60**(2), pp.173-180.

Jakhria, T., Hellewell, A.L., Porter, M.Y., Jackson, M.P., Tipping, K.W., Xue, W.F., Radford, S.E. and Hewitt, E.W. 2014. beta2-microglobulin amyloid fibrils are nanoparticles that disrupt lysosomal membrane protein trafficking and inhibit protein degradation by lysosomes. *J Biol Chem.* **289**(52), pp.35781-35794.

Jakubowski, J.M., Orr, A.A., Le, D.A. and Tamamis, P. 2020. Interactions between Curcumin Derivatives and Amyloid-beta Fibrils: Insights from Molecular Dynamics Simulations. *J Chem Inf Model.* **60**(1), pp.289-305.

Jamur, M.C. and Oliver, C. 2010. Permeabilization of cell membranes. *Methods Mol Biol.* **588**, pp.63-66.

Janelidze, S., Stomrud, E., Palmqvist, S., Zetterberg, H., van Westen, D., Jeromin, A., Song, L., Hanlon, D., Tan Hehir, C.A., Baker, D., Blennow, K. and Hansson, O. 2016. Plasma beta-amyloid in Alzheimer's disease and vascular disease. *Sci Rep.* **6**, p26801.

Jellinger, K.A. 2003. Alpha-synuclein pathology in Parkinson's and Alzheimer's disease brain: incidence and topographic distribution--a pilot study. *Acta Neuropathol.* **106**(3), pp.191-201.

Jensen, P.H., Hojrup, P., Hager, H., Nielsen, M.S., Jacobsen, L., Olesen, O.F., Gliemann, J. and Jakes, R. 1997. Binding of Abeta to alpha- and beta-synucleins: identification of segments in alpha-synuclein/NAC precursor that bind Abeta and NAC. *Biochem J.* **323 (Pt 2)**, pp.539-546.

Jin, S., Kedia, N., Illes-Toth, E., Haralampiev, I., Prisner, S., Herrmann, A., Wanker, E.E. and Bieschke, J. 2016. Amyloid-beta(1-42) Aggregation Initiates Its Cellular Uptake and Cytotoxicity. *J Biol Chem.* **291**(37), pp.19590-19606.

Jung, B.C., Lim, Y.J., Bae, E.J., Lee, J.S., Choi, M.S., Lee, M.K., Lee, H.J., Kim, Y.S. and Lee, S.J. 2017. Amplification of distinct alpha-synuclein fibril conformers through protein misfolding cyclic amplification. *Exp Mol Med.* **49**(4), pe314.

Kayed, R. and Lasagna-Reeves, C.A. 2013. Molecular mechanisms of amyloid oligomers toxicity. *J Alzheimers Dis.* **33 Suppl 1**, pp.S67-78.

Kheterpal, I., Chen, M., Cook, K.D. and Wetzel, R. 2006. Structural differences in Abeta amyloid protofibrils and fibrils mapped by hydrogen exchange--mass spectrometry with on-line proteolytic fragmentation. *J Mol Biol.* **361**(4), pp.785-795.

Kim, W.S., Kagedal, K. and Halliday, G.M. 2014. Alpha-synuclein biology in Lewy body diseases. *Alzheimers Res Ther.* **6**(5), p73.

Klucken, J., Poehler, A.M., Ebrahimi-Fakhari, D., Schneider, J., Nuber, S., Rockenstein, E., Schlotzer-Schrehardt, U., Hyman, B.T., McLean, P.J., Masliah, E. and Winkler, J. 2012. Alpha-synuclein aggregation involves a bafilomycin A 1-sensitive autophagy pathway. *Autophagy.* **8**(5), pp.754-766.

Kollmer, M., Close, W., Funk, L., Rasmussen, J., Bsoul, A., Schierhorn, A., Schmidt, M., Sigurdson, C.J., Jucker, M. and Fandrich, M. 2019. Cryo-EM structure and polymorphism of Abeta amyloid fibrils purified from Alzheimer's brain tissue. *Nat Commun.* **10**(1), p4760.

Koppen, J., Schulze, A., Machner, L., Wermann, M., Eichentopf, R., Guthardt, M., Hahnel, A., Klehm, J., Kriegeskorte, M.C., Hartlage-Rubsamen, M., Morawski, M., von Horsten, S., Demuth, H.U., Rossner, S. and Schilling, S. 2020. Amyloid-Beta Peptides Trigger Aggregation of Alpha-Synuclein In Vitro. *Molecules.* **25**(3).

Kotzbauer, P.T., Trojanowsk, J.Q. and Lee, V.M. 2001. Lewy body pathology in Alzheimer's disease. *J Mol Neurosci.* **17**(2), pp.225-232.

Kovacs, D.M., Fausett, H.J., Page, K.J., Kim, T.W., Moir, R.D., Merriam, D.E., Hollister, R.D., Hallmark, O.G., Mancini, R., Felsenstein, K.M., Hyman, B.T., Tanzi, R.E. and Wasco, W. 1996. Alzheimer-associated presenilins 1 and 2: neuronal expression in brain and localization to intracellular membranes in mammalian cells. *Nat Med.* **2**(2), pp.224-229.

Krebs, M.R., Bromley, E.H. and Donald, A.M. 2005. The binding of thioflavin-T to amyloid fibrils: localisation and implications. *J Struct Biol.* **149**(1), pp.30-37.

Kreutzmann, P., Wolf, G. and Kupsch, K. 2010. Minocycline recovers MTT-formazan exocytosis impaired by amyloid beta peptide. *Cell Mol Neurobiol.* **30**(7), pp.979-984.

Kumar, P., Nagarajan, A. and Uchil, P.D. 2018a. Analysis of Cell Viability by the Lactate Dehydrogenase Assay. *Cold Spring Harb Protoc.* **2018**(6).

Kumar, P., Nagarajan, A. and Uchil, P.D. 2018b. Analysis of Cell Viability by the MTT Assay. *Cold Spring Harb Protoc.* **2018**(6).

Lashuel, H.A., Overk, C.R., Oueslati, A. and Masliah, E. 2013. The many faces of alpha-synuclein: from structure and toxicity to therapeutic target. *Nat Rev Neurosci.* **14**(1), pp.38-48.

Lau, A., So, R.W.L., Lau, H.H.C., Sang, J.C., Ruiz-Riquelme, A., Fleck, S.C., Stuart, E., Menon, S., Visanji, N.P., Meisl, G., Faidi, R., Marano, M.M., Schmitt-Ulms, C., Wang, Z., Fraser, P.E., Tandon, A., Hyman, B.T., Wille, H., Ingelsson, M., Klenerman, D. and Watts, J.C. 2020. alpha-Synuclein strains target distinct brain regions and cell types. *Nat Neurosci.* **23**(1), pp.21-31.

Lee, J.H., McBrayer, M.K., Wolfe, D.M., Haslett, L.J., Kumar, A., Sato, Y., Lie, P.P., Mohan, P., Coffey, E.E., Kompella, U., Mitchell, C.H., Lloyd-Evans, E. and Nixon, R.A. 2015. Presenilin 1 Maintains Lysosomal Ca(2+) Homeostasis via TRPML1 by Regulating vATPase-Mediated Lysosome Acidification. *Cell Rep.* **12**(9), pp.1430-1444.

Lee, J.H., Yu, W.H., Kumar, A., Lee, S., Mohan, P.S., Peterhoff, C.M., Wolfe, D.M., Martinez-Vicente, M., Massey, A.C., Sovak, G., Uchiyama, Y., Westaway, D., Cuervo, A.M. and Nixon, R.A. 2010. Lysosomal proteolysis and autophagy require presenilin 1 and are disrupted by Alzheimer-related PS1 mutations. *Cell.* **141**(7), pp.1146-1158.

Lehtonen, S., Sonninen, T.M., Wojciechowski, S., Goldsteins, G. and Koistinaho, J. 2019. Dysfunction of Cellular Proteostasis in Parkinson's Disease. *Front Neurosci.* **13**, p457.

Leissring, M.A. 2014. Abeta degradation-the inside story. *Front Aging Neurosci.* **6**, p229.

Li, Y., Zhao, C., Luo, F., Liu, Z., Gui, X., Luo, Z., Zhang, X., Li, D., Liu, C. and Li, X. 2018. Amyloid fibril structure of alpha-synuclein determined by cryo-electron microscopy. *Cell Res.* **28**(9), pp.897-903.

Linse, S. 2017. Monomer-dependent secondary nucleation in amyloid formation. *Biophys Rev.* **9**(4), pp.329-338.

Lippa, C.F., Ozawa, K., Mann, D.M., Ishii, K., Smith, T.W., Arawaka, S. and Mori, H. 1999a. Deposition of beta-amyloid subtypes 40 and 42 differentiates dementia with Lewy bodies from Alzheimer disease. *Arch Neurol.* **56**(9), pp.1111-1118.

Lippa, C.F., Saunders, A.M., Smith, T.W., Swearer, J.M., Drachman, D.A., Ghetti, B., Nee, L., Pulaski-Salo, D., Dickson, D., Robitaille, Y., Bergeron, C., Crain, B., Benson, M.D., Farlow, M., Hyman, B.T., George-Hyslop, S.P., Roses, A.D. and Pollen, D.A. 1996. Familial and sporadic Alzheimer's disease: neuropathology cannot exclude a final common pathway. *Neurology.* **46**(2), pp.406-412.

Lippa, C.F., Schmidt, M.L., Lee, V.M. and Trojanowski, J.Q. 1999b. Antibodies to alpha-synuclein detect Lewy bodies in many Down's syndrome brains with Alzheimer's disease. *Ann Neurol.* **45**(3), pp.353-357.

Liu, C.C., Liu, C.C., Kanekiyo, T., Xu, H. and Bu, G. 2013. Apolipoprotein E and Alzheimer disease: risk, mechanisms and therapy. *Nat Rev Neurol.* **9**(2), pp.106-118.

Liu, R.Q., Zhou, Q.H., Ji, S.R., Zhou, Q., Feng, D., Wu, Y. and Sui, S.F. 2010. Membrane localization of beta-amyloid 1-42 in lysosomes: a possible mechanism for lysosome labilization. *J Biol Chem.* **285**(26), pp.19986-19996.

Liu, Y., Peterson, D.A. and Schubert, D. 1998. Amyloid beta peptide alters intracellular vesicle trafficking and cholesterol homeostasis. *Proc Natl Acad Sci U S A.* **95**(22), pp.13266-13271.

Lu, J.X., Qiang, W., Yau, W.M., Schwieters, C.D., Meredith, S.C. and Tycko, R. 2013. Molecular structure of beta-amyloid fibrils in Alzheimer's disease brain tissue. *Cell.* **154**(6), pp.1257-1268.

Luk, K.C., Song, C., O'Brien, P., Stieber, A., Branch, J.R., Brunden, K.R., Trojanowski, J.Q. and Lee, V.M. 2009. Exogenous alpha-synuclein fibrils seed the formation of Lewy body-like intracellular inclusions in cultured cells. *Proc Natl Acad Sci U S A.* **106**(47), pp.20051-20056.

Madelin, G., Kline, R., Walvick, R. and Regatte, R.R. 2014. A method for estimating intracellular sodium concentration and extracellular volume fraction in brain in vivo using sodium magnetic resonance imaging. *Sci Rep.* **4**, p4763.

Madine, J., Pandya, M.J., Hicks, M.R., Rodger, A., Yates, E.A., Radford, S.E. and Middleton, D.A. 2012. Site-specific identification of an abeta fibril-heparin interaction

site by using solid-state NMR spectroscopy. *Angew Chem Int Ed Engl.* **51**(52), pp.13140-13143.

Mahajan, S.D., Law, W.C., Aalinkeel, R., Reynolds, J., Nair, B.B., Yong, K.T., Roy, I., Prasad, P.N. and Schwartz, S.A. 2012. Nanoparticle-mediated targeted delivery of antiretrovirals to the brain. *Methods Enzymol.* **509**, pp.41-60.

Mahul-Mellier, A.L., Burtscher, J., Maharjan, N., Weerens, L., Croisier, M., Kuttler, F., Leleu, M., Knott, G.W. and Lashuel, H.A. 2020. The process of Lewy body formation, rather than simply alpha-synuclein fibrillization, is one of the major drivers of neurodegeneration. *Proc Natl Acad Sci U S A.* **117**(9), pp.4971-4982.

Mak, S.K., McCormack, A.L., Manning-Bog, A.B., Cuervo, A.M. and Di Monte, D.A. 2010. Lysosomal degradation of alpha-synuclein in vivo. *J Biol Chem.* **285**(18), pp.13621-13629.

Maltsev, A.S., Ying, J. and Bax, A. 2012. Impact of N-terminal acetylation of alpha-synuclein on its random coil and lipid binding properties. *Biochemistry.* **51**(25), pp.5004-5013.

Margallo-Lana, M., Morris, C.M., Gibson, A.M., Tan, A.L., Kay, D.W., Tyrer, S.P., Moore, B.P. and Ballard, C.G. 2004. Influence of the amyloid precursor protein locus on dementia in Down syndrome. *Neurology.* **62**(11), pp.1996-1998.

Masliah, E., Rockenstein, E., Veinbergs, I., Sagara, Y., Mallory, M., Hashimoto, M. and Mucke, L. 2001. beta-amyloid peptides enhance alpha-synuclein accumulation and neuronal deficits in a transgenic mouse model linking Alzheimer's disease and Parkinson's disease. *Proc Natl Acad Sci U S A.* **98**(21), pp.12245-12250.

Masuda, Y., Fukuchi, M., Yatagawa, T., Tada, M., Takeda, K., Irie, K., Akagi, K., Monobe, Y., Imazawa, T. and Takegoshi, K. 2011. Solid-state NMR analysis of interaction sites of curcumin and 42-residue amyloid beta-protein fibrils. *Bioorg Med Chem.* **19**(20), pp.5967-5974.

Mattsson, N., Zetterberg, H., Hansson, O., Andreasen, N., Parnetti, L., Jonsson, M., Herukka, S.K., van der Flier, W.M., Blankenstein, M.A., Ewers, M., Rich, K., Kaiser, E., Verbeek, M., Tsolaki, M., Mulugeta, E., Rosen, E., Aarsland, D., Visser, P.J., Schroder,

J., Marcusson, J., de Leon, M., Hampel, H., Scheltens, P., Pirttila, T., Wallin, A., Jonhagen, M.E., Minthon, L., Winblad, B. and Blennow, K. 2009. CSF biomarkers and incipient Alzheimer disease in patients with mild cognitive impairment. *JAMA.* **302**(4), pp.385-393.

Mawuenyega, K.G., Sigurdson, W., Ovod, V., Munsell, L., Kasten, T., Morris, J.C., Yarasheski, K.E. and Bateman, R.J. 2010. Decreased clearance of CNS beta-amyloid in Alzheimer's disease. *Science.* **330**(6012), p1774.

Mayor, S. and Pagano, R.E. 2007. Pathways of clathrin-independent endocytosis. *Nat Rev Mol Cell Biol.* **8**(8), pp.603-612.

Mazzulli, J.R., Zunke, F., Isacson, O., Studer, L. and Krainc, D. 2016. alpha-Synuclein-induced lysosomal dysfunction occurs through disruptions in protein trafficking in human midbrain synucleinopathy models. *Proc Natl Acad Sci U S A.* **113**(7), pp.1931-1936.

McGlinchey, R.P. and Lee, J.C. 2015. Cysteine cathepsins are essential in lysosomal degradation of alpha-synuclein. *Proc Natl Acad Sci U S A.* **112**(30), pp.9322-9327.

McKeith, I. 2007. Dementia with Lewy bodies. *Handb Clin Neurol.* **84**, pp.531-548.

Meilandt, W.J., Ngu, H., Gogineni, A., Lalehzadeh, G., Lee, S.H., Srinivasan, K., Imperio, J., Wu, T., Weber, M., Kruse, A.J., Stark, K.L., Chan, P., Kwong, M., Modrusan, Z., Friedman, B.A., Elstrott, J., Foreman, O., Easton, A., Sheng, M. and Hansen, D.V. 2020. Trem2 Deletion Reduces Late-Stage Amyloid Plaque Accumulation, Elevates the Abeta42:Abeta40 Ratio, and Exacerbates Axonal Dystrophy and Dendritic Spine Loss in the PS2APP Alzheimer's Mouse Model. *J Neurosci.* **40**(9), pp.1956-1974.

Meisl, G., Kirkegaard, J.B., Arosio, P., Michaels, T.C., Vendruscolo, M., Dobson, C.M., Linse, S. and Knowles, T.P. 2016. Molecular mechanisms of protein aggregation from global fitting of kinetic models. *Nat Protoc.* **11**(2), pp.252-272.

Messeter, K. and Siesjo, B.K. 1971. Regulation of the CSF pH in acute and sustained respiratory acidosis. *Acta Physiol Scand.* **83**(1), pp.21-30.

Montagnaro, S., Longo, M., Mallardo, K., Pisanelli, G., De Martino, L., Fusco, G., Baldi, L., Pagnini, U. and Iovane, G. 2008. Evaluation of a fluorescence polarization assay for

the detection of serum antibodies to Brucella abortus in water buffalo (Bubalus bubalis). *Vet Immunol Immunopathol.* **125**(1-2), pp.135-142.

Morales, R., Moreno-Gonzalez, I. and Soto, C. 2013. Cross-seeding of misfolded proteins: implications for etiology and pathogenesis of protein misfolding diseases. *PLoS Pathog.* **9**(9), pe1003537.

Morten, I.J., Gosal, W.S., Radford, S.E. and Hewitt, E.W. 2007. Investigation into the role of macrophages in the formation and degradation of beta2-microglobulin amyloid fibrils. *J Biol Chem.* **282**(40), pp.29691-29700.

Murphy, M.P. and LeVine, H., 3rd. 2010. Alzheimer's disease and the amyloid-beta peptide. *J Alzheimers Dis.* **19**(1), pp.311-323.

Nadezhdin, K.D., Bocharova, O.V., Bocharov, E.V. and Arseniev, A.S. 2011. Structural and dynamic study of the transmembrane domain of the amyloid precursor protein. *Acta Naturae.* **3**(1), pp.69-76.

Nhan, H.S., Chiang, K. and Koo, E.H. 2015. The multifaceted nature of amyloid precursor protein and its proteolytic fragments: friends and foes. *Acta Neuropathol.* **129**(1), pp.1-19.

Niemantsverdriet, E., Valckx, S., Bjerke, M. and Engelborghs, S. 2017. Alzheimer's disease CSF biomarkers: clinical indications and rational use. *Acta Neurol Belg.* **117**(3), pp.591-602.

Nixon, R.A. 2017. Amyloid precursor protein and endosomal-lysosomal dysfunction in Alzheimer's disease: inseparable partners in a multifactorial disease. *FASEB J.* **31**(7), pp.2729-2743.

O'Brien, R.J. and Wong, P.C. 2011. Amyloid precursor protein processing and Alzheimer's disease. *Annu Rev Neurosci.* **34**, pp.185-204.

Ono, K., Takahashi, R., Ikeda, T. and Yamada, M. 2012. Cross-seeding effects of amyloid beta-protein and alpha-synuclein. *J Neurochem.* **122**(5), pp.883-890.

Ovod, V., Ramsey, K.N., Mawuenyega, K.G., Bollinger, J.G., Hicks, T., Schneider, T., Sullivan, M., Paumier, K., Holtzman, D.M., Morris, J.C., Benzinger, T., Fagan, A.M.,

Patterson, B.W. and Bateman, R.J. 2017. Amyloid beta concentrations and stable isotope labeling kinetics of human plasma specific to central nervous system amyloidosis. *Alzheimers Dement.* **13**(8), pp.841-849.

Palta, P., Rippon, B., Reitz, C., He, H., Sherwood, G., Ceballos, F., Teresi, J., Razlighi, Q., Moreno, H., Brickman, A.M. and Luchsinger, J.A. 2020. Apolipoprotein E genotype and in-vivo amyloid burden in middle-aged hispanics. *Neurology.*

Paravastu, A.K., Leapman, R.D., Yau, W.M. and Tycko, R. 2008. Molecular structural basis for polymorphism in Alzheimer's beta-amyloid fibrils. *Proc Natl Acad Sci U S A.* **105**(47), pp.18349-18354.

Parhamifar, L., Andersen, H. and Moghimi, S.M. 2013. Lactate dehydrogenase assay for assessment of polycation cytotoxicity. *Methods Mol Biol.* **948**, pp.13-22.

Pauwels, K., Williams, T.L., Morris, K.L., Jonckheere, W., Vandersteen, A., Kelly, G., Schymkowitz, J., Rousseau, F., Pastore, A., Serpell, L.C. and Broersen, K. 2012. Structural basis for increased toxicity of pathological abeta42:abeta40 ratios in Alzheimer disease. *J Biol Chem.* **287**(8), pp.5650-5660.

Peduzzo, A., Linse, S. and Buell, A.K. 2020. The Properties of alpha-Synuclein Secondary Nuclei Are Dominated by the Solution Conditions Rather than the Seed Fibril Strain. *ACS Chem Neurosci.* **11**(6), pp.909-918.

Peng, C., Gathagan, R.J., Covell, D.J., Medellin, C., Stieber, A., Robinson, J.L., Zhang, B., Pitkin, R.M., Olufemi, M.F., Luk, K.C., Trojanowski, J.Q. and Lee, V.M. 2018. Cellular milieu imparts distinct pathological alpha-synuclein strains in alpha-synucleinopathies. *Nature.* **557**(7706), pp.558-563.

Petkova, A.T., Leapman, R.D., Guo, Z., Yau, W.M., Mattson, M.P. and Tycko, R. 2005. Self-propagating, molecular-level polymorphism in Alzheimer's beta-amyloid fibrils. *Science.* **307**(5707), pp.262-265.

Pieri, L., Chafey, P., Le Gall, M., Clary, G., Melki, R. and Redeker, V. 2016. Cellular response of human neuroblastoma cells to alpha-synuclein fibrils, the main constituent of Lewy bodies. *Biochim Biophys Acta.* **1860**(1 Pt A), pp.8-19.

Pinotsi, D., Buell, A.K., Galvagnion, C., Dobson, C.M., Kaminski Schierle, G.S. and Kaminski, C.F. 2014. Direct observation of heterogeneous amyloid fibril growth kinetics via two-color super-resolution microscopy. *Nano Lett.* **14**(1), pp.339-345.

Piotrowski, M., Lewandowska, J. and Wojciechowski, K. 2012. Biosurfactant-protein mixtures: Quillaja Bark Saponin at water/air and water/oil interfaces in presence of beta-lactoglobulin. *J Phys Chem B.* **116**(16), pp.4843-4850.

Qiang, W., Yau, W.M., Lu, J.X., Collinge, J. and Tycko, R. 2017. Structural variation in amyloid-beta fibrils from Alzheimer's disease clinical subtypes. *Nature.* **541**(7636), pp.217-221.

Qiang, W., Yau, W.M., Luo, Y., Mattson, M.P. and Tycko, R. 2012. Antiparallel beta-sheet architecture in Iowa-mutant beta-amyloid fibrils. *Proc Natl Acad Sci U S A.* **109**(12), pp.4443-4448.

Redmann, M., Benavides, G.A., Berryhill, T.F., Wani, W.Y., Ouyang, X., Johnson, M.S., Ravi, S., Barnes, S., Darley-Usmar, V.M. and Zhang, J. 2017. Inhibition of autophagy with bafilomycin and chloroquine decreases mitochondrial quality and bioenergetic function in primary neurons. *Redox Biol.* **11**, pp.73-81.

Robbins, A.R. 1979. Isolation of lysosomal alpha-mannosidase mutants of Chinese hamster ovary cells. *Proc Natl Acad Sci U S A.* **76**(4), pp.1911-1915.

Rodriguez-Rodriguez, C., Rimola, A., Rodriguez-Santiago, L., Ugliengo, P., Alvarez-Larena, A., Gutierrez-de-Teran, H., Sodupe, M. and Gonzalez-Duarte, P. 2010. Crystal structure of thioflavin-T and its binding to amyloid fibrils: insights at the molecular level. *Chem Commun (Camb).* **46**(7), pp.1156-1158.

Ronicke, R., Klemm, A., Meinhardt, J., Schroder, U.H., Fandrich, M. and Reymann, K.G. 2008. Abeta mediated diminution of MTT reduction--an artefact of single cell culture? *PLoS One.* **3**(9), pe3236.

Rossi, A.M. and Taylor, C.W. 2011. Analysis of protein-ligand interactions by fluorescence polarization. *Nat Protoc.* **6**(3), pp.365-387.

Rossjohn, J., Cappai, R., Feil, S.C., Henry, A., McKinstry, W.J., Galatis, D., Hesse, L., Multhaup, G., Beyreuther, K., Masters, C.L. and Parker, M.W. 1999. Crystal structure of the N-terminal, growth factor-like domain of Alzheimer amyloid precursor protein. *Nat Struct Biol.* **6**(4), pp.327-331.

Sanderson, J.B., De, S., Jiang, H., Rovere, M., Jin, M., Zaccagnini, L., Hays Watson, A., De Boni, L., Lagomarsino, V.N., Young-Pearse, T.L., Liu, X., Pochapsky, T.C., Hyman, B.T., Dickson, D.W., Klenerman, D., Selkoe, D.J. and Bartels, T. 2020. Analysis of alpha-synuclein species enriched from cerebral cortex of humans with sporadic dementia with Lewy bodies. *Brain Commun.* **2**(1), pfcaa010.

Sarell, C.J., Stockley, P.G. and Radford, S.E. 2013. Assessing the causes and consequences of co-polymerization in amyloid formation. *Prion.* **7**(5), pp.359-368.

Savage, M.J., Kalinina, J., Wolfe, A., Tugusheva, K., Korn, R., Cash-Mason, T., Maxwell, J.W., Hatcher, N.G., Haugabook, S.J., Wu, G., Howell, B.J., Renger, J.J., Shughrue, P.J. and McCampbell, A. 2014. A sensitive abeta oligomer assay discriminates Alzheimer's and aged control cerebrospinal fluid. *J Neurosci.* **34**(8), pp.2884-2897.

Scheltens, P., Blennow, K., Breteler, M.M., de Strooper, B., Frisoni, G.B., Salloway, S. and Van der Flier, W.M. 2016. Alzheimer's disease. *Lancet.* **388**(10043), pp.505-517.

Schmidt, C., Wolff, M., Weitz, M., Bartlau, T., Korth, C. and Zerr, I. 2011. Rapidly progressive Alzheimer disease. *Arch Neurol.* **68**(9), pp.1124-1130.

Schutz, A.K., Vagt, T., Huber, M., Ovchinnikova, O.Y., Cadalbert, R., Wall, J., Guntert, P., Bockmann, A., Glockshuber, R. and Meier, B.H. 2015. Atomic-resolution three-dimensional structure of amyloid beta fibrils bearing the Osaka mutation. *Angew Chem Int Ed Engl.* **54**(1), pp.331-335.

Schweighauser, M., Shi, Y., Tarutani, A., Kametani, F., Murzin, A.G., Ghetti, B., Matsubara, T., Tomita, T., Ando, T., Hasegawa, K., Murayama, S., Yoshida, M., Hasegawa, M., Scheres, S.H.W. and Goedert, M. 2020. Structures of alpha-synuclein filaments from multiple system atrophy. *Nature.*

Selkoe, D.J. 1999. Translating cell biology into therapeutic advances in Alzheimer's disease. *Nature.* **399**(6738 Suppl), pp.A23-31.

Selkoe, D.J. 2000. The origins of Alzheimer disease: a is for amyloid. *JAMA.* **283**(12), pp.1615-1617.

Selkoe, D.J. and Hardy, J. 2016. The amyloid hypothesis of Alzheimer's disease at 25 years. *EMBO Mol Med.* **8**(6), pp.595-608.

Sgourakis, N.G., Yau, W.M. and Qiang, W. 2015. Modeling an in-register, parallel "iowa" abeta fibril structure using solid-state NMR data from labeled samples with rosetta. *Structure.* **23**(1), pp.216-227.

Shahmoradian, S.H., Lewis, A.J., Genoud, C., Hench, J., Moors, T.E., Navarro, P.P., Castano-Diez, D., Schweighauser, G., Graff-Meyer, A., Goldie, K.N., Sutterlin, R., Huisman, E., Ingrassia, A., Gier, Y., Rozemuller, A.J.M., Wang, J., Paepe, A., Erny, J., Staempfli, A., Hoernschemeyer, J., Grosseruschkamp, F., Niedieker, D., El-Mashtoly, S.F., Quadri, M., Van, I.W.F.J., Bonifati, V., Gerwert, K., Bohrmann, B., Frank, S., Britschgi, M., Stahlberg, H., Van de Berg, W.D.J. and Lauer, M.E. 2019. Lewy pathology in Parkinson's disease consists of crowded organelles and lipid membranes. *Nat Neurosci.* **22**(7), pp.1099-1109.

Sidhu, A., Vaneyck, J., Blum, C., Segers-Nolten, I. and Subramaniam, V. 2018. Polymorph-specific distribution of binding sites determines thioflavin-T fluorescence intensity in alpha-synuclein fibrils. *Amyloid.* **25**(3), pp.189-196.

Sikand, K., Singh, J., Ebron, J.S. and Shukla, G.C. 2012. Housekeeping gene selection advisory: glyceraldehyde-3-phosphate dehydrogenase (GAPDH) and beta-actin are targets of miR-644a. *PLoS One.* **7**(10), pe47510.

Spillantini, M.G., Crowther, R.A., Jakes, R., Hasegawa, M. and Goedert, M. 1998. alpha-Synuclein in filamentous inclusions of Lewy bodies from Parkinson's disease and dementia with lewy bodies. *Proc Natl Acad Sci U S A.* **95**(11), pp.6469-6473.

Spillantini, M.G. and Goedert, M. 2018. Neurodegeneration and the ordered assembly of alpha-synuclein. *Cell Tissue Res.* **373**(1), pp.137-148.

Spillantini, M.G., Schmidt, M.L., Lee, V.M., Trojanowski, J.Q., Jakes, R. and Goedert, M. 1997. Alpha-synuclein in Lewy bodies. *Nature.* **388**(6645), pp.839-840.

Stewart, K.L., Hughes, E., Yates, E.A., Akien, G.R., Huang, T.Y., Lima, M.A., Rudd, T.R., Guerrini, M., Hung, S.C., Radford, S.E. and Middleton, D.A. 2016. Atomic Details of the Interactions of Glycosaminoglycans with Amyloid-beta Fibrils. *J Am Chem Soc.* **138**(27), pp.8328-8331.

Stewart, K.L., Hughes, E., Yates, E.A., Middleton, D.A. and Radford, S.E. 2017. Molecular Origins of the Compatibility between Glycosaminoglycans and Abeta40 Amyloid Fibrils. *J Mol Biol.* **429**(16), pp.2449-2462.

Strohaker, T., Jung, B.C., Liou, S.H., Fernandez, C.O., Riedel, D., Becker, S., Halliday, G.M., Bennati, M., Kim, W.S., Lee, S.J. and Zweckstetter, M. 2019. Structural heterogeneity of alpha-synuclein fibrils amplified from patient brain extracts. *Nat Commun.* **10**(1), p5535.

Sun, Y., Hou, S., Zhao, K., Long, H., Liu, Z., Gao, J., Zhang, Y., Su, X.D., Li, D. and Liu, C. 2020. Cryo-EM structure of full-length alpha-synuclein amyloid fibril with Parkinson's disease familial A53T mutation. *Cell Res.* **30**(4), pp.360-362.

Tanzi, R.E. 1999. A genetic dichotomy model for the inheritance of Alzheimer's disease and common age-related disorders. *J Clin Invest.* **104**(9), pp.1175-1179.

Teow, S.Y., Liew, K., Che Mat, M.F., Marzuki, M., Abdul Aziz, N., Chu, T.L., Ahmad, M. and Khoo, A.S. 2019. Development of a luciferase/luciferin cell proliferation (XenoLuc) assay for real-time measurements of Gfp-Luc2-modified cells in a co-culture system. *BMC Biotechnol.* **19**(1), p34.

Thal, D.R., Capetillo-Zarate, E., Del Tredici, K. and Braak, H. 2006. The development of amyloid beta protein deposits in the aged brain. *Sci Aging Knowledge Environ.* **2006**(6), pre1.

Thal, D.R., Rub, U., Orantes, M. and Braak, H. 2002. Phases of A beta-deposition in the human brain and its relevance for the development of AD. *Neurology.* **58**(12), pp.1791-1800.

Tolia, A. and De Strooper, B. 2009. Structure and function of gamma-secretase. *Semin Cell Dev Biol.* **20**(2), pp.211-218.

Tornquist, M., Michaels, T.C.T., Sanagavarapu, K., Yang, X., Meisl, G., Cohen, S.I.A., Knowles, T.P.J. and Linse, S. 2018. Secondary nucleation in amyloid formation. *Chem Commun (Camb).* **54**(63), pp.8667-8684.

Tuttle, M.D., Comellas, G., Nieuwkoop, A.J., Covell, D.J., Berthold, D.A., Kloepper, K.D., Courtney, J.M., Kim, J.K., Barclay, A.M., Kendall, A., Wan, W., Stubbs, G., Schwieters, C.D., Lee, V.M., George, J.M. and Rienstra, C.M. 2016a. Solid-state NMR structure of a pathogenic fibril of full-length human alpha-synuclein. *Nat Struct Mol Biol.* **23**(5), pp.409-415.

Tuttle, M.D., Comellas, G., Nieuwkoop, A.J., Covell, D.J., Berthold, D.A., Kloepper, K.D., Courtney, J.M., Kim, J.K., Barclay, A.M., Kendall , A., Wan, W., Stubbs, G., Schwieters, C.D., Lee, V.M., George, J.M. and Rienstra, C.M. 2016b. Solid-state NMR structure of a pathogenic fibril of full-length human α-synuclein. *Nat Struct Mol Biol.* **23**(5), pp.409-415.

Twohig, D. and Nielsen, H.M. 2019. alpha-synuclein in the pathophysiology of Alzheimer's disease. *Mol Neurodegener.* **14**(1), p23.

Tycko, R. 2014. Physical and structural basis for polymorphism in amyloid fibrils. *Protein Sci.* **23**(11), pp.1528-1539.

Ueda, K., Fukushima, H., Masliah, E., Xia, Y., Iwai, A., Yoshimoto, M., Otero, D.A., Kondo, J., Ihara, Y. and Saitoh, T. 1993. Molecular cloning of cDNA encoding an unrecognized component of amyloid in Alzheimer disease. *Proc Natl Acad Sci U S A.* **90**(23), pp.11282-11286.

Ulmer, T.S., Bax, A., Cole, N.B. and Nussbaum, R.L. 2005. Structure and dynamics of micelle-bound human alpha-synuclein. *J Biol Chem.* **280**(10), pp.9595-9603.

Uversky, V.N., Li, J. and Fink, A.L. 2001. Evidence for a partially folded intermediate in alpha-synuclein fibril formation. *J Biol Chem.* **276**(14), pp.10737-10744.

Vivekanandan, S., Brender, J.R., Lee, S.Y. and Ramamoorthy, A. 2011. A partially folded structure of amyloid-beta(1-40) in an aqueous environment. *Biochem Biophys Res Commun.* **411**(2), pp.312-316.

Volpicelli-Daley, L.A., Luk, K.C. and Lee, V.M. 2014. Addition of exogenous alpha-synuclein preformed fibrils to primary neuronal cultures to seed recruitment of endogenous alpha-synuclein to Lewy body and Lewy neurite-like aggregates. *Nat Protoc.* **9**(9), pp.2135-2146.

Walsh, D.M., Thulin, E., Minogue, A.M., Gustavsson, N., Pang, E., Teplow, D.B. and Linse, S. 2009. A facile method for expression and purification of the Alzheimer's disease-associated amyloid beta-peptide. *FEBS J.* **276**(5), pp.1266-1281.

Wang, Y. and Ha, Y. 2004. The X-ray structure of an antiparallel dimer of the human amyloid precursor protein E2 domain. *Mol Cell.* **15**(3), pp.343-353.

Warner, C.J.A., Dutta, S., Foley, A.R. and Raskatov, J.A. 2017. A Tailored HPLC Purification Protocol That Yields High-purity Amyloid Beta 42 and Amyloid Beta 40 Peptides, Capable of Oligomer Formation. *J Vis Exp.* (121).

Watanabe-Nakayama, T., Nawa, M., Konno, H., Kodera, N., Ando, T., Teplow, D.B. and Ono, K. 2020. Self- and Cross-Seeding on alpha-Synuclein Fibril Growth Kinetics and Structure Observed by High-Speed Atomic Force Microscopy. *ACS Nano.* **14**(8), pp.9979-9989.

Wilkins, H.M. and Swerdlow, R.H. 2017. Amyloid precursor protein processing and bioenergetics. *Brain Res Bull.* **133**, pp.71-79.

Wolfe, D.M., Lee, J.H., Kumar, A., Lee, S., Orenstein, S.J. and Nixon, R.A. 2013. Autophagy failure in Alzheimer's disease and the role of defective lysosomal acidification. *Eur J Neurosci.* **37**(12), pp.1949-1961.

Wroblewski, H., Burlot, R. and Johansson, K.E. 1978. Solubilization of Spiroplasma citri cell membrane proteins with the anionic detergent sodium lauroyl-sarcosinate (Sarkosyl). *Biochimie.* **60**(4), pp.389-398.

Wu, C., Cai, L., Wei, J., Pike, V.W. and Wang, Y. 2006. Lipophilic analogs of thioflavin S as novel amyloid-imaging agents. *Curr Alzheimer Res.* **3**(3), pp.259-266.

Xu, G., Fromholt, S.E., Chakrabarty, P., Zhu, F., Liu, X., Pace, M.C., Koh, J., Golde, T.E., Levites, Y., Lewis, J. and Borchelt, D.R. 2020. Diversity in Abeta deposit

morphology and secondary proteome insolubility across models of Alzheimer-type amyloidosis. *Acta Neuropathol Commun.* **8**(1), p43.

Yancopoulou, D., Xuereb, J.H., Crowther, R.A., Hodges, J.R. and Spillantini, M.G. 2005. Tau and alpha-synuclein inclusions in a case of familial frontotemporal dementia and progressive aphasia. *J Neuropathol Exp Neurol.* **64**(3), pp.245-253.

Yang, D.S., Smith, J.D., Zhou, Z., Gandy, S.E. and Martins, R.N. 1997. Characterization of the binding of amyloid-beta peptide to cell culture-derived native apolipoprotein E2, E3, and E4 isoforms and to isoforms from human plasma. *J Neurochem.* **68**(2), pp.721-725.

Yang, M. and Teplow, D.B. 2008. Amyloid beta-protein monomer folding: free-energy surfaces reveal alloform-specific differences. *J Mol Biol.* **384**(2), pp.450-464.

Yoo, S., Zhang, S., Kreutzer, A.G. and Nowick, J.S. 2018. An Efficient Method for the Expression and Purification of Abeta(M1-42). *Biochemistry.* **57**(26), pp.3861-3866.

Young, L.M., Tu, L.H., Raleigh, D.P., Ashcroft, A.E. and Radford, S.E. 2017. Understanding co-polymerization in amyloid formation by direct observation of mixed oligomers. *Chem Sci.* **8**(7), pp.5030-5040.

Zetterberg, H. and Blennow, K. 2013. Cerebrospinal fluid biomarkers for Alzheimer's disease: more to come? *J Alzheimers Dis.* **33 Suppl 1**, pp.S361-369.

Zhao, K., Li, Y., Liu, Z., Long, H., Zhao, C., Luo, F., Sun, Y., Tao, Y., Su, X.D., Li, D., Li, X. and Liu, C. 2020a. Parkinson's disease associated mutation E46K of alpha-synuclein triggers the formation of a distinct fibril structure. *Nat Commun.* **11**(1), p2643.

Zhao, K., Lim, Y.J., Liu, Z., Long, H., Sun, Y., Hu, J.J., Zhao, C., Tao, Y., Zhang, X., Li, D., Li, Y.M. and Liu, C. 2020b. Parkinson's disease-related phosphorylation at Tyr39 rearranges alpha-synuclein amyloid fibril structure revealed by cryo-EM. *Proc Natl Acad Sci U S A.* **117**(33), pp.20305-20315.

Zoltowska, K.M., Maesako, M. and Berezovska, O. 2016. Interrelationship between Changes in the Amyloid beta 42/40 Ratio and Presenilin 1 Conformation. *Mol Med.* **22**, pp.329-337.